Interaction and Dynamics in complex systems

Thesis Submitted for the degree of

Doctor of Philosophy (Science)

of

Jadavpur University

By

Kallol Mukherjee
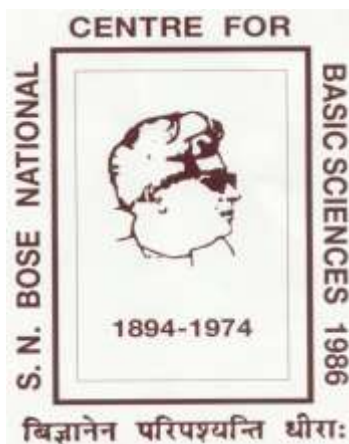
Department of Chemical, Biological and Macromolecular Sciences

S. N. Bose National Centre for Basic Sciences

Block-JD, Sector-III, Salt Lake City

Kolkata- 700106, India

September 2016

CERTIFICATE FROM THE SUPERVISOR(S)

This is to certify that the thesis entitled **"Interaction and Dynamics in complex systems"** submitted by **Sri Kallol Mukherjee** (Index no. 27/13/Chem./22), who got his name registered on 14/03/13 for the award of Ph.D. (Science) degree of Jadavpur University, is absolutely based upon his own work under the supervision of **Prof. Ranjit Biswas** and **Prof. Anjan Barman** and that neither this thesis nor any part of it has been submitted for either any degree/diploma or any other academic award anywhere before.

Dr. Ranjit Biswas

07/09/16

Professor,

Department of Chemical,

Biological and Macromolecular Sciences

S. N. Bose National Centre for

Basic Sciences

Block-JD, Sector-III, Salt Lake,

Kolkata-700106, West Bengal, India

07/09/16

Dr. Anjan Barman

Professor,

Department of Condensed Matter

Physics and Material Sciences

S. N. Bose National Centre for

Basic Sciences

Block-JD, Sector-III, Salt Lake,

Kolkata-700106, West Bengal, India

DR. RANJIT BISWAS
Professor
Dept. of Chemical, Biological & Macromolecular Sciences
S. N. Bose National Centre for Basic Sciences
Block - JD, Sector - III, Salt Lake, Kolkata - 700 098, India

DR. ANJAN BARMAN
Professor
S. N. Bose National Centre for Basic Sciences
Block - JD, Sector- III, Salt Lake,
Kolkata - 700 098, India

Dedicated to

My Father Uday Kumar Mukherjee
&
My Mother Kakali Mukherjee

Acknowledgement

I have spent about five years at S. N. Bose National Center for Basic Sciences, as a research scholar in the department of Chemical, Biological and Macromolecular Sciences (CBMS). It is a great pleasure to acknowledge the cooperation I have received from many people.

First of all, I would like to express my earnest thanks and humble gratitude to my supervisor Prof. Ranjit Biswas for his guidance and continuous support without which this work would not have been possible. His dedication to work and immense enthusiasm for solving new problems have always been motivating for me. I feel myself very much fortunate for being trained under the guidance of a person like him. The most important thing about his training is that he has always encouraged me to work independently and to think independently.

I would also like to express my sincere gratitude to my co-supervisor Prof. Anjan Barman for his untiring support and fruitful discussions in several group meetings. It has been a great privilege for me to work under his supervision for the last five years.

I want to thank CSIR for financial Support.

My sincere thanks extend to all the members of my thesis committee, Prof. Nikhil Guchhait (University of Calcutta), Dr. Punyabrata Pradhan (SNBNCBS) and Dr. Manoranjan Kumar (SNBNCBS) for dedicating valuable times from their busy schedule for me.

I want to thank my labmates Suman, Ejaj, Juriti, Atanu and Kajal from PCCP lab and Arnab, Debanjan, Chandrima, Samiran, Sucheta, Santanu, Kartik, Niraj, Anulekha, Avinash and Sourav from UFNM lab for providing a friendly atmosphere inside the labs and their unconditional helps. I also thank Dr. Biswajit Guchhait, Dr. Snehasis Daschakraborty, Dr. Tamisra Pal, Dr. Anuradha Das and Sandipa Indra for helping me in many ways.

I convey my sincere thanks to the all academic and non-academic staffs of SNBNCBS for their helps. I take the opportunity to thank security personals for their spontaneous supports.

I want to express my profound sense of regards to Dr. Parijat Das for extreme caring attitude, while I visited to her home. The sweet moments I spent with Rwitoban and Arshaman will remain cherishing for rest of my life.

I am very much thankful to two of my friends Sreeraj and Chaoba for their supports and encouragements.

I am very much grateful to one of my close friends Dr. Priyadarshi Chakraborty for his unconditional helps.

Huge appreciation extends to Sanjay da, Ganesh, Ramu, Rajiv and Kajal of SNB student mess and Bidyasagar da, Arup, Sanatan, Hari, Barun da, Sumanta Da, Subhankar and Mrinmay of SNB canteen for providing good foods.

I am grateful to all the teachers of my school (Burdwan Municipal High School), professors of my college (Vivekananda Mahavidyalay, Burdwan) and faculties of Department of Chemistry, The University of Burdwan for their guidance.

I will be ever grateful to my maternal grandfather late Sailendra Nath Banerjee (Dadamoni), my maternal grandmother Arnapurna Banerjee (Duduma) and paternal grandmother Ashalata Mukherjee (Barodidu) for their blessings. I am also thankful to all of my brothers (Papai, Rubai, Tubai, Tanai, Tunai, Ayan and Argha) and sisters (Didibhai, Mantu, Mistu and Lisa) for their care and affections.

Finally, I want to express my gratitude from the bottom of my heart to two best persons of my life, my parents, Uday Kumar Mukherjee and Kakali Mukherjee for their loves, blessings and lessons.

Abstract

In this thesis we have investigated interactions and dynamics in several complex chemical systems, which includes deep eutectic solvents (both ionic and non-ionic), aqueous macromolecular systems and polymer gel electrolytes, using dielectric relaxation and time-resolved fluorescence (TRF) spectroscopic techniques. Dielectric relaxation spectroscopic (DRS) measurements have revealed that ionic deep eutectic solvents (DESs) are different from non-ionic DESs. The dynamics of ionic DESs are slower than that of non-ionic DESs, probably due to the ionic arrest of dipolar species constituting the medium. In addition, it has been observed that the static dielectric constant (ε_0) values of acetamide and urea containing ionic DESs are significantly smaller than those of molten neat acetamide and urea, although ε_0 values of the corresponding non-ionic deep eutectics are comparable to those of neat molten systems. Temperature dependent DRS measurements further reflect on the characteristic differences between the ionic and non-ionic DESs. Interestingly, it has been found that with increasing temperature the estimated static dielectric constants of ionic DESs increase whereas for non-ionic DESs it decreases with temperature. Although exact estimation of the static dielectric constants (ε_0) for these type of conducting and highly viscous liquid systems using a frequency window $0.2 \leq \nu/\text{GHz} \leq 50$ is nontrivial, we can get a qualitative idea about the polarity of the medium from our measurements. Moreover, we have prepared a new non-ionic DES which possesses exquisite solvent properties, like high viscosity, high polarity etc and investigated it's dynamics using DRS technique. Additionally, we have examined the impact of aggregation behavior of bile salts on the solution structure and dynamics using both DRS and TRF measurements. Substantial effects from the presence of an extra hydroxyl (–OH) group on solution structure and dynamics in aqueous medium has been revealed by both time-resolved fluorescence (TRF) and DR measurements. TRF measurements have been further utilized to explore the interaction, dynamics and the heterogeneity aspect of polymer gel electrolyte systems. Note here that the experimental findings show that the polymer has a remarkable effect on the dynamics of these polymer gel electrolyte systems.

List of Publications

1. *"Dielectric Relaxations of (Acetamide + Electrolyte) Deep Eutectic Solvents in the Frequency Window, 0.2 ≤ v/GHz ≤ 50: Anion and Cation Dependence"* by **Kallol Mukherjee**, Anuradha Das, Samiran Choudhury, Anjan Barman and Ranjit Biswas ***J. Phys. Chem. B 119, 8063 (2015).***

2. *"Impact of the Aggregation Behaviour of Sodium Cholate and Sodium Deoxycholate on Aqueous Solution Structure and Dynamics: A Combined Time Resolved Fluorescence and Dielectric Relaxation Spectroscopic Study"* by **Kallol Mukherjee**, Anjan Barman and Ranjit Biswas ***J. Mol. Liq. 222, 495 (2016).***

3. *"Temperature Dependent Dielectric Relaxation in Molten Urea, and Acetamide/Urea Deep Eutectics: Polarity and the Possible Origin of the Relaxation Time Scales"* by **Kallol Mukherjee**, Suman Das, Anjan Barman and Ranjit Biswas **(Under Revision)**.

4. *"Temperature Dependent Dielectric Relaxation Dynamics of (Acetamide + Electrolyte) Deep Eutectics in the Frequency Window, 0.2 ≤ v/GHz ≤ 50 "* by **Kallol Mukherjee**, Anjan Barman and Ranjit Biswas **(Under Revision)**.

5. *"Dielectric Relaxation of (Urea + Choline Chloride) Deep Eutectic Solvents in the Frequency Window, $0.2 \leq \nu(GHz) \leq 50$: Temperature Dependence"* by **Kallol Mukherjee**, Anjan Barman and Ranjit Biswas **(to be Submitted)**.

6. *"Viscosity Coupling of Solvation and Rotation of C153 in a Polymer Gel Electrolyte System"* by **Kallol Mukherjee**, Kajal Kumbhakar, Ejaj Tarif and Ranjit Biswas **(to be Submitted)**.

7. *"Dielectric Relaxation Studies in (Acetamide + Urea + PEG) Deep Eutectic Solvent: Origin of slow relaxation"* by **Kallol Mukherjee**, Anjan Barman and Ranjit Biswas **(Manuscript in Preparation)**.

8. **"Presence of Micro-heterogeneity in Aqueous Hyaluronic Acid Gel: A probe dependent fluorescence study"* by **Kallol Mukherjee**, Ejaj Tarif and Ranjit Biswas **(Manuscript in Preparation)**.

9. *"*Composition Dependent Interaction and Dynamics of Water-Xylitol Mixtures: A Combined Time-Resolved Fluorescence and Dielectric Relaxation Study*"* by Ejaj Tarif, **Kallol Mukherjee** and Ranjit Biswas **(Manuscript in Preparation)**.

10. *"*Concentration and Temperature Dependent Dielectric Relaxation Spectroscopic Study in Aqueous Pluronic P-123 Solution*"* by **Kallol Mukherjee**, Anjan Barman and Ranjit Biswas **(Manuscript in Preparation)**.

* not included in this thesis

Contents

Chapter 1

Introduction

Understanding interaction and dynamics of complex chemical systems, such as, binary mixtures, multi-component mixtures and pure solvents has been an active area of research for a very long time. This interest stems from a desire to engineer reaction media for tailoring reactions and, in the same time, would be cost-effective, environment-friendly, easy-to-handle and recyclable. Chemistry, as a fundamental subject, has the responsibility to feed technology that demands both qualitative and quantitative knowledge about the interaction pathway and the ultimate fate of reactants. Large scale industrial usage and applications in chemical technology need knowledge of solvent impact on one-to-one interactions for a condensed phase reaction. Such a strong background constantly fuels search of new media and has led to systems, like water- alcohol,[1-3] water-surfactant,[4-9] water-polymer,[10-12] ionic liquids and their mixtures,[13-15] deep eutectic solvents,[16-18] polymer gel electrolytes[19-21] and organic electrolytes.[22-23] Medium effects on chemical reactions are now well-understood.[24-36] This knowledge of how the course of a given reaction can possibly be altered has further intensified the design of new solvent systems and their smarter use.

Polarity of a medium, which is often represented by a magnitude of the static dielectric constant (ε_0), has remarkable influence on a chemical event taking place in that medium.[37-39] It can modify the barrier that separates reactants from the products. Solvent density fluctuations, on the other hand, couples the reactive mode to the medium friction at the barrier top while crossing from the reactant well to the product surface. For a reaction medium which is dipolar in nature, density fluctuations always associate with dipole moment fluctuations. Dielectric relaxation spectroscopy (DRS) is a technique that probes this dipole density fluctuations. An oscillating electromagnetic field in the microwave (GHz) region is employed and the subsequent collective

1

polarization relaxation is tracked which then provides information regarding relaxation dynamics of the system under study.[40-47] Specifically, this experimental technique is sensitive to the reorientational motions and cooperative dynamics of the dipolar species (present in the medium) on the picosecond to nanosecond time scale. Starting from pure solvents to the complex chemical systems, this experimental tool has been rigorously used to explore their relaxation dynamics.[48-55] Application of this simple technique in electrolyte solutions not only yields information on ion-pairs but also probes ion-solvent interactions and solution dynamics in the same experiment.[52,56-58] Note for conducting solutions DRS measurements require special attention because of the conductivity divergence at $\nu \to 0$.[53,59-60] To understand the dynamics of water molecules in bulk as well as in confined environments, like reverse micelles, micelles, polymers and different biological systems, DRS has been a great technique.[47,61-69]

Interestingly, dynamics of solvent molecules can also be monitored via measuring the dynamic Stokes shift (DSS)[70-71] of a fluorescent dipolar probe molecule dissolved at a very low concentration ($\sim 10^{-5}$ mol/liter) in the system under investigation.[37,72-83] The low solute (fluorescent probe) concentration is maintained to minimize the solute-solute interaction in the solution so that the measured dynamics reflects the dynamics of the undoped (in the absence of the probe) system. A laser light with suitable energy and pulse duration is used to photo-excite the probe molecule which suddenly disturbs the equilibrium charge distribution in the fluorophore molecule, leading to a response by the surrounding solvent molecules for hosting the excited solute. This requires solvent rearrangement which, if recorded via a fast enough time resolution, can give information about time-dependent solvation process of the excited solute by the medium. Note photo-excitation modifies the dipole moment of the solute and this changed dipole moment then couples to the solvent via the medium polarization mode. Then, the time dependent fluctuations of the polarization density chart out the relaxation profile. It is therefore natural that dielectric relaxation and Stokes shift dynamics are inter-related. In one case (DRS) the medium responds to a weak external electromagnetic field and in the other (DSS) solvent responds to a sudden dipole moment change dissolved inside it. In both cases experimental results are analyzed and interpreted assuming the coupling between the solvent and the

2

perturbation (externally applied field or solute dipole moment) is weak that does not alter the inherent dynamics of the pure system (linear response).

Extensive investigation of room temperature ionic liquids (RTILs) in the last two decades have provides many useful information on structure and dynamics of these charged fluids.[82-86,87-95] Relative to RTILs, deep eutectic solvents (DESs) are newer and thus many solvent aspects are yet to be explored for this new class of solvent systems. DESs are mixtures of two or more ingredients which form molten mixtures and remain stable in the liquid phase at temperatures much lower than the individual melting temperatures (T_m's) of the mixture components. Extensive hydrogen-bonding (H-bonding) and the entropic gain are believed to be the prime reasons for forming the deep eutectic liquid mixtures out of the high melting solid components. Moreover, there exists a wide scope for selection of constituents for forming ionic[16,96] and non-ionic[97] DESs. This inherent flexibility provides the unique opportunity for tuning solvent properties and makes them suitable candidates for solvent engineering. Although several earlier studies[98-103] have suggested micro-heterogeneous solution structure for several amide based DESs, molecular length scale structures via measurements such as neutron and X-ray scattering measurements have not yet been determined. Consequently, solution heterogeneity in terms of longer-ranged static correlations and/or local clusters has not been understood. Fluorescence studies along with computer simulations have provided some indirect evidences in favor of spatio-temporal heterogeneity in these DESs.[104-107] In addition, study of collective low frequency dynamics of these systems has just begun.[108] The presence of picosecond and nanosecond dynamics in such multi-component mixtures have been revealed by time-resolved fluorescence Stokes shift measurements[97,109] and Kerr spectroscopic measurements. Recent computer simulation studies[110-111] on anion dependent H-bond relaxation dynamics and reorientational relaxation dynamics of acetamide based ionic DESs hinted at strong ion-acetamide interaction and non-Brownian angular movements.

Research described in this thesis includes dielectric relaxation (DR) dynamics of ionic and non-ionic DESs along with their temperature and composition dependent behavior measured in a frequency window $0.2 \leq \nu / GHz \leq 50$. In addition, we have measured the Stokes shift dynamics

in aqueous macromolecular systems[3,78,112-115] and polymer gel electrolytes[20,116-117] via picoseconds-resolved fluorescence measurements to complement the relevant DRS measurements.

This thesis consists of ten chapters with the first chapter being the Introduction. Chapter 2 is devoted to the discussion of experimental techniques and methods of data analyses employed while investigating the interaction and dynamics of the complex systems considered in the present Thesis. In chapter 3 we report the results of dielectric relaxation (DR) measurements for neat molten acetamide, and six different ($acetamide + electrolyte$) deep eutectic solvents.[118] Electrolytes used are: lithium salts of bromide ($LiBr$), nitrate ($LiNO_3$) and perchlorate ($LiClO_4$); sodium salts of perchlorate ($NaClO_4$) and thiocyante ($NaSCN$), and potassium thiocyanate ($KSCN$). With these electrolytes acetamide forms DESs approximately at 80:20 mole ratio. Simultaneous fits to the measured permittivity (ε') and loss (ε'') spectra of these DESs at ~293 K require a sum of four Debye (4-D) processes with relaxation times spread over pico-second to nanosecond regime. In contrast, DR spectra for neat molten acetamide (~354 K) depict 2-D relaxation with time constants ~50 ps and ~5 ps. For both the neat and ionic systems, the undetected dispersion, $\varepsilon_\infty - n_D^2$, remains to be ~3 - 4. Upon comparison, measured DR dynamics reveal pronounced anion and cation effects. Estimated static dielectric constants (ε_0) from fits for these DESs cover the range, $12 < \varepsilon_0 < 30$, and are remarkably lower than that ($\varepsilon_0 \sim 64$) measured for molten acetamide at ~354 K. Hydrodynamic effective rotation volumes (V_{eff})[37,119-120] estimated from the slowest DR relaxation time constants vary with ion identity and are much smaller than the molecular volume of acetamide. This decrease of ε_0 and V_{eff} is attributed respectively to the pinning of acetamide molecules by ions and orientation jumps, and undetected portion to the limited frequency coverage employed in these measurements.

In chapter 4, temperature dependent dielectric relaxation (DR) measurements of molten urea and ($acetamide + urea$) deep eutectics (DESs) in the frequency range, $0.2 \le \nu(GHz) \le 50$, have been reported.[121] Estimated static dielectric constant (ε_0) and dipole moment (μ) for molten urea at

406 K are found to be ~67 and ~6.0 D. The detected relaxation for molten urea requires three Debye processes with time constants ~90 ps, ~30 ps and ~5 ps and in the total relaxation process the maximum contribution comes from the 30 ps component. Similarly, we get three time components from fits of the dielectric responses of ($acetamide + urea$) DESs with a ~100 ps dominating component. However, formation of DES induces an insignificant change on ε_0 as it remains within ~68 ± 2. A connection between H-bond fluctuation and DR dynamics is discussed along with the validity of Stokes-Einstein-Debye (SED) model[37,119] while exploring the origin of the detected DR time scales. Temperature dependence of DR measurements provide an activation energy of ~21.6 kJ/mol for molten urea. Thermal decomposition of urea[122] seriously limits the accessible temperature range ($406 \leq T/K \leq 421$). Signature of urea pyrolysis is absent in the temperature dependent measurements of these DESs in the range, $335 \leq T/K \leq 363$, but the activation energy has been found to be quite similar, ~23.5 kJ/mol. This magnitude of activation energy is substantially lower than those obtained from viscosity (~31.5 kJ/mol) and dynamic fluorescence anisotropy (~32.5 kJ/mol, using C153 as probe solute) measurements.[97] Interestingly, fractional viscosity dependence for DR times has been found while the SED relation describes quantitatively the dynamic fluorescence anisotropy data in these media. The implication of this different viscosity coupling from different experiments on dynamic heterogeneity has been discussed.

In chapter 5, we have extended our work to the temperature dependent dielectric relaxation (DR) dynamics of acetamide based three deep eutectic systems (DESs).[123] DESs have been prepared by mixing three electrolytes, lithium bromide ($LiBr$), lithium nitrate ($LiNO_3$) and lithium perchlorate ($LiClO_4$), with acetamide in 20:80 molar ratio. The dielectric spectra for these DESs have been recorded over a temperature regime, $293 \leq T(K) \leq 336$. The simultaneous fitting of the real (ε') and imaginary (ε'') part of the collected dielectric responses demands a sum of four Debye (4-D) relaxation processes. The DR relaxation times are spread over picosecond to nanosecond regime. As in earlier cases, our limited frequency coverage has missed dynamical events in these media that are faster than a few picoseconds and slower than about a nanosecond.

It has been found that, like molten acetamide, these DESs follow an Arrhenius type temperature dependence and the estimated activation energies for these DESs are somewhat larger that for molten acetamide. What is even more interesting is that, unlike most of the conventional solvents, the value of the estimated static dielectric constants (ε_0) for these solvents increases with increasing temperature.

In chapter 6, we have reported temperature dependent dielectric relaxation (DR) measurements of (*urea + choline chloride*) deep eutectic solvents (DESs) in the frequency regime, $0.2 \leq \nu(GHz) \leq 50$.[124] The DESs are prepared by mixing urea and choline chloride in 60:40 and 67:33 molar ratios. Measured DR data require a sum of four Debye (4-D) relaxation processes for adequate description, with relaxation times ranging from picosecond to nanosecond, suggesting inter-species complexation and molecular rotation. Presence of choline chloride has been found to alter several properties of urea: (i) decreases static dielectric constant (ε_0) of these these DESs (molten urea, $\varepsilon_0 \approx 68$), (ii) induces a relaxation time component in the nanosecond regime, which is absent in the molten urea. Surprisingly, in contrast to the traditional solvents like water and alcohols, ε_0 for these DESs shows a continuous increase with temperature in the temperature range, $273 \leq T/K \leq 323$, with the temperature coefficient ($-d\varepsilon_S/dT$) value ~0.27 ± 0.01 K^{-1}. The activation energy estimated from the measured temperature dependent slowest dielectric relaxation time constant has been found to be substantially smaller than the activation energy from temperature dependent viscosity measurements.[125] This has been interpreted in terms of significant decoupling between solute rotation and solvent viscosity via non-Brownian moves, such as large angle jumps, during orientation relaxation.

In chapter 7, we have demonstrated the temperature dependent dielectric relaxation (DR) dynamics of a new non-ionic deep eutectic solvent (DES), containing acetamide, urea and polyethylene glycol (PEG).[126] The composition of the DES is as follows: $w[fCH_3CONH_2 + (1-f)NH_2CONH_2] + (1-w)PEG$, where w represents the weight fraction

and f represents the mole fraction. In this investigation we have kept w fixed at 0.67 and f fixed at 0.60. DR measurements have been performed in the temperature range, $308 \leq T(K) \leq 333$. The estimated static dielectric constant (ε_0) for this DES is considerably large, even larger than that for highly polar solvents like, DMSO and acetonitrile. Surprisingly, in spite of being a non-ionic DES, this system possesses a nanosecond relaxation process, which is very common for the acetamide based ionic DESs. This nanosecond component originates possibly from the collective H-bond dynamics of the acetamide (or urea) molecules connected to the polymer via H-bonding. Estimated activation energy is found to be quite high in comparison to those estimated for other acetamide based ionic and non-ionic DESs.

In chapter 8, we have presented the solute-medium coupling and solute-centred dynamics of a polymer gel electrolyte system using time-resolved fluorescence (TRF) measurement technique.[127] The polymer gel electrolyte system consists of propylene carbonate (PC) as the organic solvent media, lithium perchlorate ($LiClO_4$) as the electrolyte and $PEG\ 300$ as the polymeric component. We varied the polymer concentration from 0 wt% to 40 wt%. In the whole experiment we kept the molar ratio of PC and $LiClO_4$ fixed at 11.3. Coumarin 153 (C153), a well known fluorescent probe molecule, has been employed as a local reporter. Steady state measurements in these polymer gel electrolyte systems indicate substantial effect of polymer on the organic electrolyte system although no signature of spatial heterogeneity has been detected up to 40 wt% polymer concentration. However, TRF measurements reveal the existence of temporal heterogeneity in the medium. Fractional viscosity dependence of average rotational time has been observed. Although with increasing polymer concentration the viscosity of the medium as well as the average rotation time of the probe molecule increase, the average solvation time of the probe molecule decreases. Incorporation of polymer in the medium leads to emergence of a new nanosecond (~0.5 ns) time component, which is absent in the solvation response function of C153 in polymer-free system.

In chapter 9, we have investigated the impact of aggregation behaviour of sodium cholate (SC) and sodium deoxycholate (SDC) on aqueous solution structure and dynamics and compared by performing dielectric relaxation (DR) and time-resolved fluorescence (TRF) measurements at three different concentrations, 30 mM, 100 mM and 300 mM at ~298 K.[111] For DR studies, measurements have been carried out in the frequency range, $0.2 \leq \nu(\text{GHz}) \leq 50$. TRF measurements, on the other hand, employ a fluorescent probe, coumarin 153 (C153), as a local reporter. Both DR and TRF measurements confirm presence of surface water molecules that are characterized by sub-nanosecond timescale. This is further supported by the sub-melting features in the differential scanning calorimetric measurements. DR, dynamic Stokes shift and fluorescence anisotropy experiments indicate SDC solutions are dynamically slower than SC solutions. In addition, excitation energy dependence of steady state fluorescence emission measurements suggests SDC solutions are more heterogeneous. All these results indicate that absence of only one hydroxyl (-OH) group in SDC introduces significant difference in the aggregation behaviour between SC and SDC, affecting substantially the solution structure and dynamics. The thesis ends with chapter 10 which contains a brief concluding remark and few relevant future problems.

References

1.   A. Sukul, S. Sinhabau and N. Sukul, Br. Homeopath. J. **88**, 58 (1999).

2.   P. P. Singh and H. L. Chhabra, Br. Homeopath. J. **82**, 164 (1993).

3.   B. Bagchi, *Water in Biological and Chemical Processes: From Structure and Dynamics to Function*. (Cambridge University Press, 2013).

4.   C. A. Moody and J. A. Field, Environ. Sci. Technol. **34**, 3864 (2000).

5.   R. H. Notter, *Lung Surfactants: Basic Science and Clinical Applications*. (CRC Press, 2000).

6.   M. P. Choi, K. K. Chan, H. W. Leung and C. W. Huie, J. Chromatogr. A **983**, 153 (2003).

7.   H. D. Silva, M. Â. Cerqueira and A. A. Vicente, Food Bioprocess Technol. **5**, 854 (2012).

8.   M. Abe, *Mixed Surfactant Systems*. (CRC Press, 2004).

9.   L. L. Schramm, *Surfactants: Fundamentals and Applications in the Petroleum Industry*. (Cambridge University Press, 2000).

10.   C. A. Finch, *Chemistry and Technology of Water-soluble Polymers*. (Springer Science & Business Media, 2013).

11.   J. M. Harris, *Poly (ethylene glycol) Chemistry: Biotechnical and Biomedical Applications*. (Springer Science & Business Media, 2013).

12.   J. H. Lora and W. G. Glasser, J. Polym. Environ. **10**, 39 (2002).

13.   R. D. Rogers and K. R. Seddon, Science **302**, 792 (2003).

14.   N. V. Plechkova and K. R. Seddon, Chem. Soc. Rev. **37**, 123 (2008).

15.   P. Wasserscheid and W. Keim, Angew. Chem. Int. Ed. **39**, 3772 (2000).

16.   E. L. Smith, A. P. Abbott and K. S. Ryder, Chem. Rev. **114**, 11060 (2014).

17.   Q. Zhang, K. D. O. Vigier, S. Royer and F. Jérôme, Chem. Soc. Rev. **41**, 7108 (2012).

18.   D. V. Wagle, H. Zhao and G. A. Baker, Acc. Chem. Res. **47**, 2299 (2014).

19.   P. Wang, S. M. Zakeeruddin, I. Exnar and M. Grätzel, Chem. Commun. 2972 (2002).

20.   J. Y. Song, Y. Y. Wang and C. C. Wan, Journal of Power Sources **77**, 183 (1999).

21.   W. H. Meyer, Adv. Mater. **10**, 439 (1998).

22.   B. Scrosati and J. Garche, J. Power Sources **195**, 2419 (2010).

23.   J.-M. Tarascon and M. Armand, Nature **414**, 359 (2001).

24.   J. T. Hynes, Annu. Rev. Phys. Chem. **36**, 573 (1985).

25.   G. R. Fleming and P. G. Wolynes, Phys. Today **43**, 36 (1990).

26.   S. Mukamel and Y. J. Yan, Acc. Chem. Res. **22**, 301 (1989).

27.   J. D. Simon, Acc. Chem. Res. **21**, 128 (1988).

28.   P. J. Rossky and J. D. Simon, Nature **370**, 263 (1994).

29.   G. L. Closs and J. R. Miller, Science **240**, 440 (1988).

30.   Y. Wang and K. Eisenthal, J. Chem. Phys. **77**, 6076 (1982).

31.   E. Pines and G. R. Fleming, J. Phys. Chem. **95**, 10448 (1991).

32.   B. Bagchi, Annu. Rev. Phys. Chem. **40**, 115 (1989).

33.   H. A. Kramers, Physica **7**, 284 (1940).

34.   H. Sumi and R. A. Marcus, J. Chem. Phys. **84**, 4894 (1986).

35.   K. A. Dill, Biochemistry **29**, 7133 (1990).

36.   F. Barrière, N. Camire, W. E. Geiger, U. T. Mueller-Westerhoff and R. Sanders, J. Am. Chem. Soc. **124**, 7262 (2002).

37.   B. Bagchi, *Molecular Relaxation in Liquids*. (Oxford University Press, New York, 2012).

38.   C. Reichardt and T. Welton, *Solvents and Solvent Effects in Organic Chemistry*. (John Wiley & Sons, 2011).

39.   E. M. Kosower, J. Am. Chem. Soc. **80**, 3253 (1958).

40.   U. Kaatze and K. Giese, J. Phys. E **13**, 133 (1980).

41.   K. Asami, Prog. Polym. Sci. **27**, 1617 (2002).

42.   D. W. Davidson and R. H. Cole, J. Chem. Phys. **19**, 1484 (1951).

43.   F. Kremer and A. Schönhals, *Broadband Dielectric Measurement Techniques (10^{-6} Hz to 10^{12} Hz)*. (Springer, 2012).

44.   F. Stickel, E. W. Fischer and R. Richert, J. Chem. Phys. **102**, 6251 (1995).

45.   U. Kaatze and Y. Feldman, Meas. Sci. Technol. **17**, R17 (2005).

46.   J. Barthel, K. Bachhuber, R. Buchner and H. Hetzenauer, Chem. Phys. Lett. **165**, 369 (1990).

47.   N. Nandi, K. Bhattacharyya and B. Bagchi, Chem. Rev. **100**, 2013 (2000).

48. Y. Feldman, I. Ermolina and Y. Hayashi, IEEE Trans. Dielectr. Electr. Insul **10**, 728 (2003).

49. R. Bergman and J. Swenson, Nature **403**, 283 (2000).

50. S. Gabriel, R. Lau and C. Gabriel, Phys. Med. Biol. **41**, 2251 (1996).

51. J. Barthel, R. Buchner, P.-N. Eberspächer, M. Münsterer, J. Stauber and B. Wurm, J. Mol. Liq. **78**, 83 (1998).

52. R. Buchner, G. T. Hefter and P. M. May, J. Phys. Chem. A **103**, 1 (1999).

53. R. Buchner and G. Hefter, Phys. Chem. Chem. Phys. **11**, 8984 (2009).

54. J. Barthel, K. Bachhuber, R. Buchner, J. Gill and M. Kleebauer, Chem. Phys. Lett. **167**, 62 (1990).

55. S. Tomić, S. D. Babić, T. Vuletić, S. Krča, D. Ivanković, L. Griparić and R. Podgornik, Phys. Rev. E **75**, 021905 (2007).

56. B. Wurm, C. Baar, R. Buchner and J. Barthel, J. Mol. Liq. **127**, 14 (2006).

57. T. Chen, G. Hefter and R. Buchner, J. Phys. Chem. A **107**, 4025 (2003).

58. R. Buchner, T. Chen and G. Hefter, J. Phys. Chem. B **108**, 2365 (2004).

59. R. Buchner and J. Barthel, Annu. Rep. Prog. Chem. Sect. C **97**, 349 (2001).

60. F. Kremer and A. Schönhals, *Broadband Dielectric Spectroscopy*. (Springer, Berlin, Germany, 2003).

61. T. Shikata and S.-i. Imai, Langmuir **14**, 6804 (1998).

62. F. S. Lima, H. Chaimovich, I. M. Cuccovia and R. Buchner, Langmuir **29**, 10037 (2013).

63. K. Tielrooij, D. Paparo, L. Piatkowski, H. Bakker and M. Bonn, Biophys. J. **97**, 2484 (2009).

64. C. Cametti, S. Marchetti, C. Gambi and G. Onori, J. Phys. Chem. B **115**, 7144 (2011).

65. J. Peyrelasse and C. Boned, J. Phys. Chem. **89**, 370 (1985).

66. C. Baar, R. Buchner and W. Kunz, J. Phys. Chem. B **105**, 2906 (2001).

67. Y. Ono and T. Shikata, J. Am. Chem. Soc. **128**, 10030 (2006).

68. U. Kaatze, J. Mol. Liq. **56**, 95 (1993).

69. A. Kyritsis, P. Pissis and J. Grammatikakis, J. Polym. Sci. Part B Polym. Phys. **33**, 1737 (1995).

70. B. Bagchi, D. W. Oxtoby and G. R. Fleming, Chem. Phys. **86**, 257 (1984).

71. M. Maroncelli, J. MacInnis and G. R. Fleming, Science **243**, 1674 (1989).

72. M. Maroncelli and G. R. Fleming, J. Chem. Phys. **86**, 6221 (1987).

73. B. Bagchi and R. Biswas, Adv. Chem. Phys. **109**, 207 (1999).

74. K. Dahl, R. Biswas, N. Ito and M. Maroncelli, J. Phys. Chem. B **109**, 1563 (2005).

75. J. R. Lakowicz, *Principles of Fluorescence Spectroscopy*. (Springer Science & Business Media, 2013).

76. M. Horng, J. Gardecki, A. Papazyan and M. Maroncelli, J. Phys. Chem. **99**, 17311 (1995).

77. R. Jimenez, G. R. Fleming, P. Kumar and M. Maroncelli, Nature **369**, 471 (1994).

78. K. Bhattacharyya, Acc. Chem. Res. **36**, 95 (2003).

79. W. H. Thompson, Annu. Rev. Phys. Chem. **62**, 599 (2011).

80. M. D. Fayer, Acc. Chem. Res. **45**, 3 (2011).

81. W. P. de Boeij, M. S. Pshenichnikov and D. A. Wiersma, Annu. Rev. Phys. Chem. **49**, 99 (1998).

82. H. Shirota, A. M. Funston, J. F. Wishart and E. W. Castner Jr, J. Chem. Phys. **122**, 184512 (2005).

83. H. K. Kashyap and R. Biswas, J. Phys. Chem. B **114**, 16811 (2010).

84. M. J. Earle and K. R. Seddon, Pure Appl. Chem. **72**, 1391 (2000).

85. Y. Dai, J. van Spronsen, G.-J. Witkamp, R. Verpoorte and Y. H. Choi, Anal. Chim. Acta **766**, 61 (2013).

86. P. G. Jessop, D. J. Heldebrant, X. Li, C. A. Eckert and C. L. Liotta, Nature **436**, 1102 (2005).

87. G. Giraud, C. M. Gordon, I. R. Dunkin and K. Wynne, J. Chem. Phys. **119**, 464 (2003).

88. M. G. Del Pópolo and G. A. Voth, J. Phys. Chem. B **108**, 1744 (2004).

89. J. Hunger, A. Stoppa, S. Schrödle, G. Hefter and R. Buchner, ChemPhysChem. **10**, 723 (2009).

90. A. Samanta, J. Phys. Chem. Lett. **1**, 1557 (2010).

91. A. Stoppa, J. Hunger, R. Buchner, G. Hefter, A. Thoman and H. Helm, J. Phys. Chem. B **112**, 4854 (2008).

92. T. Yan, C. J. Burnham, M. G. Del Pópolo and G. A. Voth, J. Phys. Chem. B **108**, 11877 (2004).

93. J. N. Canongia Lopes and A. A. Pádua, J. Phys. Chem. B **110**, 3330 (2006).

94. S. Arzhantsev, N. Ito, M. Heitz and M. Maroncelli, Chem. Phys. Lett. **381**, 278 (2003).

95. H. K. Kashyap and R. Biswas, J. Phys. Chem. B **114**, 254 (2009).

96. B. Guchhait, H. Al Rasid Gazi, H. K. Kashyap and R. Biswas, J. Phys. Chem. B **114**, 5066 (2010).

97. A. Das, S. Das and R. Biswas, J. Chem. Phys. **142**, 034505 (2015).

98. G. Berchiesi, J. Mol. Liq. **83**, 271 (1999).

99. G. Berchiesi, M. De Angelis, G. Rafaiani and G. Vitali, J. Mol. Liq. **51**, 11 (1992).

100. G. Berchiesi, F. Farhat, M. de Angelis and S. Barocci, J. Mol. Liq. **54**, 103 (1992).

101. G. Berchiesi, G. Rafaiani, G. Vitali and F. Farhat, J. Therm. Anal. Calorim. **44**, 1313 (1995).

102. G. Berchiesi, G. Vitali, P. Passamonti and R. Płowiec, J. Chem. Soc., Faraday Trans. 2 **79**, 1257 (1983).

103. G. Berchiesi, G. Vitali, R. Plowiec and S. Barocci, J. Chem. Soc., Faraday Trans. 2 **85**, 635 (1989).

104. B. Guchhait, S. Das, S. Daschakraborty and R. Biswas, J. Chem. Phys. **140**, 104514 (2014).

105. B. Guchhait, H. A. R. Gazi, H. K. Kashyap and R. Biswas, J. Phys. Chem. B **114**, 5066 (2010).

106. A. Das, S. Das and R. Biswas, Chem. Phys. Lett. **581**, 47 (2013).

107. T. Pal and R. Biswas, Chem. Phys. Lett. **517**, 180 (2011).

108. R. Biswas, A. Das and H. Shirota, J. Chem. Phys. **141**, 134506 (2014).

109. B. Guchhait, S. Daschakraborty and R. Biswas, J. Chem. Phys. **136**, 174503 (2012).

110. S. Das, R. Biswas and B. Mukherjee, J. Phys. Chem. B **119**, 11157 (2015).

111. K. Mukherjee, A. Barman and R. Biswas, J. Mol. Liq. **222**, 495 (2016).

112. H. Shirota and K. Horie, J. Phys. Chem. B **103**, 1437 (1999).

113. H. Shirota, Y. Tamoto and H. Segawa, J. Phys. Chem. A **108**, 3244 (2004).

114. A. Adhikari, S. Dey, U. Mandal, D. K. Das, S. Ghosh and K. Bhattacharyya, J. Phys. Chem. B **112**, 3575 (2008).

115. B. Guchhait, R. Biswas and P. K. Ghorai, J. Phys. Chem. B **117**, 3345 (2013).

116. F. Croce, G. Appetecchi, L. Persi and B. Scrosati, Nature **394**, 456 (1998).

117. K. Xu, Chem. Rev. **104**, 4303 (2004).

118. K. Mukherjee, A. Das, S. Choudhury, A. Barman and R. Biswas, J. Phys. Chem. B **119**, 8063 (2015).

119. A. Das, R. Biswas and J. Chakrabarti, J. Phys. Chem. A **115**, 973 (2011).

120. A. Das, R. Biswas and J. Chakrabarti, Chem. Phys. Lett. **558**, 36 (2013).

121. K. Mukherjee, A. Barman and R. Biswas (under preperation).

122. S. Taniewska-Osińska, R. Łogwinienko and J. Mokrzan, Thermochimi. Acta **167**, 73 (1990).

123. K. Mukherjee, A. Barman and R. Biswas (under preperation).

124. K. Mukherjee, A. Barman and R. Biswas (under preperation).

125. A. Das and R. Biswas, J. Phys. Chem. B **119**, 10102 (2015).

126. K. Mukherjee, A. Barman and R. Biswas (under preperation).

127. K. Mukherjee, K. Khumbhakar, E. Tarif and R. Biswas (under preperation).

Chapter 2

Experimental Techniques and Data Analysis Methods

The main experimental techniques used to investigate different complex chemical systems discussed in this Thesis are Dielectric Relaxation spectroscopy, Steady State Absorption and Emission spectroscopy and Time Resolved Fluorescence Spectroscopy. This chapter includes a brief description of frequency domain dielectric measurements, steady state absorption spectroscopy and fluorescence measurements (both time dependent and steady state).

2.1 Dielectric Relaxation Spectroscopy

2.1.1 Introduction

The movements of the microscopic particles, like molecules, atoms, ions, demands specific times to reach a definite value of the polarization. Generally at room temperature the required time is 1000 ns or less. Now if an external electric field is applied whose field strength is changing within the previously mentioned time period, the microscopic particles will not be able to generate the equilibrium polarization and as a result the equilibrium polarization value will lag behind the alternating electric field. On the other hand, if the field varies slowly as compared to the motions of the microscopic particles then there will be enough time to produce an equilibrium polarization and this is called the quasi-static case.

The interaction of electromagnetic field with matter is described by Maxwell's equations[1]

$$\text{rot}\, E = -\frac{\partial}{\partial t} B \tag{2.1}$$

$$\text{rot}\, H = j + \frac{\partial}{\partial t} D \tag{2.2}$$

$$\text{div}\, D = \rho_e \tag{2.3}$$

and

$$\operatorname{div} B = 0. \tag{2.4}$$

In this set of equations E and H describe the electric and magnetic field, D the dielectric displacement, B the magnetic induction, j the current density and ρ_e the density of charges. For homogenous, non-dispersive, isotropic materials and low electric field strengths, D can be expressed by

$$D = \varepsilon^* \varepsilon_0 E, \tag{2.5}$$

where ε_0 is the dielectric permittivity of vacuum and ε^* is the complex dielectric function. According to Maxwell's equation the ε^* is time (or frequency) dependent if time dependent processes happens within the sample. For a periodic electric field, $E(t) = E_0 \exp(-i\omega t)$ where ω is the radial frequency and $i = \sqrt{-1}$, the ε^* is defined by

$$\varepsilon^*(\omega) = \varepsilon'(\omega) - i\varepsilon''(\omega), \tag{2.6}$$

where $\varepsilon'(\omega)$ and $\varepsilon''(\omega)$ are the real and imaginary part of the complex dielectric function, respectively.

2.1.2 Measurement of Dielectric Properties

2.1.2.1 Equipment

In this technique the properties of the sample cell are measured in terms of scattering parameters or "S-parameters"[2-3] of radio frequency (RF) components. S-parameters have both a magnitude and a phase component. Usually network analyzer is concerned with the accurate measurement of the ratios of the reflected signal to the incident signal, and the transmitted signal to the incident signal. During experiments the network analyzer needs a test signal, and generally a signal generator or signal source provides this. In network analyzers, we have a built-in signal generator. RF transmission lines can be prepared in a variety of transmission media such as coaxial, waveguide, twisted pair, coplanar, microstrip, stripline. The characteristic impedance (Z_0), which describes the relationship between the voltage and current travelling waves, varies

from $50\,\Omega$ to $75\,\Omega$ for different systems. It is noteworthy that the S-parameters are complex number matrices in frequency domain and for reflection mode it is generally represented as $S_{11}^{*}(\omega)$. In the case of single reflection the simple formula, $S_{11}^{*}(\omega) = \rho^{*}(\omega)$, connects reflection coefficient ($\rho^{*}(\omega)$) with the impedance of the sample

$$\rho^{*}(\omega) = \frac{Z^{*}(\omega) - Z_0}{Z^{*}(\omega) + Z_0},\tag{2.7}$$

where Z_0 is the characteristic impedance of the transmission line.

Dielectric relaxation measurements in the frequency range $0.2 \leq \nu / GHz \leq 50$ for all the complex chemical systems reported in this thesis have been carried out with a PNA-L network analyzer (N5230C) combined with a probe kit (85070E). Air, shorting block, and water were employed as open, short, and load, respectively. Fig. 2.1 represents a schematic diagram of DR measurement configuration.
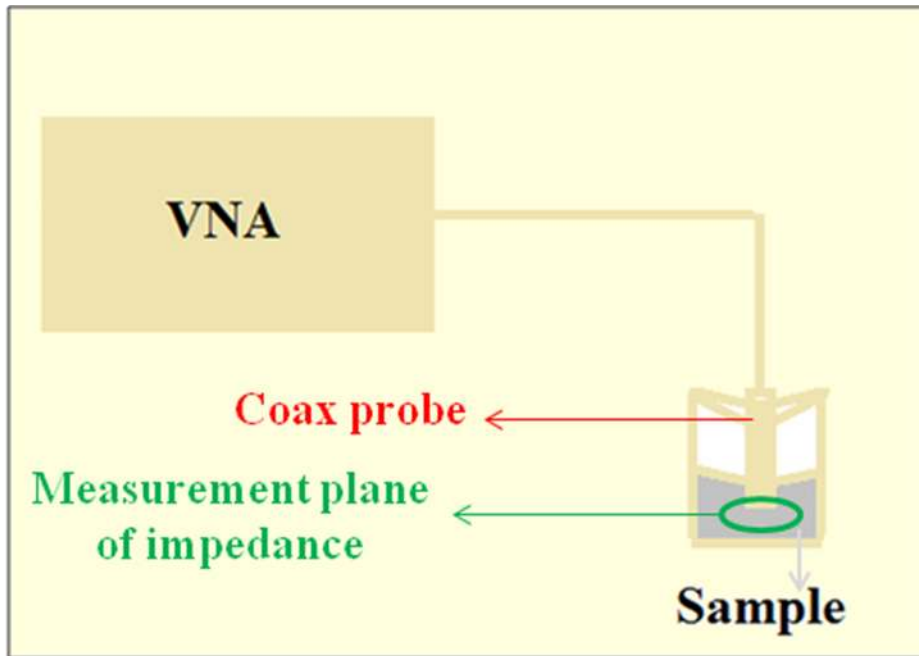
Fig. 2.1 The schematic representation of DR measurement configuration.

2.1.2.2 Mathematical Models and Data Analysis

In order to understand the characteristics of the orientational polarization, a number of mathematical model functions can be used to describe the collected DR data adequately.

2.1.2.2.1 Debye Model

The most simple ansatz to explain the complex dielectric response is given by[4-5]

$$\varepsilon^* = \varepsilon_\infty + \frac{\Delta\varepsilon}{1 + i\omega\tau_D},$$

$$(2.8)$$

where τ_D is the characteristic relaxation time, $\Delta\varepsilon = \varepsilon_0 - \varepsilon_\infty$ is the dielectric strength ($\varepsilon_0 = \varepsilon'(\omega \to 0)$ and $\varepsilon_\infty = \varepsilon'(\omega \to \infty)$)) and ω is the angular frequency. ω is related to linear frequency by $\omega = 2\pi\nu$, where ν is linear frequency.

2.1.2.2.2 Non-Debye Models

A broadening of the dielectric function can be modeled by the Cole-Cole function[6] given as

$$\varepsilon^* = \varepsilon_\infty + \frac{\Delta\varepsilon}{1 + (i\omega\tau_{CC})^{1-\alpha}},$$

$$(2.9)$$

where α is the parameter which leads to the symmetrical broadening of the relaxation function and can have any values in between, $0 \le \alpha < 1$. τ_{CC} is the corresponding relaxation time.

Moreover, for asymmetric broadening the proposed model function is

$$\varepsilon^* = \varepsilon_\infty + \frac{\Delta\varepsilon}{(1 + i\omega\tau_{CD})^\beta}.$$

$$(2.10)$$

It is called the Cole-Davidson model.[7-8] Here β is the asymmetry parameter and can have values within, $0 < \beta \le 1$ and τ_{CD} is the corresponding relaxation time.

A more general model function is Havriliak-Negami (HN) function[9] which reads

$$\varepsilon^* = \varepsilon_\infty + \frac{\Delta\varepsilon}{(1 + (i\omega\tau_{HN})^{1-\alpha})^\beta}, \tag{2.11}$$

where τ_{HN} is the corresponding relaxation time, $\alpha\,(0 \le \alpha < 1)$ and $\beta\,(0 < \beta \le 1)$ are the symmetry and asymmetry parameters, respectively.

2.1.2.2.3 Combination of Models

In real systems, the DR spectrum may be the result of a superposition of distinct relaxation modes. So the general HN function can be written as

$$\varepsilon^* = \varepsilon_\infty + \sum_j \frac{\Delta\varepsilon_j}{(1 + (i\omega\tau_j)^{1-\alpha_j})^{\beta_j}}, \tag{2.12}$$

2.1.2.2.4 Data Processing

To extract physical information from complex permittivity spectra, an appropriate mathematical description of the measured complex permittivity data has to be found. Quality of fits was determined by checking both the 'goodness-of-fit' parameter (χ^2) and residual where χ^2 was defined as follows:[10]

$$\chi^2 = \frac{1}{2m - \ell} \sum_{i=1}^{m} \left[\left(\frac{\delta\varepsilon_i'}{\sigma(\varepsilon_i')} \right)^2 + \left(\frac{\delta\varepsilon_i''}{\sigma(\varepsilon_i'')} \right)^2 \right], \tag{2.13}$$

where m denotes the number of data triples ($\nu, \varepsilon', \varepsilon''$), ℓ the number of adjustable parameters, $\delta\varepsilon_i$ and $\sigma(\varepsilon_i)$ the residuals and standard deviations of the individual data points, respectively.

2.1.2.2.5 Conductivity Corrections

The dielectric spectroscopy study of conducting samples is very complicated due to the contribution of the dc conductivity in the imaginary part of the complex dielectric response. For conductive medium the complex dielectric response is written as follows:[11-12]

$$\varepsilon^*(\nu) = \varepsilon'(\nu) - \left[i\varepsilon''(\nu) + \frac{i\kappa}{2\pi\varepsilon_p \nu} \right],$$ (2.14)

where $\nu (\nu = \omega / 2\pi)$ is the linear frequency, κ denotes the dc conductivity of the medium and ε_p is the permittivity of free space. For all the measurements, included in this thesis, carried out in conducting solutions, the contribution of the dc conductivity was eliminated.

Thus the recorded DR data, depending upon the characteristics of the medium that is conducting or non conducting, were subjected for fitting to the general HN (Eq. 2.12, mentioned above) and the fit parameters were enlisted for further understanding.

2.2 Steady State Absorption

All the steady state absorption data recorded in this thesis have been collected using UV-2600 (SHIMADZU). Fig. 2.2 displays the schematic representation of absorption spectrophotometer. Tungsten lamp and Deuterium lamp have been used as the light source and they covers both the visible and the ultra-violet regions. The illuminated light focused by a mirror passes through a filter and reaches to the monochromator which contains diffraction grating to select the specific wavelength from the source light. The monochromatic light is split into two beams before it reaches to the sample. One of the two beams goes to the sample while the other beam is used for the reference sample. The transmitted lights from the sample and the reference go to the photodiode detector. Then the signal is enhanced and processed by the analog to digital conversion to get the final absorption spectrum. According to the Lambert-Beer law, absorbance (A) depends on the path length of the sample, l, concentration of the sample, c, and the molar extinction coefficient of the sample, ε, and given by

$$A = \log(I_0 / I) = \varepsilon c l, \qquad\qquad (2.15)$$

where I_0 is intensity of the incident light and I is the intensity of the transmitted light. Our all optical measurements have been carried out keeping $l = 1$cm and c $\sim 10^{-5}$ M.
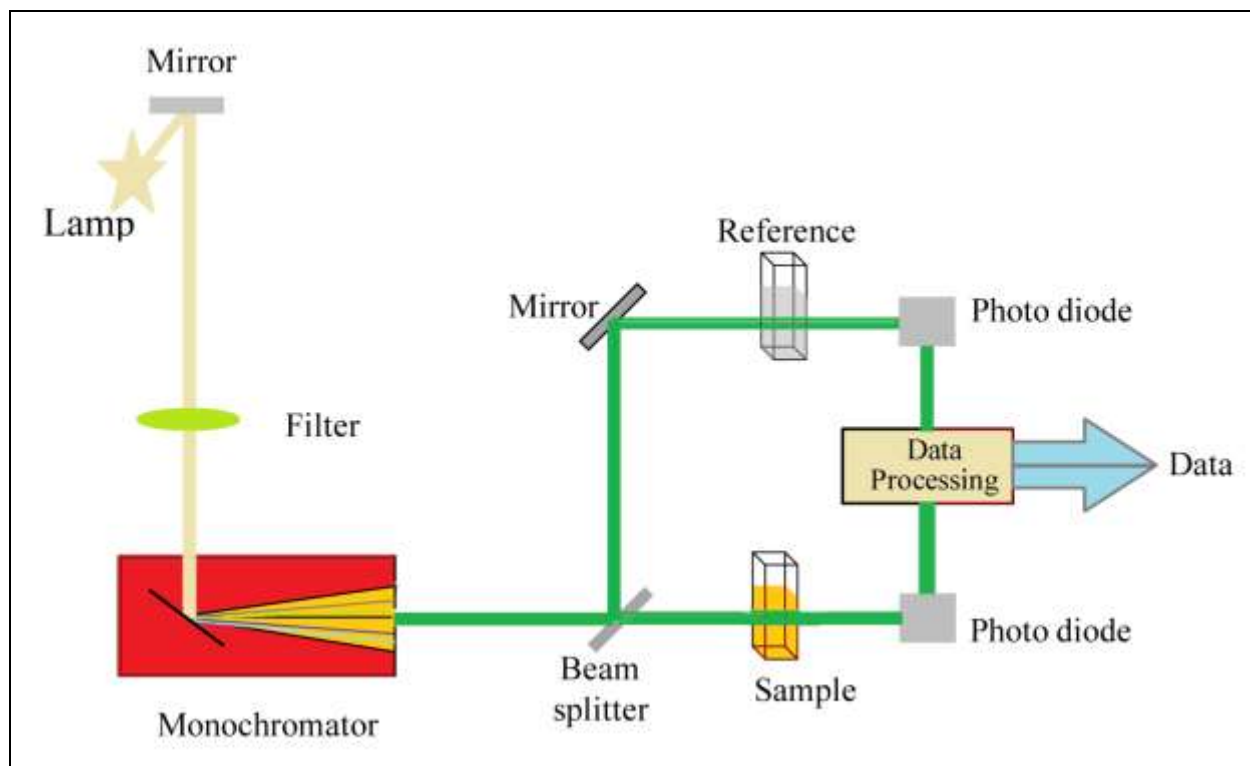
Fig. 2.2 Schematic diagram of an absorption spectrophotometer.

2.3 Steady State Fluorescence

In steady state fluorescence measurements, the sample is illuminated with a continuous light source (generally Xenon lamp) and the emission spectrum is recorded by collecting the emitting light in the perpendicular direction of the excitation light. Fig. 2.3 represents the schematic diagram of steady state fluorescence spectrophotometer. We have used a fluorimeter (Fluorolog, Jobin-Yvon, Horiba) for all the steady state emission measurements reported here.
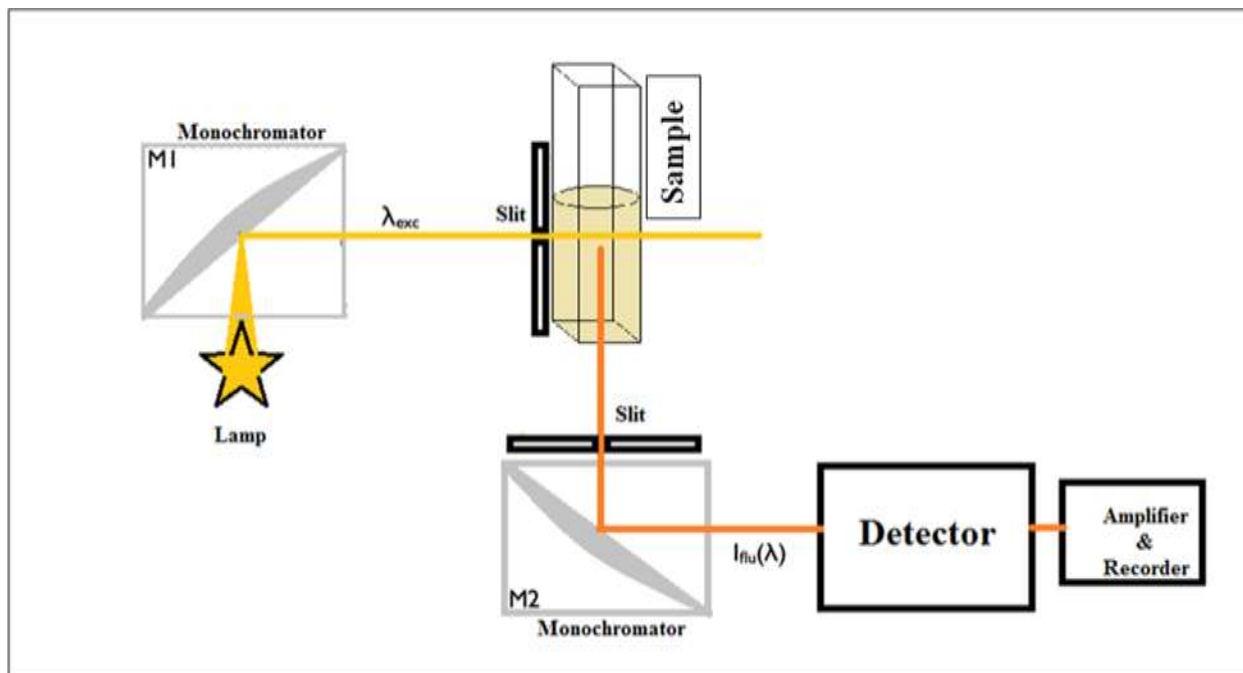
Fig. 2.3 Schematic diagram of a fluorescence spectrophotometer.

2.4 Time-resolved Fluorescence Measurements

Time-resolved fluorescence measurements have been carried out using time-correlated single photon counting (TCSPC) technique, where each photon emitted by the fluorophore is detected after the excitation with a short pulse laser light.[13-14]

2.4.1 TCSPC Technique

The principle of TCSPC relies on the concept that the probability distribution for emission of a single photon from a single fluorophore molecule following its excitation is identical to the time-dependent fluorescence intensity change of all photons emitted by the fluorophore after excitation. Fig. 2.4 represents the schematic block diagram of a typical TCSPC set-up. All the TRF measurements (included in this thesis) have been performed using a TCSPC system from

Edinburg (U.K.). At first, an excitation pulse excites the fluorophore kept in the sample cuvette to begin the experiment and simultaneously, it creates a start signal. The start signal is then passed through a constant fraction discriminator (CFD) to register the arrival time of a laser pulse and subsequently, the signal is passed to time-to-amplitude converter (TAC) to trigger the voltage ramp. Now in this voltage ramp voltage increases linearly with time and the voltage ramp gets stopped when the first photon emitted by the sample fluorophore is detected. An output pulse from the TAC is proportional to the time delay (Δt) between the start signal and stop signal. The output pulse is then sent to a multichannel analyzer (MCA) to generate the numerical value. A histogram of the decay containing photon count against time channel is generated in MCA by the repetition of the same process numerous times with the same pulse laser source.[15]
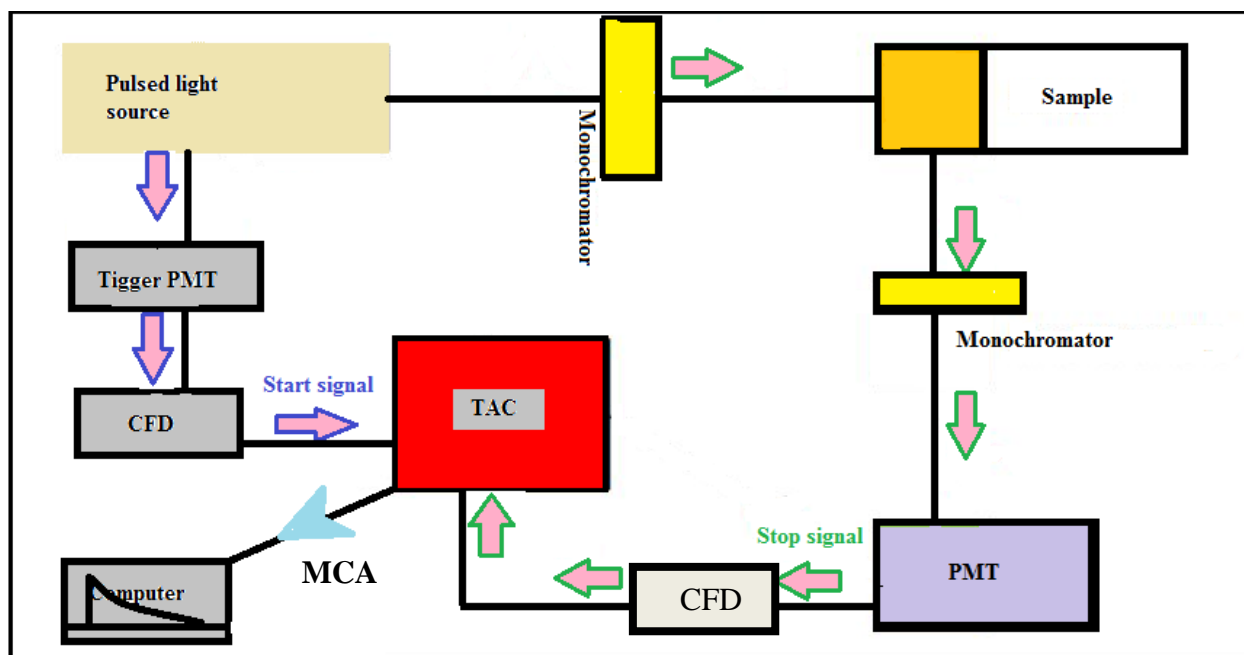
Fig. 2.4 Schematic representation of TCSPC set-up.

2.4.2 Data Analysis

2.4.2.1 Solvation Dynamics

To start the analysis, steady state absorption and emission spectra were collected and processed by solvent blank subtraction. Subsequently, a series of 14-16 magic angle decays were collected at equally spaced wavelengths across the steady state emission spectrum of the fluorophore dissolved in the liquid medium in the TCSPC set-up.

In our measurements, we used 409 nm and 445 nm diode lasers and the full width at half maxima (FWHM) of the instrument response function (IRF) was ~70-90 ps. Those samples for which the only decay in blue end and a rise followed by decay in red end, which is the signature of Stokes shift dynamics, was found, were subjected for solvation dynamics study. The recorded fluorescence decay ($N(t)$) is a convolution of IRF ($R(t)$) and sample response ($I(t)$). In order to extract $I(t)$ from the measured $N(t)$ and $R(t)$ data the iterative reconvolution method[16] using a nonlinear least square analysis was used. A sum of exponentials, $I(t) = \sum_{i=1}^{N} \alpha_i \exp(-t/\tau_i)$ (where α_i and τ_i are the pre-exponential factors and characteristic life times, respectively), was used to fit the acquired TCSPC data. To construct the time-resolved emission spectra (TRES) we followed the method mentioned in the literatures.[15,17-19] The fluorescence decays collected at different wavelengths were fitted with the following multi-exponential function

$$I(\lambda_j, t) = \sum_{i=1}^{N} \alpha_i(\lambda_j) \exp(-t/\tau_i(\lambda_j)), \qquad (2.16)$$

where $\alpha_i(\lambda_j)$ represents the pre-exponential factor and $\sum_i \alpha_i(\lambda_j) = 1$.

A new set of normalized intensity decays were generated so that the time integrated intensity at each wavelength was equal to the steady state intensity at that wavelength ($F(\lambda_j)$). The normalized factor is

$$H(\lambda_j) = \frac{F(\lambda_j)}{\int\limits_0^\infty I(\lambda_j, t) dt} = \frac{F(\lambda_j)}{\sum\limits_i \alpha_i(\lambda_j) \tau_i(\lambda_j)}. \tag{2.17}$$

The appropriate normalized intensity decay function was then obtained by,

$$I'(\lambda_j, t) = H(\lambda_j) I(\lambda_j, t) = \sum \alpha_i'(\lambda_j) \exp(-t/\tau_i(\lambda_j)), \tag{2.18}$$

where $\alpha_i'(\lambda_j) = H(\lambda_j)\alpha_i(\lambda_j)$. The values of $I'(\lambda_j, t)$ were used to calculate the intensity at any wavelength and time, and subsequently the TRES. The TRES were then converted to frequency domain for further analysis.[17] Then each time-resolved emission spectrum was fitted with a log-normal line shape function for continuous representation of the spectrum and subsequently, peak frequencies of these spectra were extracted and used for the construction solvation response function

$$S(t) = \frac{(\nu(t) - \nu(\infty))}{(\nu(0) - \nu(\infty))}, \tag{2.19}$$

where $\nu(0)$, $\nu(t)$ and $\nu(\infty)$ indicate some measure (usually peak) of frequency for the reconstructed emission spectrum at $t = 0$ (i.e. immediately after excitation), at any time t and a time sufficiently long ($t = \infty$), respectively. $S(t)$, which is a normalized function by construction, provides the information about the solvent reorganization with time in response to the sudden alteration of the equilibrium charge distribution of the fluorophore molecule on excitation. In few systems where the steady state emission does not take place from the fully relaxed state the steady state emission peak frequency becomes larger than the time-resolved emission peak frequency after sufficiently long time ($t = \infty$). Average solvation time was obtained via analytical integration of the multi-exponential fit to the previously constructed $S(t)$ decays as follows:

$$\langle \tau_S \rangle = \int\limits_0^\infty dt S(t) = \int\limits_0^\infty dt \left[\sum_i a_i \exp(-t/\tau_i) \right] = \sum_i a_i \tau_i, \tag{2.20}$$

25

where $\sum_i a_i = 1$, and a_i and τ_i denote the amplitude and time constants associated with the i-th component of $S(t)$ decay.

2.4.2.2 Rotational Dynamics

We can also use TCSPC to study the reorientational dynamics of a fluorophore molecule dissolved in a liquid medium.[15,18] This measurement is based on the principle of photoselective excitation of those fluorophore molecules whose absorption transition dipoles are parallel to the electrical vector of polarized excitation light. The fluorescence intensity decays at the parallel and perpendicular emission polarizations depend on the reorientation of the excited fluorophore. In order to understand the reorientational dynamics of a probe molecule the life time of the probe molecule has to be larger (or comparable) than the rotational diffusion timescale of the probe molecule. Time dependent fluorescence anisotropy ($r(t)$) is defined as

$$r(t) = \frac{I_{para}(t) - I_{perp}(t)}{I_{para}(t) + 2I_{perp}(t)}, \tag{2.21}$$

where $I_{para}(t)$ and $I_{perp}(t)$ denotes the vertically and horizontally polarized fluorescence decays, respectively. Note that all the emission decays are collected at the peak wavelength of the steady state emission spectrum. The polarization characteristics of the optical set-up have important consequences to the measured anisotropy. To minimize the error originating from the instrumental preference for a specific polarization, correction is required. This correction factor is usually termed as G-factor and is defined as the ratio between the transmission efficiency for vertically polarized light and that of horizontally polarized light ($G = \dfrac{I_{para}(t)}{I_{perp}(t)}$). Now the corrected $r(t)$ is represented as

$$r(t) = \frac{I_{para}(t) - GI_{perp}(t)}{I_{para}(t) + 2GI_{perp}(t)}. \tag{2.22}$$

In our analysis, the duly constructed $r(t)$ decays were fitted to multi-exponential functions as follows:

$$r(t) = r(0) \sum_i \alpha_i \exp(-t/\tau_i) \qquad (2.23)$$

where τ_i and α_i represent the time and amplitude of the i-th decay component and $\sum_i \alpha_i = 1$. In this thesis, we fixed the $r(0)$ value at 0.376 for all the measurements where C153 is the probe. The average rotational time was then estimated as follows:

$$\langle \tau_r \rangle = \int_0^\infty dt[r(t)/r(0)] = \sum_i \alpha_i \tau_i \qquad (2.24)$$

27

References

1. J. C. Maxwell, *A Treatise on Electricity and Magnetism.* (Clarendon press, 1881).

2. R. E. Collin, *Foundations for Microwave Engineering.* (John Wiley & Sons, 2007).

3. R. Clarke, A. Gregory, D. Cannell, M. Patrick, S. Wylie, I. Youngs and G. Hill, Institute of Measurement and Control, Teddington (2003).

4. P. J. W. Debye, *Polar Molecules*. (Chemical Catalog Company, Incorporated, 1929).

5. H. Pellat, presented at the Ann. Chim. Phys., 1899 (unpublished).

6. K. S. Cole and R. H. Cole, J. Chem. Phys. **9**, 341 (1941).

7. D. Davidson and R. Cole, J. Chem. Phys. **18**, 1417 (1950).

8. D. W. Davidson and R. H. Cole, J. Chem. Phys. **19**, 1484 (1951).

9. S. Havriliak and S. Negami, Polymer **8**, 161 (1967).

10. P. R. Bevington and D. K. Robinson, *Data Reduction and Error Analysis*. (McGraw–Hill, New York, New York, 2003).

11. C. J. F. Böttcher and P. Bordewijk, *Theory of Electric Polarization*. (Elsevier: Amsterdam, The Netherlands, 1978).

12. R. Buchner and J. Barthel, Annu. Rep. Prog. Chem. Sect. C: Phys. Chem. **91**, 71 (1994).

13. D. O'Connor and D. Phillips, *Time-correlated Single Photon Counting*. (Academic Press, London, 1984).

14. M. Chang, S. Courtney, A. Cross, R. Gulotty, J. Pertrich and G. R. Fleming, Analytical Instrumentation **14**, 433 (1985).

15. J. R. Lakowicz, *Principles of Fluorescence Spectroscopy*. (Springer Science & Business Media, 2013).

16. D. Birch and R. Imhof, *Topics in Fluorescence Spectroscopy, Vol. 1. Techniques*. (Plenum Press, New York, 1991).

17. M. Horng, J. Gardecki, A. Papazyan and M. Maroncelli, J. Phys. Chem. **99**, 17311 (1995).

18. M.-L. Horng, J. Gardecki and M. Maroncelli, J. Phys. Chem. A **101**, 1030 (1997).

19. K. Dahl, R. Biswas, N. Ito and M. Maroncelli, J. Phys. Chem. B **109**, 1563 (2005).

Chapter 3

Dielectric Relaxations of (Acetamide + Electrolyte) Deep Eutectic Solvents in the Frequency Window, $0.2 \leq \nu/\mathrm{GHz} \leq 50$: Anion and Cation Dependence

3.1 Introduction

Deep eutectic solvents (DESs), solvents that are multi-component melts at a temperature much lower than the individual melting points of the mixture components, are increasingly finding technological as well as industrial applications.[1-5] Many of these solvents are often biodegradable and thus offer a much cleaner alternative to the conventional organic solvents. In addition, the process of obtaining DESs through simple mixing of components followed by gentle heating offer enormous flexibility for engineering a medium suitable to a particular chemical reaction. This, and the cost-effectiveness in producing and handling the DESs provide the necessary economic viability for applications in electrodeposition, biocatalysis, cosmetic and pharmaceutical industries, biomass treatment and preparation of functional materials.[1-8] Being nonaqueous, DESs also offer a broad operational window for carrying out moisture sensitive reactions and promote green chemistry via minimizing the ecological foot print.

Solvent designing for tailoring a reaction demands a thorough understanding of medium structure and dynamics because of the proven interrelationship between reaction rate and medium effects.[9-13] Although several earlier studies[14-20] have suggested micro-heterogeneous solution structure for several DESs made of amide and electrolyte, sophisticated techniques such as neutron and X-ray scattering have not been employed yet to reveal the extent of spatial correlations present in such systems. A few recent fluorescence spectroscopic measurements combined with computer simulations have provided indirect evidences of spatial heterogeneity in several ($acetamide + electrolyte$) DESs.[21-23] However, study of dynamic (temporal)

heterogeneity via direct measurements of ultrafast solution dynamics for these systems has not been performed so far, although fast fluorescence spectroscopic measurements have revealed significant decoupling between relaxation rates and medium viscosity.[24-26] In addition, study of collective low frequency dynamics of such systems has just begun[27] with an aim to decipher the coupling between collective low frequency dynamics and solution heterogeneity.[28-32] Dielectric relaxation spectroscopy (DRS) is an important experimental technique which can probe both the inherent medium dynamics and its connection to solution structure,[33-39] and complement information accessed via time-dependent fluorescence Stokes shift (TDFSS) measurements.[40-44] This motivates the current DRS measurements with the focus being placed on relaxation in the gigahertz (GHz) region where interconnection between the fast solution dynamics observed via DRS and TDFSS techniques is the most prominent.

We note, however, here that the present measurements are not the first DRS measurements for these systems as dielectric relaxations of a few ($acetamide + electrolyte$) DESs within the frequency window, $10^{-7} \leq \nu/\text{MHz} \leq 10^{2}$, have already been reported.[19,20] These relatively low frequency measurements have suggested inhomogeneous relaxation kinetics and colossal static dielectric constant (ε_0). Temperature dependent relaxation times detected in these measurements have been found to spread over half-of-a-second to a couple of nanoseconds, suggesting extremely slow relaxation originating from movements of nano-sized domains formed via the interaction between amide molecules and electrolytes.[19,20] Our frequency coverage ($0.2 \leq \nu/\text{GHz} \leq 50$) cannot probe these slow dynamics of aggregated structures and hence we would refrain from drawing any conclusion on relaxation dynamics possessing time scales longer than approximately a nanosecond. Since faster relaxation time scales are more relevant for simple chemical reactions (for example, cis-trans isomerization) as relevant reactive modes are coupled to fast density fluctuations on a barrier top,[45-47] DRS measurements with frequency coverage, $0.2 \leq \nu/\text{GHz} \leq 50$, bridge an important information gap for dipolar density fluctuations possessing time scales between nanosecond and sub-hundred picoseconds. In addition, we report here the DR relaxation of neat molten acetamide and compare the data with those for several ($acetamide + electrolyte$) DESs to uncover differences in interaction between

ions and acetamide (CH_3CONH_2) molecules in these multi-component melts. Such a study has not been done before and constitutes the main theme of the present paper.

Electrolytes used here readily form DESs with acetamide approximately at the same mole ratio (*acetamide:electrolyte*::80:20) and remain as a stable liquid at ~293 K after melting at a relatively higher temperature and subsequent cooling.[21-27] Six DESs with the following compositions were considered: (i) *0.78CH$_3$CONH$_2$ + 0.22LiBr*, (ii) *0.78CH$_3$CONH$_2$ + 0.22LiNO$_3$*, (iii) *0.75CH$_3$CONH$_2$ + 0.25NaSCN*, (iv) *0.75CH$_3$CONH$_2$ + 0.25KSCN*, (v) *0.81CH$_3$CONH$_2$ + 0.19LiClO$_4$*, and (vi) *0.81CH$_3$CONH$_2$ + 0.19NaClO$_4$*. Except for the $NaClO_4$ containing DES, details regarding sample preparation for other DESs could be found elsewhere as these systems have already been studied via fluorescence[21,22,24-26] and femtosecond Raman-induced Kerr effect spectroscopic (fs-RIKES)[27] techniques. [*0.81CH$_3$CONH$_2$ + 0.19NaClO$_4$*] DES was obtained by following the method employed for [*0.81CH$_3$CONH$_2$ + 0.19LiClO$_4$*] system. Measured glass transition temperatures (T_g's) of these DESs are in ~190-200 K range[21] and, therefore, our measurement temperature is ~100 K above the respective T_g's but much lower than the melting temperatures of the individual components. Note here that the current measurements and subsequent comparisons have been made among multi-component melt systems where compositions slightly vary. This slight mismatch is deliberately allowed to ensure a qualitative comparison of the measured DR time scales with those observed earlier in either time-resolved fluorescence[21,24,25] or fs-RIKES[27] measurements. This assumes importance given that the frequency window employed here is not sufficiently wide for detecting the full DR dynamics, and subsequently relaxation parameters have been obtained via fits to model functions. In addition, these compositions correspond to approximately 25-30 electrolyte molecules per 100 acetamide molecules, and as a result, drastic variation in relaxation dynamics due to a small variation in electrolyte concentration is not expected.

3.2 Experimental Details

3.2.1 Materials and Methods

Acetamide (≥98%, Merck, India), sodium thiocyanate (≥99%, Sigma Aldrich), potassium thiocyanate (≥99%, Sigma Aldrich), lithium nitrate (≥99%, SRL, India), lithium bromide (≥99%,

Sigma Aldrich), lithium perchlorate (≥99%, Fluka) and sodium perchlorate (≥98%, Alfa aesar), were vacuum-dried (~300 K) overnight before use. Briefly, ~10g of sample were prepared for each composition by quickly transferring the required amounts of each of these compounds in 20mL sample vial at room temperature. Sample preparations and measurements were carried out in a tightly humidity-controlled (humidity level maintained to 37%) laboratory environment. Subsequently, the sample vials were sealed and heated slowly to ~350 K until it formed a uniform melt. Each of these molten samples were then allowed for sufficient time to attain the room temperature $(293 \pm 0.5$ K) before any measurements. Refractive indices (n_D) were measured by using aliquots of these samples employing an automated temperature-controlled refractometer (RUDOLPH, J357). DR measurements for neat molten acetamide was carried out after carefully melting solid acetamide employing a heating plate (MS-H-Pro from SCILOGEX, USA) and maintaining the temperature at T $=354 \pm 0.5$ K.

3.2.2 DR Measurement Details

The DR data acquisition technique and the corresponding analysis procedures are essentially the same as described in chapter 2 and in refs.[48-50] Approximately 8mL of the thermally equilibrated molten sample (DESs and neat acetamide) and properly humidity-controlled environment were used for measurements in each case. We took 501 data points for each DR measurements.

3.3 Results and Discussion

3.3.1 DR of Molten Neat Acetamide

Before we investigate the ion dependence of DR in ionic DESs considered here, let us first present the results for molten neat acetamide. Fig. 3.1 displays the real (ε') and imaginary (ε'') components of the complex dielectric spectra for acetamide measured at ~354 K along with the 2-D fits. Fits considering models other than 2-D relaxation (for example, Cole-Davidson) produced worse description of the measured spectra. Note the plateau in $\varepsilon'(\nu)$ at the low frequency (ν) limit which is typical for non-conducting dipolar medium.[51] In addition, $\varepsilon''(\nu)$ shows a peak at $\nu_{peak} \approx 3$ GHz. Fit parameters summarized inside the figure indicate ~97% of the total detected relaxation is carried out by the slower (τ_1=55 ps) of the these two time scales. This

matches with the characteristic relaxation time constant, $\tau_{peak} = 1/2\pi\nu_{peak} \approx 53\,ps$. Interestingly, Stokes-Einstein-Debye (SED) equation,[52-56] $\tau_r = 3V_{eff}\eta/k_BT$, predicts a value of ~60 ps at ~354 K for single particle rotation time for acetamide if a molecular diameter (σ) of 4.5Å and viscosity (η) of 2 cP[24] are used. V_{eff}, effective volume, in such a calculation is taken as molecular volume, $V_m = 2\pi\sigma^3/3$. The relationship between the single particle and the collective rotation times is, $\tau_r = \dfrac{\ell(\ell+1)}{2}\times\tau$, τ denoting a time constant associated with collective orientational relaxation of rank ℓ. For DR, $\ell=1$, and therefore, $\tau_r = \tau$.
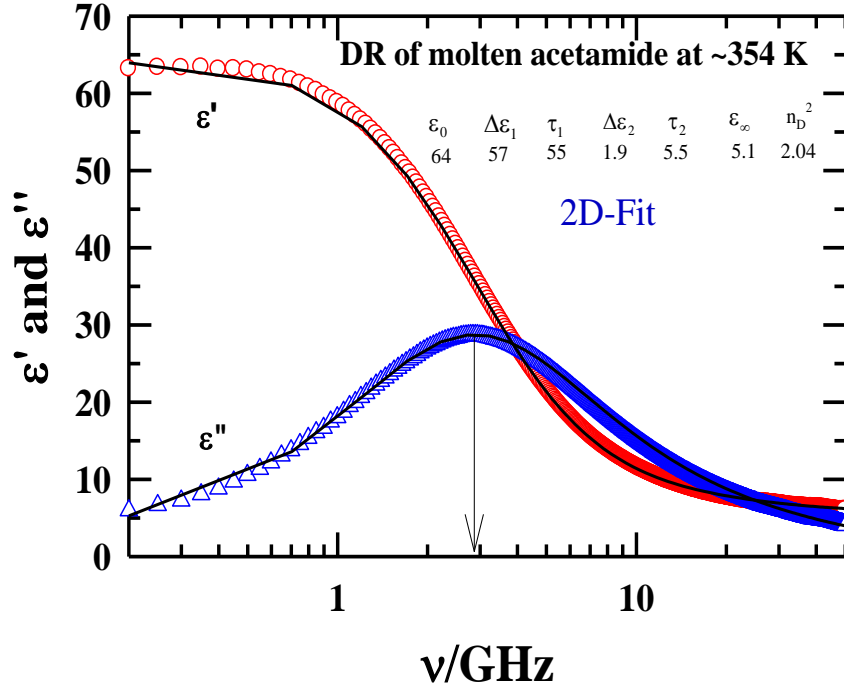
Fig. 3.1: Dielectric relaxation of molten neat acetamide at ~354 K. Measured real (ε') and imaginary (ε'') components of the complex DR spectrum are shown by circles and triangles, respectively. Solid lines through these data represent simultaneous fits using 2-Debye relaxation model. Fit parameters are: $\varepsilon_0 = 64$, $\Delta\varepsilon_1 = 57$, $\tau_1 = 55$ ps, $\Delta\varepsilon_2 = 1.9$, $\tau_2 = 5.5$ ps, $\varepsilon_\infty = 5.1$. The refractive index (n_D) of molten acetamide has been reported[62] to be 1.4274 and thus $n_D^2 \approx 2.04$. Therefore, $\varepsilon_\infty - n_D^2 = 3.06$, which has remained undetected in the present measurements. The arrow indicates the characteristic relaxation frequency corresponding to τ_1.

33

This identity then suggests that the measured slowest DR time ($\tau_1 = 55$ ps) originates from, as in N,N-dimethylacetamide (DMA),[50] the isotropic rotational diffusion of acetamide molecule. This similarity between τ_1 and τ_r is somewhat perplexing given that molten acetamide is a H-bonded (two H-bonds per acetamide molecule on an average[57]) liquid. Interestingly, all-atom simulation study of H-bond structural relaxation, $C_{HB}(t)$, of molten acetamide at 368 K reports a relaxation component possessing a time scale of ~54 ps.[58] Therefore, the close proximity between τ_1 and τ_r may be fortuitous, and the slowest relaxation in molten acetamide can be dictated by, as in other H-bonded amides,[50] the waiting time for finding another H-bonding partner arriving at a suitable location with preferred orientation after breaking an already existing H-bond.

Next we comment on the possible origin of ~5 ps time scale (τ_2) for molten acetamide which contributes ~3% to the total detected relaxation. Such a small amplitude, however, does not, suggest this fast component is unrealistic for the following reasons. First, this time scale is similar to the sub-10 ps time scale observed in the simulations of orientational relaxation for N-H bond vector and acetamide backbone in molten neat acetamide.[58] It is therefore possible that this ~5 ps DR component originates from the reorientation of acetamide backbone or N-H bond vector. A hint to the involvement of H-bond breaking and reformation with this bond vector reorientation emerges from the simulated $C_{HB}(t)$, which possesses a significant component (~55%) that decays with a time constant of ~8 ps.[58] Note here that fs-RIKES measurements of ionic acetamide deep eutectics considered here have detected a relaxation component with time scale in ~1-3 ps range.[27] In addition, previous DR studies of water and monohydroxy alcohols have detected ~1-3 ps time scale and interpreted in terms of flipping motion of –OH groups, and breaking and reformation of H-bond between pairs involving centre-of-mass translation.[59] All these suggest that the ~ 5 ps time scale detected here is linked to N-H bond vector reorientation coupled with H-bond relaxation of acetamide molecules.

DR spectra shown in Fig. 3.1 also indicate $\varepsilon_0 = 64$ for molten acetamide at ~354 K, which is in good agreement with earlier report of $\varepsilon_0 = 61$ at ~367 K.[60,61] Moreover, the missing dispersion

amplitude, $\varepsilon_\infty - n_D^2 = 5.1 - 2.04^{62} = 3.06$, reflects presence of liquid dynamics faster than detectable in the current measurements. Note such high frequency DR components in liquid amides[63,64] and other H-bonded systems[65-68] have been found to be critical for generating ultrafast solvent response. In addition, measurements of intermolecular collective dynamics in amides and substituted amides have reported librational response in the terra-hertz (1 THz = 10^{12} Hz) regime.[69-71] Therefore, DR experiments employing a wider coverage at the high frequency regime, followed by THz measurements are required for a complete characterization of polarization dynamics of molten acetamide and acetamide containing DESs.

3.3.2 DR Time Scales in (*acetamide + electrolyte*) DESs: Anion Dependence

Anion dependence of dielectric relaxation of (*acetamide + electrolyte*) DESs is demonstrated in Fig. 3.2 where the upper panels present the measured spectra for (*acetamide + LiX*) systems with X= Br^-, NO_3^- and ClO_4^-, and the lower panel shows those for (*acetamide + NaX*) systems with X=SCN^- and ClO_4^-. Note here that neither a plateau in $\varepsilon'(\nu)$ nor a peak in $\varepsilon''(\nu)$ can be observed in these spectra, making estimation of ε_0 and characteristic relaxation time a non-trivial task. 4-Debye fits through the data are shown by the solid lines while the fit parameters are summarized in Table 3.1. Residuals shown in Figs. A.a.1 and A.a.2 (Appendix) suggest that these fits, though not perfect, provide a reasonable description of both the real (ε') and imaginary (ε'') components of the dielectric spectra recorded. Note a semi-quantitative description of the relaxation dynamics is only expected because the present measurements cannot access the relaxations outside the frequency window employed. Note all these DESs, as neat molten acetamide would, require a fast Debye relaxation component for adequately describing the measured spectra, although the amplitude associated with this component has been found to be very small (~1-3% of the total detected dispersion). We believe that this fast, sub-10 ps component is real for the following reasons: (i) DR of neat molten acetamide suggest presence of such a fast time scale. (ii) 3-Debye fits neglecting this fast component led to relatively poor description of the measured spectra. A comparison between residuals in Fig. A.a.3 (Appendix) obtained via 3-Debye and 4-Debye fits to the DR spectra measured for (acetamide + LiClO₄) system demonstrates this. Since an unconstrained 4-Debye fit to this system produced a time

scale of 4 ps, fit to data for other systems were performed after fixing this fastest time constant. (iii) A considerable part of the high frequency dispersion, $\varepsilon_\infty - n_D^2 \approx 4$, remained undetected in the present measurements. Interestingly, a similar magnitude of total dispersion has also remained undetected for neat molten acetamide. All these considerations strongly suggest that this fast, sub-10 picosecond component is real and connected to N-H bond vector reorientation of acetamide molecule. The undetected dispersion is then attributed to the intermolecular librational and interaction-induced reorientational motions of acetamide molecules[69-71] forming these DESs.
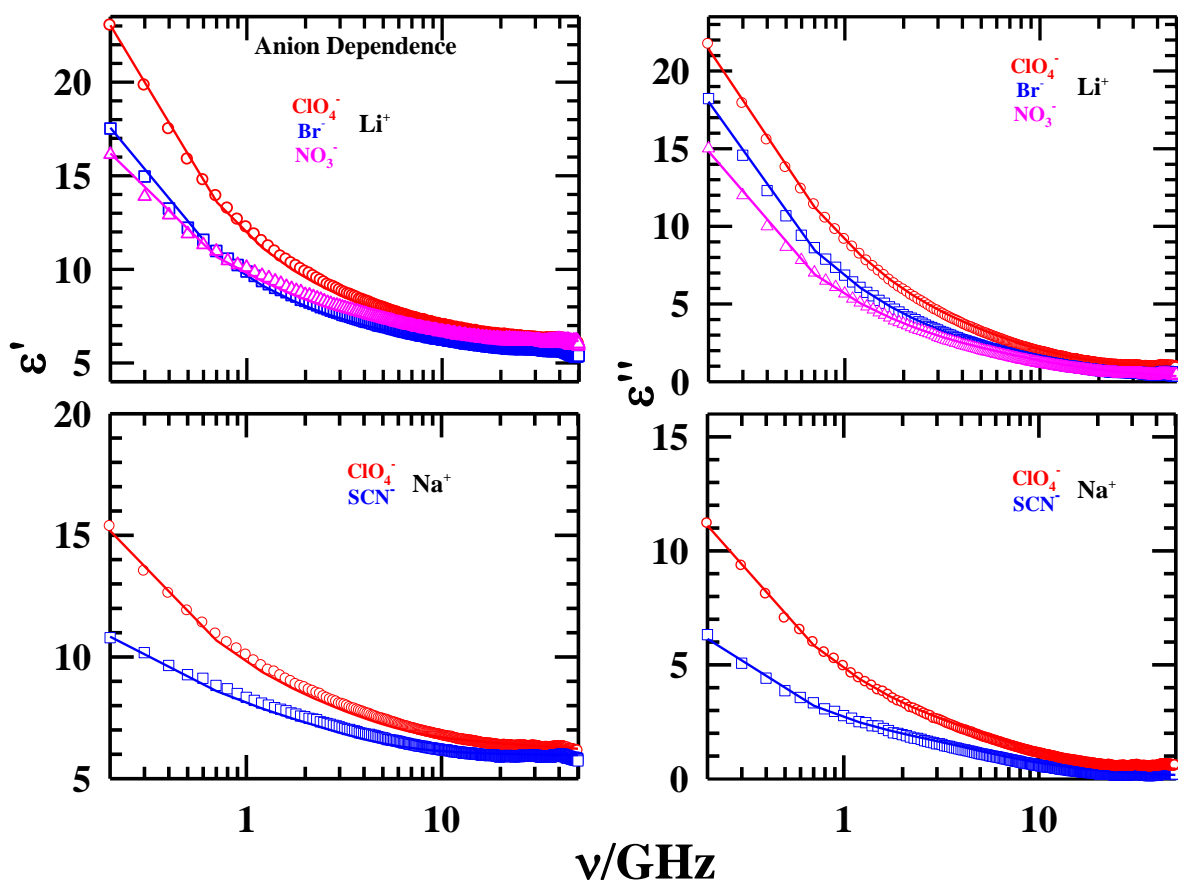
Fig. 3.2: Anion dependence of the real (ε') and imaginary (ε'') parts of the measured DR spectra for the ionic deep eutectics, (Acetamide + Electrolyte) at ~293 K. The specific identity of the electrolytes are shown in insets. Upper panel shows real and imaginary parts for deep eutectics with lithium salts (perchlorate, bromide and nitrate), and the lower panel presents those with sodium salts (perchlorate and thiocyanate). Representations are color-coded.

Table 3.1: Fit parameters obtained from simultaneous fits of real (ε') and imaginary (ε'') parts of the measured DR spectra for the ionic deep eutectics, ($acetamide + electrolyte$) at ~293 K.

Electrolyte	ε_0	$\Delta\varepsilon_1$	$\tau_1{}^b$ (ps)	$\Delta\varepsilon_2$	τ_2 (ps)	$\Delta\varepsilon_3$	τ_3 (ps)	$\Delta\varepsilon_4$	τ_4 (ps)	ε_∞	χ^2	$n_D{}^c$	$<\tau_{av}>^d$ (ps)
LiBr	23.6	13.3 (74%)^a	715	3.0 (17%)	131	1.4 (8%)	30	0.2 (1%)	4	5.6	0.014	1.407	605
LiNO$_3$	21.9	11.4 (72%)	790	2.8 (18%)	126	1.4 (9%)	29	0.1 (1%)	4	6.1	0.013	1.385	657
LiClO$_4$	29.4	16.2 (69%)	630	4.4 (19%)	160	2.3 (9%)	38	0.8 (3%)	4	5.8	0.016	1.371	528
NaClO$_4$	18	8 (67%)	600	2.3 (19%)	158	1.2 (10%)	41	0.4 (4%)	4	6.1	0.012	1.369	502
NaSCN	12.8	3.2 (47%)	867	2.0 (29%)	255	1.6 (23%)	54	0.06 (1%)	4	5.9	0.011	1.418	633
KSCN	25.3	13.3 (70%)	557	3.7 (19%)	120	1.8 (9%)	28	0.3 (2%)	4	6.2	0.015	1.413	463

a) number in parenthesis indicates dispersion amplitude of a given dispersion step in percentage.

b) τ_i (i=1-3) are better within ±5% of the reported values (based on 3-5 independent measurements).

c) Measured refractive index.

d) $<\tau_{av}> = \dfrac{\sum_{i=1}^{=2} a_i \tau_i}{\sum_{i=1}^{2} a_i}$, where $\sum_{i=1}^{n} a_i = 1$ and $a_i = \dfrac{\Delta\varepsilon_i}{\sum_{i=1}^{n} \Delta\varepsilon_i}$.

Next we comment on the possible origins for the other time scales observed in the present DR measurements. First, the slowest time scale (τ_1), which is in ~0.5 - 1 ns range with an amplitude of ~50-70% of the total dispersion detected, is ~10-20 times slower than τ_1 for molten acetamide, and indicates strong ion-acetamide interactions. In addition, this time scale does not follow the viscosity (η) trend (see Table A.a.4 in the Appendix for η values).[21,27] The fact that this time scale or the amplitude-averaged time scale considering τ_1 and τ_2 (that is,

$$\langle \tau_{av} \rangle = \sum_{i=1}^{2} a_i \tau_i \Big/ \sum_{i=1}^{2} a_i$$) does not follow the viscosity trend of these DESs suggests difference in

ion-acetamide interactions upon the change in ion identity. Evidences for electrolyte dependent interaction and dynamics have already been reflected in the fluorescence and simulation studies of these ionic acetamide deep eutectics earlier,[21-26] and the present DR data reconfirm this general observation. Interestingly, insertion of these time scales (τ_1 or $\langle \tau_{av} \rangle$) in the SED relation,[52-56] $V_{eff} = k_B T \tau_r / 3\eta$, leads not only to a much smaller V_{eff} for acetamide than its V_m but predicts also a wild variation of V_{eff} upon the change in electrolyte. This suggests that τ_1 does not involve either the full molecular rotation of acetamide in these ionic deep eutectics or the rotating moiety does not experience the full frictional resistance exerted by the macroscopic viscosity of the medium. Similar observation has also been made for ionic liquids while connecting the rotation volume of the dipolar ion to the slowest measured DR times.[34,37]

Note these ionic DESs are heterogeneous media,[21-26] and therefore the hydrodynamic relation between the orientational relaxations at the collective (that is DR) and single particle limits is expected to break down. Prediction for wildly varying rotational volumes for acetamide may suggest involvement of cooperative small-amplitude motions and/or reorientational jumps.[58,72,73] The cooperativity may arise, as discussed in earlier works,[18,19] from the formation of H-bonded complexes between ions and acetamide molecules extended over a few-to-several molecular diameters, promoting small amplitude collective rotation at the expense of molecular rotation. In such a scenario, breaking and reformation of H-bonds for acetamide molecules of ion-acetamide complexes can be a source for the observed slowing down. Our initial simulation results on

$C_{HB}(t)$ decay in one of these ionic DESs indeed suggest presence of a slow time scale in ~0.5 ns regime.

The other two DR time scales, τ_2 and τ_3, respectively in ~100-200 ps and ~25-50 ps ranges, also do not show any specific dependence on medium viscosity or electrolyte volume[74] (see Table A.a.5, Appendix). Note OHD-RIKES measurements of thiocyanate ion and lithium ion containing deep eutectics considered here have reported decay components with time scales in 100 ps and ~10-20 ps ranges.[27] This suggests that the collective molecular motions that produced the above OHD-RIKES time scales also contribute to the τ_2 and τ_3 in these DR measurements. This is because both OHD-RIKES and DR measurements respond to long wavelength polarization fluctuations of the system. Furthermore, dynamic Stokes shift measurements of these DESs employing a limited time-resolution (~75 ps) have reported solvation decay components with time constant in the ~100 ps and ~0.5-1 ns ranges along with a substantial missing faster component.[21,24,25] All these Kerr spectroscopic and time-resolved fluorescence measurements therefore support the presence of time scales detected by the present DR measurements for these ionic DESs.

3.3.3 DR Time Scales: Cation Dependence

Fig. 3.3 displays the cation dependence of the DR spectrum for (*acetamide + Li/NaClO₄*) and (*acetamide + K/NaSCN*) DESs at ~293 K along with the corresponding 4-D fits. Fit parameters are, as before, summarized in Table 3.1. Note that for both the perchlorate (ClO_4^-) and thiocyanate (SCN^-) DESs, τ_1 or $<\tau_{av}>$ follows the change in η upon change in the counter metal ion of the accompanying electrolyte. However, τ_1 values for these DESs also indicate, as before for anion dependent cases, much smaller V_{eff} and a wide variation of it with cation identity (Li^+/Na^+ for ClO_4^- DES and Na^+/K^+ for SCN^- DES). The inadequacy of the SED relation is further highlighted in larger τ_1 values for (*acetamide + NaSCN*) DES than that for (*acetamide + LiBr*) system although the former is less viscous than the latter. It is therefore evident that the detected reorientational dynamics in these systems cannot be interpreted in terms of isotropic molecular rotation of acetamide, and non-hydrodynamic mode such as jumps may be

involved. We also mention here that electrolytes in these DESs may produce ion pairs and other higher order complex species which would contribute to the relaxation process by adding, due to larger sizes, further slower relaxation time scales.[75] More complete measurements using wider frequency window are therefore required to capture the full DR dynamics of these complex molten systems.
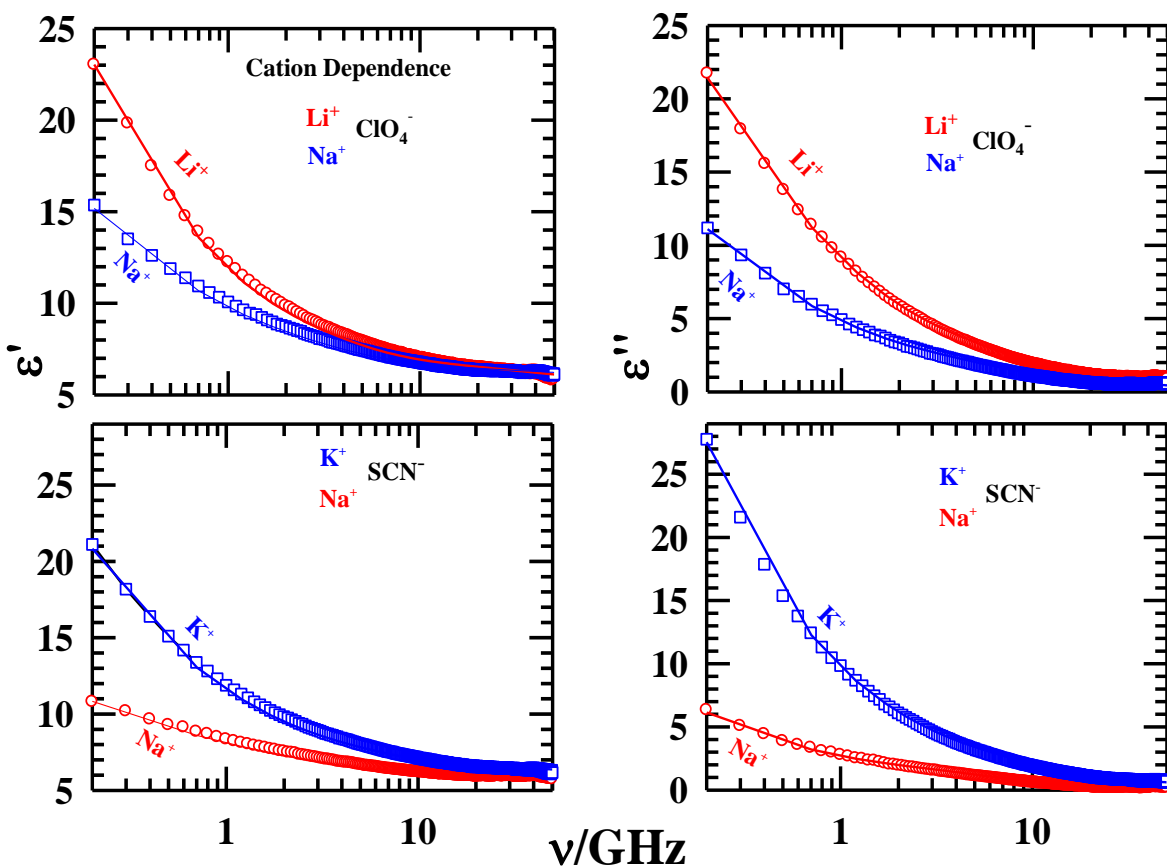
Fig. 3.3: Cation dependence of the real (ε') and imaginary (ε'') parts of the measured DR spectra for the ionic deep eutectics, ($acetamide + electrolyte$) at ~293 K. Upper panel shows spectra for perchlorate salts of lithium and sodium, and lower panel presents thiocyanate salts of sodium and potassium. Representations are color-coded.

3.3.4 Static Dielectric Constant, ε_0, from Fit: Anion and Cation Dependence

Data in Table 3.1 indicate that ε_0 values from fits vary in the range ~13-30, and exhibit a dependence on both cation and anion identity. Note this range of ε_0 may involve a large uncertainty because the lowest frequency accessed is 200 MHz, and dipolar relaxation at $\nu < 200\,\text{MHz}$, if any, has remained completely unaccounted for during fits. Such a possibility may exist as a characteristic plateau of $\varepsilon'(\nu)$ in the limit of lower frequencies is absent in the DR spectra recorded for all these ionic deep eutectics. Analyses of multiple data sets for a given system recorded in the employed frequency window suggest an over-all error bar of ±2.5 for these estimated ε_0 values. This large error bar notwithstanding, such a range of ε_0 for these DESs is striking because it reflects a drastic decrease from the value (ε_0 = 64) measured for molten neat acetamide at ~354 K. This decrease appears even more dramatic if one considers that the measurements for molten acetamide were done at a temperature ~61 K higher than that for these DESs, and that a rise in solution temperature decreases ε_0 via reducing long-ranged orientational spatial correlations.[34,48] The observed decrease for these DESs may, however, take place if formation of ion-acetamide complex quenches, partially or fully, the rotational degrees of freedom of the surrounding acetamide molecules. Formation of such 'irrotationaly bound' solvent molecules via ion-solvent electrostatic interactions has been proposed before while explaining the marked decrease in static dielectric constant upon addition of electrolyte in aqueous and non-aqueous media at ambient condition.[76-78] Note dilution of dipole density upon addition of electrolyte also contributes to the observed reduction in ε_0 but is likely to be overwhelmed by the reduction due to freezing of surrounding dipolar acetamide molecules ($\mu_{\text{acetamide}} = 3.7\,\text{D}$)[60] via ion-acetamide interaction. Kinetic polarization deficiency arising from a coupling between the rotation of the acetamide (dipolar) molecules and the translation of the ions may also contribute to the observed reduction of ε_0 values.[79,80] Note calculated dynamic Stokes shift magnitudes for a dipolar solvation probe in these ionic DESs (except in presence of NaClO$_4$) assuming $\varepsilon_0 \sim 30$ were found to be in reasonable agreement with experimental values.[21,24-25] This provides a support to the ε_0 range observed in the present DR

41

measurements. Ion solvation by acetamide leading to quenching of acetamide rotation coupled with electrolyte-induced break-down of H-bond network,[76-78] and kinetic depolarization effects,[79,80] may therefore, be the reasons for the observed reduction in ε_0 for these ionic DESs.

Data in Table 3.1 also reveals that among the (*acetamide + LiX*) systems, ClO_4^- -containing DES possesses the largest ε_0. The same is also true when we compare ε_0 between (*acetamide + NaX*) DESs. For the SCN^--containing DESs, ε_0 in presence of Na^+ is found to be nearly half of that found for the corresponding K^+ -containing one. A comparison between (*acetamide + Na/LiClO_4*) deep eutectics also reveals that ε_0 for Na^+ -containing deep eutectic system is ~1.6 time lower than that for the corresponding Li^+ -containing system. Considering the chemistry of these systems one can suggest that cation solvation and the reduction of the Kirkwood factor due to the electrolyte-induced breakdown of the H-bond network of the liquid acetamide are probably among the dominant reasons[76-78] for the observed decrease of ε_0. A simulation study probing the ion dependences for both the kinetic depolarization effects[79,80] and lifetime of the acetamide-ion complexes can examine this proposition.

Note here that, as the current measurements cover only a part of the total relaxation, finding the 'true' fit model is somewhat problematic. Consequently, the observed adequacy of multi-Debye fits for DESs spectra may be fortuitous. Fortunately, collected DR spectra for molten neat acetamide provide semi-quantitatively correct estimates for ε_0 and the slowest relaxation time scale. These form the basis for a discussion on ion effects on DR of these ionic DESs. Comparison with relaxation time scales from time-resolved fluorescence[21,24.25] and Kerr spectroscopic[27] measurements provide additional fidelity to the DR time scales obtained via 4-D fits. The general applicability of 4-D description for the detected part of the relaxation in these DESs is shown representatively in Fig. A.a.6 and Fig. A.a.7 along with the relevant fit parameters summarized in Table A.a.8 (see Appendix). It is evident from these figures and the table that 4-D fits provide a uniform general description of the measured spectra for these DESs, without strictly assigning any specific mechanism to the relaxation modes. Interestingly,

adoption of such a generalized description can be found in earlier works investigating the effects of molecular solvents on DR of ionic liquids.[34,81,82]

3.4 Conclusion

In summary, the present DR measurements of neat molten acetamide and six different (*acetamide + MX*) deep eutectics in the frequency window $0.2 \leq \nu/\text{GHz} \leq 50$ have revealed marked dependence of relaxation parameters on the identity of the electrolytes. Drastic decrease of ε_0 has been found for each of the six systems studied, and the range $12 < \varepsilon_0 < 30$ resembles to that reported for various types of ionic liquids.[34-39,83] Multi-Debye fits have been found to describe the detected relaxation dynamics, with the fastest time constant appears to be connected to N-H bond vector relaxation. The slowest sub-nanosecond relaxation time scales for these DESs deviate strongly from hydrodynamic predictions, and suggest involvement of either collective small amplitude rotation or orientational jump followed by structural H-bond relaxation. Although the present measurements have missed relaxation dynamics at both the low frequency ($\nu < 0.2\,\text{GHz}$) and high frequency ($\nu > 50\,\text{GHz}$) wings, fit parameters describing the measured DR spectra corroborates well with dynamic Stokes shift results from experiments and calculations.[21,24-26] In addition, several features of DR dynamics of these ionic deep eutectics resemble to those observed for room temperature ionic liquids and electrolyte solutions.

Because DR measurements of these conducting media involve non-trivial problem of dealing with conductivity divergence at $\nu \to 0$, care must be exercised to protect estimated ε_0 values for such solutions from turning anything between erroneous to completely wrong. Our confidence for the reported range of ε_0 for these ionic deep eutectics arises from correctly reproducing the reported ε_0 values and slowest DR time constants for neat water, several non-aqueous media and their electrolyte solutions at ambient condition. This is exemplified in Table A.a.9 (Appendix) which provides a comparison between DR fit parameters from our measurements and those available in the literature[84-86] for aqueous solutions of sodium chloride (NaCl) and potassium chloride (KCl) at a few electrolyte concentrations. Representative fits along with residuals are provided in Fig. A.a.10 and Fig. A.a.11(see Appendix). In addition, when (*acetamide + urea*)

deep eutectics[87] have been subjected to DR measurements, we find $\varepsilon_0 \approx 69$ at ~333 K which, as observed earlier for aqueous urea solutions,[88] increases with urea concentration. Temperature - dependent DR measurements of these ionic and nonionic DESs and their simulation interpretations will constitute our future works. Further, one needs to investigate the interplay between H-bond frustration[89] and locally preferred structures[90] for a molecular level understanding of the interconnection between the depression of freezing point and heterogeneity for these and other deep eutectics.

References

1. D. V. Wagle, H. Zhao and G. A. Baker, Acc. Chem. Res. **47**, 2299 (2014).

2. Q. Zhang, K. D. O. Vigier, S. Royer and F. Jérôme, Chem. Soc. Rev. **41**, 7108 (2012).

3. A. P. Abbott, G. Capper, D. L. Davies, R. K. Rasheed and V. Tambyrajah, Chem. Commun. 70 (2003).

4. A. P. Abbott, D. Boothby, G. Capper, D. L. Davies and R. K. Rasheed, J. Am. Chem. Soc. **126**, 9142 (2004).

5. M. Francisco, A. van den Bruinhorst and M. C. Kroon, Angew. Chem. Int. Ed. **52**, 3074 (2013).

6. M. Francisco, A. van den Bruinhorst and M. C. Kroon, Green Chem. **14**, 2153 (2012).

7. H. Zhao and G. A. Baker, J. Chem. Technol. Biotechnol. **88**, 3 (2013).

8. D. Carriazo, M. C. Serrano, M. C. Gutiérrez, M. L. Ferrer and F. del Monte, Chem. Soc. Rev. **41**, 4996 (2012).

9. G. van der Zwan and J. T. Hynes, Chem. Phys. **152**, 169 (1991).

10. G. van der Zwan and J. T. Hynes, J. Chem. Phys. **78**, 4174 (1983).

11. A. Nitzan, *Chemical Dynamics in Condensed Phases*. (Oxford University Press, Oxford, U.K 2006).

12. T. Pradhan and R. Biswas, J. Phys. Chem. A **111**, 11514 (2007).

13. T. Pradhan, H. A. R. Gazi and R. Biswas, J. Chem. Phys. **131**, 054507 (2009).

14. G. Berchiesi, G. Rafaiani, G. Vitali and F. Farhat, J. Therm. Anal. Calorim. **44**, 1313 (1995).

15. G. Berchiesi, G. Vitali, P. Passamonti and R. Płowiec, J. Chem. Soc., Faraday Trans. 2 **79**, 1257 (1983).

16. G. Berchiesi, F. Farhat, M. de Angelis and S. Barocci, J. Mol. Liq. **54**, 103 (1992).

17. G. Berchiesi, G. Vitali, R. Plowiec and S. Barocci, J. Chem. Soc. Faraday Trans. 2 **85**, 635 (1989).

18. G. Berchiesi, J. Mol. Liq. **83**, 271 (1999).

19. A. Amico, G. Berchiesi, C. Cametti and A. Di Biasio, J. Chem. Soc. Faraday Trans. 2 **83**, 619 (1987).

20. G. Berchiesi, M. De Angelis, G. Rafaiani and G. Vitali, J. Mol. Liq. **51**, 11 (1992).

21. B. Guchhait, S. Das, S. Daschakraborty and R. Biswas, J. Chem. Phys. **140**, 104514 (2014).

22. A. Das, S. Das and R. Biswas, Chem. Phys. Lett. **581**, 47 (2013).

23. T. Pal and R. Biswas, Chem. Phys. Lett. **517**, 180 (2011).

24. B. Guchhait, H. A. R. Gazi, H. K. Kashyap and R. Biswas, J. Phys. Chem. B **114**, 5066 (2010).

25. B. Guchhait, S. Daschakraborty and R. Biswas, J. Chem. Phys. **136**, 174503 (2012).

26. H. A. R. Gazi, B. Guchhait, S. Daschakraborty and R. Biswas, Chem. Phys. Lett. **501**, 358 (2011).

27. R. Biswas, A. Das and H. Shirota, J. Chem. Phys. **141**, 134506 (2014).

28. D. Xiao, J. R. Rajian, A. Cady, S. Li, R. A. Bartsch and E. L. Quitevis, J. Phys. Chem. B **111**, 4669 (2007).

29. D. Xiao, L. G. Hines Jr, R. A. Bartsch and E. L. Quitevis, J. Phys. Chem. B **113**, 4544 (2009).

30. D. Xiao, J. R. Rajian, S. Li, R. A. Bartsch and E. L. Quitevis, J. Phys. Chem. B **110**, 16174 (2006).

31. A. L. Sturlaugson, K. S. Fruchey and M. D. Fayer, J. Phys. Chem. B **116**, 1777 (2012).

32. H. Shirota and R. Biswas, J. Phys. Chem. B **116**, 13765 (2012).

33. D. A. Turton, J. Hunger, A. Stoppa, G. Hefter, A. Thoman, M. Walther, R. Buchner and K. Wynne, J. Am. Chem. Soc. **131**, 11140 (2009).

34. J. Hunger, A. Stoppa, S. Schrödle, G. Hefter and R. Buchner, ChemPhysChem. **10**, 723 (2009).

35. A. Stoppa, J. Hunger, R. Buchner, G. Hefter, A. Thoman and H. Helm, J. Phys. Chem. B **112**, 4854 (2008).

36. M.-M. Huang, S. Bulut, I. Krossing and H. Weingärtner, J. Chem. Phys. **133**, 101101 (2010).

37. C. Daguenet, P. J. Dyson, I. Krossing, A. Oleinikova, J. Slattery, C. Wakai and H. Weingärtner, J. Phys. Chem. B **110**, 12682 (2006).

38. K. Nakamura and T. Shikata, ChemPhysChem. **11**, 285 (2010).

39. M. Mizoshiri, T. Nagao, Y. Mizoguchi and M. Yao, J. Chem. Phys. **132**, 164510 (2010).

40. M. Horng, J. Gardecki, A. Papazyan and M. Maroncelli, J. Phys. Chem. **99**, 17311 (1995).

41. B. Bagchi and R. Biswas, Adv. Chem. Phys. **109**, 207 (1999).

42. H. K. Kashyap and R. Biswas, J. Phys. Chem. B **112**, 12431 (2008).

43. S. Daschakraborty and R. Biswas, J. Phys. Chem. B **118**, 1327 (2014).

44. S. Daschakraborty, T. Pal and R. Biswas, J. Chem. Phys. **139**, 164503 (2013).

45. R. F. Grote and J. T. Hynes, J. Chem. Phys. **73**, 2715 (1980).

46. G. R. Fleming and P. G. Wolynes, Phys. Today **43**, 36 (1990).

47. R. Biswas and B. Bagchi, J. Chem. Phys. **105**, 7543 (1996).

48. C. J. F. Böttcher and P. Bordewijk, *Theory of Electric Polarization*. (Elsevier: Amsterdam, The Netherlands, 1978).

49. F. Kremer and A. Schönhals, *Broadband Dielectric Spectroscopy*. (Springer, Berlin, Germany, 2003).

50. P. Bevington, *Data Reduction and Error Analysis for the Physical Sciences*. (McGraw-Hill: New York, 1969).

51. J. Barthel, R. Buchner and B. Wurm, J. Mol. Liq. **98**, 51 (2002).

52. B. Bagchi, *Molecular Relaxation in Liquids*. (Oxford University Press, New York, 2012).

53. J. L. Dote, D. Kivelson and R. N. Schwartz, J. Phys. Chem. **85**, 2169 (1981).

54. M.-L. Horng, J. Gardecki and M. Maroncelli, J. Phys. Chem. A **101**, 1030 (1997).

55. A. Das, R. Biswas and J. Chakrabarti, J. Phys. Chem. A **115**, 973 (2011).

56. A. Das, R. Biswas and J. Chakrabarti, Chem. Phys. Lett. **558**, 36 (2013).

57. S. Nasr, M. Ghédira and R. Cortes, J. Chem. Phys. **110**, 10487 (1999).

58. S. Das, R. Biswas and B. Mukherjee, J. Phys. Chem. B **119**, 274 (2015).

59. J. Barthel, K. Bachhuber, R. Buchner and H. Hetzenauer, Chem. Phys. Lett. **165**, 369 (1990).

60. R. A. Wallace, Inorg. Chem. **11**, 414 (1972).

61. D. Kerridge, Chem. Soc. Rev. **17**, 181 (1988).

62. en.wikipedia.org/wiki/Acetamide.

63. R. Biswas and B. Bagchi, J. Phys. Chem. **100**, 1238 (1996).

64.   H. K. Kashyap, T. Pradhan and R. Biswas, J. Chem. Phys. **125**, 174506 (2006).

65.   S. Roy and B. Bagchi, J. Chem. Phys. **99**, 9938 (1993).

66.   R. Biswas, N. Nandi and B. Bagchi, J. Phys. Chem. B **101**, 2968 (1997).

67.   J. Kindt and C. Schmuttenmaer, J. Phys. Chem. **100**, 10373 (1996).

68.   S. Daschakraborty, T. Pal and R. Biswas, J. Chem. Phys. **139**, 164503 (2013).

69.   Y. J. Chang and E. W. Castner Jr, J. Chem. Phys. **99**, 113 (1993).

70.   K. Goossens, L. Smeller and K. Heremans, J. Chem. Phys. **99**, 5736 (1993).

71.   O. F. Nielsen, P.-A. Lund and E. Praestgaard, J. Chem. Phys. **77**, 3878 (1982).

72.   D. Laage and J. T. Hynes, Science **311**, 832 (2006).

73.   D. Laage and J. T. Hynes, J. Phys. Chem. B **112**, 14230 (2008).

74.   H. D. B. Jenkins, H. K. Roobottom, J. Passmore and L. Glasser, Inorg. Chem. **38**, 3609 (1999).

75.   P. Eberspächer, E. Wismeth, R. Buchner and J. Barthel, J. Mol. Liq. **129**, 3 (2006).

76.   J. Barthel, R. Buchner, P.-N. Eberspächer, M. Münsterer, J. Stauber and B. Wurm, J. Mol. Liq. **78**, 83 (1998).

77.   R. Buchner, Pure Appl. Chem. **80**, 1239 (2008).

78.   R. Buchner and J. Barthel, Annu. Rep. Prog. Chem., Sect. C **97**, 349 (2001).

79.   J. Hubbard, L. Onsager, W. van Beek and M. Mandel, Proc. Natl. Acad. Sci. U. S. A. **74**, 401 (1977).

80.   J. Hubbard and L. Onsager, J. Chem. Phys. **67**, 4850 (1977).

81.   A. Stoppa, J. Hunger, G. Hefter and R. Buchner, J. Phys. Chem. B **116**, 7509 (2012).

82.   X.-X. Zhang, M. Liang, J. Hunger, R. Buchner and M. Maroncelli, J. Phys. Chem. B **117**, 15356 (2013).

83.   O. Zech, J. Hunger, J. R. Sangoro, C. Iacob, F. Kremer, W. Kunz and R. Buchner, Phys. Chem. Chem. Phys. **12**, 14341 (2010).

84.   J. Barthel, M. Kleebauer and R. Buchner, J. Solution Chem. **24**, 1 (1995).

85.   K. Nörtemann, J. Hilland and U. Kaatze, J. Phys. Chem. A **101**, 6864 (1997).

86.   T. Chen, G. Hefter and R. Buchner, J. Phys. Chem. A **107**, 4025 (2003).

87.   A. Das, S. Das and R. Biswas, J. Chem. Phys. **142**, 034505 (2015).

88.   Y. Hayashi, Y. Katsumoto, S. Omori, N. Kishii and A. Yasuda, J. Phys. Chem. B **111**, 1076 (2007).

89.   H. Shintani and H. Tanaka, Nat. Phys. **2**, 200 (2006).

90.   G. Tarjus, C. Alba-Simionesco, M. Grousson, P. Viot and D. Kivelson, J. Phys. Condens. Matter **15**, S1077 (2003).

Chapter 4

Temperature Dependent Dielectric Relaxation in Molten Urea, and Acetamide/Urea Deep Eutectics: Polarity and the Possible Origin of the Relaxation Time Scales

4.1 Introduction

Deep eutectic solvents (DESs), by virtue of their exquisite solvent properties, economical viability, and easy preparation and transport protocol, are fast emerging as solvents for large scale industrial and technological applications.[1-7] DESs are multi-component molten mixtures which constitute a new class by themselves because they remain as stable liquids after melting at temperatures much lower than the melting temperatures ($T_m s$) of the individual mixture components. Extensive inter-species hydrogen bonding (H-bonding) and entropic gain for being in the liquid phase are the principal factors that assist in accessing the liquid phase through the extensive depression of freezing points. For some DESs, bio-degradable nature of the mixture components imparts certain degree of 'greenness',[8-10] fuelling solvent engineering to design environmentally benign DESs that can tailor reaction products. Ability of a solvent to steer a reaction lies in the static and dynamic solvent control of a reaction.[11-15] While the static control emerges from the polarity of a reaction medium and thus principally related to the medium dipole density, the dynamic control arises from the coupling of the reactive mode with the dipole fluctuation time scale during the barrier crossing. These controlling parameters can be easily tuned for DESs as a particular DES with desired properties can be prepared by choosing components from a wide range of ionic and non-ionic compounds. For example, acetamide can form deep eutectics with a variety of electrolytes[16-23] as well as with urea,[24-26] producing molten mixtures with very different polarities and viscosity coefficients.

Although DESs possess huge potential for large scale application as reaction media, both the structural and dynamical aspects of these systems have remained largely unexplored. Time-resolved fluorescence Stokes shift[16-20] and Kerr spectroscopic[22] measurements performed in

the last few years have revealed presence of picosecond and nanosecond dynamics in ($acetamide + electrolyte$) deep eutectics near room temperature. In addition, these fluorescence measurements have suggested a partial decoupling between diffusion and viscosity, and the consequent break-down of the conventional hydrodynamics.[16-19,21] This and a strong excitation wavelength dependence of steady state fluorescence emission of a dissolved dipolar probe[17,19] strongly suggest that these ionic DESs are spatio-temporally heterogeneous, a conclusion already hinted at by a few earlier studies.[27-30] Dielectric relaxation measurements of several ionic acetamide DESs in the frequency window $0.2 \leq \nu/GHz \leq 50$ have provided further support to the dynamic heterogeneity picture of these solutions.[31] Interestingly, recent fluorescence measurements of ($acetamide + urea$) deep eutectics, a representative of non-ionic DES, have revealed homogeneous solution character and demonstrated that accessing liquid phase via depression of freezing points of mixture components does not automatically guarantee solution inhomogeneity.[26] However, observation of heterogeneity signatures of a host solvent via fluorescence measurements depends critically on the fluorescence lifetime ($\langle \tau_{life} \rangle$) of the probe used.[20,32-34] Naturally then one asks the following question: is the observed opposing solution characteristics indicative of any fundamental difference between the ionic and non-ionic acetamide deep eutectics or just a reflection of relatively much faster density fluctuation time scales in ($acetamide + urea$) deep eutectics compared to the $\langle \tau_{life} \rangle$ of the probes used?

We investigate the above question via carrying out temperature dependent dielectric relaxation (DR) measurements in the frequency window $0.2 \leq \nu/GHz \leq 50$ of ($acetamide + urea$) deep eutectics having a eutectic temperature of ~319 K at 0.62 mole fraction of acetamide,[26] with the general composition [f CH_3CONH_2+$(1-f)$ NH_2CONH_2] at $f = 0.6$ and 0.7 within the temperature range, $335 \leq T/K \leq 363$. Earlier study[24-26] ensures that ($acetamide + urea$) deep eutectics with the above compositions remain accessible to the proposed DR measurements. In addition, DR measurements of molten urea at ~406 K have been performed. Note DR investigation of molten urea and ($acetamide + urea$) DESs has not been carried out before. DR data obtained here for molten urea together with our earlier results for molten acetamide (~354 K)[31] assist in exploring the origin of DR time scales measured for the ($acetamide + urea$) DESs considered. It has been reported that urea and acetamide can form both intra- and inter-species H- bonding to generate the conjugates at low

urea concentration and polymeric chains at high concentration.[35,36] These DR measurements are expected to shed light on this proposition. Moreover, DR time scales for (*acetamide* + *urea*) DESs found here should help qualitatively understand the solvation time scales reported earlier via dynamic Stokes shift measurements,[26] and stimulate further experiments using more sophisticated techniques.

4.2 Experimental Details

4.2.1 Materials and Methods

Acetamide ($\geq$98%, Merck, India), and Urea (>99%, SRL, India) were vacuum-dried (~300 K) overnight before use. Samples were prepared and relevant experiments were done in a tightly humidity-controlled environment. Further details regarding sample preparation could be found elsewhere as these DESs were already studied via fluorescence measurements.[26] Briefly, the sample vials were sealed and heated slowly to ~355 K until it formed a clear melt and then the DR measurements were performed. Refractive indices (n_D) were measured by employing an automated temperature-controlled refractometer (RUDOLPH, J357).

4.2.2 DRS Measurement Details

The DR data collection technique and the data analysis procedures are the same as mentioned in chapter 2 and in refs.[37-39] Approximately 10 mL of the thermally equilibrated molten sample (DESs and neat molten urea) and properly humidity-controlled environment were used for measurements in each case. We took 1001 data points for each DR measurements. Temperature dependent DR measurements for these DESs were carried out by using a heating plate (MS-H-Pro from SCILOGEX, USA). In all measurements desired experimental temperatures were sufficiently stable for conducting repeat (at least three) recordings.

4.3 Results and Discussion

4.3.1 DR of Molten Urea at ~406 K

We first present the results for molten urea because these data along with those for molten acetamide are prerequisites for exploring the origin of DR time scales in (*acetamide* + *urea*) DESs presented later. In addition, being an excellent solvent in liquid condition,[40] molten urea requires characterization of its polarity properties. Fig. 4.1 presents the DR spectra for

molten urea measured at ~406 K where the real (ε') and the imaginary (ε'') components are shown along with the 3-Debye (3-D) fits and fit parameters. Note that for molten urea, unlike in molten acetamide, the slowest (τ_1) of the three steps accounts for near about 11% of the total dielectric relaxation detected.
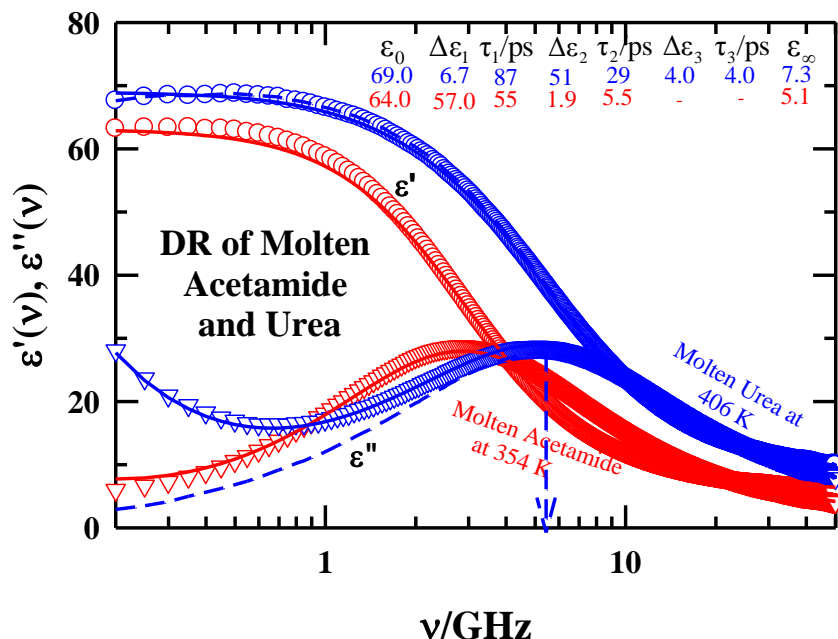
Fig. 4.1: DR of molten acetamide (354K) and molten urea (406 K) detected within the frequency window, $0.2 \leq \nu/\text{GHz} \leq 50$. Measured real ($\varepsilon'$) and imaginary ($\varepsilon''$) components of the recorded spectra are shown by circles and triangles, respectively. Solid lines through these data represent simultaneous 3-Debye fits with fit parameters shown as inset. Short dashed lines going through the urea data are reconstruction after conductivity correction (due to urea pyrolysis[41]).

In addition, the second slowest time constant having maximum (~88%) contribution in the total relaxation, $\tau_2 = 29\ ps$, corroborates well with the time corresponding to the peak frequency ($\nu_{peak} \sim 5.5\,\text{GHz}$) of the $\varepsilon''(\nu)$, $\tau_{peak} = 1/2\pi\nu_{peak} \approx 30\,\text{ps}$. A comparison with the DR data for molten acetamide (~354 K),[31] shown in the same figure, clearly indicates that the relaxation in molten urea is faster than that in molten acetamide. Higher experimental temperature for urea than acetamide may be a reason for this, although the static dielectric

constant for molten urea ($\varepsilon_0 \sim 70$) is found to be somewhat larger than that ($\varepsilon_0 \sim 64$) for molten acetamide.

Next we estimate the viscosity (η) of urea at 406 K from these DR data assuming that the time constant ($\tau_2 = 29\ ps$), having maximum contribution in the total relaxation process, originates from the molecular rotation of urea. Because DR probes orientational relaxation of rank 1 ($\ell = 1$), the single particle orientation time (τ_r) connects to the collective DR time as follows:[42] $\tau_r = \dfrac{\ell(\ell+1)}{2} \times \tau_{DR} = \tau_2$. Consequently, the Stokes-Einstein-Debye (SED) relation,[43-46] $\tau_r = 3V\eta/k_B T$, provides $\eta \sim 2.4$ cP at 406 K if we approximate the rotating urea molecule as a sphere of radius,[47-48] $r = 1.8$ Å (molecular volume $V = 4\pi r^3/3$, $k_B T$ being the Boltzmann constant times the temperature). While such a viscosity value for urea at 406 K appears plausible, this may not be accurate because the hydrodynamic radius[47] used in the above estimation can differ from the bare molecular radius. This is indeed the case as we obtain $\eta \sim 0.9$ cP if the hard-sphere radius of urea,[49-50] $r_{HS} = 2.5$ Å, is used, and this viscosity value is very close to our simulated viscosity value, $\eta \sim 0.7 \pm 0.2$ cP (see Appendix A.b.8). In such a scenario the viscosity ratio, $\eta_{354K}^{acetamide}/\eta_{406K}^{urea}$, becomes ~ 2.2 which correlates rather well with τ_2 (which has the maximum contribution) in molten urea being ~ 1.9 times shorter than the major DR time component of molten acetamide. Though here we have simulated the viscosity of molten urea, an independent measurement of viscosity for molten urea is necessary to ascertain whether τ_2 originates from molecular rotation of urea or it involves non-Brownian moves such as jumps.[51] Given that molten urea is an extensively H-bonded liquid,[52] roles for the collective H-bond relaxation dynamics and waiting time for finding a neighbor with suitable orientation (for forming a new H-bond after breaking a pre-existing one followed by rotation)[51,53] need to be independently understood before assigning a microscopic mechanism to the first two (τ_1 and τ_2) measured DR time scales.

Access to ε_0 for molten urea now enables one to estimate the dipole moment (μ) of urea in its liquid phase via the Onsager relation,[54] $(\varepsilon_0 - 1)(2\varepsilon_0 + 1)/9\varepsilon_0 = 4\pi\rho\mu^2/9k_B T$, where ρ denotes the solvent number density. In the absence of density data for molten urea we

follow the measurements for (*acetamide* + *urea*) deep eutectics[25] to approximate the density of molten urea at ~406 K as 1.25 g/cc, and obtain $\mu \approx 6.7$ D. This lies in between the two different measurements of dipole moment of urea in dilute solutions of dioxane at ~298 K which are 8.6 D[55] and 4.6 D.[56] In contrast, the current estimate is larger than the value (μ =5.3 D)[52] obtained from quantum chemical calculations at the single molecule level using the self-consistent field (SCF) wave function with atomic natural orbital (ANO) basis sets. Use of Cavell equation,[57-58] on the other hand, leads to μ =6.0 D which is quite close to our estimated value. Considering the absence of the effects due to the collective inter-molecular H-bonding network of molten urea in both the dioxane measurements[56] and quantum calculations,[52] a liquid phase dipole moment of 6.7 D for molten urea at ~406 K estimated here appears to be plausible.

We may now comment on the origin of the third time constant, τ_3 = 4 ps, which carries nearly 7% of the total detected relaxation. Note similar sub-10 ps relaxation has been observed earlier for molten acetamide and acetamide/electrolyte deep eutectics,[31] and assigned to the N-H bond vector reorientation.[51] Presence of N-H unit in urea as in acetamide and urea possessing two such units probably explains the appearance of the similar sub-10 ps component in molten urea with nearly double of its amplitude compared to that in molten acetamide. Note ε_∞ for molten urea is ~1.5 times larger than that measured for molten acetamide in the same frequency window, suggesting more weight to the high-frequency collective inter-molecular dynamics in the former than in the latter. This together with the shorter DR time scales will ensure not only a faster Stokes shift dynamics in molten urea than in molten acetamide[59-61] but also trigger ultrafast solvation response[62-66] in these neat molten media and in DESs made of them. Indeed, dynamic Stokes shift measurements have already hinted at the presence of a large ultrafast solvation component in (*acetamide* + *urea*) DESs.[26] This is further supported by the observation that more than 50% of the measured total solvation response in liquid formamide at ~295 K is composed of sub-picosecond component[67] which has been shown later[59,61,68] to arise from a combined participation of the fast DR time constant and the collective solvent intermolecular modes.

4.3.2 DR of Molten Urea: Temperature Dependence

Onset of pyrolysis[41] at $T > 400\,K$ seriously limits an extensive temperature dependent DR study for molten urea. We have therefore chosen a very narrow temperature window, $406 \leq T/K \leq 421$, in which the extent of decomposition remains negligible and the quality of the measured DR spectra acceptable within the frequency range, $0.2 \leq \nu/GHz \leq 50$. Note measurements within such a narrow temperature range will probably provide only a qualitative idea about how medium friction couples with the collective orientational relaxation in molten urea. Fig. 4.2 presents the collected temperature dependent DR spectra along with their 3-D fits where fits to the spectra are also shown in separate panels. These fits clearly demonstrate a shift of the ν_{peak} in $\varepsilon''(\nu)$ to higher frequency upon raising the temperature, suggesting faster relaxation at higher temperature. DR parameters obtained from 3-D fits summarized in Table A.b.1 (Appendix) indicate shortening of τ_2 (connected to ν_{peak}) by ~21% upon increasing the temperature from 406 K to 421 K, although ε_0 remains nearly unchanged at $\sim 70 \pm 1$ within this temperature variation. The fastest time constant, τ_3, does not show any temperature dependence as it was constrained at 4 ps during the simultaneous fits to the DR spectra at all these temperatures and the slowest component (τ_1) shows very small dependence (~10% change) on temperature. An Arrhenius-type of temperature dependence with an activation energy, $E_a^{urea}(\tau_2)$ ~21.64 kJ/mol and $E_a^{urea}(\langle \tau_{av}^{DR} \rangle)$ ~30.45 kJ/mol, for τ_2 and $\langle \tau_{av}^{DR} \rangle$ ($\langle \tau_{av}^{DR} \rangle = \sum_{i=1}^{2} a_i \tau_i \Big/ \sum_{i=1}^{2} a_i$ where the amplitudes (a_i) and the time constants (τ_i) are taken from Table A.b.1, Appendix) have been observed within this temperature range (see Fig. A.b.2, Appendix). This may be compared to the activations energies for several H-bonded small molecular liquids: $E_a^{formamide}(\tau_1) = 17.2$ kJ/mol,[53] $E_a^{water}(\tau_1) = 17.5$ kJ/mol,[69] $E_a^{ethanol}(\tau_1) = 19.9$ kJ/mol,[70] and $E_a^{propanol}(\tau_1) = 26$ kJ/mol.[70] Similar activation energies therefore suggest that τ_2 in molten urea is connected to the relaxation processes involving the H-bonding network.
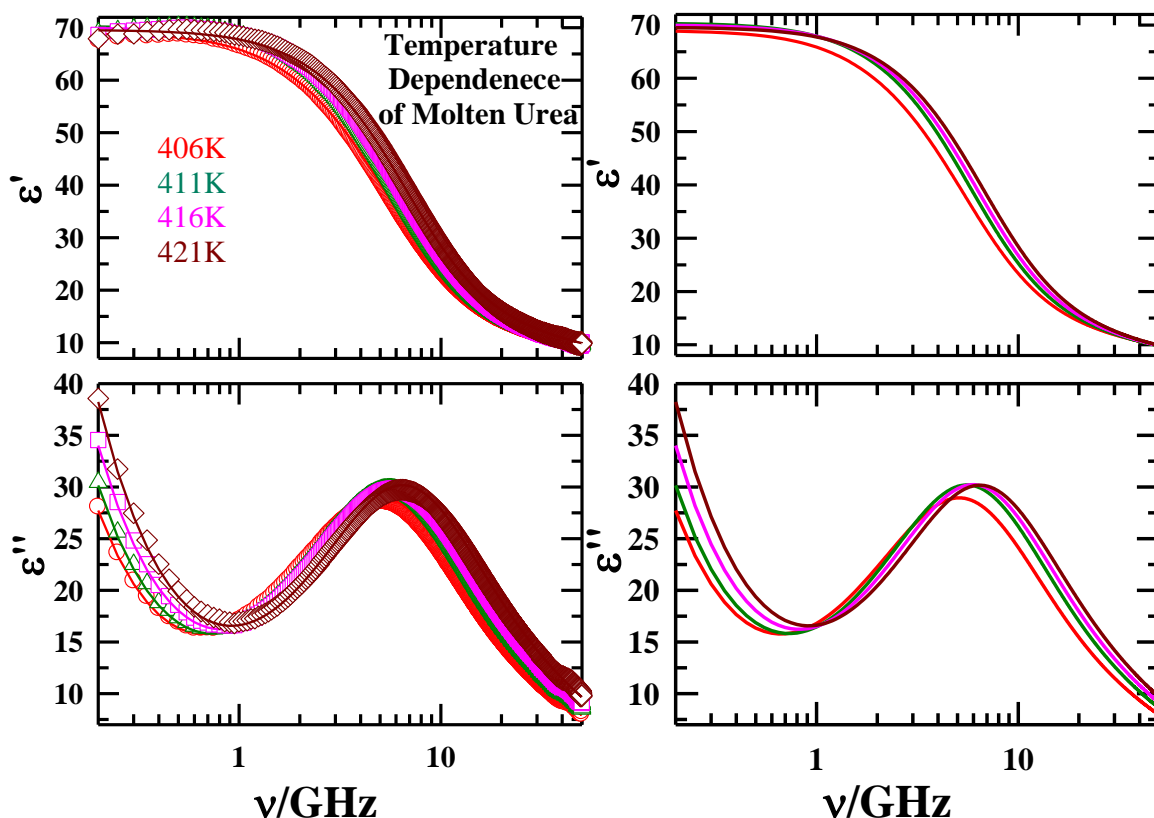
Fig. 4.2: Temperature dependent DR of molten urea. Collected spectra along with 3-Debye fits are presented in the left panel while only fits are shown in the right panel. All the representations are color coded. DR spectra are shown for the frequency regime $0.2 \leq \nu / \mathrm{GHz} \leq 50$.

4.3.3 DR in $(acetamide + urea)$ **DESs: Temperature Dependence**

Fig. 4.3 shows the temperature dependent DR spectra of the $(acetamide + urea)$ DES at f =0.6 along with the 3-D fits. The corresponding spectra and their fits for the DES at f =0.7 are shown in Fig. A.b.3 (see Appendix). A representative comparison between the 3-D and 2-D fits is provided in Fig. A.b.4 (see Appendix) which shows 3-D model provides a relatively better description of the spectra than that by the 2-D model. Note the plateau in $\varepsilon'(\nu)$ at all these temperatures as the frequency approaches its' limiting value at the lower wing. Such a behavior is typical for DR of systems composed of purely dipolar species.[53] A closer inspection of $\varepsilon'(\nu)$ at the low frequency wing suggests a gradual decrease of $\varepsilon(\nu \to 0)$ with temperature.
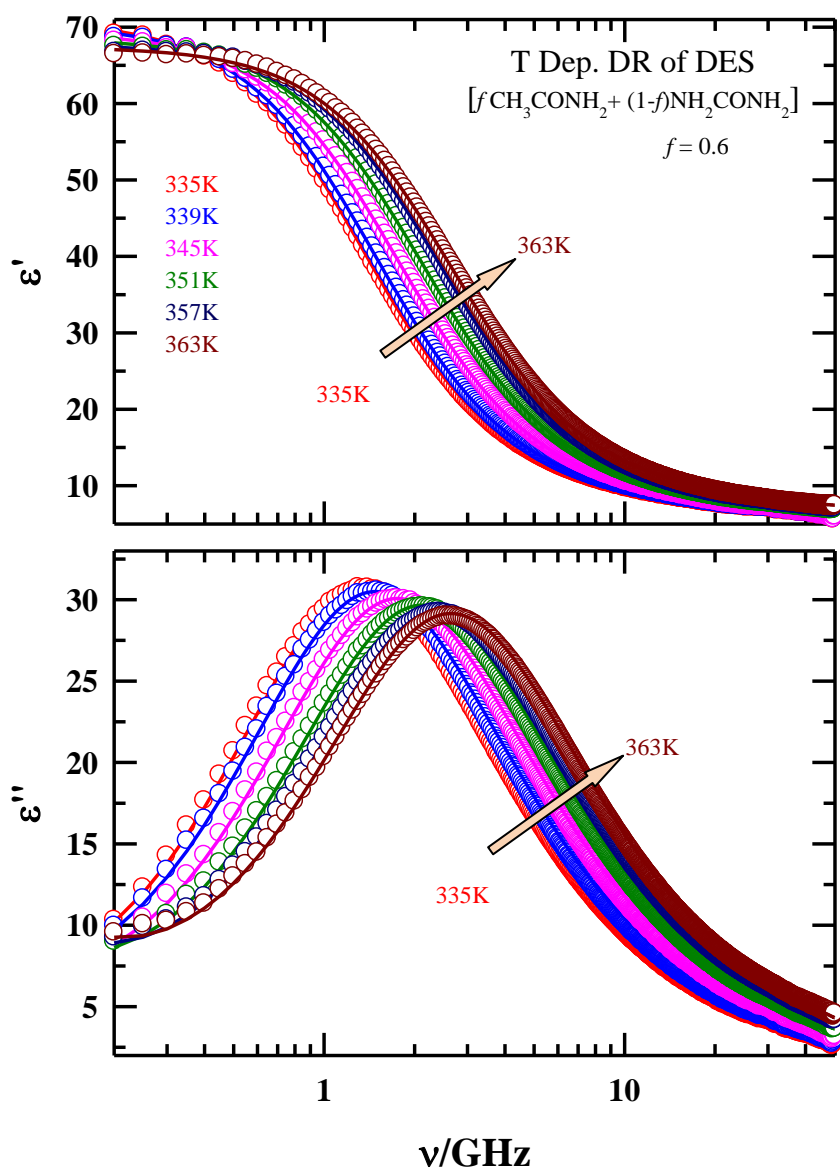
Fig. 4.3: Temperature dependence of DR of the (*acetamide* + *urea*) DES at $f = 0.6$ within the frequency regime $0.2 \leq \nu / GHz \leq 50$. Solid lines through the measured spectra represent simultaneous 3-Debye fits. All the representations are color coded. Arrow indicates the direction of temperature increase.

In addition, the peak frequency (ν_{peak}) of $\varepsilon''(\nu)$ moves to higher frequency as the solution temperature is increased. This shift of ν_{peak} is expected because η for these media decreases with temperature,[26] inducing faster relaxation at higher temperature. Sequential increase of the value of $\varepsilon''(\nu)$ at $\nu = 50\,GHz$ with temperature further reflects faster relaxation at higher temperature. This means that the extent of the inaccessible high frequency dynamics

becomes increasingly larger with the rise in solution temperature. Interestingly, $\varepsilon''(\nu)$ for these DESs, unlike in the case of molten urea, do not show any rise as $\nu \to 0$, suggesting absence of urea decomposition at these temperatures.

The temperature dependence discussed above is more quantitatively presented in Table 4.1 where the 3-D fit parameters obtained at f =0.6 and 0.7 are summarized along with the measured refractive indices (n_D) and the difference, $\varepsilon_\infty - n_D^2$. These fits provide three different time scales - τ_1 ~60-120 ps, τ_2 ~40-55 ps, and τ_3 ~5-7 ps. Note this ~5-7 ps timescale has already been observed in the DR of molten acetamide and ($acetamide + electrolyte$) DESs and attributed to the N-H bond vector reorientation coupled to H-bond relaxation.[31,51] However, no nanosecond time scale has been detected for these systems and this reflects, at least from the DR point of view, a clear difference between the ($acetamide + urea$) and ($acetamide + electrolyte$)[31] DESs. Note the measured τ_1 in these deep eutectics is slower than those detected for the molten acetamide and urea, suggesting inter-species H-bond interactions being responsible for this time scale.

Let us now examine various aspects of the slowest relaxation component characterized by the time constant, τ_1. Note τ_1 is associated with the maximum dispersion at nearly all the temperatures considered for the two compositions studied. In fact, a temperature dependence of this dispersion amplitude is very clear in Table 4.1 at both the compositions. At 335 K and f=0.6, a value of ~120 ps for τ_1 correlates well with the corresponding ν_{peak} of $\varepsilon''(\nu)$ at ~1.3 GHz, $\tau_{peak} = 1/2\pi\nu_{peak} = 122\,\text{ps}$. This correlation extends to all the other cases studied as well, indicating that the main relaxation for these DESs resides within the frequency window employed here. Next we ask: what could be the likely origin for τ_1 - collective orientational relaxation coupled to the inter-molecular H-bond relaxation or molecular rotation of either of the free species, urea or acetamide? SED analyses as done before for molten acetamide[31] and urea leads to a radius of ~1.7 Å at 335 K with η=9.9 cP for the rotating dipolar species in this DES at f=0.6. Interestingly, SED provides very similar values for the rotating radius (~1.6 - 1.8 Å) at all other temperatures and also for the composition, f=0.7.

Table 4.1: Parameters obtained from simultaneous 3-Debye fits to real (ε') and imaginary (ε'') components of the measured DR spectra for ($acetamide + urea$) DESs at various temperatures.[a]

T (K)	ε_0	$\Delta\varepsilon_1$	τ_1 (ps)	$\Delta\varepsilon_2$	τ_2 (ps)	$\Delta\varepsilon_3$	τ_3 (ps)	ε_∞	n_D	$\varepsilon_\infty - n_D^2$
				$f = 0.6$						
335	70.9	58.1(90%)	121	4.6(7%)	39	2.2	6	6.0	1.395	4.05
339	70.3	57.7(90%)	111	4.4(7%)	37	2.2	6	6.1	1.395	4.15
345	69.3	55.9(88%)	94	4.9(8%)	38	2.4	6	6.1	1.394	4.16
351	68.5	53.4(86%)	79	6.2(10%)	39	2.4	6	6.5	1.394	4.56
357	67.8	50.1(82%)	70	8.5(14%)	40	2.6	6	6.6	1.393	4.66
363	67.4	49.0(81%)	64	9.0(15%)	38	2.7	6	6.7	1.393	4.76
				$f = 0.7$						
335	69.5	55.8(88%)	121	5.3(8%)	50	2.2	6	6.2	1.389	4.27
339	69.1	53.8(85%)	107	6.9(11%)	52	2.4	6	6.2	1.389	4.27
345	68.2	49.6(80%)	92	9.7(16%)	54	2.6	6	6.3	1.388	4.37
351	67.2	43.1(71%)	81	14.9(24%)	55	2.9	6	6.3	1.388	4.37
357	66.3	38.2(63%)	73	18.8(31%)	54	3.1	7	6.2	1.387	4.28
363	65.7	17.0(29%)	73	39.2(66%)	55	3.2	6	6.3	1.387	4.38

a) Error bar for ε_0 is typically ± 2, and time constants are better than $\pm 5\%$ of the tabulated values. Numbers within parenthesis indicate percentages of the dispersion amplitudes with respect to the total dispersion detected.

Note such a value for the rotating radius is quite close to the hydrodynamic radius of urea molecule (r $=1.8$ Å)[47] but somewhat smaller than both the hard sphere radius of urea ($r_{HS} = 2.5$ Å)[49,50] and the radius of acetamide (r = 2.25 Å)[31]. However, considering the uncertainty involved in determining the rotating radius by using the SED for H-bonded non-spherical molecular liquids and the small difference between the radius of acetamide and that from SED for urea, it is difficult to unambiguously assign τ_1 to the molecular rotation of

either free urea or acetamide. In addition, this range of rotating radius negates the involvement of individual rotations of polymeric species[36] formed via H-bonding between urea and acetamide molecules. However, presence of extensive H-bond interactions between acetamide and urea may lead to a DR time scale very similar to that associated with the collective inter-species H-bond relaxation. This is reminiscent of what we have observed before for molten acetamide[31,51] and therefore a cooperative mechanism for τ_1 cannot be ruled out. It is noteworthy that in molten urea we have also observed a time constant of ~90 ps though the viscosity of the medium is almost ten times smaller than the viscosity of the DES systems. So the hundreds of picoseconds component, which is common for both pure and doped systems, is probably arising due to the collective H-bond dynamics and as the DESs contain extensive H-bonds, this component is the major relaxation process for DESs.

The second, relatively faster time constant, τ_2, lies in ~40-55 ps range which bears a close resemblance to the slowest time constant (~55 ps) detected for neat molten acetamide,[31] and second slowest time component (~30 ps) for molten urea. The corresponding dispersion amplitude ($\Delta\varepsilon_2$) for τ_2 is uniformly larger at all temperatures in the DES with higher acetamide concentration (f =0.7). Moreover, the temperature dependence for $\Delta\varepsilon_2$ is stronger than for τ_2 with $\Delta\varepsilon_2$ exhibiting greater temperature effects at f =0.7 than at f =0.6. Note that the ratio, τ_1/τ_2, becomes even less than 2 at higher temperatures, questioning the acceptability of the resulting 3-D fit parameters. A refit of these data using 2-D model, however, provides a worse description than that obtained by 3-D model (see Fig. A.b.4), justifying the use of the latter for a uniform description of all the DR spectra collected here.

We next estimate the activation energies ($E_a^{DES}(\langle \tau_{av}^{DR} \rangle)$) associated with the slower components of the DR in these DESs from the amplitude-averaged relaxation times, $\langle \tau_{av}^{DR} \rangle = \sum_{i=1}^{2} a_i \tau_i \Big/ \sum_{i=1}^{2} a_i$, where the amplitudes (a_i) and the time constants (τ_i) are taken from Table 4.1. Fig. 4.4 presents the temperature dependence of the average relaxation times which depicts an Arrhenius-type of temperature dependence with activation energies, 23.6 kJ/mol at f=0.6 and 23.3 kJ/mol at f=0.7, respectively. Temperature dependence of τ_1 alone (not shown here) also provides similar activation energies: 23.9 kJ/mole at f=0.6 and 22.8

kJ/mol at f=0.7. These activation energies are quite similar to that (21.6 kJ/mol) obtained for molten urea but lower than those for η (shown in Fig. A.b.5, Appendix) which are 32.3 kJ/mole at f=0.6 and 30.8 kJ/mol at f=0.7.
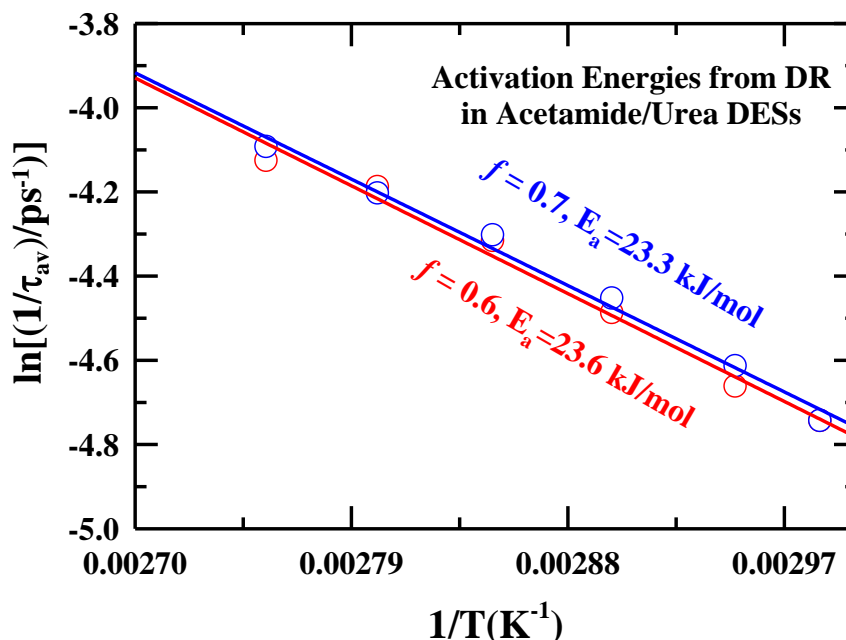
Fig. 4.4: Composition dependent activation energies from DR times in acetamide/urea DESs via Arrhenius plots. Inverse of the amplitude-averaged times considering only the first two slow time constants (τ_1 and τ_2) are shown as a function of inverse temperature in semi-logarithmic fashion. Solid lines represent linear fits through the respective data sets. Representations are color-coded.

Interestingly, temperature dependent fluorescence anisotropy measurements using a dipolar probe, coumarin 153 (C153), in these DESs provide activation energies for solute rotation (33.9 kJ/mol and 31.2 kJ/mol at f=0.6 and 0.7, respectively)[26] which are quite close to those from η but ~1.3-1.5 times larger than those from DR measurements. This probably reflects a difference in the coupling to the viscous friction between the rotational relaxations probed by dynamic fluorescence anisotropy measurements (using a foreign dipolar solute) and DR measurements (where rotating dipolar moiety is a part of the un-doped system itself). Fig. 4.5 explores the viscosity coupling of $\left\langle \tau_{av}^{DR} \right\rangle$ by showing the $(\eta/T)^p$ dependence of the average DR times in a double-logarithmic fashion. For a comparison, results obtained from

fluorescence anisotropy measurements using C153 in these DESs[26] are also shown. Viscosity coupling for τ_1 is examined in Fig. A.b.6 (Appendix) and compared with C153 rotation data. These two figures clearly show that C153 interacts more extensively with η during anisotropy relaxation than the rotating moiety during DR because the fraction power (p) for C153 is near unity and larger than that ($p \sim 0.6\text{-}0.7$) obtained from DR measurements.

Note a difference in viscosity coupling can emerge for rotating bodies of disparate sizes in heterogeneous media due to a competition between the rotor size and the dynamically correlated domain size (heterogeneity length-scale).[71-73] Therefore, the contrasting p values observed here may be attributed to the varying sizes of the rotors involved with these two different experiments. Such an observation also suggests that ($acetamide + urea$) DESs are dynamically heterogeneous media although they may not be as heterogeneous as ($acetamide + electrolyt\,e$) systems.[16-20]
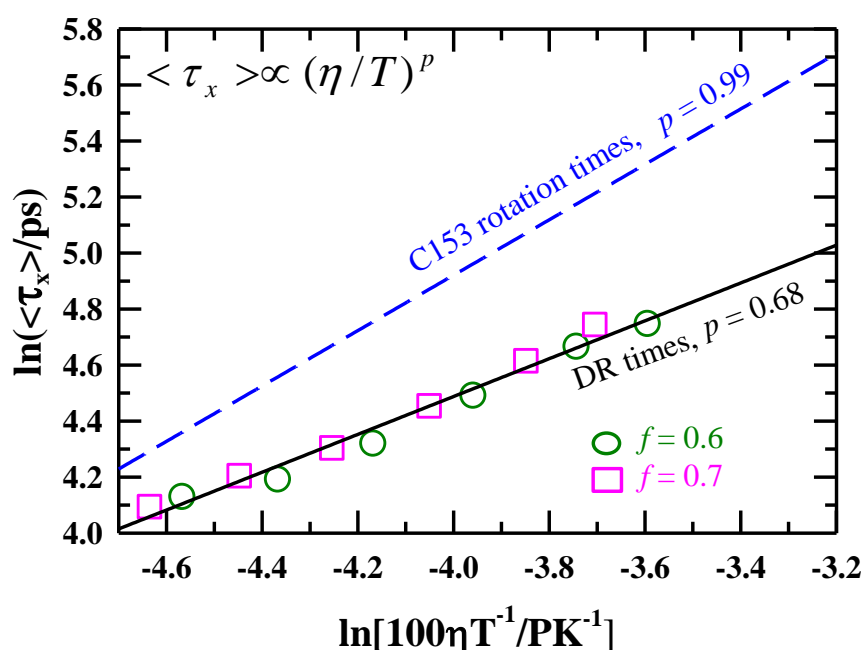
Fig. 4.5: A comparison of viscosity coupling to rotation times between DR and dynamic fluorescence anisotropy relaxation. Measured average relaxation times are shown as a function of temperature-reduced viscosity, $\left(\dfrac{\eta}{T}\right)$. DR times for both the compositions are shown by different symbols. Fit through these data points (considering a single set) is denoted by the black solid line. Fit obtained from C153 rotation times in these DESs reported in Ref. 26 is shown by the blue dashed line.

Inter-twining of rotation with structural H-bond relaxation can make dynamic heterogeneity more prominent for DR. In contrast, rotational relaxation of a relatively larger foreign solute, C153, predominantly involves orientational displacements of the surrounding solvent molecules, experiencing the full frictional resistance from the medium. A comparison between dielectric and fluorescence anisotropy relaxations for ($urea + choline\ chloride$) deep eutectics would be interesting in this regard as these systems appeared 'homogeneous' in fluorescence anisotropy relaxation measurements.[74]

4.4 Conclusion

In summary, the present paper reports first dielectric relaxation measurements of molten urea and ($acetamide + urea$) deep eutectics, characterizing the polarization relaxations in the frequency range, $0.2 \leq \nu/\text{GHz} \leq 50$. Large values for the static dielectric constant ($\varepsilon_0 \sim 67$) and dipole moment ($\mu \sim 6.0\,D$) explains the extensive solvating power of molten urea. The detected relaxation for molten urea, like in acetamide, requires two Debye processes for adequate description whereas a third slower Debye process emerges when urea forms deep eutectics with acetamide. Estimated ε_0 values for these DESs ($\varepsilon_0 \sim 65-70$) are not very different from that either for molten urea or for molten acetamide ($\varepsilon_0 \sim 64$). This is in contrast to what we have observed for ($acetamide + electrolyte$) DESs before[31] and means that not only the solvating power of the mixture components is preserved in the deep eutectics but this power is now accessible also at temperatures much lower than the individual melting temperatures of both the components. Large scale industrial applications for ($acetamide + urea$) DESs stem from these important solvent and economic aspects. Interestingly, the static dielectric constant for molten urea ($\varepsilon_0 \sim 67$) found here is much larger than that ($\varepsilon_0 = 3$) reported for urea in the solid state.[56]

The temperature dependence of ε_0 for these DESs reveals, like many common dipolar solvents and their mixtures,[75-77] a decreases of ε_0 with increase of temperature due to thermal randomization of the constituent dipoles. The temperature coefficient, -dε_0/dT, for these DESs has been found to be ~0.13 (see Fig. A.b.7) which is smaller than that (~0.37) estimated for water[75] but larger than those reported for several imidazolium cation based ionic liquids.[70] Polarities represented by the difference in reaction field factor,[67,77]

$$\Delta f(\varepsilon_0, n_D) = \frac{\varepsilon_0 - 1}{\varepsilon_0 + 2} - \frac{n_D^2 - 1}{n_D^2 + 2},$$ for both molten urea and these (*acetamide* + *urea*) DESs are similar to several strongly polar common solvents, such as, acetonitrile, propylene carbonate, ethanol, methanol and formamide. In addition, similar values of $\Delta f(\varepsilon_0, n_D)$ for both molten urea and (*acetamide* + *urea*) DESs explain composition independence of spectral properties observed in earlier fluorescence measurements.[26]

Temperature dependent DR measurements of (*acetamide* + *urea*) deep eutectics provide activation energies very similar to that for molten urea but significantly lower than those from both temperature dependent viscosity and fluorescence anisotropy measurements. An inspection of the viscosity coupling to the rotational motions probed by these different experiments (DR and fluorescence anisotropy) reveals fractional viscosity dependence for the slowest DR time scale but a hydrodynamic behavior for fluorescence anisotropy relaxation. This contrasting observation may be construed as DR being more efficient in probing the heterogeneous dynamics of a given medium than fluorescence anisotropy relaxation. This is a distinct possibility as DR in these extensively H-bonded systems couples dipolar rotation to H-bond relaxation via the waiting time for finding a suitable partner at a proper orientation to form a new H-bond after breaking a pre-existing one and subsequent rotation. The observed time scales obtained from the experiments are also in good agreement with the simulated H-bond correlations (for details see A.b.8 in Appendix). Note, we have separately considered various types of H-bonds in (*acetamide* + *urea*) DESs for a better understanding of the microscopic details. Temperature and ion dependent DR relaxation of various industrially relevant DESs along with simulated interpretations will constitute our future works.

References

1. D. V. Wagle, H. Zhao and G. A. Baker, Acc. Chem. Res. **47**, 2299 (2014).

2. Q. Zhang, K. D. O. Vigier, S. Royer and F. Jérôme, Chem. Soc. Rev. **41**, 7108 (2012).

3. A. P. Abbott, G. Capper, D. L. Davies, R. K. Rasheed and V. Tambyrajah, Chem. Commun. 70 (2003).

4. A. P. Abbott, D. Boothby, G. Capper, D. L. Davies and R. K. Rasheed, J. Am. Chem. Soc. **126**, 9142 (2004).

5. M. Francisco, A. van den Bruinhorst and M. C. Kroon, Angew. Chem. Int. Ed. **52**, 3074 (2013).

6. P. Liu, J.-W. Hao, L.-P. Mo and Z.-H. Zhang, RSC Adv. (2015).

7. G. García, S. Aparicio, R. Ullah and M. Atilhan, Energy Fuels **29**, 2616 (2015).

8. D. Carriazo, M. C. Serrano, M. C. Gutiérrez, M. L. Ferrer and F. del Monte, Chem. Soc. Rev. **41**, 4996 (2012).

9. M. Francisco, A. van den Bruinhorst and M. C. Kroon, Green Chem. **14**, 2153 (2012).

10. H. Zhao and G. A. Baker, J. Chem. Technol. Biotechnol. **88**, 3 (2013).

11. G. van der Zwan and J. T. Hynes, Chem. Phys. **152**, 169 (1991).

12. G. van der Zwan and J. T. Hynes, J. Chem. Phys. **78**, 4174 (1983).

13. A. Nitzan, *Chemical Dynamics in Condensed Phases.* (Oxford University Press, Oxford, U.K, 2006).

14. T. Pradhan and R. Biswas, J. Phys. Chem. A **111**, 11514 (2007).

15. T. Pradhan, H. A. R. Gazi and R. Biswas, J. Chem. Phys. **131**, 054507 (2009).

16. B. Guchhait, H. A. R. Gazi, H. K. Kashyap and R. Biswas, J. Phys. Chem. B **114**, 5066 (2010).

17. B. Guchhait, S. Daschakraborty and R. Biswas, J. Chem. Phys. **136**, 174503 (2012).

18. H. A. R. Gazi, B. Guchhait, S. Daschakraborty and R. Biswas, Chem. Phys. Lett. **501**, 358 (2011).

19. B. Guchhait, S. Das, S. Daschakraborty and R. Biswas, J. Chem. Phys. **140**, 104514 (2014).

20. A. Das, S. Das and R. Biswas, Chem. Phys. Lett. **581**, 47 (2013).

21. T. Pal and R. Biswas, Chem. Phys. Lett. **517**, 180 (2011).

22. R. Biswas, A. Das and H. Shirota, J. Chem. Phys. **141**, 134506 (2014).

23. S. N. Tripathy, Z. Wojnarowska, J. Knapik, H. Shirota, R. Biswas and M. Paluch, J. Chem. Phys. **142**, 184504 (2015).

24. L. Walbrugh, "Amitraj solid dosage form," M.S. thesis (University of Pretoria, Pretoria, South Africa, 2006).

25. S. Rajkhowa, A. Das, S. Mahiuddin and R. Biswas, J. Chem. Eng. Data **57**, 3467 (2012).

26. A. Das, S. Das and R. Biswas, J. Chem. Phys. **142**, 034505 (2015).

27. G. Berchiesi, J. Mol. Liq. **83**, 271 (1999).

28. G. Berchiesi, G. Vitali, R. Plowiec and S. Barocci, J. Chem. Soc. Faraday Trans. 2 **85**, 635 (1989).

29. G. Berchiesi, G. Vitali, P. Passamonti and R. Płowiec, J. Chem. Soc. Faraday Trans. 2 **79**, 1257 (1983).

30. G. Berchiesi, G. Rafaiani, G. Vitali and F. Farhat, J. Therm. Anal. Calorim. **44**, 1313 (1995).

31. K. Mukherjee, A. Das, S. Choudhury, A. Barman and R. Biswas, J. Phys. Chem. B **119**, 8063 (2015).

32. P. K. Mandal, M. Sarkar and A. Samanta, J. Phys. Chem. A **108**, 9048 (2004).

33. Z. Hu and C. J. Margulis, Proc. Natl. Acad. Sci. U.S.A. **103**, 831 (2006).

34. T. Pradhan, P. Ghoshal and R. Biswas, J. Phys. Chem. A **112**, 915 (2008).

35. M. C. Stumpe and H. Grubmüller, J. Phys. Chem. B **111**, 6220 (2007).

36. A. S. Mahadevi, Y. I. Neela and G. N. Sastry, Phys. Chem. Chem. Phys. **13**, 15211 (2011).

37. C. J. F. Böttcher and P. Bordewijk, *Theory of Electric Polarization.* (Elsevier: Amsterdam, The Netherlands, 1978).

38. F. Kremer and A. Schönhals, *Broadband Dielectric Spectroscopy.* (Springer, Berlin, Germany, 2003).

39. P. R. Bevington and D. K. Robinson, *Data Reduction and Error Analysis.* (McGraw–Hill, New York, 2003).

40. S. Taniewska-Osińska, R. Łogwinienko and J. Mokrzan, Thermochim. Acta **167**, 73 (1990).

41. P. M. Schaber, J. Colson, S. Higgins, D. Thielen, B. Anspach and J. Brauer, Thermochim. Acta **424**, 131 (2004).

42. B. Bagchi, *Molecular Relaxation in Liquids.* (Oxford University Press, New York, 2012).

43. J. L. Dote, D. Kivelson and R. N. Schwartz, J. Phys. Chem. **85**, 2169 (1981).

44. M.-L. Horng, J. Gardecki and M. Maroncelli, J. Phys. Chem. A **101**, 1030 (1997).

45. A. Das, R. Biswas and J. Chakrabarti, J. Phys. Chem. A **115**, 973 (2011).

46. A. Das, R. Biswas and J. Chakrabarti, Chem. Phys. Lett. **558**, 36 (2013).

47. S. G. Schultz and A. K. Solomon, J. Gen. Physiol. **44**, 1189 (1961).

48. G. Jones and S. K. Talley, J. Am. Chem. Soc. **55**, 624 (1933).

49. S. Cabani, P. Gianni, V. Mollica and L. Lepori, J. Solution Chem. **10**, 563 (1981).

50. G. Graziano, J. Phys. Chem. B **105**, 2632 (2001).

51. S. Das, R. Biswas and B. Mukherjee, J. Phys. Chem. B **119**, 11157 (2015).

52. P. O. Åstrand, A. Wallqvist, G. Karlström and P. Linse, J. Chem. Phys. **95**, 8419 (1991).

53. J. Barthel, R. Buchner and B. Wurm, J. Mol. Liq. **98**, 51 (2002).

54. C. G. Gray, K. E. Gubbins and C. G. Joslin, *Theory of Molecular Fluids 2: Applications. International Series of Monographs on Chemistry.* (Oxford University Press, 2011).

55. E. Bergmann and A. Weizmann, Trans. Faraday Soc. **34**, 783 (1938).

56. W. Kumler and G. M. Fohlen, J. Am. Chem. Soc. **64**, 1944 (1942).

57. E. A. Cavell, P. Knight and M. Sheikh, Trans. Faraday Soc. **67**, 2225 (1971).

58. M. Bešter-Rogač, A. Stoppa, J. Hunger, G. Hefter and R. Buchner, Phys. Chem. Chem. Phys. **13**, 17588 (2011).

59. R. Biswas and B. Bagchi, J. Chem. Phys. **105**, 7543 (1996).

60. R. Biswas and B. Bagchi, J. Phys. Chem. A **103**, 2495 (1999).

61. H. K. Kashyap, T. Pradhan and R. Biswas, J. Chem. Phys. **125**, 174506 (2006).

62. S. Daschakraborty, T. Pal and R. Biswas, J. Chem. Phys. **139**, 164503 (2013).

63. S. Daschakraborty and R. Biswas, J. Chem. Phys. **137**, 114501 (2012).

64. N. Nandi, S. Roy and B. Bagchi, J. Chem. Phys. **102**, 1390 (1995).

65. S. Roy and B. Bagchi, J. Chem. Phys. **99**, 9938 (1993).

66. S. Roy and B. Bagchi, J. Chem. Phys. **99**, 1310 (1993).

67. M. Horng, J. Gardecki, A. Papazyan and M. Maroncelli, J. Phys. Chem. **99**, 17311 (1995).

68. B. Bagchi and R. Biswas, Adv. Chem. Phys. **109**, 207 (1999).

69. C. Ro, L. Thrane, P.-O. Åstrand, A. Wallqvist and K. V. Mikkelsen, J. Chem. Phys. **107**, 5319 (1997).

70. J. Hunger, A. Stoppa, S. Schrödle, G. Hefter and R. Buchner, ChemPhysChem. **10**, 723 (2009).

71. M. D. Ediger, Annu. Rev. Phys. Chem. **51**, 99 (2000).

72. W. Huang and R. Richert, Philos. Mag. **87**, 371 (2007).

73. T. Pal and R. Biswas, J. Chem. Phys. **141**, 104501 (2014).

74. A. Das and R. Biswas, J. Phys. Chem. B **119**, 10102 (2015).

75. R. Buchner, J. Barthel and J. Stauber, Chem. Phys. Lett. **306**, 57 (1999).

76. P. Petong, R. Pottel and U. Kaatze, J. Phys. Chem. A **104**, 7420 (2000).

77. H. A. R. Gazi and R. Biswas, J. Chem. Sci. **123**, 265 (2011).

Chapter 5

Temperature Dependent Dielectric Relaxation Dynamics of (Acetamide + Electrolyte) Deep Eutectics in the Frequency Window, $0.2 \leq \nu(GHz) \leq 50$

5.1 Introduction

Deep eutectic solvents (DESs) are fast evolving as probable replacements for ionic liquids (ILs). This is because DESs can offer desired solvent properties at a much lower cost and, in several cases, they leave minimum ecological footprints.[1-5] The "greenness" of ILs is now intensely debated for they are poorly biodegradable and biocompatible, raising concern regarding their use a sustainable reaction media.[6-8] DESs, in contrast, are in many cases environmentally benign and thus becoming a good alternative to ILs in industrial applications.[9-10] For example, DESs have found application in organic synthesis,[11] catalysis,[12] gas absorption,[13] electrochemistry[14] etc. Moreover, these DESs can be both ionic and non-ionic in character whereas ILs are always ionic. DESs are mixtures of two or more solid substances in a certain mole fraction where the mixtures, upon melting at a temperature much lower than the melting temperatures of the individual components, can sustain a stable liquid phase for a very long time. It is believed that extensive interspecies H-bonding and the entropic gain for being in the liquid state are the main driving force behind the formation of stable liquid phase.

Although DESs offer exquisite solvent systems, microscopic understanding of interactions and dynamics is still lacking. The importance of such an understanding arises because several physico-chemical properties, such as, polarity, viscosity, and conductivity, can play key roles in deciding the rate of a reaction occurring in them.[15-19] Excitation wavelength dependent steady

70

state fluorescence emission measurements[20-21] have already suggested presence of spatial heterogeneity in several ($acetamide + electrolyte$) DESs.[22-25] Subsequently, time resolved fluorescence (TRF) experiments along with simulation studies have reported that some of these DESs are dynamically heterogeneous too.[26-27] Interestingly, although the TRF studies in the ($acetamide + urea$) non-ionic DESs suggest homogeneity in solution dynamics,[28] DR measurements may reveal a different feature as dynamic fluorescence anisotropy and DR measurements probe dipolar rotation of different ranks. Interestingly, recent simulation studies of DESs containing acetamide have revealed presence of large angle orientation jumps for acetamide molecules in these multi-component molten systems. [29-32]

In this work, we have investigated the temperature dependence of DR dynamics and anion effects on it for three ($acetamide + electrolyte$) DESs. Although several attempts [26-27,33-37] have already been made to understand the temperature and ion effects of deep eutectic dynamics, there remain several aspects that need to be understood for smarter use of these solvent systems. The present work investigates solution dynamics to gain understanding in this direction. Here we have chosen lithium salts of bromide, nitrate and perchlorate because these systems have been examined before by steady state and time-resolved fluorescence spectroscopy and thus previous reports will help to generate a proper interpretation of the measured DR data. These DESs are prepared with the mole ratio, acetamide:electrolyte:: 80:20, and remain as a stable liquid at 293 K after melting at higher temperature. Reported glass transition temperatures (T_gs) of these DESs are ~200 K [20,27] and there the temperature range considered in our study is ~100 -160 K above the respective T_gs.

DRS probes the collective response of a medium to a time-dependent electrical field.[38-40] It is a useful technique to study the collective reorientation dynamic of dipolar molecules in liquid state.[41-46,67] Because these systems support extensive H-bonding, DR will bear signature of H-bond relaxation dynamics as well. Note the present measurements are done within a frequency window, $0.2 \leq \nu(GHz) \leq 50$, and therefore, slower dynamics beyond nanosecond cannot be probed. This is a serious limitation of the present endeavour; however, the attempt being the first would be useful to gain qualitative understanding of collective orientational relaxation in these complex systems.

5.2 Experimental Details

5.2.1 Materials and Methods

Acetamide ($\geq$99%, Sigma-Aldrich, India), lithium bromide ($\geq$99%, Sigma-Aldrich), lithium nitrate ($\geq$99%, SRL, India) and lithium perchlorate ($\geq$99%, Fluka) were vacuum-dried (~300 K) overnight before use. Samples were prepared and relevant experiments were done in a tightly humidity - controlled environment. Further details regarding sample preparation could be found elsewhere as these DESs were already studied via fluorescence measurements.[20,27] Briefly, the sample vessels were sealed and heated slowly to ~350 K until it formed a clear melt. Once a liquid phase is obtained, the heat-source was removed and the melt was allowed slowly to reach the room temperature or the lowest temperature it is known to be in liquid phase. Aliquots from this were then used for measurements.

5.2.2 DR Measurement Details

The DR data collection technique and the data analysis procedures are the same as described in chapter 2 and in previous works.[47-48] Approximately 8-10 mL of thermally equilibrated molten sample (DESs and neat acetamide) in a properly humidity-controlled environment were used for measurements in each case. We took 1001 data points for each DR measurements. Temperature dependent DR measurements for these DESs were carried out by using a heating plate (MS-H-Pro from SCILOGEX, USA). We used a thermometer which was set at the same plane of the probe end to estimate the temperature more accurately and to avoid the misinterpretation of sample temperature which can arise due to gradient heating as we were using a heating plate. In all measurements desired experimental temperatures were sufficiently stable for conducting repeat (at least three) recordings.

5.3 Results and Discussion

5.3.1 ε_0 of ($acetamide + electrolyte$) DESs: Temperature Dependence

Fig. 5.1 depicts the temperature dependent ε_0 values for the three DESs. Before going to our results, let us concentrate on the temperature dependent behaviour of ε_0 for the conventional solvents, like water,[49] alcohols,[50] amides[51] etc. For most of the solvents it has been found that

with increasing temperature ε_0 value decreases.[52] For example, if we look at the temperature dependent dielectric response of pure water,[49] we will find that an increase of 35°C in temperature results ~10% depression in ε_0 value. For all the three DESs, the ε_0 value increases with temperature, except for ClO_4^- containing system. For this system, ε_0 increases first then decreases. Interestingly, the pattern of increase in ε_0 value depends on the anion identity of the electrolyte and the extent of increase is the maximum (~63%) for Br^- and the minimum (~7%) for ClO_4^-. It is noteworthy that neither a plateau in $\varepsilon'(\nu)$ nor a peak in $\varepsilon''(\nu)$ is observed in the DR spectra (see Fig. 5.2), especially in the low temperature spectra, so making an accurate estimation of ε_0 value for these DESs associates with large error bar. But from our estimated temperature dependent ε_0 values it is clear that with increasing temperature the polarity of the medium increases.

Although the increase of ε_0 with temperature is rare for conventional solvents, few carboxylic acids, such as, acetic acid and trifluoroacetic acid show similar temperature dependent behaviour.[52] With increasing temperature ε_0 decreases because of the increased thermal randomization of the dipolar static correlations. The increase in ε_0 for those carboxylic acids has been explained in terms of breakage of dimers that have formed with anti-parallel orientation of their intrinsic dipoles into monomers releasing the individual dipoles to contribute constructively to the medium polarity. For these carboxylic acids, therefore, the temperature –assisted dissociation of dimers is reflected on the temperature-induced increase of ε_0. It is well known that these DESs posses extensive inter- and intra-species H-bonding. Hence, we propose that those acetamide molecules which, due to ion solvation, were irrotationally bound [53-54] to the ions, are increasingly released upon successive increase of temperature and allowed to participate to the medium dielectric relaxation. As a result, the ε_0 value of the system increases, overriding the effects of thermal randomization.
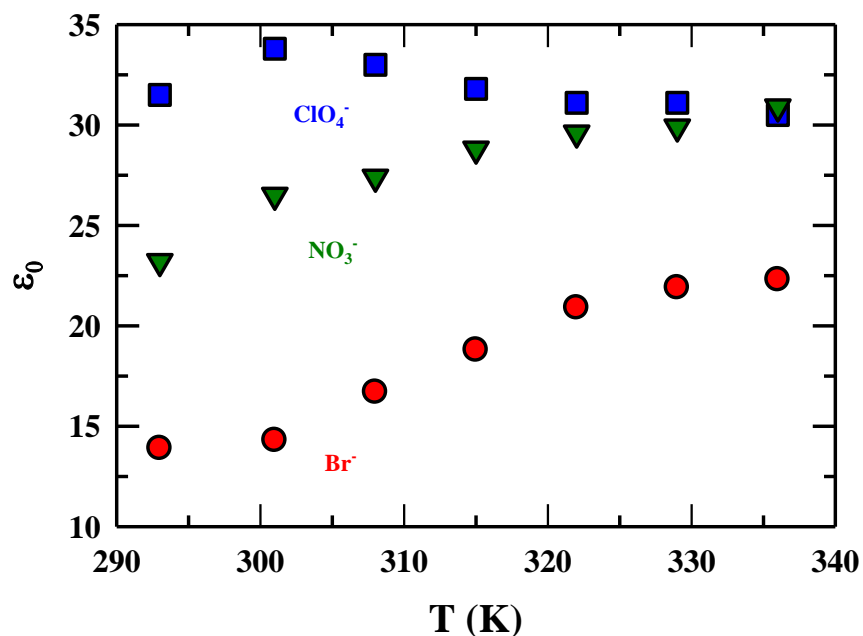
Fig. 5.1: Temperature dependence of estimated static dielectric constant (ε_0) for the three DESs. Specific identities of ion-containing DESs are color coded.

Now we will concentrate on the effects of anion identity on the temperature dependent behaviour of ε_0 for these DESs. From Fig. 5.1, it is clear that ClO_4^- system behaves somewhat differently from the other two systems. Initially, the ε_0 for the ClO_4^- system increases with temperature and then decreases, whereas for the other two systems the ε_0 values increase continuously with temperature up to 336 K. The reason may be that the number of irrotationally bound acetamide molecules in ClO_4^- system is not as many as in the other two systems. Note that not only the ε_0 value but also the ε_∞ value depends on the anion identity (see Table A.c.4, Appendix).

5.3.2 DR Time Scales in (*acetamide* + *electrolyte*) DESs: Temperature Dependence

5.3.2.1 Temperature Effect on τ_4

Fig. 5.2 and Figs. A.c.1 and A.c.2 (Appendix) represent the temperature dependent DR spectra of the three (*acetamide* + *electrolyte*) DESs. Fig. A.c.3 is the representative plot which displays the residuals of DR data fitting. The extracted parameters from the DR spectra are tabulated in Table 5.1. We have attempted different fitting models such as multi-Debye, Cole-Cole and Cole-Davidson; it has been found that 4-Debye model, in most of the cases, produces the best description of the collected DR spectra. It has already been observed that a fast Debye relaxation component is required [55] to represent the measured spectra. An unconstrained fitting of these DR data produces a sub-10 ps component which (the timescale) remains nearly insensitive to the solution temperature. As a result, this timescale has been kept fixed. Note that in *LiBr* system, the contribution of this fast component is much lower compared to the other two systems. We believe that this fast, sub-10 ps component arises due to the N-H bond vector reorientation of the acetamide molecules.

5.3.2.2 Temperature Effects on τ_1 & τ_2

Next we discuss the possible origin and temperature dependence of τ_1 and τ_2. These ion-induced slow relaxations (τ_1 & τ_2) contribute ~80% to the total dielectric response. Although τ_1, the slowest time constant with the maximum contribution to the total DR response, follows the viscosity trend (see Table 5.1), τ_2 does not. However, the amplitude-averaged time scale considering τ_1 and τ_2 (that is, $\left\langle \tau_{av}^{DR} \right\rangle = \sum_{i=1}^{2} a_i \tau_i \left/ \sum_{i=1}^{2} a_i \right.$) follows the viscosity trend ($\eta_{bromide} > \eta_{nitrate} > \eta_{perchlorate}$). Interestingly, insertion of these time scales (τ_1 or $\left\langle \tau_{av}^{DR} \right\rangle$) in the SED relation,[56-60] $V_{eff} = k_B T \tau_r / 3\eta$, leads to a much smaller V_{eff} for acetamide than its V_m.
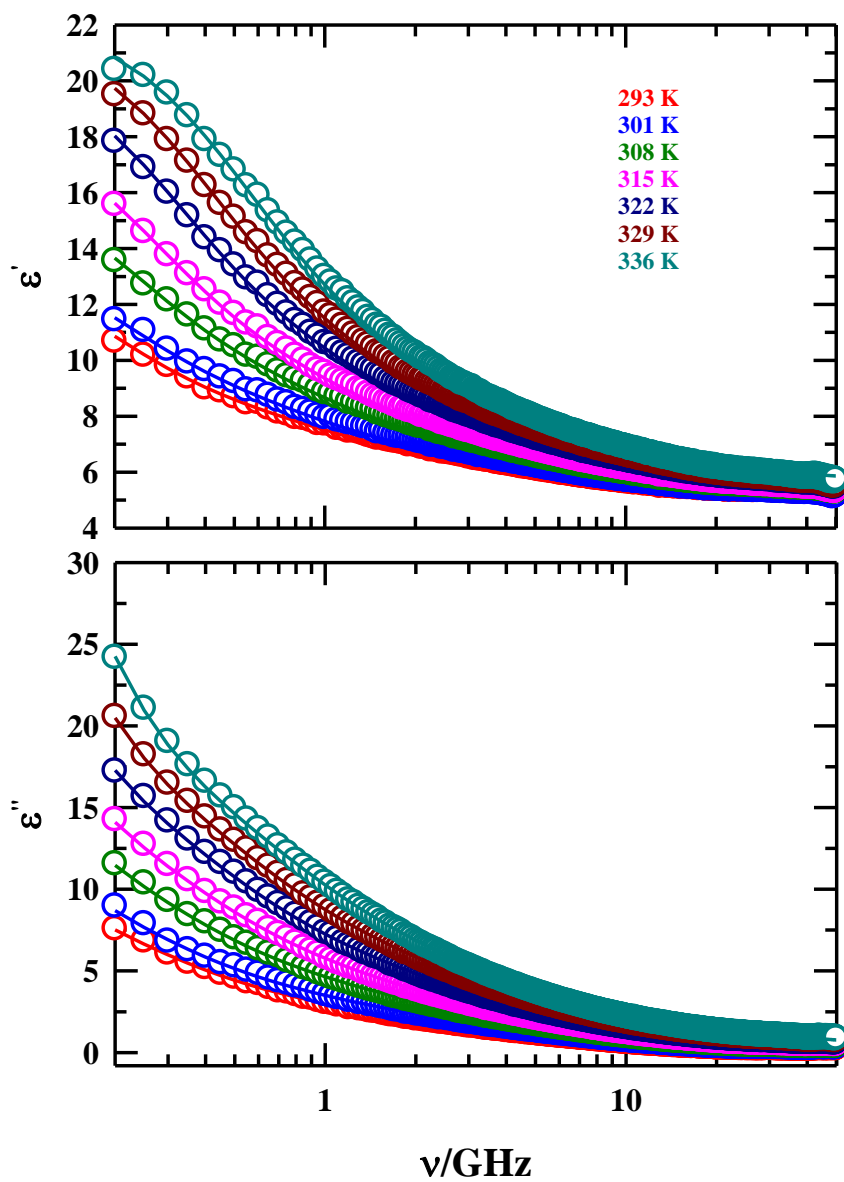
Fig. 5.2: Temperature dependence of the real (ε') and imaginary (ε'') parts of the measured DR spectra for ($acetamide + LiBr$) DES within the frequency regime $0.2 \leq \nu/\mathrm{GHz} \leq 50$. Solid lines through these data represent simultaneous fits using 4-Debye relaxation model.

Table 5.1: Parameters obtained from simultaneous 4-Debye fits to real (ε') and imaginary (ε'') components of the measured DR spectra for, ($acetamide + elecrolyte$), DES at various temperatures.

DESs	Temp.	ε_0 [a]	$\Delta\varepsilon_1$	τ_1 [c] (ps)	$\Delta\varepsilon_2$	τ_2 (ps)	$\Delta\varepsilon_3$	τ_3 (ps)	$\Delta\varepsilon_4$	τ_4 (ps)	ε_∞	χ^2	$\left\langle\tau_{av}^{DR}\right\rangle$ [d] (ps)
Acetamide + LiBr	293 K	13.9	5.7 (66%) [b]	832	1.7 (20%)	160	1.1 (13%)	36	0.1 (1%)	5	5.3	0.009	676
	301 K	14.3	5.6 (62%)	761	2.1 (23%)	162	1.2 (13%)	35	0.1 (1%)	5	5.3	0.010	599
	308 K	16.7	7.3 (65%)	667	2.5 (22%)	142	1.3 (11%)	32	0.2 (2%)	5	5.4	0.011	534
	315 K	18.8	8.9 (66%)	585	2.2 (16%)	131	1.4 (10%)	31	0.3 (2%)	5	5.4	0.013	496
	322 K	21.0	10.4 (67%)	491	3.2 (21%)	114	1.5 (10%)	28	0.4 (2%)	5	5.5	0.015	401
	329 K	21.9	10.9 (66%)	394	3.5 (21%)	100	1.5 (9%)	26	0.5 (3%)	5	5.5	0.017	323
	336 K	22.3	11.5 (69%)	300	3.2 (19%)	78	1.4 (8%)	24	0.5 (3%)	5	5.7	0.019	252
Acetamide + LiNO₃	293K	23.2	12.5 (72%)	702	2.9 (17%)	135	1.4 (8%)	38	0.5 (3%)	4	5.9	0.013	593
	301K	26.5	14.5 (71%)	560	3.6 (17%)	123	1.7 (8%)	34	0.6 (3%)	4	6.0	0.016	476
	308K	27.4	15.3 (71%)	460	3.9 (18%)	107	1.6 (7%)	30	0.8 (4%)	4	5.8	0.018	389
	315K	28.8	15.9 (69%)	385	4.5 (20%)	100	1.6 (7%)	27	1.0 (4%)	4	5.8	0.021	321
	322K	29.6	15.6 (66%)	325	5.3 (22%)	97	1.8 (8%)	25	1.0 (4%)	4	5.9	0.024	268
	329K	29.9	15.2 (63%)	275	5.8 (24%)	88	1.8 (8%)	23	1.2 (5%)	4	5.9	0.027	223
	336K	30.3	14.8 (61%)	233	6.5 (27%)	80	1.7 (7%)	21	1.3 (5%)	4	6.0	0.032	177
Acetamide + LiClO₄	293K	31.5	16.8 (66%)	592	4.6 (18%)	194	2.8 (11%)	52	1.2 (5%)	4	6.1	0.017	507
	301K	33.8	13.5 (49%)	490	9.1 (33%)	192	3.3 (12%)	45	1.5 (5%)	4	6.4	0.024	370
	308K	33.0	11.6 (43%)	376	10.2 (38%)	168	3.2 (12%)	42	1.7 (6%)	4	6.3	0.025	278
	315K	31.8	10.0 (39%)	282	10.0 (39%)	157	3.7 (15%)	41	1.8 (7%)	4	6.3	0.025	225
	322K	31.1	18.3 (74%)	168	-	-	4.2 (17%)	41	2.1 (9%)	4	6.5	0.031	168
	329K	30.5	17.9 (75%)	137	-	-	3.9 (16%)	36	2.2 (9%)	4	6.5	0.034	137
	336K	30.5	17.5 (73%)	117			4.0 (17%)	34	2.4 (10%)	4	6.6	0.041	117

a) ε_0 values are associated with error bar ± 2.0 (based on three independent measurements).

b) Numbers within the parenthesis indicates the amplitude of the dispersion step in percentage.

c) $\tau_i (i=1\text{-}3)$ are better within $\pm 5\%$ of the enlisted values (based on three independent measurements).

d) $\left\langle \tau_{av}^{DR} \right\rangle = \sum_{i=1}^{2} a_i \tau_i \bigg/ \sum_{i=1}^{2} a_i =$ amplitude-averaged DR times.

This suggests that τ_1 does not involve either the full molecular rotation of acetamide in these ionic deep eutectics or the rotating moiety does not experience the full frictional hindrance exerted by the macroscopic viscosity of the medium. Recently reported simulation studies on reorientational dynamics and H-bond dynamics in ($acetamide + electrolyte$) DESs suggests that both the reorientational relaxation and structural H-bond fluctuation dynamics contain nanosecond relaxation components for these DESs and these relaxations arise due to the ion-acetamide interactions.[68] It has been proposed that ion-acetamide interaction is the main reason behind the slow dynamics of acetamide molecules in ionic ionic acetamide deep eutectics. Interestingly, it has been observed that the total amplitude of τ_1 and τ_2 in our measurements remain more or less constant (except for $LiClO_4$ at higher temperatures) throughout the temperature range considered, which indicates that the origin of this two time components are probably the same – ion-complexed acetamide molecules. DR measurements, with proper elimination of the conductivity contribution at the low frequency regime (< 100 MHz) should be carried out to examine this proposition.

Fig. 5.3 depicts the temperature dependence of $\left\langle \tau_{av}^{DR} \right\rangle$ which reflects an Arrhenius type temperature dependence. Subsequently, we have estimated the activation energies ($E_a{}^{DR}$) for the three DESs. It has been observed that the three $E_a{}^{DR}$ are, to some extent, higher than the E_a^{DR} for molten acetamide[69] and they show significant anion dependence. Since solvation time scales closely follows the DR time scales, it will be appropriate to have a comparison between these two activation energies for each DESs which is presented in Table 5.2. And such a comparison shows that these E_a^{DR} values are close to the activation energies estimated from average solvation time of a fluorescent dipolar probe molecule [27] in these DESs. Moreover, similar kinds of activation energies have been reported for the slow DR relaxation of ionic liquids. [43] In order to understand the viscosity coupling of $\left\langle \tau_{av}^{DR} \right\rangle$ we plotted $\left\langle \tau_{av}^{DR} \right\rangle$ as a function of temperature-scaled viscosity, (η/T), in Fig. 5.4. Subsequently, it has been found that the $\left\langle \tau_{av}^{DR} \right\rangle$ exhibits fractional power law, $\langle \tau_{av}^{DE} \rangle \propto (\eta/T)^p$, where p values depend on anion identity. This type of power law dependence of the relaxation times has already been observed for the time-resolved

fluorescence studies in these DESs[20,27] and it is the manifestation of temporal heterogeneity.[61-65] Table 5.2 displays the comparison between the p values extracted from DR measurements and solvation dynamics studied for these three DESs. Table 5.2 clearly shows that the values of the enlisted parameters (E_a^X and p) for the two different experimental techniques are very similar.
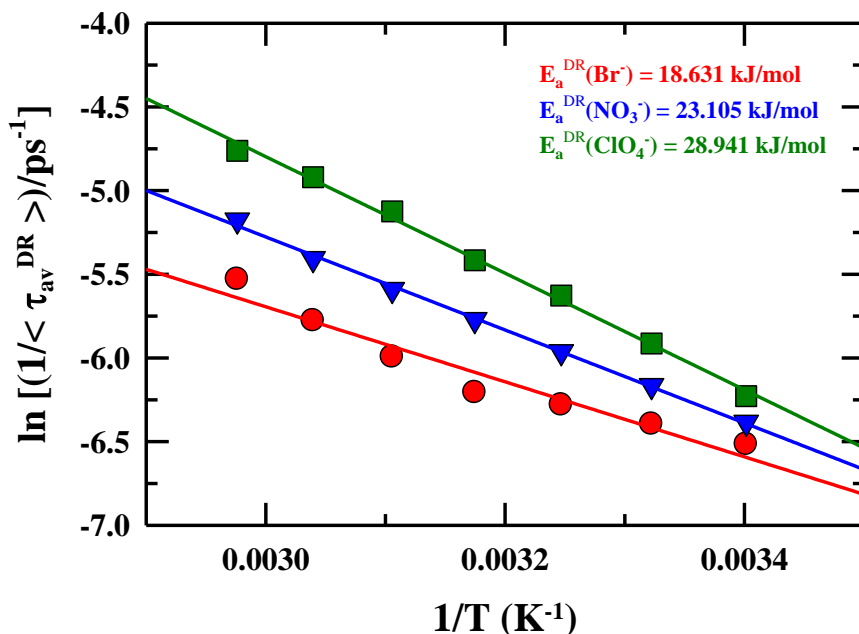
Fig. 5.3: Anion dependent activation energies from amplitude-averaged DR times ($\left\langle \tau_{av}^{DR} \right\rangle = \sum_{i=1}^{2} a_i \tau_i \Big/ \sum_{i=1}^{2} a_i$) in (*acetamide + electrolyte*) DESs via Arrhenius plots. Inverse of the $\left\langle \tau_{av}^{DR} \right\rangle$ is shown as a function of inverse temperature in semi-logarithmic fashion. Solid lines represent linear fits through the respective data sets. Representations are, as before, color coded.
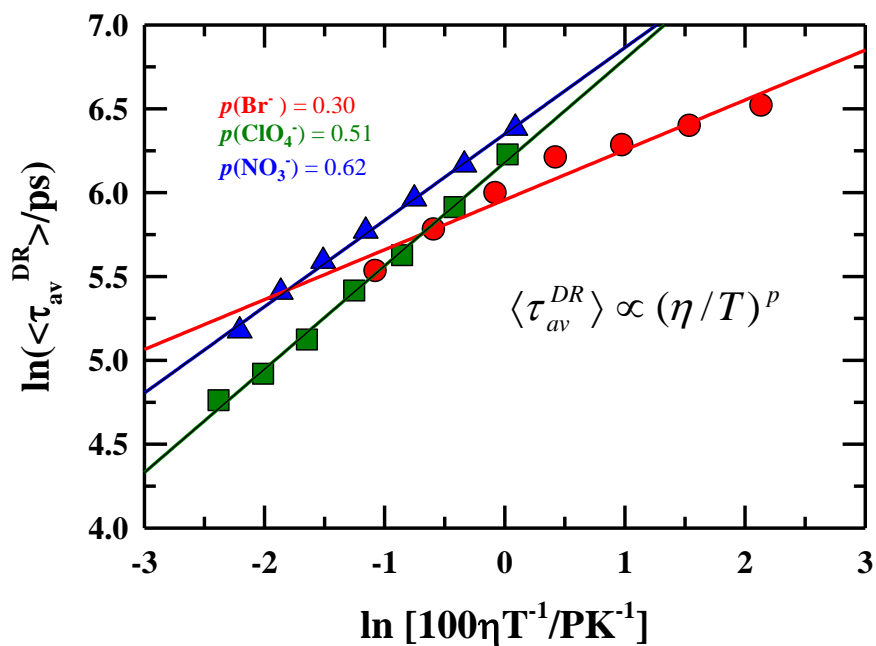
Fig. 5.4: $\left(\dfrac{\eta}{T}\right)$ dependence of amplitude-averaged DR time ($\langle \tau_{av}^{DR} \rangle$) for the three DESs. Solid lines represent the fits through the all $\langle \tau_{av}^{DR} \rangle$ data. Specific identities of anions are shown in the inset.

5.3.2.3 Temperature Effect on τ_3

Next we discuss the effects of temperature on τ_3. Similar relaxation timescale has already been reported for molten acetamide. In our previous dielectric study in ($acetamide + urea$) system,[69] we have also observed a similar DR timescale which correlates to the H-bond relaxation through reorientation of acetamide molecules. Now the question is- what is the origin of this relaxation time component in these ionic DESs, where the viscosity of the medium is ~1000 times higher than the viscosity of molten acetamide?

Table 5.2: Comparison between the activation energies and p values, estimated from dielectric relaxation study and solvation dynamics study,[e] for all the three DESs.

Anion Identity	E_a^{DR}	p (DR)	E_a^{SD}	p (SD)
Br^-	18.63 kJ/mol	0.30	26.72 kJ/mol	0.37
NO_3^-	23.11 kJ/mol	0.51	23.13 kJ/mol	0.43
ClO_4^-	28.94 kJ/mol	0.62	30.05 kJ/mol	0.57

e) The data collected from the ref. 27 and ref. 20

We propose that this relaxation time somehow related to the dynamics of the acetamide molecules. We have two reasons behind this suggestion: i) this relaxation processes is common for all acetamide based deep eutectics, both in ionic and non-ionic ones, and ii) recent simulation studies in these DESs have reported a similar time component for the acetamide-acetamide H-bond relaxation.[68] Further studies are required to characterize the exact origin of this relatively fast time component.

5.4 Conclusion

In summary, the present work demonstrates the effects of temperature on DR dynamics of acetamide based three ionic deep eutectic systems. With increasing temperature the estimated static dielectric constants (ε_0) of these DESs increase. Although the exact estimation of ε_0 is nontrivial for these type of conducting viscous liquids, estimated ε_0 values helps us to get an idea about the polarity of these mediums. As we miss the low frequency relaxation processes due to frequency limitation of our instrument, frequency dependent DR study in theses DESs with a broader frequency window can be useful to estimate the ε_0 values more exactly.

Although the magnitude of τ_4 has been kept fixed, the other three relaxation processes exhibit considerable temperature dependence. It has been observed that the activation energy associated with $\left\langle \tau_{av}^{DR} \right\rangle$ is somewhat greater than the same for molten acetamide and comparable with the

activation energy for solvation of a dipolar probe molecule in theses DESs. Moreover, this activation energies, associated with the slower two time components ($\tau_1 \& \tau_2$), does not follow viscosity trend. Further studies using more sophisticated experimental techniques, like small angle neutron scattering and 2D IR spectroscopy, may be helpful in this regard. Molecular dynamics simulation of the temperature dependent dielectric relaxation[66] of these DESs will also help to understand the changes in the medium polarity with temperature.

References

1.   D. V. Wagle, H. Zhao and G. A. Baker, Acc. Chem. Res. **47**, 2299 (2014).

2.   A. P. Abbott, G. Capper, D. L. Davies, R. K. Rasheed and V. Tambyrajah, Chem. Commun. 70 (2003).

3.   A. P. Abbott, D. Boothby, G. Capper, D. L. Davies and R. K. Rasheed, J. Am. Chem. Soc. **126**, 9142 (2004).

4.   M. Francisco, A. van den Bruinhorst and M. C. Kroon, Angew. Chem. Int. Ed. **52**, 3074 (2013).

5.   Q. Zhang, K. D. O. Vigier, S. Royer and F. Jérôme, Chem. Soc. Rev. **41**, 7108 (2012).

6.   A. Romero, A. Santos, J. Tojo and A. Rodríguez, J. Hazard. Mater. **151**, 268 (2008).

7.   A. Paiva, R. Craveiro, I. Aroso, M. Martins, R. L. Reis and A. R. C. Duarte, ACS Sustainable Chem. Eng. **2**, 1063 (2014).

8.   R. J. Bernot, E. E. Kennedy and G. A. Lamberti, Environ. Toxicol. Chem. **24**, 1759 (2005).

9.   E. L. Smith, A. P. Abbott and K. S. Ryder, Chem. Rev. **114**, 11060 (2014).

10. H. Zhao and G. A. Baker, J. Chem. Technol. Biotechnol. **88**, 3 (2013).

11. S. Handy and K. Lavender, Tetrahedron Lett. **54**, 4377 (2013).

12. D. Lindberg, M. de la Fuente Revenga and M. Widersten, J. Biotechnol. **147**, 169 (2010).

13. G. García, S. Aparicio, R. Ullah and M. Atilhan, Energy Fuels **29**, 2616 (2015).

14. A. P. Abbott, G. Capper, K. J. McKenzie and K. S. Ryder, J. Electroanal. Chem. **599**, 288 (2007).

15. G. van der Zwan and J. T. Hynes, Chem. Phys. **152**, 169 (1991).

16. G. van der Zwan and J. T. Hynes, J. Chem. Phys. **78**, 4174 (1983).

17. A. Nitzan, *Chemical Dynamics in Condensed Phases*. (Oxford University Press, Oxford, 2006).

18. T. Pradhan and R. Biswas, J. Phys. Chem. A **111**, 11514 (2007).

19. T. Pradhan, H. A. R. Gazi and R. Biswas, J. Chem. Phys. **131**, 054507 (2009).

20. B. Guchhait, S. Das, S. Daschakraborty and R. Biswas, J. Chem. Phys. **140**, 104514 (2014).

21. A. Das, S. Das and R. Biswas, Chem. Phys. Lett. **581**, 47 (2013).

22. G. Berchiesi, G. Rafaiani, G. Vitali and F. Farhat, J. Therm. Anal. Calorim. **44**, 1313 (1995).

23. G. Berchiesi, G. Vitali, R. Plowiec and S. Barocci, J. Chem. Soc., Faraday Trans. 2 **85**, 635 (1989).

24. G. Berchiesi, G. Vitali, P. Passamonti and R. Płowiec, J. Chem. Soc., Faraday Trans. 2 **79**, 1257 (1983).

25. G. Berchiesi, J. Mol. Liq. **83**, 271 (1999).

26. B. Guchhait, H. A. R. Gazi, H. K. Kashyap and R. Biswas, J. Phys. Chem. B **114**, 5066 (2010).

27. B. Guchhait, S. Daschakraborty and R. Biswas, J. Chem. Phys. **136**, 174503 (2012).

28. A. Das, S. Das and R. Biswas, J. Chem. Phys. **142**, 034505 (2015).

29. D. Laage and J. T. Hynes, Science **311**, 832 (2006).

30. D. Laage and J. T. Hynes, J. Phys. Chem. B **112**, 14230 (2008).

31. S. Das, R. Biswas and B. Mukherjee, J. Phys. Chem. B **119**, 11157 (2015).

32. S. Das, R. Biswas and B. Mukherjee, J. Phys. Chem. B **119**, 274 (2015).

33. T. Pal and R. Biswas, Chem. Phys. Lett. **517**, 180 (2011).

34. A. Das and R. Biswas, J. Phys. Chem. B **119**, 10102 (2015).

35. R. Biswas, A. Das and H. Shirota, J. Chem. Phys. **141**, 134506 (2014).

36. H. A. R. Gazi, B. Guchhait, S. Daschakraborty and R. Biswas, Chem. Phys. Lett. **501**, 358 (2011).

37. S. N. Tripathy, Z. Wojnarowska, J. Knapik, H. Shirota, R. Biswas and M. Paluch, J. Chem. Phys. **142**, 184504 (2015).

38. R. Buchner, Pure Appl. Chem. **80**, 1239 (2008).

39. R. Buchner and J. Barthel, Annu. Rep. Prog. Chem. Sect. C: Phys. Chem. **91**, 71 (1994).

40. U. Kaatze and K. Giese, J. Phys. E **13**, 133 (1980).

41. D. A. Turton, J. Hunger, A. Stoppa, G. Hefter, A. Thoman, M. Walther, R. Buchner and K. Wynne, J. Am. Chem. Soc. **131**, 11140 (2009).

42. A. Stoppa, J. Hunger, R. Buchner, G. Hefter, A. Thoman and H. Helm, J. Phys. Chem. B **112**, 4854 (2008).

43. J. Hunger, A. Stoppa, S. Schrödle, G. Hefter and R. Buchner, ChemPhysChem. **10**, 723 (2009).

44. C. Daguenet, P. J. Dyson, I. Krossing, A. Oleinikova, J. Slattery, C. Wakai and H. Weingärtner, J. Phys. Chem. B **110**, 12682 (2006).

45. M. Mizoshiri, T. Nagao, Y. Mizoguchi and M. Yao, J. Chem. Phys. **132**, 164510 (2010).

46. R. Biswas, N. Rohman, T. Pradhan and R. Buchner, J. Phys. Chem. B **112**, 9379 (2008).

47. C. J. F. Böttcher and P. Bordewijk, *Theory of Electric Polarization*. (Elsevier: Amsterdam, The Netherlands, 1978).

48. P. R. Bevington and D. K. Robinson, *Data Reduction and Error Analysis*. (McGraw–Hill, New York, 2003).

49. R. Buchner, J. Barthel and J. Stauber, Chem. Phys. Lett. **306**, 57 (1999).

50. B. Lone, P. Undre, S. Patil, P. Khirade and S. Mehrotra, J. Mol. Liq. **141**, 47 (2008).

51. S. Bass, W. Nathan, R. Meighan and R. Cole, J. Phys. Chem. **68**, 509 (1964).

52. Y. Marcus, *The Properties of Solvents*. (Wiley Chichester, Chichester, 1998).

53. J. Barthel, R. Buchner, P.-N. Eberspächer, M. Münsterer, J. Stauber and B. Wurm, J. Mol. Liq. **78**, 83 (1998).

54. R. Buchner, Pure Appl. Chem. **80**, 1239 (2008).

55. K. Mukherjee, A. Das, S. Choudhury, A. Barman and R. Biswas, J. Phys. Chem. B **119**, 8063 (2015).

56. B. Bagchi, *Molecular Relaxation in Liquids*. (Oxford University Press, New York, 2012).

57. J. L. Dote, D. Kivelson and R. N. Schwartz, J. Phys. Chem. **85**, 2169 (1981).

58. M.-L. Horng, J. Gardecki and M. Maroncelli, J. Phys. Chem. A **101**, 1030 (1997).

59. A. Das, R. Biswas and J. Chakrabarti, J. Phys. Chem. A **115**, 973 (2011).

60. A. Das, R. Biswas and J. Chakrabarti, Chem. Phys. Lett. **558**, 36 (2013).

61. M. D. Ediger, Annu. Rev. Phys. Chem. **51**, 99 (2000).

62. M. D. Ediger, C. Angell and S. R. Nagel, J. Phys. Chem. **100**, 13200 (1996).

63. H. Sillescu, J. Non-Cryst. Solids **243**, 81 (1999).

64. D. Chakrabarti and B. Bagchi, Phys. Rev. Lett. **96**, 187801 (2006).

65. C. Angell, J. Chem. Phys. **46**, 4673 (1967).

66. M. Neumann, J. Chem. Phys. **85**, 1567 (1986).

67. K. Mukherjee, A. Barman and R. Biswas, J. Mol. Liq. **222**, 495 (2016).

68.   S. Das, R. Biswas and B. Mukherjee, J. Phys. Chem. (under minor revision)

69.   K. Mukherjee, A. Barman and R. Biswas, J. Phys. Chem. B (under revision)

Chapter 6

Dielectric Relaxation of (Urea + Choline Chloride) Deep Eutectic Solvents in the Frequency Window, $0.2 \le \nu(GHz) \le 50$: Temperature Dependence

6.1 Introduction

From the beginning of the twenty first century, deep eutectic solvents are emerging as an alternative to the ionic liquids (ILs) due to their less expensive and easy accessible nature.[1-4] Application of deep eutectic solvents (DESs) in synthetic chemistry[5-7] and electrochemistry[8-10] as reaction media is increasing day by day for their less toxicity, low vapor pressure and good solvent properties over a wide temperature range. DESs can be ionic[3,11-14] or nonionic,[15] depending upon the nature of the constituent elements and this is one of the additional advantages of DESs over ILs. The biodegradable [16]and readily available nature of choline chloride, a quaternary ammonium salt having similarities to the vitamin B complex-group, turns it into a promising candidate for selection as one of the constituent elements in preparation of DESs. The choline chloride based DESs,[2,17] which are already been accepted as the green solvent systems,[18,19] are being extensively used in the field of organic synthesis,[20,21] gas absorption,[22] selective metal extraction[23] and electrochemistry.[24] DESs are prepared by mixing two or more solid elements in a certain molar ratio and annealing them at higher temperature to transform them into liquids from their solid mixtures. It has been found that these liquids remain stable at a much lower temperature (mostly at or near room temperature) than the individual melting temperatures of the constituents for quite a long time. Extensive interspecies hydrogen bonding and the gain in entropy for being in the liquid phase are the main driving forces behind the stability of these room temperature DESs in the liquidus form.

Quaternary ammonium salts, possessing high melting points, have been found to form ionic DESs with any of the following compounds:[24,25] sugars, amides and alcohols. Thus, this wide window for the selection of constituents creates opportunities to study the interactions and dynamics of these quaternary ammonium salt containing DESs in detail. Acetamide based ionic deep eutectics have already been studied rigorously by fluorescence spectroscopy,[12-15,26] dielectric relaxation spectroscopy (DRS),[27-28] computer simulation[29,30] and femtosecond Raman-induced Kerr effect spectroscopy,[31] and the outcome of all these studies corroborates well with the previous nuclear magnetic resonance,[32] viscoelastic,[33] ultrasonic measurements[34] indicating complex solution character[35] of these media. Moreover, presence of temporal heterogeneity in some of the acetamide based ionic and nonionic DESs has been proposed by observing the fractional viscosity dependence of the solvation and rotation rates of dipolar fluorescent probe molecules in time-resolved fluorescence spectroscopy and in DR measurements.[16,17,19,27]

The widely used choline chloride based DESs is choline chloride (melting point-475K) and urea (melting point-406K) system with 1:2 molar ratio and this DES has the melting temperature and glass transition temperature at 285 K and~200 K, respectively.[18,36] The biocompatiable choline chloride is an important ingredient in animal and poultry food industry.[37-38] On the other hand, urea is an important ingredient in fertilizer industry[39] and also plays an important role in microbial metabolism in aquatic systems.[40] So the DESs made up of these two ecologically important components are good examples of environmentally benign solvents though very little information about the interactions and dynamics of these solvents are available. Several physic-chemical properties, such as, densities,[41] viscosities,[18,41,42] conductivity values[18] and molar heat capacities[43] of these DESs at various temperatures are already reported in literature. Steady state fluorescence spectroscopic measurements[37,44] have been carried out using different fluorescent probe molecules and subsequently, from these measurements the dielectric constants for these DESs have been estimated though direct measurements to estimate the polarity of these multi-component mixtures are still lacking. Recent FTIR measurements along with simulation studies[45,46] have revealed the presence of H-bonding between the Cl^- of choline chloride molecule and the $-NH_2$ group of the urea molecule which was predicted by earlier works also.[17]

Time resolved fluorescence spectroscopic measurements in these DESs employing C153 as a fluorescent probe molecule have revealed the decoupling of the solvation and rotation times of the probe molecule from the medium friction and a pronounced effect of temperature on the dynamics of these solvents.[37] Interestingly, the pulsed field gradient NMR spectroscopic study[47] in choline chloride based DESs have proposed that the molecular diffusions do not follow the random walk model; rather they follow a jump mechanism which is usual for the DESs[28,31] and ionic liquids.[48-50] In spite of the above mentioned few experimental and simulation studies, their molecular dynamics, like rotational dynamics, H-bond dynamics, and their physical properties, like polarity, are still not well explored and understood yet.

A thorough understanding about the properties of the medium is essential[51-54] to steer a chemical reaction occurring in a given medium at a desired rate. This requires a good knowledge of solution dynamics and frictional resistance. In this scenario dielectric relaxation spectroscopy (DRS)[55] can be a good option to study the dynamics of these DESs and the effect of temperature on their dynamics. DRS mainly probes the fluctuations of collective dipole moment in presence of an externally oscillating electromagnetic field. It is a powerful technique to examine the cooperative reorientation of dipolar species.[56,57] Note that in this DES both choline chloride and urea molecule possess high dipole moment;[58,59] even the choline cation also has moderate dipole moment.[58] In this work, as we can access the frequency regime $0.2 \leq \nu(GHz) \leq 50$ with our instrument and, as a result, we will refrain from making any comment about the time scales that are slower than 1 ns. Here we have studied the dielectric response of two DESs of general composition [*f urea + (1-f) choline chloride*] for *f* = 0.60 and 0.67 at six different temperatures, within the temperature regime $293 \leq T/K \leq 323$, for each DES.

6.2 Experimental Details

6.2.1 Materials and Methods

Choline chloride (≥99%, Sigma-Aldrich) and urea (≥99%, SRL) were vacuum-dried at room temperature for 48 h before use. Samples were prepared and relevant experiments were done in a

tightly humidity-controlled environment. Further details regarding sample preparation could be found elsewhere as these DESs were already studied via fluorescence measurements.[37] Briefly, the sample vessels were sealed and heated slowly to ~340 K until it formed a clear melt. Then the DR measurements were carried out after cooling it to the desired temperature.

6.2.2 DR Measurement Details

The DR data collection technique and the data analysis procedures are the same as described in chapter 2 and in refs.[60-61] Approximately 8mL of the each mixture were subjected for DR measurements after proper thermal equilibriation in an appropriately humidity-controlled environment. Temperature dependent DR measurements for these DESs were carried out by using a heating plate (MS-H-Pro from SCILOGEX, USA). We used a thermometer which was set at the same plane of the probe end to estimate the temperature more accurately and to avoid the misinterpretation of sample temperature which can arise due to gradient heating as we were using a heating plate. During all measurements desired experimental temperatures were sufficiently stable for conducting repeat (at least three) data acquisition.

6.3 Results and Discussion

6.3.1 Estimation of Static Dielectric Constant (ε_0) and Its' Temperature Dependence

The values of the DR parameters extracted from fitting the experimental data, presented in Fig. 6.1 and Fig. A.d.1, using HN equation (Eq. 2.12) have been summarized in the Table 6.1. First, we concentrate on the value of static dielectric constant. Data in Table 6.1 suggests that for both the compositions the value of static dielectric constant ε_0 increases with increasing temperature. Though for these kind of highly viscous conducting liquids the exact estimation of ε_0 is difficult and contains large uncertainties as the plateau in the real part and the characteristic peak in the imaginary part of the dielectric response is absent. Moreover, when we approach towards the lower frequency regime the conductivity term which contains the $1/\nu$ divergence at $\nu \rightarrow 0$ limit starts to dominate the total DR response, making the data erroneous data. However, estimated ε_0 values from our measurements are in good agreement with those predicted from steady state fluorescence peak shifts.[37] Usually, for traditional solvents like water, alcohols and amides the ε_0 value decreases with increase in temperature due to the thermal randomization of the

91

constituent dipoles.[62] For many ionic liquids, with increasing temperature the ε_0 value decreases.[63] There are a few solvents,[62] like acetic acid, acetic anhydride, which shows increment in ε_0 value with increase in temperature. This anomaly has been addressed in terms of breakage of molecular association into single molecules upon increasing solution temperature, enhancing the dipole density.[62] With increasing temperature the association of molecules with anti-parallel dipoles breaks and the number of contributing dipoles increases, which ultimately dominates over the effects of thermal randomization and increases ε_0 with temperature.

One of the probable reasons may be that in these types of ionic DESs a huge number of dipolar constituents remain irrotationaly bound[64-66] to the ionic species and with increasing temperature they start to respond in the relaxation process as their attachment becomes weaker. On the other hand, the presence of a characteristic peak in the imaginary part as well as a plateau in the real part of the DR response in the lower frequency regime may result this type of increment in ε_0 values with temperature. Although the presence of molecular associations in these DESs has already been established by different experimental and simulation studies, the question is- are they arranged in such an orientation that their intrinsic dipoles remain antiparallel? To address the question, assuming the DESs as a one component system, we employed the Onsager-Kirkwood-Frohlich equation,[67]

$$\frac{(\varepsilon_0-\varepsilon_\infty)(2\varepsilon_0+\varepsilon_\infty)}{\varepsilon_0(\varepsilon_\infty+2)^2}=\frac{\rho\mu^2}{9\varepsilon_p k_\beta T}g_k \;,\tag{6.1}$$

Table 6.1: Parameters obtained from simultaneous 4-Debye fits to real (ε') and imaginary (ε'') components of the measured DR spectra for [f urea + (1-f) choline chloride], $f = 0.60$ and 0.67, DESs at various temperatures.

Temp.	ε_0	$\Delta\varepsilon_1$	τ_1 (ps)	$\Delta\varepsilon_2$	τ_2 (ps)	$\Delta\varepsilon_3$	τ_3 (ps)	$\Delta\varepsilon_4$	τ_4 (ps)	ε_∞	n_D	κ_{fit} (S/m)	χ^2
					$f = 0.60$								
293K	13.2[a]	3.2(52%)[b]	553[e]	1.6(26%)	141	1.4	35	0.1	4	7.1	1.439[c]	0.057[d]	0.012
303K	14.5	3.6(47%)	503	1.9(25%)	147	1.7	35	0.4	4	6.9	1.436	0.092	0.015
308K	16.6	4.8(50%)	482	2.3(24%)	122	1.9	35	0.5	4	7.1	1.434	0.144	0.016
313K	18.1	5.3(49%)	463	2.8(26%)	125	2.1	32	0.7	4	7.2	1.433	0.205	0.018
318K	19.6	6.2(50%)	444	3.0(24%)	121	2.3	32	0.9	4	7.2	1.432	0.278	0.021
323K	20.8	7.0(51%)	428	3.2(24%)	115	2.4	32	1.0	4	7.2	1.430	0.331	0.025
					$f = 0.67$								
293K	15.4	5.0(58%)	549	2.1(24%)	110	1.4	30	0.1	5	6.8	1.438	0.052	0.041
303K	16.8	5.6(56%)	494	2.6(26%)	109	1.5	30	0.3	5	6.8	1.436	0.103	0.053
308K	18.3	6.5(57%)	475	2.8(25%)	102	1.7	29	0.4	5	6.9	1.435	0.145	0.052
313K	19.8	7.2(56%)	459	3.1(24%)	104	1.9	29	0.6	5	7.0	1.433	0.194	0.050
318K	21.3	7.9(56%)	444	3.5(25%)	104	2.1	29	0.7	5	7.2	1.432	0.263	0.052
323K	23.2	9.1(57%)	427	3.8(24%)	103	2.3	29	0.8	5	7.2	1.431	0.359	0.057

a) ε_0 values have error bar ±2.0 (based on three independent measurements).

b) Numbers within the parenthesis indicates the amplitude of the dispersion step in percentage.

c) Measured refractive index.

d) Extracted dc conductivity value from the fitting of the experimental data points.

e) τ_i (i=1-3) are better within $\pm5\%$ of the enlisted values (based on three independent measurements).

where ρ denotes the solvent number density, ε_0 is the static dielectric constant, ε_p is the vacuum permittivity , μ the dipole moment of constituting dipoles and g_k the Kirkwood factor which is taken unity here. We get the effective dipole moment value ~0.8 D at 293K which is smaller by an order of magnitude than the gas phase dipole moment of choline chloride (~8.0 D)[59] and substantially smaller than the same for urea (~3.83 D).[60] Moreover, if we use Cavell equation[68] to estimate the dipole moment of the species associated with the slowest relaxation process it gives a value ~0.7 D. Now in a system where the constituting elements have high gas phase dipole moment values, (urea has dipole moment ~6.0 D in the molten state[28]) such a substantially smaller value of the effective dipole moment may be a manifestation of molecular association. In associating liquids the value of g_k is known to deviate from unity, we have tried to make a rough estimate of the value of Kirkwood factor, g_k, for urea molecules, neglecting the dipole moment of choline chloride molecules, for this medium. Drastic deviation of g_k ($g_k \approx 0.2$) from unity indicates presence of strong association between the dipolar species and the smaller value than unity may be the signature of antiparallel arrangement. With increasing temperature (up to 323K) the value of the effective dipole moment, estimated from Onsager equation, increases and shows a ~40% increase at 323K with respect to the same at 293K which may be the resultant of continuous breakdown of molecular associations with increase in temperature. Fig. 6.1 and Fig. A.d.1 (Appendix) represent the temperature dependent dielectric response of the DES with f =0.60 and f =0.67, respectively. Fig. 6.2 describes the temperature dependence of ε_0 (for both f =0.60 and 0.67) and from this plot we have estimated the temperature coefficient, $-d\varepsilon_0/dT$, which has been found to be ~ 0.27 ±0.01 K^{-1} and independent of f.

6.3.2 DR Time Scales in (*urea + choline chloride*) DESs: Temperature Dependence

Fig. 6.1 and Fig. A.d.1 (Appendix) contain the temperature dependent dielectric response of (*urea + choline chloride*) DESs for f =0.60 and f =0.67 respectively. The straight lines passing through the experimental data points indicate the 4-Debye (4D) fitting. Though the fastest time component (τ_4) in our measurement has very small (~ 5%) contribution in the total dielectric response, we cannot neglect it as: i) The 3D fitting produces poorer description, shown in Fig. A.d.2 (Appendix), compared to 4-D fitting, ii) This type of time component has also been

observed in molten acetamide, molten urea and their DESs by both simulation[31,69] and experimental[28] studies and iii) A significant amount of dispersion ($\varepsilon_\infty - n_D{}^2$) remains inaccessible in our measurements.
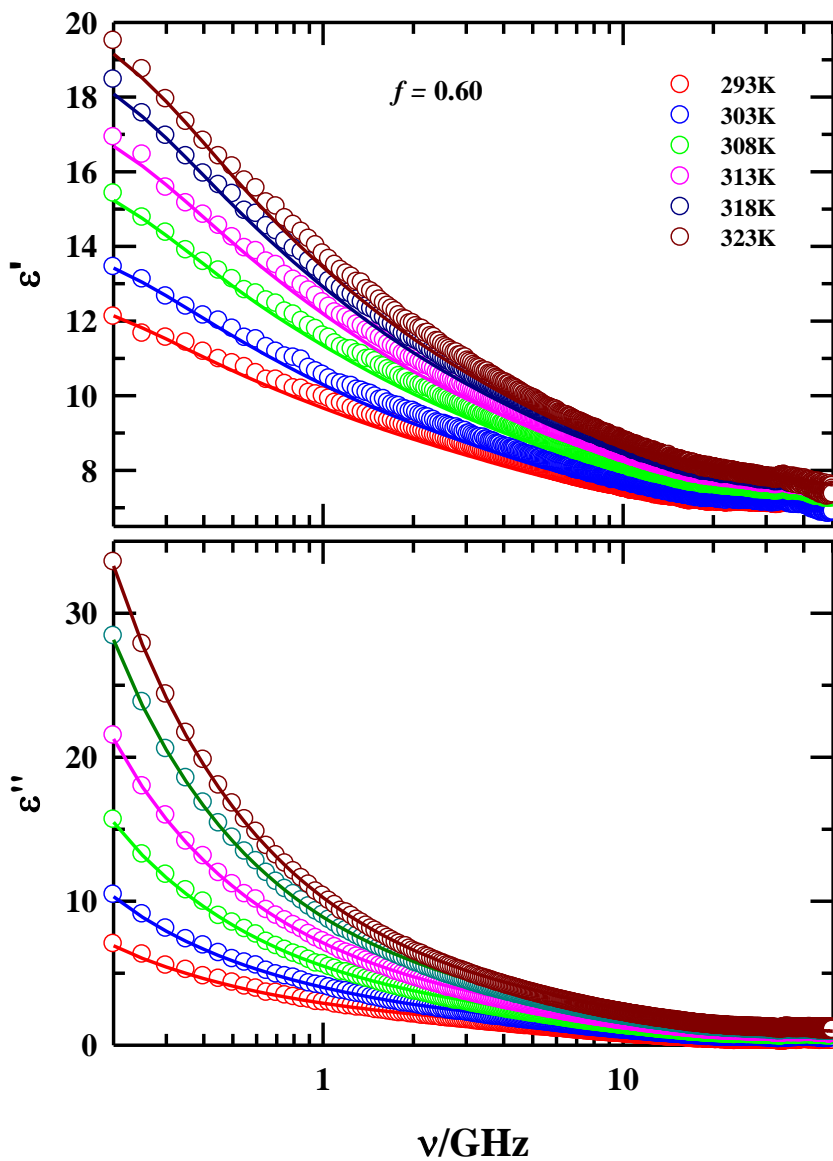
Fig. 6.1: Temperature dependence of the real (ε') and imaginary (ε'') parts of the measured DR spectra for ($urea + choline\ chloride$) DES at f = 0.60 within the frequency regime $0.2 \leq \nu / \mathrm{GHz} \leq 50$. Solid lines through these data represent simultaneous fits using 4-Debye relaxation model. Representations are color-coded.

Note that, during the fitting of the measured data we kept the fast component fixed at ~5 ps (for f = 0.60 at 4 ps and for f = 0.67 at 5 ps) . This fast relaxation process has been attributed to the N-H bond vector reorientation coupled to H-bond relaxation and the undetected fast part ($\varepsilon_\infty - n_D^2$) can be connected to the intermolecular librations. Similar kind of fast time component (~1-2 ps) has already been observed in formamide and N-methyl formamide by DR[70] and OHD-OKE measurements.[71]
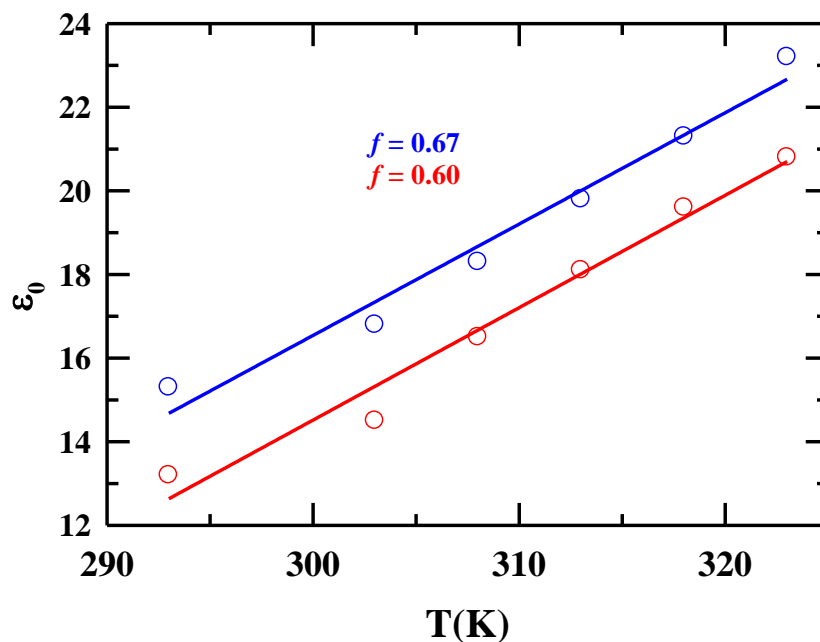
Fig. 6.2: Temperature dependence of estimated static dielectric constant (ε_0) for f = 0.60 and f = 0.67. Specific identities of compositions are color-coded.

Next we concentrate on τ_3 and τ_2 time constants which are contributing ~15-20% and ~20-25% respectively in the measured relaxation dynamics. If we can recall the DR dynamics of molten urea,[72] there is also a relaxation time constant of ~30 ps, though the contribution of that component is maximum in the total dielectric response of urea. For molten urea, this time component has been attributed to the hydrogen bond relaxation coupled with single particle rearrangement dynamics of urea molecules. Similar mechanism could be operative here also but the decrement in the amplitude indicates less abundance of single molecular dynamics.

96

Moreover, in molten urea the collective molecular dynamics via rearrangement of H-bond network happens in the time scale of ~90 ps. In the ($urea + choline\ chloride$) DESs the 100-150 ps timescale, which has a contribution of one quarter in the accessible dielectric response, can be attributed to the collective molecular dynamics via rearrangement of urea - urea H-bond network. These two time components (τ_3 and τ_2) are not new; similar timescales have been observed during the DR and OHD-RIKES measurements in the acetamide based ionic deep eutectics.[28,32] Furthermore, dynamic Stokes shift measurements have reported solvation decay component with time constant of ~100-200 ps.[37]

Now the most interesting part is that, like ($acetamide + electrolyte$) DESs, the ion induced DR dynamics is also present in these DESs. τ_1, which is absent in the DR dynamics of molten urea and almost six times larger than the slowest DR time of molten urea,[72] is the major (~50%) relaxation component in the DR dynamics of these DESs. We would try to correlate the slowest time component (τ_1) with the viscosity of the medium (η) through the Stokes-Einstein-Debye (SED) relation[73-76], $\tau_r = 3V\eta/k_B T$, as DR probes orientational relaxation of rank 1 ($\ell = 1$). The single particle orientation time (τ_r) connects to the collective DR time as follows:[77]

$\tau_r = \dfrac{\ell(\ell+1)}{2} \times \tau_{DR} = \tau_1$. Following this we get the effective molecular radius ~0.46 Å which is much smaller than the reported molecular radius of urea (1.8Å).[78,79] Moreover, if we put τ_{PG} (

$\tau_{PG} = \dfrac{2\varepsilon_S + \varepsilon_\infty}{3\varepsilon_S}\tau_1$), calculated from Powles–Glarum equation,[80-81] in the SED relation then the

effective radius becomes even smaller. This suggests that either τ_1 does not correspond to the full molecular rotation of the smallest dipolar molecule, urea in this case, or it does not experience the full frictional resistance exerted by the microscopic viscosity of the medium. The breakdown of SED relation in this heterogeneous[37,82] ionic deep eutectic system is expected. The small value of molecular radius of the relaxing species may be an indication of non-Brownian moves such as jumps.[82,70] In acetamide based ionic deep eutectics, with the variation of electrolytes, similar type of relaxation times (~0.5 -1ns) has already been reported by DR measurements.[27] Note that, ionic liquids which are quite similar in nature with these DESs have been found to undergo similar kind of non-Brownian angular dynamics.[64] Note the presence of

non-Brownian dynamics in ($urea + choline\ chloride$) DES has already been hinted by pulsed field gradient NMR spectroscopy.[48]

It is now clear that the amplitudes associated with τ_1 and τ_2 remain more or less insensitive towards the temperature variation and the amplitudes of τ_3 and τ_4 vary somewhat with temperature. The slight increase in the contribution of τ_4 can be explained by considering the temperature induced speeding up of the dynamics of the system. Our initial data for the temperature dependent dielectric measurements in ($acetamide + electrolyte$) DESs also indicates similar increment in the amplitude of the fastest time component with increase in temperature. Next we have estimated the activation energies ($E_a^{DR}(\langle \tau_{av}^{DR} \rangle)$) associated with the slower components of the DR in these DESs from the amplitude-averaged relaxation times, $\langle \tau_{av}^{DR} \rangle = \sum_{i=1}^{2} a_i \tau_i \Big/ \sum_{i=1}^{2} a_i$, where the amplitudes ($a_i$) and the time constants (τ_i) are presented in Table 6.1. Note $1/\langle \tau_{av}^{DR} \rangle$ vs $1/T$ plot suggests an Arrhenius-type behavior and Fig. 6.3 depicts the temperature dependence of $\langle \tau_{av}^{DR} \rangle$ for both the compositions, $f = 0.60$ and $f = 0.67$. The estimated activation energy (E_a^{DR}) does not show much change with the variation in f value. Here we get a substantially small value for E_a^{DR} (~6 kJ/mole) compared to the same of molten urea and molten acetamide. Fig. A.d.3 (Appendix) represents the temperature dependence of the slowest relaxation time (τ_1) and the estimation of the activation energies ($E_a^{DR,slowst}$) are very close to the activation energies (E_a^{DR}) from the $1/\langle \tau_{av}^{DR} \rangle$ vs $1/T$ plots. Estimation of activation energy associated with the average solvation rate and average rotation rate of a dipolar fluorescent probe molecule in these DESs produces quite large values and these values are comparable with the same for viscosity.[37]
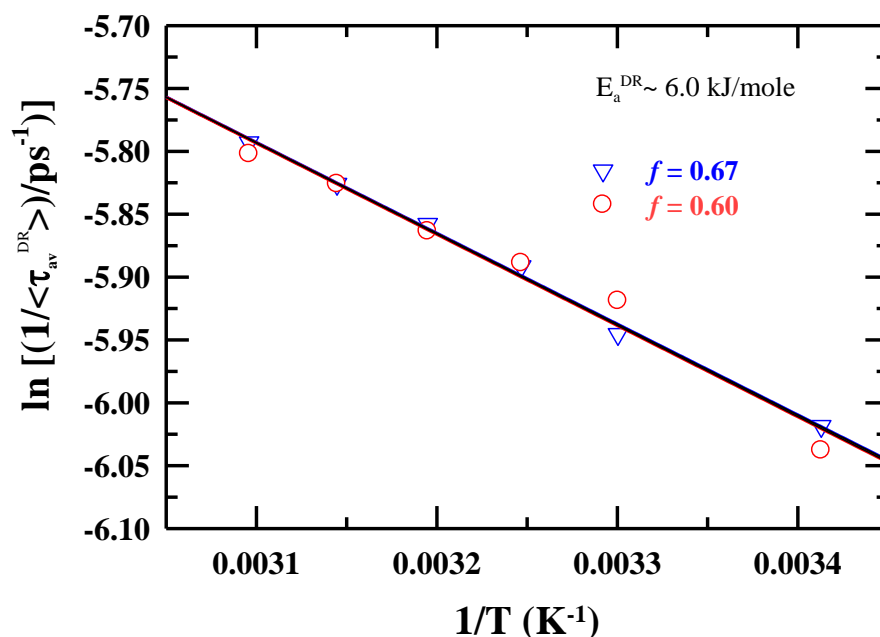
Fig. 6.3: Composition dependent activation energies from amplitude-averaged DR times ($\left\langle \tau_{av}^{DR} \right\rangle = \sum_{i=1}^{2} a_i \tau_i \Big/ \sum_{i=1}^{2} a_i$) in (*urea + choline chloride*) DESs via Arrhenius plots. Inverse of the $\left\langle \tau_{av}^{DR} \right\rangle$ is shown as a function of inverse temperature in semi-logarithmic fashion. Solid lines represent linear fits through the respective data sets. Representations are color-coded.

Fig. 6.4 depicts the $(\eta/T)^p$ dependence of the slowest time component, τ_1, and from this plot we have extracted the p value for both the compositions. Comparison between the p values obtained from solvation ($p = 0.7$ to 0.8) and rotation dynamics ($p = 0.8$ to 0.9) of C153 in these DESs and the p value obtained from DR measurements ($p = 0.1$) shows a huge difference. Now this observation indicates that the DR dynamics of these DESs are substantially decoupled from the viscosity of the medium though the probes, constituent dipoles for DR measurements and C153 for fluorescence measurements, are not the same for the two measurement techniques.
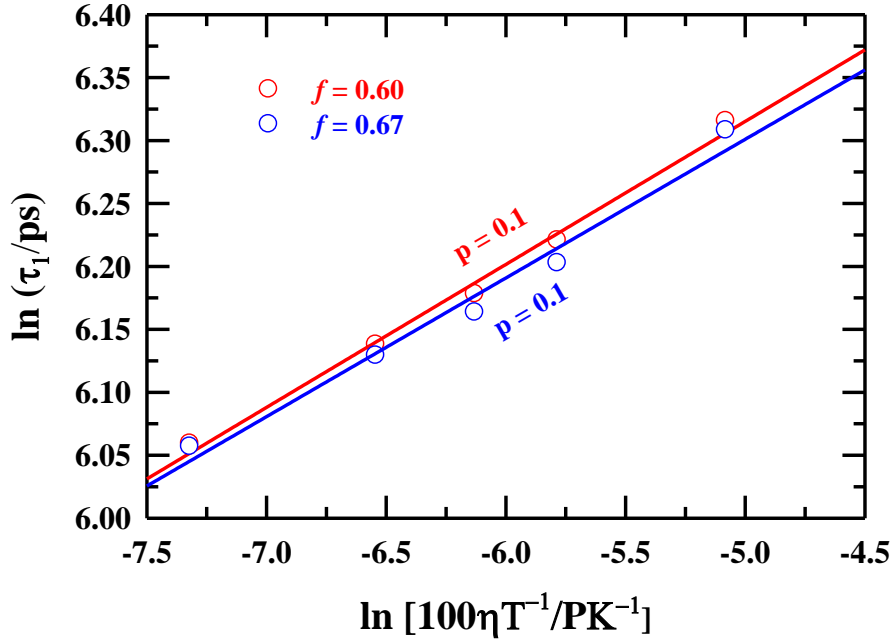
Fig. 6.4: $\left(\dfrac{\eta}{T}\right)$ dependence of slowest DR time (τ_1) for the two different compositions. Solid lines represent the fits through the all (f = 0.60 and 0.67) τ_1 data. Specific identities of compositions are shown in the inset.

6.4 Conclusion

In summary, the present work reports dielectric relaxation study in ($urea + choline\ chloride$) DESs for the first time in the frequency regime, $0.2 \le \nu/\mathrm{GHz} \le 50$. Estimated static dielectric constant (ε_0) for molten urea gets substantially reduced in presence of choline chloride and reaches a value which is almost five times smaller than that of molten urea (~68 at 406K). Solvation of ions by the dipolar specie may be one of the reasons behind the huge decrement in the value of estimated static dielectric constant. Elevation of temperature causes increase in the value of ε_0 and the temperature coefficient -dε_0/dT is quite high. Abnormally low value (though rough estimation) of the Kirkwood factor, g_k, for urea molecules in the medium indicates presence of association with antiparallel molecular dipoles. The dc-conductivity values obtained from our fitting are in good agreement with previously enlisted conductivity data.[18]

References

1. M. Francisco, A. van den Bruinhorst and M. C. Kroon, Angew. Chem. Int. Ed. **52**, 3074 (2013).

2. A. P. Abbott, D. Boothby, G. Capper, D. L. Davies and R. K. Rasheed, J. Am. Chem. Soc. **126**, 9142 (2004).

3. Q. Zhang, K. D. O. Vigier, S. Royer and F. Jérôme, Chem. Soc. Rev. **41**, 7108 (2012).

4. D. V. Wagle, H. Zhao and G. A. Baker, Acc. Chem. Res. **47**, 2299 (2014).

5. P. Liu, J.-W. Hao, L.-P. Mo and Z.-H. Zhang, RSC Adv. (2015).

6. D. Carriazo, M. C. Serrano, M. C. Gutiérrez, M. L. Ferrer and F. del Monte, Chem. Soc. Rev. **41**, 4996 (2012).

7. H. G. Liao, Y. X. Jiang, Z. Y. Zhou, S. P. Chen and S. G. Sun, Angew. Chem. Int. Ed. **120**, 9240 (2008).

8. C. Gu, X. Xu and J. Tu, J. Phys. Chem. C **114**, 13614 (2010).

9. J. Vijayakumar, S. Mohan, S. A. Kumar, S. R. Suseendiran and S. Pavithra, Int. J. Hydrogen Energy **38**, 10208 (2013).

10. A. P. Abbott, G. Capper, D. L. Davies, K. J. McKenzie and S. U. Obi, J. Chem. Eng. Data **51**, 1280 (2006).

11. B. Guchhait, H. A. R. Gazi, H. K. Kashyap and R. Biswas, J. Phys. Chem. B **114**, 5066 (2010).

12. B. Guchhait, S. Daschakraborty and R. Biswas, J. Chem. Phys. **136**, 174503 (2012).

13. H. A. R. Gazi, B. Guchhait, S. Daschakraborty and R. Biswas, Chem. Phys. Lett. **501**, 358 (2011).

14. B. Guchhait, S. Das, S. Daschakraborty and R. Biswas, J. Chem. Phys. **140**, 104514 (2014).

15. A. Das, S. Das and R. Biswas, J. Chem. Phys. **142**, 034505 (2015).

16. B.-Y. Zhao, P. Xu, F.-X. Yang, H. Wu, M.-H. Zong and W.-Y. Lou, ACS Sustainable Chem. Eng. **3**, 2746 (2015).

17. A. P. Abbott, G. Capper, D. L. Davies, R. K. Rasheed and V. Tambyrajah, Chem. Commun. 70 (2003).

18. H. Zhao, C. Zhang and T. D. Crittle, J. Mol. Catal. B: Enzym. **85**, 243 (2013).

19.	H. Zhao and G. A. Baker, J. Chem. Technol. Biotechnol. **88**, 3 (2013).

20.	A. Zhu, T. Jiang, B. Han, J. Zhang, Y. Xie and X. Ma, Green Chem. **9**, 169 (2007).

21.	Y. A. Sonawane, S. B. Phadtare, B. N. Borse, A. R. Jagtap and G. S. Shankarling, Org. Lett. **12**, 1456 (2010).

22.	D. Yang, M. Hou, H. Ning, J. Zhang, J. Ma, G. Yang and B. Han, Green Chem. **15**, 2261 (2013).

23.	A. P. Abbott, G. Capper, D. L. Davies, R. K. Rasheed and P. Shikotra, Inorg. Chem. **44**, 6497 (2005).

24.	E. L. Smith, A. P. Abbott and K. S. Ryder, Chem. Rev. **114**, 11060 (2014).

25.	Z. Maugeri and P. D. de María, RSC Adv. **2**, 421 (2012).

26.	A. Das, S. Das and R. Biswas, Chem. Phys. Lett. **581**, 47 (2013).

27.	K. Mukherjee, A. Das, S. Choudhury, A. Barman and R. Biswas, J. Phys. Chem. B **119**, 8063 (2015).

28.	S. N. Tripathy, Z. Wojnarowska, J. Knapik, H. Shirota, R. Biswas and M. Paluch, J. Chem. Phys. **142**, 184504 (2015).

29.	T. Pal and R. Biswas, Chem. Phys. Lett. **517**, 180 (2011).

30.	S. Das, R. Biswas and B. Mukherjee, J. Phys. Chem. B **119**, 11157 (2015).

31.	R. Biswas, A. Das and H. Shirota, J. Chem. Phys. **141**, 134506 (2014).

32.	G. Berchiesi, G. Rafaiani, G. Vitali and F. Farhat, J. Therm. Anal. Calorim. **44**, 1313 (1995).

33.	G. Berchiesi, G. Vitali, P. Passamonti and R. Płowiec, J. Chem. Soc., Faraday Trans. 2 **79**, 1257 (1983).

34.	G. Berchiesi, G. Vitali, R. Plowiec and S. Barocci, J. Chem. Soc. Faraday Trans. 2 **85**, 635 (1989).

35.	G. Berchiesi, J. Mol. Liq. **83**, 271 (1999).

36.	A. Das and R. Biswas, J. Phys. Chem. B **119**, 10102 (2015).

37.	M. E. Griffin, K. A. Wilson, M. R. White and P. B. Brown, J. Nutr. **124**, 1685 (1994).

38.	V. Ravindran and R. Blair, World's Poult. Sci. J. **49**, 219 (1993).

39.	C. A. Jones, R. T. Koenig, J. W. Ellsworth, B. D. Brown and G. D. Jackson, *Management of Urea Fertilizer to Minimize Volatilization*. (Montana State University Extension, 2007).

40. C. M. Solomon, J. L. Collier, G. M. Berg and P. M. Glibert, Aquat. Microb. Ecol. **59**, 67 (2010).

41. A. Yadav and S. Pandey, J. Chem. Eng. Data **59**, 2221 (2014).

42. F. S. Mjalli and J. Naser, Asia Pac. J. Chem. Eng. **10**, 273 (2015).

43. R. B. Leron and M.-H. Li, Thermochim. Acta **530**, 52 (2012).

44. A. Pandey and S. Pandey, J. Phys. Chem. B **118**, 14652 (2014).

45. S. L. Perkins, P. Painter and C. M. Colina, J. Chem. Eng. Data **59**, 3652 (2014).

46. S. L. Perkins, P. Painter and C. M. Colina, J. Phys. Chem. B **117**, 10250 (2013).

47. C. D'Agostino, R. C. Harris, A. P. Abbott, L. F. Gladden and M. D. Mantle, Phys. Chem. Chem. Phys. **13**, 21383 (2011).

48. J. Habasaki and K. Ngai, J. Chem. Phys. **129**, 194501 (2008).

49. D. A. Turton, J. Hunger, A. Stoppa, G. Hefter, A. Thoman, M. Walther, R. Buchner and K. Wynne, J. Am. Chem. Soc. **131**, 11140 (2009).

50. J. Hunger, T. Sonnleitner, L. Liu, R. Buchner, M. Bonn and H. J. Bakker, J. Phys. Chem. Lett. **3**, 3034 (2012).

51. G. van der Zwan and J. T. Hynes, Chem. Phys. **152**, 169 (1991).

52. G. van der Zwan and J. T. Hynes, J. Chem. Phys. **78**, 4174 (1983).

53. A. Nitzan, *Chemical Dynamics in Condensed Phases*. (Oxford University Press, Oxford, 2006).

54. T. Pradhan and R. Biswas, J. Phys. Chem. A **111**, 11514 (2007).

55. U. Kaatze and K. Giese, J. Phys. E **13**, 133 (1980).

56. J. Barthel, K. Bachhuber, R. Buchner and H. Hetzenauer, Chem. Phys. Lett. **165**, 369 (1990).

57. A. Stoppa, J. Hunger, R. Buchner, G. Hefter, A. Thoman and H. Helm, J. Phys. Chem. B **112**, 4854 (2008).

58. S. Shaukat, der Universität Regensburg, 2013.

59. R. Brown, P. Godfrey and J. Storey, J. Mol. Spectrosc. **58**, 445 (1975).

60. C. J. F. Böttcher and P. Bordewijk, *Theory of Electric Polarization*. (Elsevier: Amsterdam, The Netherlands, 1978).

61. P. Bevington, *Data Reduction and Error Analysis for the Physical Sciences*. (McGraw-Hill: New York, 1969).

62.   Y. Marcus, *The Properties of Solvents*. (Wiley Chichester, Chichester, 1998).

63.   J. Hunger, A. Stoppa, S. Schrödle, G. Hefter and R. Buchner, ChemPhysChem. **10**, 723 (2009).

64.   K. Tielrooij, D. Paparo, L. Piatkowski, H. Bakker and M. Bonn, Biophys. J . **97**, 2484 (2009).

65.   R. Buchner, G. T. Hefter and P. M. May, J. Phys. Chem. A **103**, 1 (1999).

66.   R. Buchner and G. Hefter, Phys. Chem. Chem. Phys. **11**, 8984 (2009).

67.   H. Fröhlich, *Theory of Dielectrics: Dielectric Constant and Dielectric Loss*. (Clarendon Press, 1958).

68.   E. A. Cavell, P. Knight and M. Sheikh, Trans. Faraday Soc. **67**, 2225 (1971).

69.   S. Das, R. Biswas and B. Mukherjee, J. Phys. Chem. B **119**, 274 (2015).

70.   B. Wurm, C. Baar, R. Buchner and J. Barthel, J. Mol. Liq. **127**, 14 (2006).

71.   Y. J. Chang and E. W. Castner Jr, J. Chem. Phys. **99**, 113 (1993).

72.   K. Mukherjee, A. Barman and R. Biswas, J. Chem. Phys. (To be submitted).

73.   J. L. Dote, D. Kivelson and R. N. Schwartz, J. Phys. Chem. **85**, 2169 (1981).

74.   M.-L. Horng, J. Gardecki and M. Maroncelli, J. Phys. Chem. A **101**, 1030 (1997).

75.   A. Das, R. Biswas and J. Chakrabarti, J. Phys. Chem. A **115**, 973 (2011).

76.   A. Das, R. Biswas and J. Chakrabarti, Chem. Phys. Lett. **558**, 36 (2013).

77.   B. Bagchi, *Molecular Relaxation in Liquids*. (Oxford University Press, New York, 2012).

78.   S. G. Schultz and A. K. Solomon, J. Gen. Physiol. **44**, 1189 (1961).

79.   G. Jones and S. K. Talley, J. Am. Chem. Soc. **55**, 624 (1933).

80.   J. Powles, J. Chem. Phys. **21**, 633 (1953).

81.   S. H. Glarum, J. Chem. Phys. **33**, 1371 (1960).

82.   M. D. Ediger, Annu. Rev. Phys. Chem. **51**, 99 (2000).

83.   D. Laage and J. T. Hynes, Science **311**, 832 (2006).

Chapter 7

Dielectric Relaxation Studies in (Acetamide + Urea + PEG) Deep Eutectic Solvent: Origin of Slow Relaxation

7.1 Introduction

Designing new kind of reaction media, which will be commercially viable and at the same time eco-friendly in nature, has been a subject of immense interest for the last few decades.[1-4] Room temperature ionic liquids(RTILs),[5-7] room temperature super critical fluids (RTSFs)[8-9] and deep eutectic solvents (DESs)[10] are termed as green solvents, though recently the 'greenness' of ionic liquids has been questioned.[11-13] DESs are biodegradable,[14-17] less toxic and cheap to produce,[18] whereas the other two solvents (RTILs and RTSFs) are relatively costly. Moreover, day by day the application of DESs in industry is increasing due to their exquisite solvent properties.[19-22] DESs are molten mixture of two or more components which are stable in the liquid state at temperatures much lower than the individual melting temperatures (T_m's). These multi-component mixtures can be both ionic[10] and non-ionic[23] in nature. In this work we have prepared a non-ionic DES which contains acetamide, urea and polyethylene glycol and investigated the dynamics of this system using frequency domain dielectric relaxation spectroscopy in the frequency window, $0.2 \leq \nu / GHz \leq 50$. The composition of these DESs can be presented as $w[fCH_3CONH_2 + (1-f)NH_2CONH_2] + (1-w)PEG$, where w represents the weight fraction and f represents the mole fraction. In this study we have kept w fixed at 0.67 and f fixed at 0.6. We have tried to prepare DESs by varying the weight fraction of *PEG* in the medium (keeping f value fixed at 0.6), but it has been found that this is the minimum weight fraction required to make the DESs stable near the room temperature (~ 305 K).

Previous nuclear magnetic resonance,[24] viscoelastic,[25] ultrasonic[26] and dielectric relaxation studies[27-28] in the acetamide based DESs have revealed the presence of micro-heterogeneity in the medium. Steady state and picoseconds-resolved fluorescence measurements along with

simulation studies[29-32] have also found the existence of spatial and temporal heterogeneities[33-35] in the medium. The signature of temporal heterogeneity in DESs was reflected in the fractional viscosity dependence of the measured solvation and rotation rates. Similar kind of solute-medium decoupling has already been observed in several ILs.[36-37] Very recently a molecular dynamics simulation study on X-ray and neutron scattering structures of deep eutectic solvents (DESs) reported presence of spatial heterogeneity in molecular length scales.[38] Moreover, dielectric studies in the frequency regime, $0.2 \leq \nu/GHz \leq 50$, for six different ionic DESs[39] and femtosecond Raman-induced Kerr effect spectroscopy (fs-RIKES) measurements[40] have explored the ion dependent dynamics and structure of these acetamide based DESs. Later, anion dependent simulation studies of the acetamide based DESs have pointed out the origin of the slow relaxation processes observed by DR measurements[41] and the effects of anion identity on the jump dynamics of these DESs.

Interestingly, a slow nanosecond ion-induced DR dynamics has been found in all the ionic DESs studied. Time-resolved fluorescence measurements have revealed homogeneous structure and dynamics for ($acetamide + urea$) DESs, although DR measurements suggest temporal heterogeneity in the medium.[42] Unfortunately, very few studies have been carried out on the dynamics of non-ionic DESs in the last few years. In order to understand the dynamics of these non-ionic DESs comprehensively, more investigations are required. The reasons that motivated us to take up this study are as follows. First, this is a non-ionic DES, and a DR study of this will add to the database. Second, the DR dynamics of the ($acetamide + urea$) DESs in the $0.2 \leq \nu/GHz \leq 50$ frequency regime are already reported[42] so it will help us to understand the interaction and dynamics better. Third, the DR dynamics of pure polyethylene glycol is also available.[43-44] Fourth, this DES is accessible at 305 K whereas the ($acetamide + urea$) DESs are stable up to 328 K. This provides an opportunity to study a room temperature deep eutectics.

Dielectric relaxation spectroscopy (DRS) is a useful tool to understand the inherent medium dynamics and its correlation with the liquid structure of the medium.[45-49] This technique has already been used to explore the dynamics of pure solvents,[50-52] aqueous electrolytes,[53-55] organic electrolytes,[56-57] binary solvent mixtures,[58-59] and ionic liquids.[60-62] As our frequency coverage spans a narrow range ($0.2 \leq \nu/GHz \leq 50$), we cannot probe the slow relaxation

processes happening in the multi-nanoseconds time scale and the fast relaxations occurring in the sub-picoseconds time scale. Note that to the best of our knowledge, this is the first DR study on this type of ternary non-ionic room temperature DES.

7.2 Experimental Details

7.2.1 Materials and Methods

Acetamide ($\geq$99%, Sigma-Aldrich) and Urea (>99%, SRL, India) were vacuum-dried (~300 K) overnight before use. Polyethylene glycol of number-averaged molecular weight 300 (*PEG 300*, Sigma-Aldrich) was used as received. Samples were prepared and relevant experiments were done in a tightly humidity-controlled environment. Briefly, the sample was prepared as follows: First, we prepared the (*acetamide* + *urea*) DES and the details regarding this preparation could be found elsewhere as these DESs were already studied via fluorescence measurements.[23] Then we added *PEG* of required amount in the medium at 333 K. After mixing the *PEG* well, we kept the mixture at ~308 K for 2 hours. Refractive indices (n_D) were measured by employing an automated temperature-controlled refractometer (RUDOLPH, J357).

7.2.2 DR Measurement Details

The DR data collection technique and the data analysis procedures are the same as described in chapter 2 and in refs.[63-64] Approximately 10 mL of the each mixture was subjected for DR measurements after proper thermal equilibriation in an appropriately humidity-controlled environment. Temperature dependent DR measurements for these DESs were carried out by using a heating plate (MS-H-Pro from SCILOGEX, USA). We used a thermometer which was set at the same plane of the probe end to estimate the temperature more accurately and to avoid the misinterpretation of sample temperature which can arise due to gradient heating as we were using a heating plate. During all measurements desired experimental temperatures were sufficiently stable for conducting repeat (at least three) data acquisition.

7.3 Results and Discussion

7.3.1 Static Dielectric Constant, ε_0, from Fit

Fig. 7.1 and Table 7.1 represent the temperature dependent DR spectra of the DES and fit parameters, respectively. Interestingly, it has been found that, like in ionic DESs,[39] in the low temperature (308 K) DR spectra of the DES the plateau in the real part as well as the characteristic peak in the imaginary part is missing. This, we think, is the manifestation of our limited frequency coverage. When the solution temperature is increased, the characteristic peak in the imaginary part of the dielectric spectrum appears and shifts to the higher frequency with temperature. The estimated ε_0 value for this DES is quite high, even larger than that of DMSO.[65] Although the ε_0 value of this DES is to some extent smaller than the ε_0 of ($acetamide + urea$) DESs,[42] it is appreciably larger than the previously reported ε_0 of the ionic DESs at a comparable temperature.[66] The temperature dependence of ε_0 has been plotted in Fig. A.e.1(Appendix) and it indicates negligible effects of temperature on ε_0 of this DES; Acetamide based ionic DESs, on the contrary, have shown pronounced temperature effect on ε_0.[66] It is noteworthy that the closeness of the ε_0 values at 308 K (the imaginary part does not contain any characteristic peak) and 318 K (the characteristic peak in the imaginary part starts to creep in) for this DES signifies that in spite of missing plateau in the real part and characteristic peak in the imaginary part, we have been able to successfully estimate the ε_0 value at 308 K. Note that due to limited frequency coverage, a significant portion ($\varepsilon_\infty - n_D^2$) remains inaccessible to the present measurements.
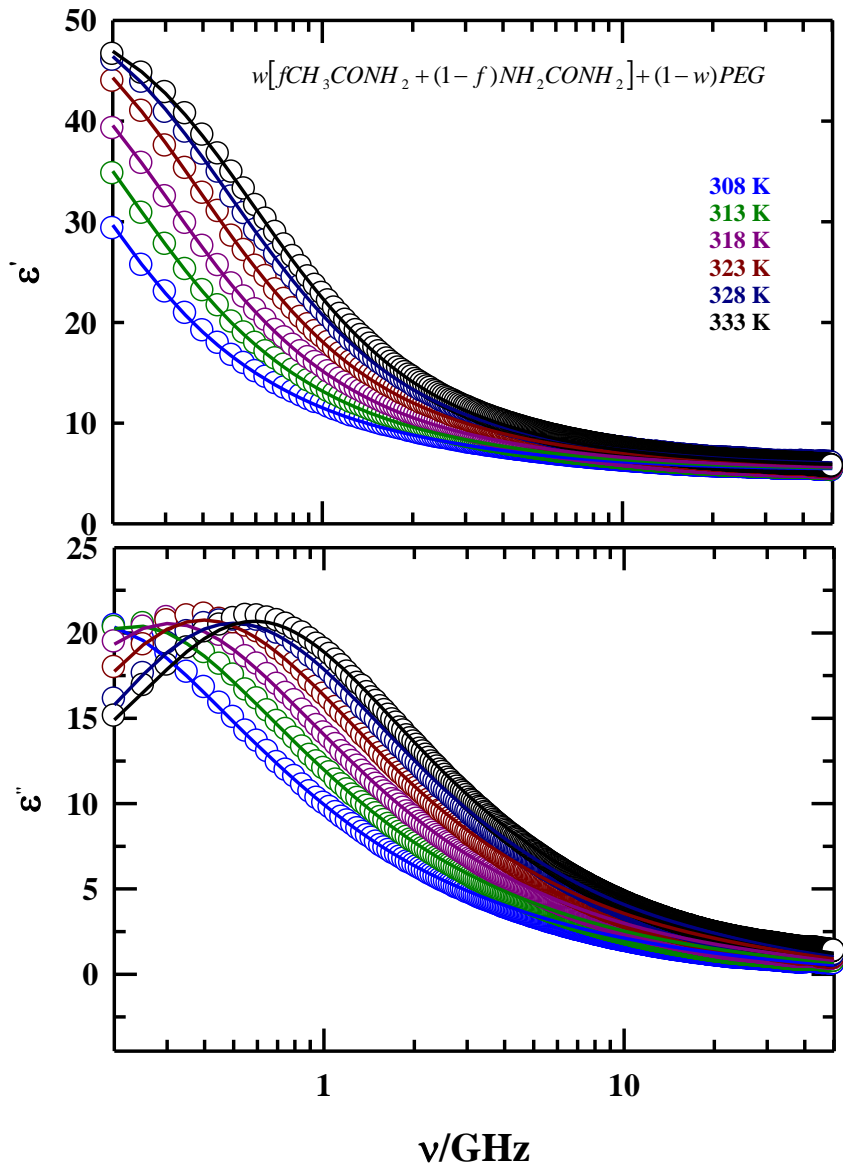
Fig. 7.1: Temperature dependence of the real (ε') and imaginary (ε'') parts of the measured DR spectra for $w\left[fCH_3CONH_2 + (1-f)NH_2CONH_2\right]+(1-w)PEG$ DES within the frequency regime, $0.2 \leq \nu/\text{GHz} \leq 50$. Solid lines through these data represent simultaneous fits using 1CC3D relaxation model. CC denotes the Cole-Cole and D the Debye descriptions. Representations are color-coded.

7.3.2 DR Time Scales and Their Possible Origins

Simultaneous fit of the real and imaginary parts of the collected DR spectra produce four relaxation time components spread over sub-10 ps to 1 ns. First, we will discuss about the probable origin of the slowest component, τ_1. Note that no nanosecond relaxation time component, like τ_1 in the present DES, has been observed in the DR dynamics of ($acetamide + urea$) DESs.[42] Moreover, if we compare the DR dynamics of ($acetamide + urea$) and ($acetamide + urea + PEG$) DESs at a comparable temperature (~335 K), we can see that in the ($acetamide + urea + PEG$) DES the slowest time constant (τ_1) is ~3 times longer than the slowest DR time component of ($acetamide + urea$) DESs. Larger viscosity (~ 2 times) of the medium can partly account for this slower dynamics. In order to understand the viscosity coupling of τ_1, we have plotted τ_1 as a function of temperature-scaled viscosity (η / T) in Fig. 7.2 which strongly suggests that the slowest DR time constant follows a fractional viscosity dependence. Now the question is what is the origin of this time component? What is the role for collective H-bond dynamics and how much of it is single particle orientation? We have estimated the single particle reorientation time, using SED relation,[67-71] for acetamide molecules (which is the smallest one in the medium) in this DESs at 333 K which is almost double of the slowest DR time constant measured. Our initial DR measurements in ($PEG + acetamide / urea$) system at 303 K (not included here) shows that with increasing acetamide (or urea) concentration in PEG, a slow (in nanosecond scale) DR time constant appears which is totally absent in the DR dynamics of pure PEG.[43]

Furthermore, we have investigated the temperature dependence of τ_1, presented in Fig. A.e.2 (Appendix) which suggests that τ_1 follows an Arrhenius type temperature dependence. Subsequently, we have estimated the activation energy associated with the slowest DR process and it is ~ 37 kJ/mol which is substantially larger than the activation energy associated with the slowest time component of ($acetamide + urea$) DESs, ~24 kJ/mol.[42]

Table 7.1: Parameters obtained from simultaneous 1CC3D fits to real (ε') and imaginary (ε'') components of the measured DR spectra for, ($w[fCH_3CONH_2 + (1-f)NH_2CONH_2] + (1-w)PEG$), DES at various temperatures.

Temp. (K)	ε_0	$\Delta\varepsilon_1$	$\tau_1^{\,b}$ (ps)	α	$\Delta\varepsilon_2$	τ_2 (ps)	$\Delta\varepsilon_3$	τ_3 (ps)	$\Delta\varepsilon_4$	τ_4 (ps)	ε_∞	χ^2	$n_D^{\,c}$	$<\tau_{av}>^d$ (ps)
308	53.4	40.2 (84%)[a]	960	0.04	5.0 (10%)	212	2.1 (4%)	49	0.7 (2%)	12	5.4	0.013	1.401	828
313	53.0	40.1 (84%)	696	0.05	4.7 (10%)	164	2.0 (4%)	40	0.7 (2%)	9	5.4	0.015	1.399	601
318	52.5	38.5 (82%)	540	0.04	5.7 (12%)	144	2.1 (4%)	35	0.7 (2%)	8	5.5	0.017	1.398	460
323	53.9	32.7 (68%)	484	0.01	11.3 (23%)	180	3.1 (4%)	43	1.0 (2%)	9	5.8	0.023	1.398	370
328	52.8	29.9 (64%)	392	0.005	12.7 (27%)	157	3.2 (7%)	40	1.1 (2%)	9	5.9	0.027	1.397	293
333	51.7	33.9 (74%)	301	0.02	8.5 (18%)	118	2.7 (6%)	31	0.9 (2%)	7	5.7	0.027	1.395	244

a) Number in parenthesis indicates dispersion amplitude of a given dispersion step in percentage.

b) τ_i ($i=1$-3) are better within ±5% of the reported values (based on 3-5 independent measurements).

c) Measured refractive index.

d) $<\tau_{av}> = \dfrac{\sum\limits_{i=1}^{=2} a_i \tau_i}{\sum\limits_{i=1}^{2} a_i}$, where $\sum\limits_{i=1}^{n} a_i = 1$ and $a_i = \dfrac{\Delta\varepsilon_i}{\sum\limits_{i=1}^{n} \Delta\varepsilon_i}$.

Next we concentrate on τ_2 which is the second slowest relaxation component in the DR dynamics of ($acetamide + urea + PEG$) DES. This hundreds of picoseconds time constant is also present in the DR dynamics of ($acetamide + urea$) DESs. Moreover, dielectric relaxation with similar timescale has also been observed in our initial measurements of ($acetamide + PEG$) system at 20 wt% acetamide concentration. We propose that, like ($acetamide + urea$) DESs,[42]

this timescale arises due to the acetamide-acetamide or acetamide-urea collective H-bond dynamics, though the contributions of the dipolar $C-O-C$ unit of PEG, which has a relaxation time ~ 100 ps[43] at ~ 298 K, cannot be neglected. Interestingly, it has been found that the total contribution of these two relaxation processes (τ_1 and τ_2) in the total DR dynamics remains nearly constant (~ 90 %) throughout the whole temperature range considered. We think that these two relaxation processes are somehow interlinked. The calculated amplitude-averaged relaxation times, $\left\langle \tau_{av}^{DR} \right\rangle = \sum_{i=1}^{2} a_i \tau_i \Big/ \sum_{i=1}^{2} a_i$, from the slower two components of the observed DR dynamics of this DES are provided in Table 7.1. It has been found that the $\left\langle \tau_{av}^{DR} \right\rangle$ follows an Arrhenius type temperature dependence and the estimated activation energy (see Fig. A.e.3, Appendix) associated with these slower relaxation processes is comparable to the activation energy estimated from the slowest relaxation time (τ_1).
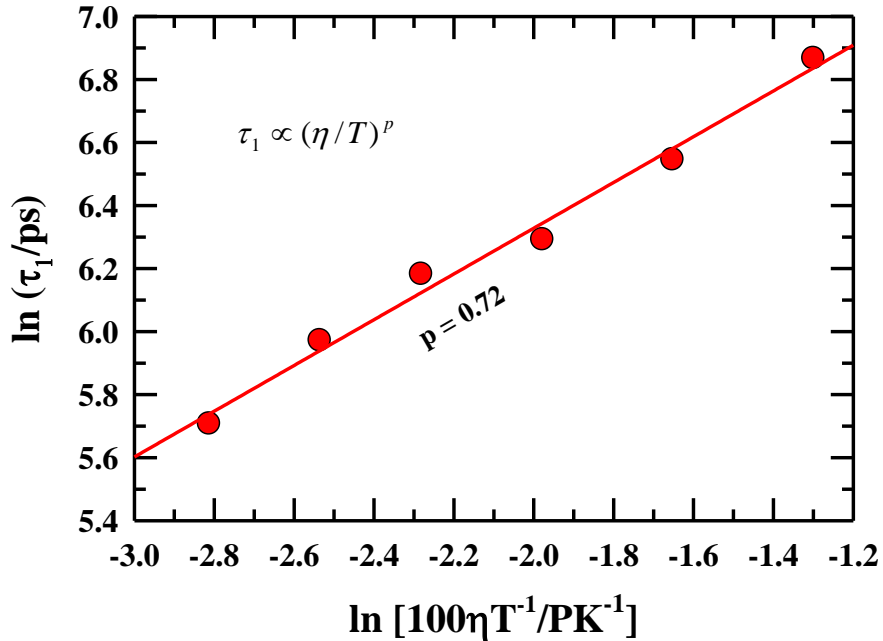
Fig. 7.2: $\left(\dfrac{\eta}{T}\right)$ dependence of slowest DR time (τ_1) for the $w\left[fCH_3CONH_2 + (1-f)NH_2CONH_2\right]+(1-w)PEG$ DES. Solid line represents the fit through the all τ_1 data.

Now we inspect the other two fast relaxation processes. We think that the ~10 ps time component (τ_4) contains the contributions from both, the "crankshaft motion" of the oligomer backbone[43] as well as the $N-H$ bond vector reorientation of the acetamide (or urea) molecules.[39,72] Note that the time scales associated with these two relaxation processes are too close to resolve their individual contributions in the total DR response. The third slowest DR time component (τ_3) may be linked to the rearrangement of acetamide molecules due to the following reasons. First, this time component is missing in the DR dynamics of pure PEG[43]. Second, similar relaxation timescale has been observed in both acetamide based ionic[39] and non-ionic[42] DESs. Third, in our initial DR results of ($PEG + acetamide$) we have found that, upon addition of acetamide in PEG, a ~40 ps time component appears in the DR dynamics which is completely absent in the DR response of pure PEG.

7.4 Conclusion

In summary, the present work investigates the DR dynamics of a new non-ionic DES having composition: $w[fCH_3CONH_2 + (1-f)NH_2CONH_2] + (1-w)PEG$, where w ($=$ 0.33) represents the weight fraction and f ($=$ 0.6) the mole fraction. Interestingly, viscosity of the present DES is comparable to the viscosity of pure PEG though their dielectric constant values are very different: the ε_0 value of the DES (~53, at 308 K) is ~ 4 times larger than the ε_0 value of pure PEG (~ 14, at 308 K). A combination of high viscosity and high polarity makes this solvent a unique one for regulating the diffusion controlled reactions involving polar species. On the other hand, unlike previously reported non-ionic DES[23], this DES is stable near room temperature. We think all these properties of this non-ionic DES will make it an excellent solvent for industrial applications, though rigorous studies using different experimental techniques are required to generate further understanding about the structure and dynamics of this DES.

Moreover, our recent excitation wavelength dependent emission study[31,73-74] in this DES (not included here) reveals that this system is more or less spatially homogeneous, though in DR study we have got the signature of presence of temporal heterogeneity in the medium. Like ionic DESs, this non-ionic DES also possesses a nanosecond time component in its DR dynamics which arises due to the collective H-bond dynamics of the acetamide (or urea) molecules

attached to the polymer molecules. Temperature dependent DR dynamics study of this DES shows that the activation energy associated with the slow time components (τ_1 and τ_2) is quite high. It is noteworthy that a significant part of the fast DR dynamics remains inaccessible to us due to our frequency limitation. Terahertz spectroscopic studies can be very useful to investigate the fast part of the DR dynamics of this DES. A simulation study focusing on the orientational relaxation and H-bond fluctuation dynamics of the acetamide (or urea) molecules will be very helpful to explore the origin of the DR time scales reported in the present work.

References

1. J. H. Clark and S. J. Tavener, Org. Process Res. Dev. **11**, 149 (2007).

2. P. T. Anastas and J. C. Warner, Green chemistry: Theory and practice 29 (1998).

3. W. M. Nelson, Perspective and practice. New York, NY: Oxford University Press (2003).

4. J. M. DeSimone, Science **297**, 799 (2002).

5. M. J. Earle and K. R. Seddon, Pure Appl. Chem. **72**, 1391 (2000).

6. R. D. Rogers and K. R. Seddon, Science **302**, 792 (2003).

7. M. Armand, F. Endres, D. R. MacFarlane, H. Ohno and B. Scrosati, Nature materials **8**, 621 (2009).

8. S. V. Dzyuba and R. A. Bartsch, Angew. Chem. Int. Ed. **42**, 148 (2003).

9. P. T. Anastas and M. M. Kirchhoff, Acc. Chem. Res. **35**, 686 (2002).

10. E. L. Smith, A. P. Abbott and K. S. Ryder, Chem. Rev. **114**, 11060 (2014).

11. A. Paiva, R. Craveiro, I. Aroso, M. Martins, R. L. Reis and A. R. C. Duarte, ACS Sustainable Chem. Eng. **2**, 1063 (2014).

12. T. Welton, Green Chemistry **13**, 225 (2011).

13. M. Cvjetko, K. Radošević, A. Tomica, I. Slivac, J. Vorkapić-Furač and V. Srček, Archives of Industrial Hygiene and Toxicology **63**, 15 (2012).

14. A. P. Abbott, D. Boothby, G. Capper, D. L. Davies and R. K. Rasheed, J. Am. Chem. Soc. **126**, 9142 (2004).

15. A. P. Abbott, G. Capper, D. L. Davies, R. K. Rasheed and V. Tambyrajah, Chem. Commun. 70 (2003).

16. D. V. Wagle, H. Zhao and G. A. Baker, Acc. Chem. Res. **47**, 2299 (2014).

17. M. Francisco, A. van den Bruinhorst and M. C. Kroon, Angew. Chem. Int. Ed. **52**, 3074 (2013).

18. P. D. de María and Z. Maugeri, Curr. Opin. Chem. Biol. **15**, 220 (2011).

19. G. García, S. Aparicio, R. Ullah and M. Atilhan, Energy Fuels **29**, 2616 (2015).

20. A. P. Abbott, G. Capper, K. J. McKenzie and K. S. Ryder, J. Electroanal. Chem. **599**, 288 (2007).

21. S. Handy and K. Lavender, Tetrahedron Lett. **54**, 4377 (2013).

22. E. R. Parnham, E. A. Drylie, P. S. Wheatley, A. M. Slawin and R. E. Morris, Angew. Chem. Int. Ed. **118**, 5084 (2006).

23. A. Das, S. Das and R. Biswas, J. Chem. Phys. **142**, 034505 (2015).

24. G. Berchiesi, G. Rafaiani, G. Vitali and F. Farhat, J. Therm. Anal. Calorim. **44**, 1313 (1995).

25. G. Berchiesi, G. Vitali, P. Passamonti and R. Płowiec, J. Chem. Soc., Faraday Trans. 2 **79**, 1257 (1983).

26. G. Berchiesi, G. Vitali, R. Plowiec and S. Barocci, J. Chem. Soc., Faraday Trans. 2 **85**, 635 (1989).

27. A. Amico, G. Berchiesi, C. Cametti and A. Di Biasio, J. Chem. Soc. Faraday Trans. **83**, 619 (1987).

28. G. Berchiesi, M. De Angelis, G. Rafaiani and G. Vitali, J. Mol. Liq. **51**, 11 (1992).

29. A. Das, S. Das and R. Biswas, Chem. Phys. Lett. **581**, 47 (2013).

30. B. Guchhait, S. Das, S. Daschakraborty and R. Biswas, J. Chem. Phys. **140**, 104514 (2014).

31. B. Guchhait, S. Daschakraborty and R. Biswas, J. Chem. Phys. **136**, 174503 (2012).

32. B. Guchhait, H. Al Rasid Gazi, H. K. Kashyap and R. Biswas, J. Phys. Chem. B **114**, 5066 (2010).

33. M. D. Ediger, Annu. Rev. Phys. Chem. **51**, 99 (2000).

34. M. D. Ediger, C. Angell and S. R. Nagel, J. Phys. Chem. **100**, 13200 (1996).

35. C. Angell, J. Chem. Phys. **46**, 4673 (1967).

36. H. Jin, X. Li and M. Maroncelli, J. Phys. Chem. B **111**, 13473 (2007).

37. S. K. Das, P. K. Sahu and M. Sarkar, J. Phys. Chem. B **117**, 636 (2013).

38. S. Kaur, A. Gupta and H. K. Kashyap, J. Phys. Chem. B (2016).

39. K. Mukherjee, A. Das, S. Choudhury, A. Barman and R. Biswas, J. Phys. Chem. B **45**, (2015).

40. R. Biswas, A. Das and H. Shirota, J. Chem. Phys. **141**, 134506 (2014).

41. S. Das, R. Biswas and B. Mukherjee, J. Chem. Phys. (under minor revision).

42. K. Mukherjee, S. Das, A. Barman and R. Biswas, J. Chem. Phys. (under preperation).

43. S. Schrödle, R. Buchner and W. Kunz, J. Phys. Chem. B **108**, 6281 (2004).

44. C. Mali, S. Chavan, K. Kanse, A. Kumbharkhane and S. Mehrotra, Indian J. Pure Appl. Phys. **45**, 476 (2007).

45. D. A. Turton, J. Hunger, A. Stoppa, G. Hefter, A. Thoman, M. Walther, R. Buchner and K. Wynne, J. Am. Chem. Soc. **131**, 11140 (2009).

46. J. Hunger, A. Stoppa, S. Schrödle, G. Hefter and R. Buchner, ChemPhysChem. **10**, 723 (2009).

47. R. Buchner, Pure Appl. Chem. **80**, 1239 (2008).

48. R. Biswas, N. Rohman, T. Pradhan and R. Buchner, J. Phys. Chem. B **112**, 9379 (2008).

49. U. Kaatze and K. Giese, J. Phys. E **13**, 133 (1980).

50. J. Barthel, K. Bachhuber, R. Buchner and H. Hetzenauer, Chem. Phys. Lett. **165**, 369 (1990).

51. S. Bass, W. Nathan, R. Meighan and R. Cole, J. Phys. Chem. **68**, 509 (1964).

52. R. Buchner, J. Barthel and J. Stauber, Chem. Phys. Lett. **306**, 57 (1999).

53. R. Buchner, T. Chen and G. Hefter, J. Phys. Chem. B **108**, 2365 (2004).

54. R. Buchner, G. T. Hefter and P. M. May, J. Phys. Chem. A **103**, 1 (1999).

55. T. Chen, G. Hefter and R. Buchner, J. Phys. Chem. A **107**, 4025 (2003).

56. J. Barthel, R. Buchner, P.-N. Eberspächer, M. Münsterer, J. Stauber and B. Wurm, J. Mol. Liq. **78**, 83 (1998).

57. R. Buchner and J. Barthel, Annu. Rep. Prog. Chem. Sect. C: Phys. Chem. **91**, 71 (1994).

58. T. Sato and R. Buchner, J. Chem. Phys. **118**, 4606 (2003).

59. T. Sato and R. Buchner, J. Phys. Chem. A **108**, 5007 (2004).

60. C. Wakai, A. Oleinikova, M. Ott and H. Weingärtner, J. Phys. Chem. B **109**, 17028 (2005).

61. M.-M. Huang, S. Bulut, I. Krossing and H. Weingärtner, J. Chem. Phys. **133**, 101101 (2010).

62. C. Daguenet, P. J. Dyson, I. Krossing, A. Oleinikova, J. Slattery, C. Wakai and H. Weingärtner, J. Phys. Chem. B **110**, 12682 (2006).

63. C. J. F. Böttcher and P. Bordewijk, *Theory of Electric Polarization*. (Elsevier: Amsterdam, The Netherlands, 1978).

64. P. R. Bevington and D. K. Robinson, *Data Reduction and Error Analysis*. (McGraw–Hill, New York, 2003).

65. Z. Lu, E. Manias, D. D. Macdonald and M. Lanagan, J. Phys. Chem. A **113**, 12207 (2009).

66. K. Mukherjee, A. Barman and R. Biswas, J. Chem. Phys. (under preperation).

67. B. Bagchi, *Molecular Relaxation in Liquids*. (Oxford University Press, New York, 2012).

68. J. L. Dote, D. Kivelson and R. N. Schwartz, J. Phys. Chem. **85**, 2169 (1981).

69. M.-L. Horng, J. Gardecki and M. Maroncelli, J. Phys. Chem. A **101**, 1030 (1997).

70. A. Das, R. Biswas and J. Chakrabarti, J. Phys. Chem. A **115**, 973 (2011).

71. A. Das, R. Biswas and J. Chakrabarti, Chem. Phys. Lett. **558**, 36 (2013).

72. S. Das, R. Biswas and B. Mukherjee, J. Phys. Chem. B **119**, 274 (2014).

73. P. K. Mandal, M. Sarkar and A. Samanta, J. Phys. Chem. A **108**, 9048 (2004).

74. Z. Hu and C. J. Margulis, Proc. Natl. Acad. Sci. U.S.A. **103**, 831 (2006).

Chapter 8

Viscosity Coupling of Solvation and Rotation of C153 in a Polymer Gel Electrolyte System

8.1 Introduction

Nowadays major research attempts are being focused on the invention of new materials for rechargeable batteries to reduce the consumption of non-renewable resources.[1-5] Polymer gel electrolytes are one of the promising electrolyte materials that can be used in energy storage devices, super capacitors, dye-sensitized solar cells, fuel cells etc.[6-9] Polymer gel electrolyte systems are composed of organic electrolytes and polymers dissolved in it. It has already been reported that solutions of lithium salts, like lithium perchlorate ($LiClO_4$), lithium fluoroborate ($LiBF_4$), lithium trifluoromethanesulfonate ($LiCF_3SO_3$), in liquid propylene carbonate (PC), ethylene carbonate (EC), and dimethyl carbonate (DMC) or their mixtures have immense industrial applications due to their use as electrolytes in rechargeable lithium batteries.[10-11] In particular, a useful electrolyte must be able to act as a mechanical separator, an electronic insulator, and a good ionic conductor. As these solutions can simultaneously provide high ionic conductivity of organic electrolyte and high viscosity of polymer solution at the same time, they have been used as an electrolyte of electrochemical devices. In this work, we have taken the ($PC + LiClO_4$) mixture as organic electrolyte and polyethylene glycol (PEG) as the polymer molecule to investigate the solution dynamics.

Although a number of investigations have been carried out to elucidate the solution structure and the dynamics of the ($PC + LiClO_4$) systems using different spectroscopic techniques,[12-16] there are many things those are still not fully understood. It has been reported that the solution structure as well as the dynamics of the medium changes of these type of systems significantly

with the variation in the salt concentration of the system.[17-18] Not only PC but also different solvent mixtures, like $PC + EC$, $PC + DMC$, have been employed to have a better understanding about the ion solvation and transportation of the ions in these medium. Polymer gel electrolyte is medium where another component (polymer) is added in an organic electrolyte to increase the efficiency and the sustainability of the batteries. The conductivity of a pure polymer electrolyte is closely linked to the polymer segmental mobility[19-21] and this is why the conductivity of the pure polymer electrolyte is much lower than the conductivity of organic electrolytes. Our ultimate goal is to combine two features, high mechanical and chemical stability of pure polymer electrolytes and the high conductivity of organic electrolytes. Recently, several attempts have been made to understand the structure and dynamics of the polymer gel electrolyte systems with various polymer molecules.[22-26] Polyethylene oxide (PEO) is the most rigorously used polymer among all in these attempts. It is noteworthy that the conductivity of these polymer gel electrolyte is much higher than the corresponding pure polymer electrolyte system. Here we are interested to examine the effect of a polymer, PEG, an example of hydrophilic polymer and lower homolog of PEO, in the dynamics of these organic electrolytes by time resolved fluorescence spectroscopic technique. We preferably selected the PEG over other polymers as it has many technological and biochemical applications.[27-28] Moreover, it has been observed, through the excitation wavelength dependent emission studies[29-31] of a fluorescent probe molecule in a PEG containing pure polymer electrolyte,[32] that the interaction of the polymer molecules with the alkali metal ions induces spatial heterogeneity in the medium. QENS study of a polymer gel electrolyte system, containing $PMMA$, have revealed the information on both the spatial and temporal behaviors of the system and proposed two dynamical processes in the picosecond-nanosecond range: a faster one of rotational character and a slower one of translational character.[23] Moreover, the QENS investigation estimated the heterogeneity length scale ~5-20 Å for the same polymer gel electrolyte system which arises due to the polymer matrix.

In this paper, we have studied the fluorescence Stokes shift dynamics and rotational relaxation of a dipolar solute, Coumarin 153,[33-41] in a polymer gel electrolyte composite, composed of PC, $LiClO_4$ and PEG. Here we have varied the wt% of PEG in the medium, keeping the

PC / $LiClO_4$ molar ratio fixed at ~11.3, which corresponds to ~1mol/lit concentration of $LiClO_4$ and the reason behind the selection of this specific $LiClO_4$ concentration is: close to this $LiClO_4$ concentration (~ 1.3 mol/lit) dc conductivity reaches to a maximum value.[17] We have picked this polymer gel electrolyte composite for investigation due to the following reasons. First, the structure and dynamics of the organic electrolyte (PC + $LiClO_4$) has already been studied by different techniques. Second, the physico-chemical properties of similar type of pure polymer electrolyte composite are also available in the relevant literature[42]. Third, photo-physical properties of C153 in the pure polymer electrolyte have already been reported.[32] The solute-medium dynamical coupling is also an interesting aspect to look into, when it has already been reported that the Walden rule is not valid in this type of systems.[24]

8.2 Experimental Details

8.2.1 Materials and Methods

Laser grade Coumarin 153 was used as received (Exciton). Polyethylene glycol of number-averaged molecular weight 300 ($PEG300$), lithium perchlorate ($LiClO_4$) and propylene carbonate (PC) were used as received (Sigma-Aldrich). The experimental solutions were prepared by mixing of required amount of electrolyte, PC and PEG. Proper care was taken to ensure complete dissolution of the added electrolyte and to avoid moisture absorption. Concentration of C153 in each of these samples was maintained at ~10^{-5} M. Temperature was maintained via a temperature controller (Julabo), and sufficient time was allowed for achieving thermal equilibrium for each sample before measurement. The sample temperature was maintained within ± 0.5 K of the desired temperature.

8.2.2 Steady State Measurements

Steady state absorption and emission spectra were recorded by using a UV-Visible spectrophotometer (UV-2600, Shimadzu), and a fluorimeter (Fluorolog, Jobin-Yvon, Horiba), respectively. The solvent-blank subtracted spectra were processed accordingly before further analyses and frequency determination.[32, 43-44] Details about the measurement techniques are the same as described in chapter 2.

8.2.3 Viscosity and Sound Velocity Measurements

Sound velocity and viscosity coefficients (η) measurements were performed by using an automated temperature-controlled density-cum-sound analyzer (Anton Paar, model DSA 5000) and micro viscometer (AMVn, Anton Paar), respectively.[45-46]

8.2.4 Conductivity Measurements

Conductivity of the polymer gel electrolyte systems were measured by a Bench-top multi-parameter electrochemical meter (SESHIN BIOTECH, Model: ECM-610). All the conductivity data were collected at room temperature (~298 K).

8.2.5 Time-resolved Fluorescence Measurements

Time-resolved fluorescence measurements were performed with a time-correlated single-photon counting (TCSPC) system described earlier in chapter 2 and in refs .[47-48] The full width at half-maximum (fwhm) of the instrument response function (IRF) was ~80 ps.

8.3 Results and Discussion

8.3.1 Steady State Spectral Features: A Comparison between Pure Solvents and Polymer Gel Electrolytes

UV-VIS absorption and fluorescence emission spectra of C153 dissolved in these polymer gel electrolyte systems with different PEG concentrations are presented in Fig. 8.1.With increasing polymer concentration both spectra (absorption and emission) show blue shift due to the decreased average polarity of the system upon addition of less polar substance (PEG, $\varepsilon_0 = 15$) in the medium.[49-50] Steady state spectral features of the polymer gel electrolyte system along with the same of pure solvents are presented in Table 8.1 where numerical values for average frequencies[51-52] and widths (fwhm) are summarized. If we closely look at Table 8.1, we find that with the addition of $LiClO_4$ in PC the absorption spectra shifts by ~600 cm^{-1} to the lower
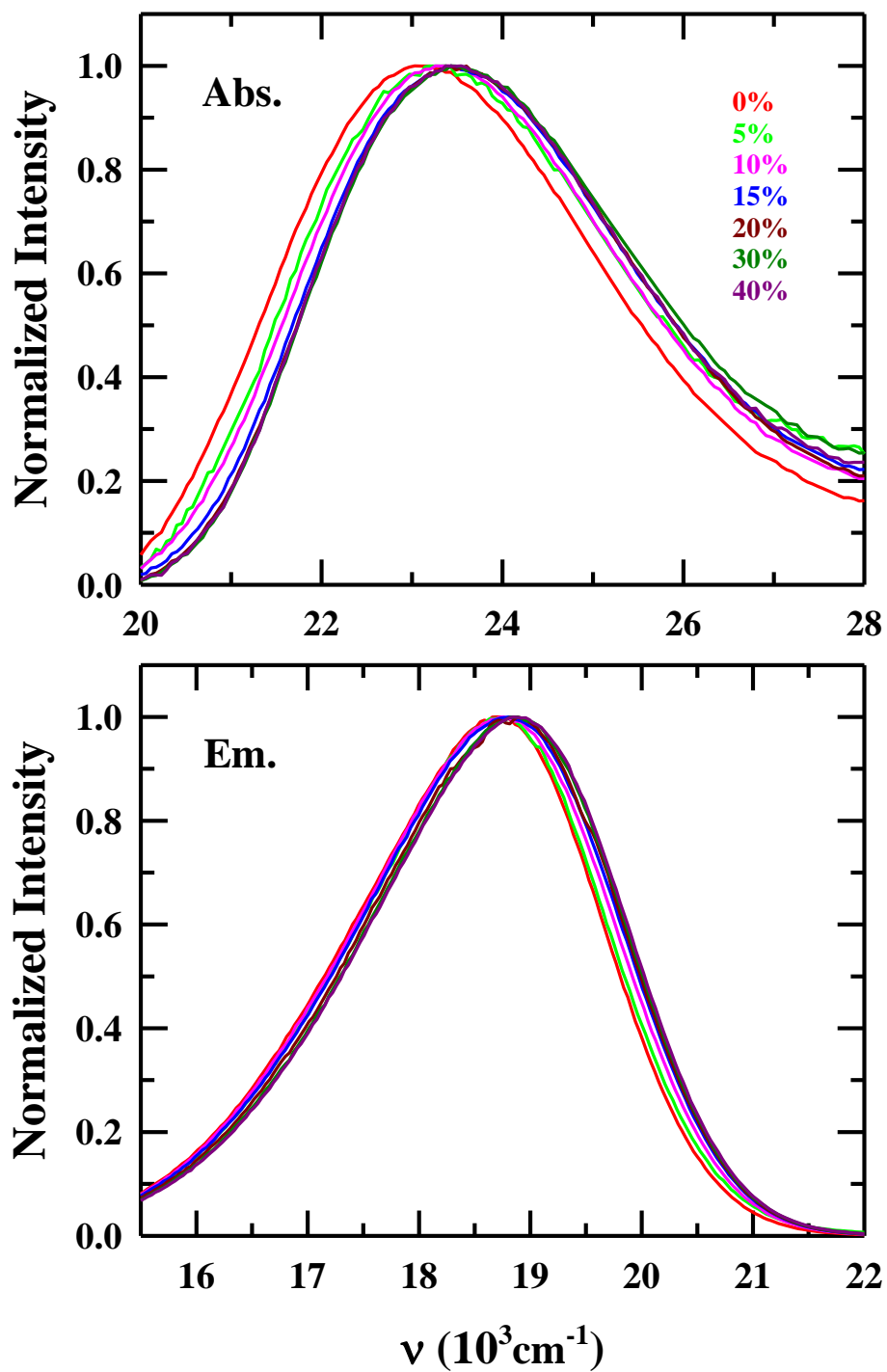
Fig. 8.1: Representative absorption (upper panel) and emission (lower panel) spectra of C153 in polymer gel electrolytes at different polymer concentrations at ~298 K. Spectra at different polymer concentrations are color-coded.

frequency side. More interestingly, upon addition of *PEG* the absorption spectra moves towards higher frequency and at 40 wt% *PEG* it reaches a value very close to the absorption peak frequency of C153 in pure *PEG* . Similar trend has also been observed in the emission spectra, though the emission spectrum of C153 in 40 wt% *PEG* system is ~200 cm^{-1} red-shifted from the emission spectrum of the same in pure *PEG* . It is noteworthy that the width of both absorption and emission spectra for the polymer gel electrolyte systems do not undergo monotonic changes with increasing polymer concentration; however, the spectral widths are not very much different from the same taken in pure *PC* and pure *PEG* .

Table 8.1: A comparison of spectral frequencies and widths between pure solvents and polymer gel electrolytes at ~ 298 K. Typical error bars for the frequencies and widths are within ± 200 cm^{-1}.

System	$\nu_{abs.}$ $(10^3 cm^{-1})$	$\nu_{em.}$ $(10^3 cm^{-1})$	$\Gamma_{abs.}$ $(10^3 cm^{-1})$	$\Gamma_{em.}$ $(10^3 cm^{-1})$
Only PC	24.041	18.998	4.378	2.864
PC+ $LiClO_4$ + 0% PEG	23.434	18.522	4.240	2.655
PC+ $LiClO_4$ + 5% PEG	23.626	18.571	4.367	2.647
PC+ $LiClO_4$ + 10% PEG	23.688	18.583	4.229	2.738
PC+ $LiClO_4$ + 15% PEG	23.794	18.621	4.253	2.765
PC+ $LiClO_4$ + 20% PEG	23.816	18.673	4.197	2.732
PC+ $LiClO_4$ + 30% PEG	23.865	18.687	4.270	2.720
PC+ $LiClO_4$ + 40% PEG	23.824	18.699	4.177	2.720
Only PEG	23.859	18.881	4.297	2.731

Although, it has already been reported that $LiClO_4$ induces spatial heterogeneity in *PEG* ,[32] in polymer gel electrolytes (where both $LiClO_4$ and *PEG* are present in sufficient amount), we have not observed any signature of spatial heterogeneity. This is shown in Table A.f.1 (Appendix). Both pure *PEG* [32] and 40 wt% *PEG* system show similar excitation wavelength dependent emission features. Our temperature dependent study (up to 318 K) reveals very minimal effect of temperature on both absorption and emission spectra. So it can be said that the

system remains quite stable up to 318 K, which is essential for rechargeable batteries. Now the question is: are these polymer gel electrolyte media really homogeneous in nature? To answer this question we have performed time resolved fluorescence measurements.

8.3.2 Time-resolved Fluorescence Anisotropy, $r(t)$: Viscosity Coupling

Fig. 8.2 compares the $r(t)$ decays for C153 in 0 wt% and 40 wt% *PEG* concentrations at 298 K along with the bi-exponential fits (line) through them. With increasing polymer concentration the slowing down of probe rotation is observable. Table 8.2 represents the fit parameters from the bi-exponential fits to the $r(t)$ decays at different *PEG* concentrations at different temperatures.
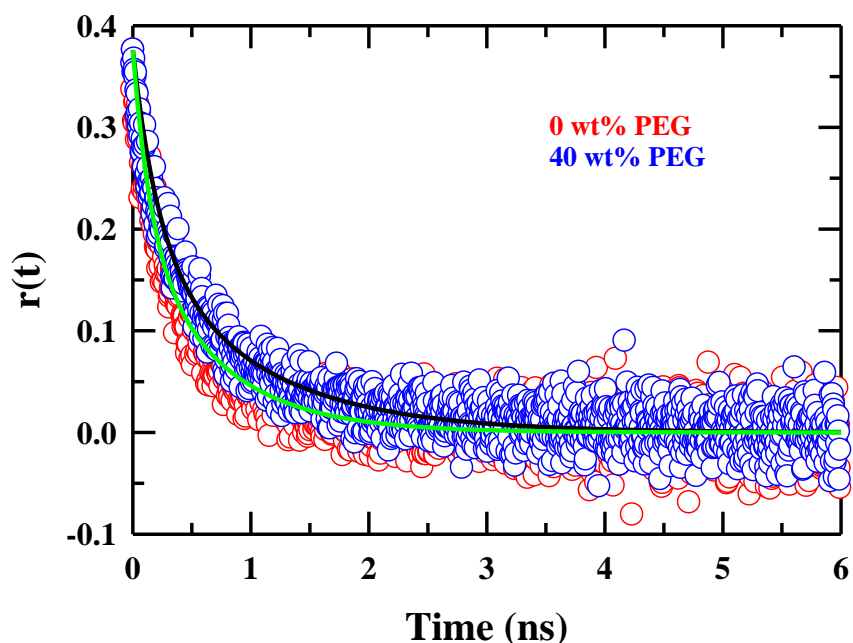
Fig. 8.2: Representative time-resolved fluorescence anisotropy ($r(t)$) decays for C153 in polymer gel electrolytes at 0 wt% and 40 wt% polymer concentrations. The solutions were excited at 298 K using a laser light of 409 nm. Solid lines passing through the data points denote bi-exponential fits through them. Representations are color-coded.

First, we consider the effects of $LiClO_4$ in *PC* , and it has been found that the incorporation of electrolytes in the medium elevates the viscosity by a factor of ~ 3 compared to that of pure *PC* .[53] As a result, the average rotational time ($\langle \tau_r \rangle$) of C153 increases in comparison to pure

125

PC .When polymer is added in the medium, viscosity changes. This is presented in Table 8.2 with polymer concentration. Fig. 8.3 represents the concentration (in terms of viscosity of the system) dependence of average rotational time ($\langle \tau_r \rangle$ vs $(\eta/T)^{p_r(C)}$ plot) at 298 K. Interestingly, the partial viscosity dependence, with $p_r(C)$ value ~ 0.5, of solute reorientation is quite significant here. This signifies the presence of temporal heterogeneity[54-57] in the medium. In order to further investigate the solute-medium coupling in these polymer gel electrolytes, we have estimated the rotation times of solute from the modified Stokes-Einstein-Debye(SED),[34, 58-61] $\tau_r^h = V\eta C f_s / k_B T$, where V and f_s are the volume and shape factor of solute (C153), respectively, and C is the coupling parameter of solute with surrounding environment.[62-63] We have used V = 246 Å^3, f_s = 1.71, and C = 0.24 (slip boundary condition) and 1 (stick boundary condition). Interestingly, the measured $\langle \tau_r \rangle$ are close to the slip rotation times (displayed in Fig. A.f.2, Appendix).

Next we move to the temperature dependent behavior of $\langle \tau_r \rangle$ in different polymer containing systems. Two time components, one is in 0.1-0.2 ns range (τ_1) and the other in 0.5-1 ns regime (τ_2), are observable in both polymer-free and polymer-gel electrolyte systems though their amplitudes and magnitudes change with polymer concentration. Average rotational times ($\langle \tau_r \rangle$) have been calculated for each polymer concentration at all the temperatures, presented in Table 8.2. It is clear from Table 8.2 that with increasing temperature the rotation of the probe molecule becomes faster due to the decrease of medium viscosity. Furthermore, we have tried to find out the viscosity coupling of $\langle \tau_r \rangle$ by varying the temperature for a fixed polymer concentration. Interestingly, here also, we get a fractional viscosity dependence of $\langle \tau_r \rangle$, presented in Fig. A.f.3 (Appendix), and subsequently, $p_r(T)$ values 0.75 ± 0.1 for all the polymer gel electrolyte systems considered here.

Table 8.2: Fit parameters extracted from r(t) decays measured with C153 in polymer gel electrolytes at different polymer concentrations for various temperatures. [a]

PEG Conc. (wt/wt)%	Temp. (K)	Viscosity (cP)	a_1	τ_1 (ps)	a_2	τ_2 (ps)	$\langle \tau_r \rangle$ (ps)
0	293	8.326	0.38	180	0.62	718	514
	298	7.299	0.46	146	0.54	671	430
	303	6.376	0.48	191	0.52	580	393
	308	5.622	0.49	145	0.51	568	361
	313	4.998	0.54	118	0.46	550	317
	318	4.475	0.56	100	0.44	537	292
5	293	8.209	0.50	143	0.50	812	477
	298	7.102	0.54	204	0.46	717	440
	303	6.205	0.57	162	0.43	708	397
	308	5.471	0.65	161	0.35	673	340
	313	4.863	0.58	124	0.42	614	330
	318	4.352	0.62	97	0.38	565	275
10	293	8.112	0.48	130	0.52	712	433
	298	7.017	0.55	133	0.45	692	384
	303	6.132	0.56	131	0.44	650	359
	308	5.405	0.72	127	0.28	642	271
	313	4.803	0.56	117	0.44	459	267
	318	4.298	0.56	99	0.44	427	243
15	293	8.330	0.61	187	0.39	830	438
	298	7.190	0.62	165	0.38	773	396
	303	6.269	0.62	162	0.38	721	374
	308	5.524	0.64	170	0.36	628	335
	313	4.900	0.73	144	0.27	622	273
	318	4.388	0.74	139	0.26	624	265
20	293	9.302	0.58	133	0.42	904	457
	298	7.968	0.64	168	0.36	820	403
	303	6.904	0.69	157	0.31	855	373
	308	6.043	0.72	158	0.28	819	343
	313	5.361	0.73	101	0.27	771	282
	318	4.779	0.73	111	0.27	664	260
30	293	12.926	0.48	98	0.52	912	521
	298	10.839	0.51	155	0.49	804	473
	303	9.216	0.54	171	0.46	746	436
	308	7.928	0.57	156	0.43	597	346
	313	6.896	0.60	137	0.40	621	331
	318	6.052	0.63	121	0.37	567	286
40	293	18.372	0.44	117	0.56	1117	677
	298	15.098	0.48	211	0.52	971	606
	303	12.573	0.51	197	0.49	851	517
	308	10.590	0.54	191	0.46	790	466
	313	9.104	0.56	141	0.44	759	413
	318	7.860	0.58	122	0.42	680	356

a) Fit parameters have been obtained after fixing the r_0 value at 0.376. Individual time constants are better than $\pm 5\%$ of the reported values.

Now the question: why these two p_r ($p_r(T)$ and $p_r(C)$) values are different? We think that as we are increasing the concentration of the polymer in the medium the system as a whole changes and as a result the interactions and the dynamics of the medium also change; in contrast, when we increase the temperature of the medium, keeping polymer concentration fixed, the system remains the same only the temperature-induced effects on interactions and dynamics that changes. So it is expected that the two p_r values will differ. But the important aspect is that both the p_r values indicate presence of substantial temporal heterogeneity in the medium.
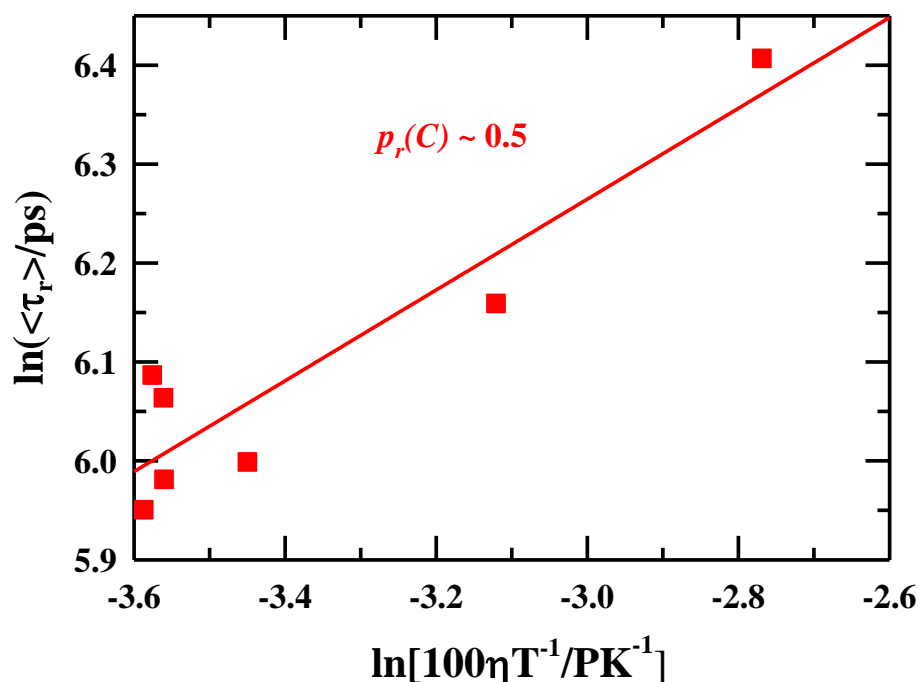
Fig. 8.3: (η/T) dependence of average rotational time ($\langle \tau_r \rangle$) for C153 in the polymer gel electrolyte systems. Solid line passing through the data points represents the fit.

8.3.3 Time-resolved Solvation Dynamics, $S(t)$: Viscosity Coupling

A comparison between the dynamical solvation response of C153 in these polymer gel electrolyte systems with the variation in polymer concentration at 298 K has been presented in Fig.8.4. A representative figure for the corresponding fluorescent transients at the red (630 nm) and blue (490 nm) wavelengths for the two different polymer concentrations (0% and 40%) are

shown in Fig. A.f.4 (Appendix). Tri-exponential fits going through the data are also presented along with the fit parameters. From this figure signature of Stokes shift dynamics can be clearly seen; only decay at blue (higher energy, relative to the peak of the steady state emission spectrum) wavelengths and rise followed by decay at the red (lower energy) wavelengths is present here.
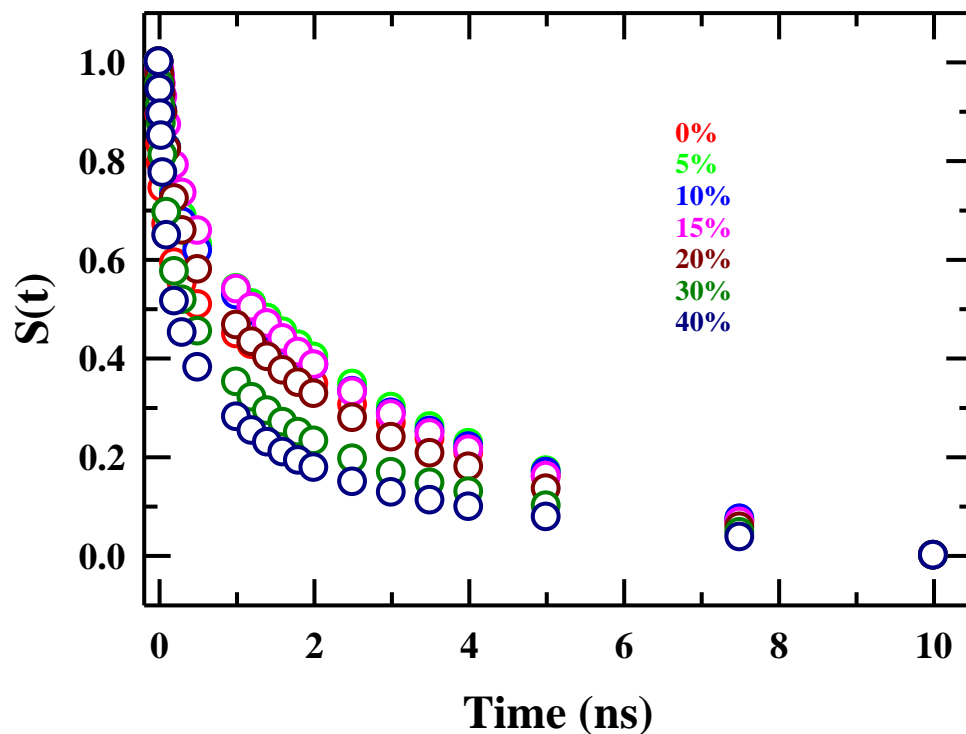
Fig. 8.4: Solvation response functions ($S(t)$) decay for C153 in the polymer gel electrolytes with different polymer concentrations at 298 K. Polymer concentrations are color-coded.

The dynamic Stokes shift, $\Delta v'_{Obs}$, has been obtained after constructing the TRES from these intensity decays and it has been presented in the Table 8.3 along with the missing percentages.[64] A representative plot of the duly constructed TRES has been shown in Fig. A.f.5. Note that we have missed a substantial amount of the total solvation response (60-70%) because a broad time resolution employed in the present measurements. Here we have used a well known

approximation procedure[65] to estimate the total dynamic Stokes shift for all the polymer gel electrolyte systems.

Table 8.3: Estimated ($\Delta\nu^t_{est}$) and observed ($\Delta\nu^t_{obs}$) dynamic Stokes shifts and percentage of missing portion of the total dynamics for C153 in (*PC+LiClO₄*) with various *PEG* concentrations at 298 K.

PEG conc. (wt%)	$\Delta\nu^t_{est}$ (10^3 cm^{-1})	$\Delta\nu^t_{obs}$ (10^3 cm^{-1})	% missed
0	1.622	0.578	64
5	1.817	0.522	71
10	1.865	0.595	68
15	1.929	0.549	72
20	1.905	0.583	69
30	1.895	0.537	72
40	1.825	0.666	64

Subsequently, fit parameters to the solvation response functions are displayed in Table 8.4. In polymer-free medium the solvation response function contains two time components, one sub-100 ps and another multi-nanosecond. The fast component is arising due to the "free" solvent molecules, as similar timescale has already been reported in pure *PC* at 252K.[37] We think that the slow component is arising due to the slow movement of the solvent molecules associated with the ions.[17] Recent simulation study[66] in this type of organic electrolytes, containing $LiBF_4$ salt at low concentrations, suggests that the solvent molecules are so strongly bound to the cations that no exchange of molecules can take place between the first and the second solvation shells of lithium ion within 100 ps timescale, whereas many exchanges are visible for the anion within the same time interval. Furthermore, it has been reported that the interaction energy for one solvent molecule at the neighborhood of cation is 10 times larger than the same for the anion. So it is more probable that the slow multi-nanosecond timescale is arising from the solvent molecules bound to Li^+. Moreover, a relaxation around 100 MHz, which corresponds to a similar time component to our measured slow time constant, has been reported by dielectric relaxation studies in these organic electrolytes.[67] As we have chosen the composition (*PC* : $LiClO_4$) at which the conductivity of the organic electrolyte close to maximum, we can expect

minimum ion pair formation in the medium and our measured dc conductivity of the polymer free system is in well agreement with previous report.[17] Even in Raman spectroscopic study, no contact ion pair has been detected at low salt concentrations.[17] So the contribution of the contact ion pairs in the solvation response function is anticipated to be much less than the contribution of the ion bound solvent molecules, which are likely to be present at large numbers participating in dynamic equilibrium with the available free solvent molecules.

Table 8.4: Fit parameters for the $S(t)$ decays in polymer gel electrolytes with various polymer concentrations at ~ 298 K. [a]

PEG conc. (wt%)	η (cP)	a_1	τ_1 (ps)	a_2	τ_2 (ps)	a_3	τ_3 (ps)	$\langle \tau_r \rangle$ (ps)
0	7.30	0.39	45	-	-	0.61	3532	2171
5	7.10	0.27	118	-	-	0.73	3344	2479
10	7.02	0.29	132	-	-	0.71	3328	2391
15	7.19	0.10	119	0.17	306	0.73	3184	2388
20	7.97	0.21	117	0.17	384	0.62	3143	2048
30	10.84	0.38	85	0.21	654	0.41	3362	1538
40	15.10	0.43	81	0.27	598	0.31	3409	1239

a) Individual time constants are better than $\pm 5\%$ of the reported values.

Now with the addition of *PEG* in the medium a third time component in the nanosecond regime (0.3-0.7 ns) emerges. The contribution of this component increases with increasing polymer concentration though the values of the other two time components remain more or less the same. The new relaxation time in the solvent response function can be connected to the cooperative intermolecular dynamics of the terminal $C-O-H$ group of the polymer molecules acting as H-bond donor or acceptor.[68] It is unexpected that flexibility of these polymer molecules[69-72] would allow the rigid-rotor mode. Moreover, similar solvent relaxation has already been observed by in the Stokes shift dynamics study of C153 in pure *PEG*. Furthermore, recent dielectric relaxation study in pure *PEG*300 have reported a similar slow component (~0.2 ns) at 298 K.[73] We have

calculated the average solvation time ($\langle\tau_s\rangle$) for each polymer concentrations. Surprisingly, with increasing polymer concentration, $\langle\tau_s\rangle$ decreases and at 40 wt% *PEG* concentration it reaches to a value which is almost half of the $\langle\tau_s\rangle$ measured for 0 wt% *PEG* (see Table 8.4). Fig. 8.5 depicts the concentration dependence (in terms of viscosity of the medium) of $\langle\tau_s\rangle$ at a constant temperature (298 K). Note that $\langle\tau_s\rangle$ follows the fractional viscosity dependence with a negative $p_s(C)$ value, $p_s(C) \sim -0.8$.

We know that in solvation dynamics we actually examine the relaxation of the solvent molecules around the excited probe molecule. With increasing polymer concentration the abundance of the polymer molecules around the probe molecule increases by replacing the ion-solvent adducts. Thus, the contribution of the polymer molecules in the solvation dynamics of the probe molecule increases resulting faster solvation of the probe molecules. Fluorescence anisotropy measurements, which suggests the presence of temporal heterogeneity in the medium, also supports the partial viscosity decoupling of $\langle\tau_s\rangle$. The intermolecular H-bond relaxation dynamics of the polymer molecules is the dictating factor to the solvation dynamics of C153.
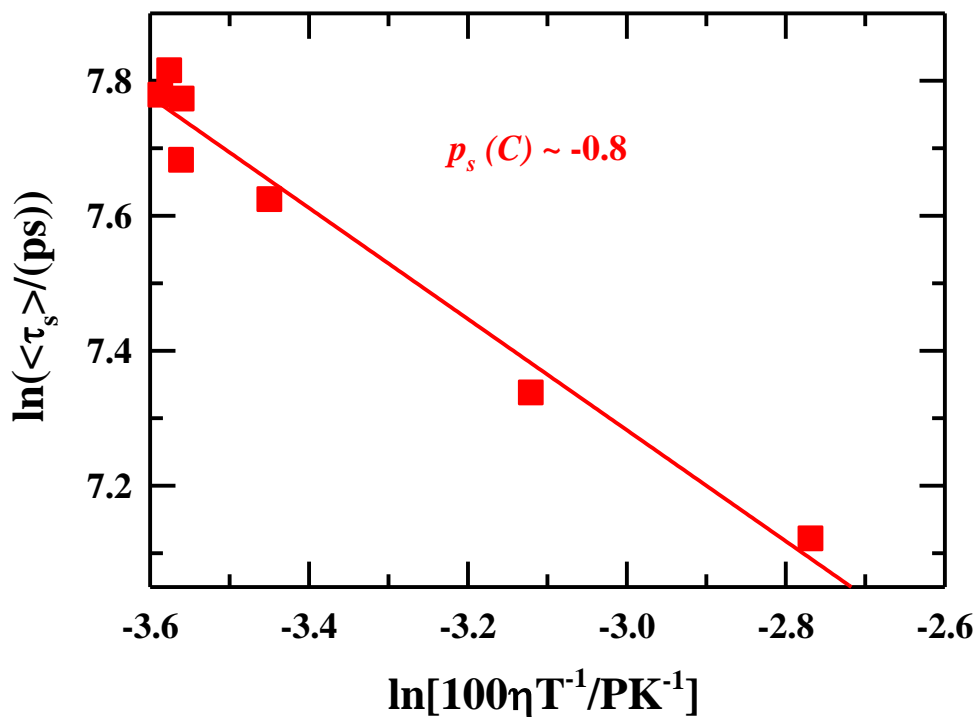
Fig. 8.5: (η/T) dependence of average solvation time ($\langle \tau_s \rangle$) for C153 in the polymer gel electrolyte systems. Solid line passing through the data points represents the fit.

Dielectric relaxation spectroscopy in gigahertz to terahertz frequency regime can be very helpful to understand the unexplored fast dynamics of these systems. At elevated temperature (~ 303K), we miss almost 80% of the total solvation response, and this restricts us to study the temperature dependent solvation dynamics of C153 in these complex systems.

8.4 Conclusion

In summary, the above work presented here clearly depicts the viscosity decoupling of rotation and solvation of C153 in the polyethylene glycol based polymer gel electrolyte system although the dc conductivity (κ) of the medium follows the Walden law, i.e. $\eta\kappa$ = constant, reasonably well, presented in Fig. A.f.6 (Appendix). Excitation wavelength dependent emission studies reveal that these systems are spatially homogeneous though the TRF studies indicate something

different. The fractional viscosity dependence of the average rotation time of C153 has been observed for polymer-free as well as polymer containing systems. Both temperature and concentration dependent p ($p_r(T)$ and $p_r(C)$) values deviate substantially from unity which can be ascribed as the manifestation of temporal heterogeneity, present in the medium. Complete viscosity decoupling of the average solvation time of C153 re-emphasizes the presence of temporal heterogeneity in the medium. The decrease in average solvation time with increasing polymer concentration, rather with increasing viscosity of the medium, signifies remarkable effect of polymer in the solvation dynamics of the photo-excited probe molecule. The appearance of a new time component in the solvation response function of C153 in the polymer containing systems (above 15 wt% of polymer) and the close similarity of this time component with the previously reported DR and solvation time constants of C153 in pure $PEG300$ re-establishes the impact of the polymer in the solution structure of these polymer gel electrolytes. Realistic simulation studies in these complex chemical systems can be very helpful to understand the interactions and dynamics of these systems.

References

1.   M. Armand and J.-M. Tarascon, Nature **451**, 652 (2008).

2.   J.-M. Tarascon and M. Armand, Nature **414**, 359 (2001).

3.   Y.-C. Lu, Z. Xu, H. A. Gasteiger, S. Chen, K. Hamad-Schifferli and Y. Shao-Horn, J. Am. Chem. Soc. **132**, 12170 (2010).

4.   P. Simon and Y. Gogotsi, Nat. Mater. **7**, 845 (2008).

5.   T. Ogasawara, A. Débart, M. Holzapfel, P. Novák and P. G. Bruce, J. Am. Chem. Soc. **128**, 1390 (2006).

6.   A. M. Stephan, Eur. Polym. J. **42**, 21 (2006).

7.   O. Ileperuma, Mater. Technol. **28**, 65 (2013).

8.   J. Wu, Z. Lan, J. Lin, M. Huang, Y. Huang, L. Fan and G. Luo, Chem. Rev. **115**, 2136 (2015).

9.   H. Yu, J. Wu, L. Fan, Y. Lin, K. Xu, Z. Tang, C. Cheng, S. Tang, J. Lin, M. Huang and Z. Lan, J. Power Sources **198**, 402 (2012).

10.   F. Croce, G. Appetecchi, L. Persi and B. Scrosati, Nature **394**, 456 (1998).

11.   K. Xu, Chem. Rev. **104**, 4303 (2004).

12.   B. Klassen, R. Aroca, M. Nazri and G. Nazri, J. Phys. Chem. B **102**, 4795 (1998).

13.   L. Yang, A. Xiao and B. L. Lucht, J. Mol. Liq. **154**, 131 (2010).

14.   E. Cazzanelli, P. Mustarelli, F. Benevelli, G. B. Appetecchi and F. Croce, Solid State Ionics **86**, 379 (1996).

15.   H. L. Yeager and H. Reid, J. Phys. Chem. **80**, 850 (1976).

16.   H. L. Yeager, J. D. Fedyk and R. J. Parker, J. Phys. Chem. **77**, 2407 (1973).

17.   D. Battisti, G. Nazri, B. Klassen and R. Aroca, J. Phys. Chem. **97**, 5826 (1993).

18.   K. Kondo, M. Sano, A. Hiwara, T. Omi, M. Fujita, A. Kuwae, M. Iida, K. Mogi and H. Yokoyama, J. Phys. Chem. B **104**, 5040 (2000).

19.   Z. Gadjourova, Y. G. Andreev, D. P. Tunstall and P. G. Bruce, Nature **412**, 520 (2001).

20.   W. Gorecki, P. Donoso, C. Berthier, M. Mali, J. Roos, D. Brinkmann and M. Armand, Solid State Ionics **28**, 1018 (1988).

21.   A. Triolo, V. Arrighi, R. Triolo, S. Passerini, M. Mastragostino, R. Lechner, R. Ferguson, O. Borodin and G. Smith, Physica B: Condensed Matter **301**, 163 (2001).

22.   P. Carlsson, R. Zorn, D. Andersson, B. Farago, W. Howells and L. Börjesson, J. Chem. Phys. **114**, 9645 (2001).

23.   D. Andersson, D. Engberg, J. Swenson, C. Svanberg, W. Howells and L. Börjesson, J. Chem. Phys. **122**, 234905 (2005).

24.   T. Yamaguchi, R. Matsui and S. Koda, J. Phys. Chem. B **117**, 7077 (2013).

25.   J. Song, Y. Wang and C. Wan, J. Power Sources **77**, 183 (1999).

26.   C. Svanberg, J. Adebahr, H. Ericson, L. Börjesson, L. Torell and B. Scrosati, J. Chem. Phys. **111**, 11216 (1999).

27.   H. Saito, A. S. Hoffman and H. I. Ogawa, J. Bioact. Compat. Polym. **22**, 589 (2007).

28.   C. Fruijtier-Pölloth, Toxicology **214**, 1 (2005).

29.   A. Samanta, J. Phys. Chem. B **110**, 13704 (2006).

30.   B. Guchhait, S. Das, S. Daschakraborty and R. Biswas, J. Chem. Phys. **140**, 104514 (2014).

31.   B. Guchhait, S. Daschakraborty and R. Biswas, J. Chem. Phys. **136**, 174503 (2012).

32.   B. Guchhait and R. Biswas, J. Chem. Phys. **138**, 114909 (2013).

33.   R. Baumann, C. Ferrante, E. Kneuper, F.-W. Deeg and C. Bräuchle, J. Phys. Chem. A **107**, 2422 (2003).

34.   M.-L. Horng, J. Gardecki and M. Maroncelli, J. Phys. Chem. A **101**, 1030 (1997).

35.   S. Indra and R. Biswas, J. Chem. Phys. **142**, 204501 (2015).

36.   R. Karmakar and A. Samanta, J. Phys. Chem. A **106**, 4447 (2002).

37.   M. Maroncelli and G. R. Fleming, J. Chem. Phys. **86**, 6221 (1987).

38.   D. Roy, S. K. Mondal, K. Sahu, S. Ghosh, P. Sen and K. Bhattacharyya, J. Phys. Chem. A **109**, 7359 (2005).

39.   P. Hazra, D. Chakrabarty and N. Sarkar, Chem. Phys. Lett. **371**, 553 (2003).

40.   L. Reynolds, J. Gardecki, S. Frankland, M. Horng and M. Maroncelli, J. Phys. Chem. **100**, 10337 (1996).

41.   K. Mukherjee, A. Barman and R. Biswas, J. Mol. Liq. **222**, 495 (2016).

42.   G. Kalita, K. G. Sarma and S. Mahiuddin, J. Chem. Eng. Data **45**, 912 (2000).

43.   T. Pradhan and R. Biswas, J. Phys. Chem. A **111**, 11514 (2007).

44.   H. A. R. Gazi, B. Guchhait, S. Daschakraborty and R. Biswas, Chem. Phys. Lett. **501**, 358 (2011).

45. A. Das and R. Biswas, J. Phys. Chem. B **119**, 10102 (2015).

46. H. A. R. Gazi, H. K. Kashyap and R. Biswas, J. Chem. Sci. **127**, 61 (2015).

47. T. Pradhan, H. A. R. Gazi, B. Guchhait and R. Biswas, J. Chem. Sci. **124**, 355 (2012).

48. R. Biswas, A. R. Das, T. Pradhan, D. Touraud, W. Kunz and S. Mahiuddin, J. Phys. Chem. B **112**, 6620 (2008).

49. T. Pradhan, P. Ghoshal and R. Biswas, J. Chem. Sci. **120**, 275 (2008).

50. S. Indra, B. Guchhait and R. Biswas, J. Chem. Phys. **144**, 124506 (2016).

51. R. Biswas, J. Lewis and M. Maroncelli, Chem. Phys. Lett. **310**, 485 (1999).

52. J. Lewis, R. Biswas, A. Robinson and M. Maroncelli, J. Phys. Chem. B **105**, 3306 (2001).

53. A. Pal, G. Dass and A. Kumar, J. Chem. Eng. Data **43**, 738 (1998).

54. M. D. Ediger, Annu. Rev. Phys. Chem. **51**, 99 (2000).

55. M. D. Ediger, C. Angell and S. R. Nagel, J. Phys. Chem. **100**, 13200 (1996).

56. H. Sillescu, J. Non-Cryst. Solids **243**, 81 (1999).

57. C. Angell, J. Chem. Phys. **46**, 4673 (1967).

58. B. Bagchi, *Molecular Relaxation in Liquids*. (Oxford University Press, New York, 2012).

59. J. L. Dote, D. Kivelson and R. N. Schwartz, J. Phys. Chem. **85**, 2169 (1981).

60. A. Das, R. Biswas and J. Chakrabarti, J. Phys. Chem. A **115**, 973 (2011).

61. A. Das, R. Biswas and J. Chakrabarti, Chem. Phys. Lett. **558**, 36 (2013).

62. H. Jin, G. A. Baker, S. Arzhantsev, J. Dong and M. Maroncelli, J. Phys. Chem. B **111**, 7291 (2007).

63. C. M. Hu and R. Zwanzig, J. Chem. Phys. **60**, 4354 (1974).

64. B. Guchhait, R. Biswas and P. K. Ghorai, J. Phys. Chem. B **117**, 3345 (2013).

65. R. Fee and M. Maroncelli, Chem. Phys. **183**, 235 (1994).

66. J.-C. Soetens, C. Millot and B. Maigret, J. Phys. Chem. A **102**, 1055 (1998).

67. T. Yamaguchi, M. Hayakawa, T. Matsuoka and S. Koda, J. Phys. Chem. B **113**, 11988 (2009).

68. S. Schrödle, R. Buchner and W. Kunz, J. Phys. Chem. B **108**, 6281 (2004).

69. Y. Kuroda and M. Kubo, J. Polym. Sci. **26**, 323 (1957).

70. K. J. Liu and R. Ullman, J. Chem. Phys. **48**, 1158 (1968).

71. G. D. Smith, D. Y. Yoon, C. G. Wade, D. O'Leary, A. Chen and R. L. Jaffe, J. Chem. Phys. **106**, 3798 (1997).

72. L. Livadaru, R. Netz and H. Kreuzer, J. Chem. Phys. **118**, 1404 (2003).

73. C. Mali, S. Chavan, K. Kanse, A. Kumbharkhane and S. Mehrotra, Indian J. Pure Appl. Phys. **45**, 476 (2007).

Chapter 9

Impact of the Aggregation Behaviour of Sodium Cholate and Sodium Deoxycholate on Aqueous Solution Structure and Dynamics: A Combined Time Resolved Fluorescence and Dielectric Relaxation Spectroscopic Study

9.1 Introduction

Amphiphilic bile salts are the prime by-products of cholesterol metabolism and, biologically, they are important surfactant molecules for human body system.[1-6] Physiological activities of bile salts include transportation of lipid molecules,[4] controlling of the biosynthesis of bile acid and cholesterol by a negative feedback mechanism and their complexation with cations to enhance the intestinal absorption of Ca^{2+} [5] etc. The chemical structures, presented in A.g.1 (Appendix), of these salt molecules, containing hydrophobic and hydrophilic faces instead of polar head and non-polar tail groups, are markedly different from that of the conventional surfactant (ionic or non-ionic) molecules.[7] The concave side (the hydrophilic face) of the molecule is containing the hydroxyl and the carboxylate groups whereas the convex side (the hydrophobic side) is holding the methyl groups. The aggregation of these molecules in water is driven by this typical structure. Sodium cholate (SC) and sodium deoxycholate (SDC) are the two bile salts which have been studied previously[8-16] but several aspects have still remained unexplored. For example, how does the presence of an additional hydroxyl group in SC (please see Fig. A.g.1, Appendix) affect the aggregation behaviour in aqueous medium and alter the over-all aqueous dynamics? How different are SC and SDC in their hydrophobic characters?

Interestingly, both experimental [8,17-22] and simulation [23-24] studies have reported dependence of size and shape of the aggregates on bile salt concentration in aqueous solutions. Different aggregation mechanisms [25-27] have been invoked to explain this atypical micellization behaviour. The first of them (primary-secondary micelle model) assumes that the primary aggregation, occurring just above the critical micellar concentration (CMC[1]), is the formation of small

aggregates via interaction among a few to several monomers (2 to 10 monomers) through their hydrophobic faces.[1] At higher concentrations (CMC[2]), the primary aggregates form larger aggregates (secondary micelles) via hydrogen bond formation and hydrophobic interaction. Our study here involves three concentrations to cover the primary and secondary micellization regions. Bile salt aggregates, containing sites of differing polarities, are good candidates for trapping hydrophobic molecules[28-29] and can fulfil various application purposes.[30-33] Vehicular roles for bile acids as drug carriers in live cell systems have also been explored of late.[34-36]

In this work, time resolved fluorescence (TRF) and dielectric relaxation (DR) measurements have been carried out for aqueous solutions of SC and SDC at three different milli-molar (mM) concentrations, 30 mM, 100 mM and 300 mM. TRF is a useful technique for exploring the environmental dynamics for a variety of media,[37-43,46] and we focus here on the concentration dependent slow dynamics of these aqueous bile salt solutions using a temporal resolution <100 ps. C153 is chosen as the fluorescent solute probe because experimental studies and quantum mechanical calculations have shown that this molecule is one of the best suited polarity probes[48-60] for the kind of measurements proposed here. However, different fluorescent probes have been used earlier to characterize the CMCs[61-64] of these salts and Stokes shift dynamics of aqueous SDC solutions at 100 mM concentration.[10,38] These studies indicate that primary aggregation in aqueous medium for both of these bile salts is complete within ~20 mM concentration and secondary aggregates form at concentrations <60 mM. Our present study therefore sheds light on aqueous solution dynamics that predominantly contains primary aggregates and compare that with the medium where secondary aggregates dominate. In this way, the dependence of solution dynamics on the aggregation state is explored, facilitating a comparison between the solution dynamics containing SC and SDC at comparable concentrations. The solution dynamics is further examined via DR measurements in the frequency range, $0.2 \leq \nu(\text{GHz}) \leq 50$, for providing fidelity to the Stokes shift dynamics time scales and assistance in interpreting the measured fluorescence dynamics in terms of solvent orientational polarization relaxation[65-71]. Such a combined and comparative study of aqueous bile salt solution dynamics via DR and TRF measurements is new and presented here. Note here that dynamics of aqueous macromolecular solutions has been explored extensively through DR measurements[72-81] which have reported

presence of both bulk-like free and bound water molecules. Our present study reveals a concentration dependence of such differing time scales in aqueous SC and SDC solutions.

9.2 Experimental Details

9.2.1 Materials and Methods

Laser grade Coumarin 153 was used as received (Exciton). Bile salts (SDC and SC) were purchased from Sisco Research Laboratories (SRL) and vacuum dried before use. Millipore water was used for preparing the aqueous solutions of the surfactants. Solutions of three different concentrations (30 mM, 100 mM and 300 mM) were prepared by dissolving the requisite amounts of bile salts in water and stirring. Concentration of C153 in each of these samples was maintained at $\sim 10^{-5}$ M. Temperature was maintained via a temperature controller (Julabo), and sufficient time was allowed for achieving temperature equilibrium for each sample before measurement. The sample temperature was maintained within $\pm 0.5\,\mathrm{K}$ of the desired temperature.

9.2.2 Steady State Measurements

Steady state absorption and emission spectra were collected by using a UV-Visible spectrophotometer (UV-2600, Shimadzu), and a fluorimeter (Fluorolog, Jobin-Yvon, Horiba), respectively. Spectra were then solvent-blank subtracted and processed accordingly before further analyses and frequency determination.[82-84] Details about the measurement techniques are the same as described in chapter 2.

9.2.3 Differential Scanning Calorimetric (DSC) Measurements

To investigate the presence of bound water molecules, DSC (TA Instruments Q2000) technique was applied. The samples were hermetically sealed in an aluminium pan (40 μl, Tzero, TA Instruments) to prevent evaporation during the measurements.

9.2.4 Viscosity and Sound Velocity Measurements

Sound velocity and viscosity coefficients (η) were measured by using an automated temperature-controlled density-cum-sound analyzer (Anton Paar, model DSA 5000) and micro viscometer (AMVn, Anton Paar), respectively.[85-86]

9.2.5 Time-resolved Fluorescence Measurements

Time-resolved fluorescence measurements were performed with a time-correlated single-photon counting (TCSPC) system described earlier in chapter 2 and in refs .[47,87-89] The full width at half-maximum (fwhm) of the instrument response function (IRF) was ~80 ps.

9.2.6 DR Measurement Details

The DR data collection technique and the data analysis procedures are the same as described in chapter 2 and in refs.[91-94] Approximately, 10 mL of the each mixture were subjected for DR measurements after proper thermal equilibriation in an appropriately humidity-controlled environment.

9.3 Results and Discussion

9.3.1 Steady State Spectral Features: A Comparison between SC and SDC Solutions

UV-VIS absorption and fluorescence emission spectra of C153 dissolved in these aqueous media at three different concentrations are shown in Fig. 9.1. Absorption and emission spectra of C153 in cyclohexane are also shown in these panels in order to indicate the vibrational features that are common to C153 spectra in non-polar solvents also appear in the spectra obtained for aqueous SDC solutions. Interestingly, absorption and emission spectra in presence of both these bile salts show concentration dependent blue shift although the extent of shift is larger for solutions with SC. Furthermore, emission spectra in aqueous SC solutions are much narrower than those for SDC solutions although the absorption spectra in both these media are characterized by comparable widths (full width at half maximum abbreviated as fwhm and denoted by $\Gamma_{em./abs.}$). These spectral features are quantitatively presented in Table 9.1 where average frequencies[95-96] and widths (fwhm) are summarized. A closer look to this table also indicate that the absorption and emission spectral frequencies for C153 in SDC solution at each of the concentrations studied are blue-shifted compared to the corresponding frequencies in SC solution. The relatively blue-shifted spectra and larger emission widths in SDC solutions suggest that local environments around C153 in these solutions are different from those in SC solutions. This difference can be attributed to the additional –OH group that is present in SC affecting the aggregation behaviour in solution.
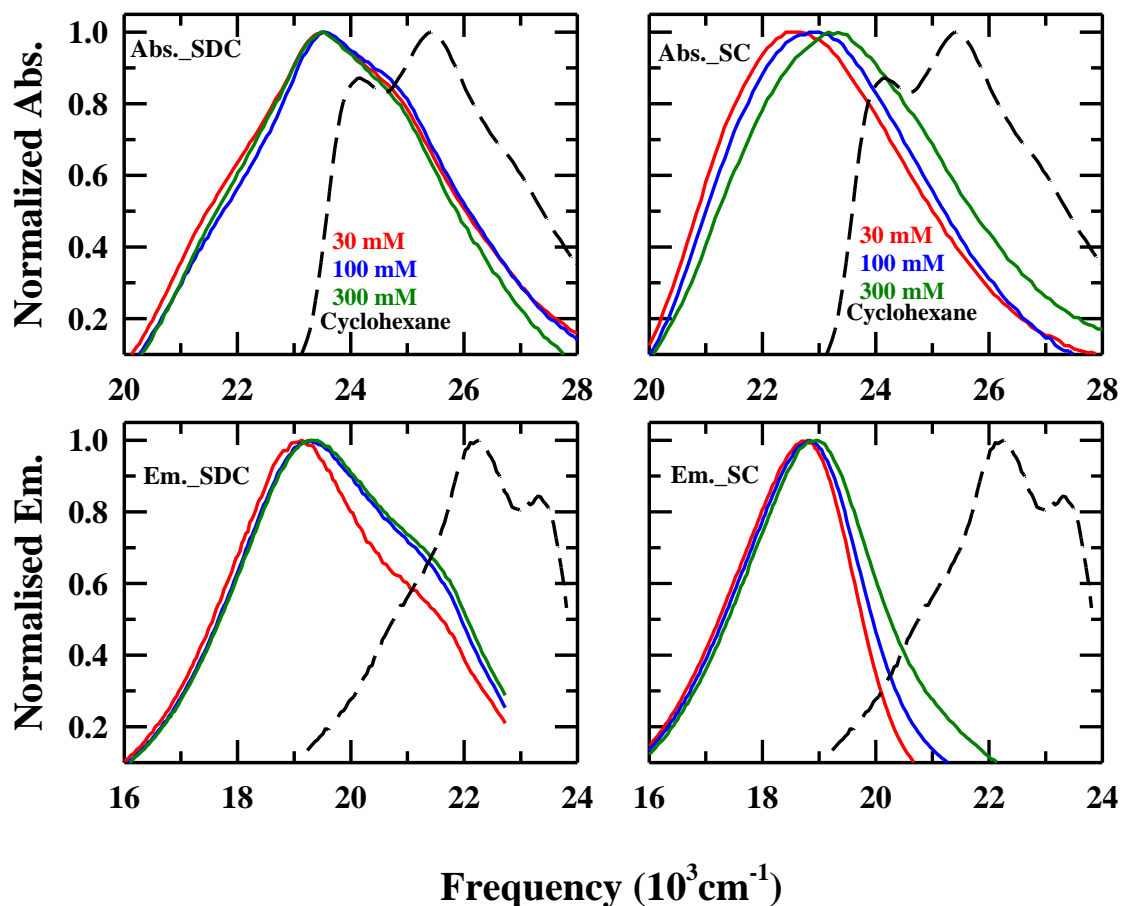
Fig. 9.1: Representative absorption (upper panel) and emission (lower panel) spectra of C153 in aqueous solutions of SC and SDC at three different concentrations at ~298 K. Spectra of the same solute in cyclohexane are also shown (dashed lines). Spectra at different concentrations are color-coded.

The aggregation behaviour of these bile salts in aqueous solutions (that is, formation of micelles) then naturally brings in the issue of solution heterogeneity. This can be probed by conducting excitation wavelength ($\lambda_{exc.}$) dependence of the emission spectral width ($\Gamma_{em.}$) of a dissolved fluorescent solute. Because spectral widths derive contributions from both solute-medium interaction and distribution of solvation environment around the solute, $\lambda_{exc.}$ dependence of $\Gamma_{em.}$ reflects photo-selection of solvation environments that are stable during the period of the fluorescence lifetime.[97-100]

Table 9.1: A comparison of spectral frequencies and widths between aqueous SC and SDC solutions at ~298 K. Typical error bars for the frequencies and widths are within ± 250 cm^{-1}.

System	$v_{abs.}$ (10^3cm^{-1})	$v_{em.}$ (10^3cm^{-1})	$\Gamma_{abs.}$ (10^3cm^{-1})	$\Gamma_{em.}$ (10^3cm^{-1})
30 mM SC	22.895	18.553	4.228	2.540
100 mM SC	23.107	18.690	4.164	2.636
300 mM SC	23.483	18.887	4.528	2.859
30 mM SDC	23.778	19.373	4.573	4.031
100 mM SDC	23.870	19.563	4.335	4.288
300 mM SDC	23.711	19.617	4.243	4.363
Cyclohexane	25.362	22.076	3.593	3.034

Fig. 9.2 presents results of such a study using C153 in both of these solutions at the three different concentrations. Upon changing the $\lambda_{exc.}$ from 390 nm to 490 nm $\Gamma_{em.}$ shows a dispersion of ~2000 cm^{-1} for SDC solutions at all the three concentrations whereas the maximum dispersion for SC solutions is found to be ~900 cm^{-1} at 300 mM concentration. Qualitatively similar behaviour has also been observed for the $\lambda_{exc.}$ dependent emission peak frequencies ($v_{em.}$) shown in Fig. A.g.2 (Appendix). These results strongly indicate that aqueous SDC solutions are more heterogeneous than the SC containing ones. Temperature dependent emission spectra in SC and SDC solutions at 300 mM concentration, presented in Fig. A.g.3 (Appendix), indicate that the shoulder at high frequency end softens up with the increase of solution temperature; the extent of softening is more pronounced for SDC solutions than for SC solutions. This provides further support in favour of SDC solutions being more heterogeneous than SC solutions.
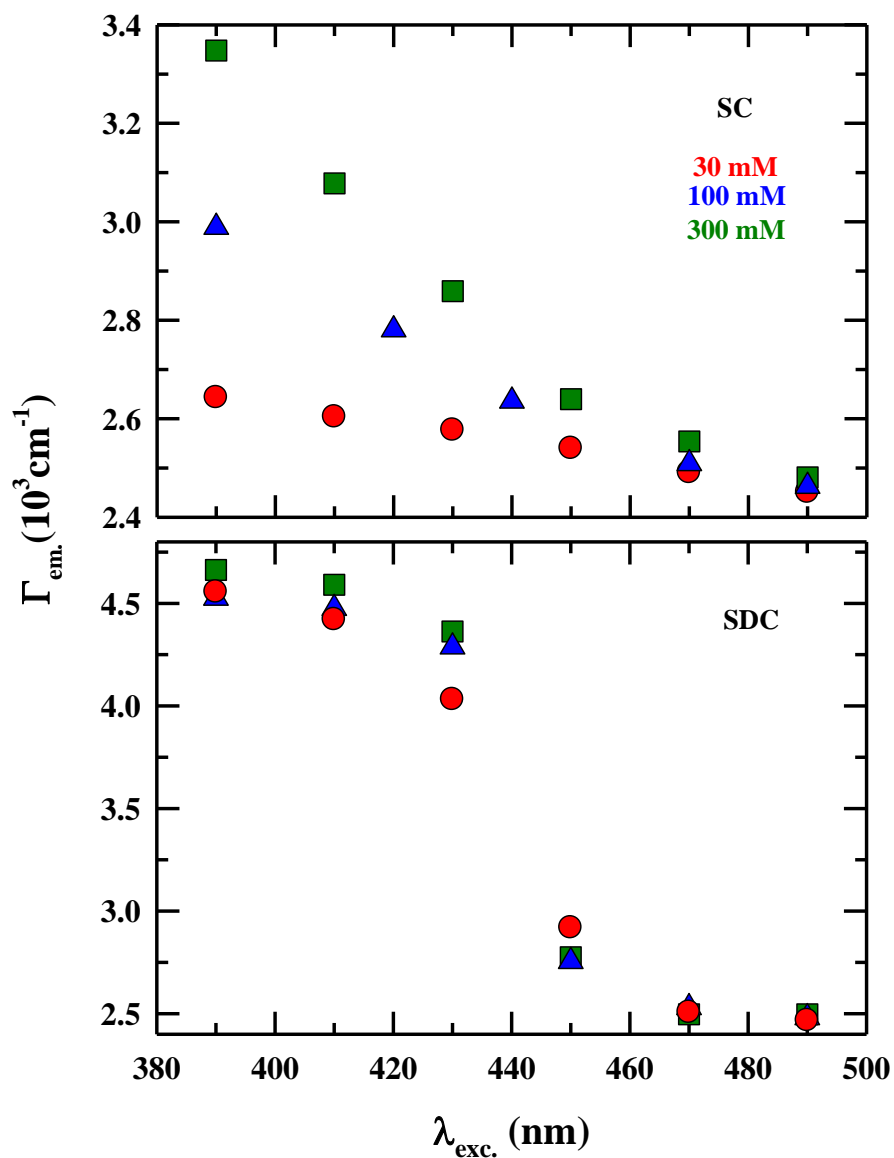
Fig. 9.2: Excitation wavelength ($\lambda_{exc.}$) dependence of emission spectral width (full width at half maximum, fwhm) of C153 in SC (upper panel) and SDC (lower panel) solutions at three different concentrations and ~298 K. Circles indicate the 30 mM concentration whereas the triangles and the squares represent the 100 mM and 300 mM concentrations, respectively. Representations are color-coded.

9.3.2 Time-resolved Fluorescence Anisotropy, *r(t)*: Slower Solute Rotation in SDC Solutions

Fig. 9.3 compares the *r(t)* decays for C153 in aqueous SC and SDC solutions at 30 mM (upper panel) and 300 mM (lower panel) concentrations at 298 K along with the bi-exponential fits (line) through them. A representative figure showing the collected $I_{para}(t)$ and $I_{perp}(t)$ decays are presented in Fig. A.g.4 along with residuals from a fit to *r(t)* in Fig. A.g.5 (Appendix). These figures suggest the typical quality of fits obtained for the *r(t)* decays discussed here. Note in Fig. 9.3 that *r(t)* decay in SDC solutions is slower than that in SC solutions and the slowing down becomes more pronounced at higher concentrations. This can be qualitatively understood from the measured temperature dependent η provided in Table A.g.6 (Appendix). Fit parameters summarized in Table 9.2 indicate that anisotropy decay in both the systems possess well separated time scales which may or may not reflect distribution of C153 in different solvation environments.[45] The relatively slower solute rotation can be understood from the measured temperature dependent viscosity coefficients η provided in Table A.g.6 (Appendix). For example, at 300 mM concentration the ratio between the average rotation times in SDC and SC solutions $(\langle\tau_r\rangle_{SDC}/\langle\tau_r\rangle_{SC})$ is ~1.9 which correlates well with the ratio between the corresponding solution viscosities, η_{SDC}/η_{SC} ~1.6. Another feature to note is that the slower nanosecond component dominates the *r(t)* decays at all concentrations for both the systems, producing average rotation times in the ~1-3 ns regime. Given that the extrapolated value of $\langle\tau_r\rangle$ for C153 in water is ~40 ps,[45] these slower rotation times suggest location of C153 near the aggregated surface in these aqueous bile salt solutions. Stronger aggregation behaviour for SDC then leads to slower solute rotation compared to that in SC solutions. This corroborates well with the $\lambda_{exc.}$ dependent fluorescence emission results presented earlier in Fig. 9.2.
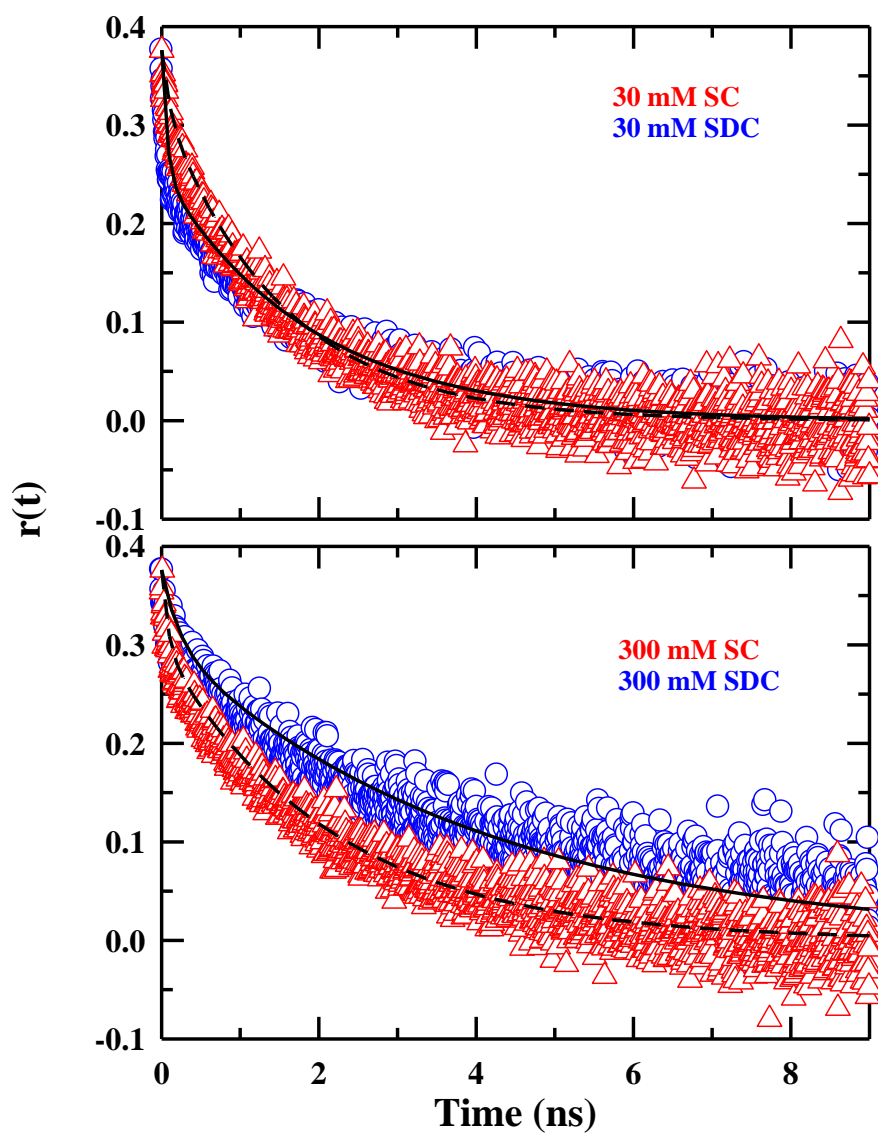
Fig. 9.3: Representative time-resolved fluorescence anisotropy ($r(t)$) decays for C153 in aqueous SC and SDC solutions at 30 mM (upper panel) and 300 mM (lower panel) concentrations. The solutions were excited at 298 K using a laser light of 445 nm. Red triangles indicate the data at 30 mM concentration and blue circles those at 300 mM concentration. Black (dashed for SC and solid for SDC) lines passing through the data points denote the bi-exponential fits through them.

Table 9.2: Fit parameters required for the bile salt concentration dependent *r(t)* decays measured with C153 in SC and SDC solutions at ~298 K.

SC_Excitation at 445 nm							
Concentration (mM)	$a_1^{\ b}$	τ_1 (ns)	a_2	τ_2 (ns)	$<\tau_r>$ (ns)	χ^2	$r_0^{\ c}$
30	14%	0.094	86%	1.5	1.303	0.0004	0.38±0.02
100	16%	0.068	84%	1.678	1.420	0.0004	0.34±0.02
300	20%	0.084	80%	2.153	1.739	0.0004	0.36±0.02
SDC_Excitation at 445 nm							
Concentration (mM)	$a_1^{\ b}$	τ_1 (ns)	a_2	τ_2 (ns)	$<\tau_r>$ (ns)	χ^2	$r_0^{\ c}$
30	33%	0.065	67%	1.888	1.286	0.0004	0.41±0.04
100	14.7%	0.074	85.3%	2.483	2.129	0.0007	0.33±0.02
300	19%	0.227	81%	3.962	3.252	0.0006	0.30±0.02

b) Fit parameter have been obtained after fixing the r_0 value at 0.376. Individual time constants are better than ± 5% of the reported values.

c) r_0 values obtained from unconstrained fits.

9.3.3 Dynamic Stokes Shift Measurements: Slower Solvation Response in SDC Solutions

A comparison between the dynamical solvation response measured by using C153 in SC and SDC aqueous solutions is depicted in Fig. 9.4 where the measured decays of the solvation response functions, *S(t),* at 300 mM bile salt concentration and 298 K is shown as a function of time. Corresponding fluorescent transients at the red (610 nm) and blue (470 nm) wavelengths are shown in Fig. A.g.7(Appendix). Tri-exponential fits going through the data are also presented here along with the fit parameters. It is evident from this figure that, like solute rotation, solute solvation is also slower in SDC compared to that in SC. Qualitatively similar results have also been found at the other two concentrations studied.
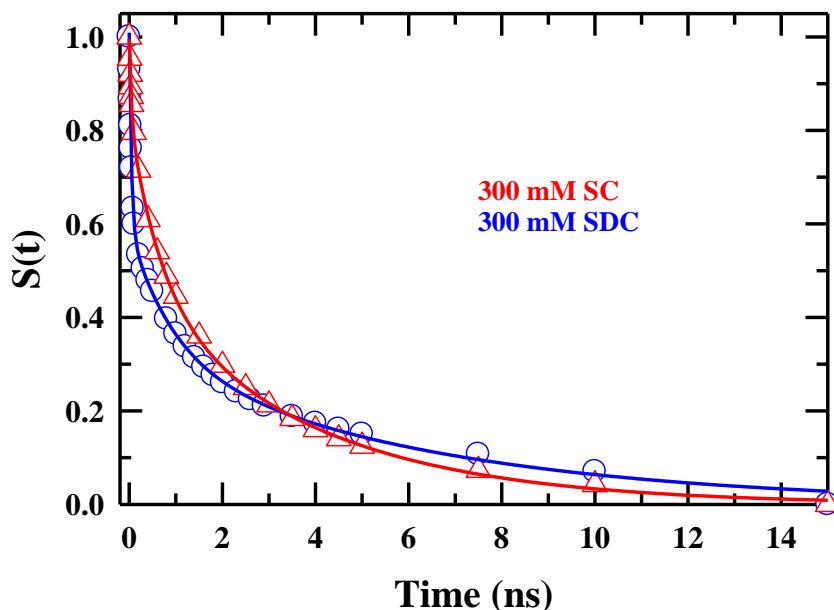
Fig. 9.4: Representative decay of measured solvation response functions (*S(t)*) for C153 in 300 mM SC and SDC solutions at ~298 K. Blue circles (for SDC) and red triangles (for SC) represent the experimental data points; solid lines through them are tri-exponential fits.

Fit parameters summarized in Table 9.3 suggest that the measured responses are characterized by sub-100 ps, nanosecond and multi-nanoseconds solvation components with dynamic shift magnitudes ~400-500 cm^{-1}. Note here that the use of broad temporal resolution in these

measurements has led to the missing of the ultrafast sub-100 femtosecond component reported for bulk water,[101-102] amplitude of which could be quite large for these systems. Interestingly, the sub-100 ps and nanosecond components are very similar to those observed earlier for the aqueous micelles[40,42,46] and reverse micelles (RMs) of sodium bis(2-ethylhexyl) sulfosuccinate (AOT) and Igepal CO-520(IGPAL).[37] Computer simulation studies of solvation dynamics in these RMs have further suggested that the nanosecond component is linked to the surface-bound water molecules in these confined environments.[37]

Table 9.3: Observed dynamic Stokes shift magnitudes and fit parameters of the $S(t)$ decays at in aqueous solutions at various bile salt concentrations and ~298 K.

System	Excitation	Observed Dynamic Stokes Shift $(10^3 cm^{-1})$	a_1	τ_1 $(ps)^a$	a_2	τ_2 (ps)	a_3	τ_3 (ps)	$<\tau_{av}>$ (ps)
30 mM SDC	Excitation-445 nm	0.483	0.60	21	0.19	1236	0.22	6296	1632
100 mM SDC		0.519	0.59	21	0.19	1130	0.23	6199	1652
300 mM SDC		0.471	0.42	48	0.26	900	0.32	6150	2222
30 mM SC	Excitation-445 nm	0.348	0.30	73	0.31	500	0.37	2539	1116
100 mM SC		0.429	0.24	68	0.35	708	0.41	3140	1551
300 mM SC		0.529	0.16	46	0.35	654	0.47	3774	2010

a) Individual time constants are better than $\pm 5\%$ of the reported values.

We therefore ascribe the sub-100 ps and nanosecond solvation components in these systems to the slow water molecules near the surface of the bile salt aggregates that are participating in the bound-to-free dynamical equilibrium.[81, 103] The slowest component with timescale in the 3-6 ns regime may have arisen from the stiffened movement of the alkyl chain containing the carboxylate (-$CH_2CH_2COO^-$) group. Further studies are required to examine this proposition as the role of counter-ions in producing the slower component is under debate.[104]

9.3.4 Dielectric Relaxation Measurements: Observation of Slow Water

Fig. 9.5 presents the DR spectra of SC and SDC systems at the three different concentrations considered here. Simultaneous 4-Debye fits to the permittivity ($\varepsilon'(v)$) and loss ($\varepsilon''(v)$) components of the spectra are also shown.
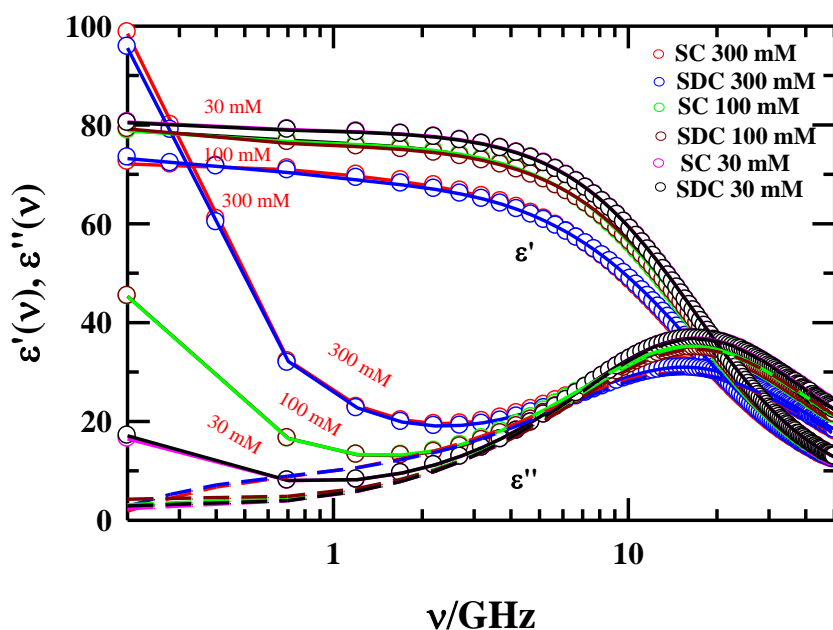
Fig. 9.5: Concentration dependence of the real (ε') and imaginary (ε'') parts of the measured complex DR spectra for aqueous SC and SDC solutions at three different bile salt concentrations. Solid lines are simultaneous 4-Debye fits through the real and imaginary components. Dashed lines depict the data points constructed after subtracting the conductivity contribution ($\frac{\kappa}{2\pi v}$) from the imaginary component of the DR spectrum. Spectra at different concentrations are color coded. Measurements are done at ~293 K.

Note that in the same figure fits to $\varepsilon''(v)$ subtracting the conductivity contribution[90,94] are also presented (dashed lines). Needless to mention that such an exercise did not change the fit parameters summarized in Table 9.4. Notice that the 9 ps DR component accounts for ~80-90% of the total dispersion. This component represents the cooperative relaxation of bulk-like water molecules[105-108] that are present in these solutions. Likewise, the 1 ps component (kept fixed during fit) which appears with a tiny amplitude due to our limited coverage at the high frequency end may be related to the single particle rotation of free water.[105] The presence of the bile salts in these aqueous media is then reflected via the other two much slower relaxations which are in ~200-1000 ps range and ~20-40 ps range. Interestingly, these time scales have also been observed in our dynamic Stokes shift measurements (see Table 9.3). This correspondence between the DR and dynamic Stokes shift time scales is expected because both the measurements probe the orientational polarization relaxation of the environment.[65] Following the arguments provided during the discussion of Stokes shift dynamics time scales, these slow DR times (τ_1 and τ_2) are attributed to the slow water molecules that are near the surface of the aggregates (formed by SC and SDC in aqueous solution) and participating in the bound-to-free dynamic equilibrium.[72,80,81] The presence of surface water in SC and SDC solutions is further evidenced by the sub-melting peak in differential scanning calorimetric (DSC) curves (see Fig. A.g.8, Appendix).[109] It should, however, be mentioned here that relaxation of the ion-pairs formed at the aggregated surface may also contribute at this slow time regime.[73]

Data in Table 9.4 further indicate that τ_1 for SC solutions are faster at each concentration than that obtained for SDC solutions. This relatively slower dynamics for SDC solutions has also been observed in the dynamic Stokes shift measurements, and is a reflection of comparatively higher viscosity. What is more interesting is that τ_1 decreases with bile salt concentration for both the solutions although viscosity increases. This may be explained in terms of curvature of the aggregated structure as follows. At lower bile salt concentration, the aggregates are relatively smaller in size[11,17] which can bind surface water more tightly. At higher concentration the aggregated structures become bigger in size, accommodating larger number of water molecules at the surface allowing more flexibility. As a result, τ_1 becomes faster with bile salt concentration. Such an argument in terms of curvature effect has been put forward earlier while

explaining the shortening of average solvation time scales in aqueous reverse micelles with the increase of confining diameter.[37]

Table 9.4: Parameters obtained from the fitting of the complex dielectric response functions of SC and SDC for all the three concentrations.[a]

System	ε_0	$\Delta\varepsilon_1$	τ_1 (ps)	$\Delta\varepsilon_2$	τ_2 (ps)	$\Delta\varepsilon_3$	τ_3 (ps)	$\Delta\varepsilon_4$	τ_4 (ps)	ε_∞	n_D	κ_{fit} (S/m)	χ^2
30 mM SC	81.8	2.9 (4%)	680	2.2 (3%)	20	71.4 (92.8%)	9	0.2 (0.2%)	1	5.1	1.333	0.16	0.008
100 mM SC	80.7	4.3 (5%)	690	3.5 (5%)	30	67.1 (89%)	9	0.8 (1%)	1	5.0	1.338	0.47	0.005
300 mM SC	72.3	3.8 (6%)	150	12.8 (19%)	20	49.3 (74%)	9	0.7 (1%)	1	5.7	1.352	1.08	0.012
30 mM SDC	83.0	4.1 (5%)	1000	1.2 (2%)	27	72.4 (93%)	9	0.2	1	5.1	1.333	0.16	0.003
100 mM SDC	82.5	6.5 (8%)	804	2.7 (4%)	35	67.6 (87%)	9	0.6 (1%)	1	5.1	1.339	0.46	0.003
300 mM SDC	73.8	5.2 (8%)	291	7.5 (11%)	29	54.7 (80%)	9	1.0 (1%)	1	5.5	1.353	1.03	0.011

a) Error bar for ε_0 is typically ±0.5, and time constants are better than $\pm5\%$ of the tabulated values. Numbers within parenthesis indicate percentages of the dispersion amplitudes with respect to the total dispersion detected

9.4 Conclusion

In summary, the present study reveals that aqueous SDC solutions exhibit more heterogeneous and slower dynamical features than SC solutions although SDC possesses hydroxyl (-OH) groups only one less than those in SC. The presence of slow water is revealed in DR, TRF and DSC measurements. A correlation between the dielectric relaxation and solvation time scales observed here further supports the presence of slow water in these systems. The present study, however, cannot confirm the role of counter ions in producing slow DR and Stokes shift dynamics. An appropriate simulation study is warranted here for a more complete understanding of these complex biologically relevant systems. A comparative study of bile salt concentration dependent dynamical heterogeneity of water molecules would be helpful in understanding the surface water in these systems.[110-111]

References

1. D. M. Small, P. Nair and D. Kritchevsky, *The Bile Acids: Chemistry, Physiology and Metabolism*. (Plenum Press, New York, 1971).

2. P. Nair, *The Bile Acids Chemistry, Physiology, and Metabolism: Volume 1: Chemistry*. (Springer Science & Business Media, 2013).

3. H. Danielsson and J. Sjövall, *Sterols and Bile Acids*. (Elsevier Publishing Company, 1985).

4. S. Mukhopadhyay and U. Maitra, Curr. Sci. **87**, 1666 (2004).

5. A. F. Hofmann and K. J. Mysels, Colloids Surf. **30**, 145 (1987).

6. A. F. Hofmann and D. M. Small, Annu. Rev. Med. **18**, 333 (1967).

7. D. M. Small, *The Physical Chemistry of Cholanic Acids*. (Springer, 1971).

8. G. Esposito, E. Giglio, N. V. Pavel and A. Zanobi, J. Phys. Chem. **91**, 356 (1987).

9. S. Sen, P. Dutta, S. Mukherjee and K. Bhattacharyya, J. Phys. Chem. B **106**, 7745 (2002).

10. A. Adhikari, S. Dey, U. Mandal, D. K. Das, S. Ghosh and K. Bhattacharyya, J. Phys. Chem. B **112**, 3575 (2008).

11. A. Roda, A. F. Hofmann and K. J. Mysels, J. Biol. Chem. **258**, 6362 (1983).

12. C. Ju and C. Bohne, J. Phys. Chem. **100**, 3847 (1996).

13. G. Conte, R. Di Blasi, E. Giglio, A. Parretta and N. V. Pavel, J. Phys. Chem. **88**, 5720 (1984).

14. A. Coello, F. Meijide, E. Rodriguez Nunez and J. Vazquez Tato, J. Phys. Chem. **97**, 10186 (1993).

15. D. M. Small and W. Admirand, Nature **221**, 265 (1969).

16. D. Small, S. Penkett and D. Chapman, Biochim. Biophys. Acta, Lipids Lipid Metab. **176**, 178 (1969).

17. N. A. Mazer, M. C. Carey, R. F. Kwasnick and G. B. Benedek, Biochemistry **18**, 3064 (1979).

18. M. Gomez-Mendoza, M. L. Marin and M. A. Miranda, J. Phys. Chem. Lett. **2**, 782 (2011).

19. M. Gomez-Mendoza, M. L. Marin and M. A. Miranda, J. Phys. Chem. B **116**, 14776 (2012).

20. J. Zakrzewska, V. Markovic, D. Vucelic, L. Feigin, A. Dembo and L. Mogilevsky, J. Phys. Chem. **94**, 5078 (1990).

21. A. Bonincontro, A. A. D'Archivio, L. Galantini, E. Giglio and F. Punzo, Langmuir **16**, 10436 (2000).

22. D. Madenci and S. U. Egelhaaf, Curr. Opin. Colloid Interface Sci. **15**, 109 (2010).

23. L. B. Pártay, P. Jedlovszky and M. Sega, J. Phys. Chem. B **111**, 9886 (2007).

24. L. B. Pártay, M. Sega and P. Jedlovszky, Langmuir **23**, 12322 (2007).

25. R. Li, E. Carpentier, E. D. Newell, L. M. Olague, E. Heafey, C. Yihwa and C. Bohne, Langmuir **25**, 13800 (2009).

26. G. Li and L. B. McGown, J. Phys. Chem. **97**, 6745 (1993).

27. D. Oakenfull and L. Fisher, J. Phys. Chem. **81**, 1838 (1977).

28. M. Gomez-Mendoza, E. Nuin, I. Andreu, M. L. Marin and M. A. Miranda, J. Phys. Chem. B **116**, 10213 (2012).

29. A. Baldridge, A. Amador and L. M. Tolbert, Langmuir **27**, 3271 (2011).

30. M. Pattabiraman, L. S. Kaanumalle and V. Ramamurthy, Langmuir **22**, 2185 (2006).

31. U. Mandal, S. Ghosh, D. K. Das, A. Adhikari, S. Dey and K. Bhattacharyya, J. Chem. Sci. **120**, 15 (2008).

32. C. M. Hebling, L. E. Thompson, K. W. Eckenroad, G. A. Manley, R. A. Fry, K. T. Mueller, T. G. Strein and D. Rovnyak, Langmuir **24**, 13866 (2008).

33. K. W. Eckenroad, L. E. Thompson, T. G. Strein and D. Rovnyak, Magn. Reson. Chem. **45**, 72 (2007).

34. M. Stojančević, N. Pavlović, S. Goločorbin-Kon and M. Mikov, Front. Life Sci. **7**, 112 (2013).

35. Y. S. R. Elnaggar, Int. J. Nanomedicine **10**, 3955 (2015).

36. J. Li, X. Wang, T. Zhang, C. Wang, Z. Huang, X. Luo and Y. Deng, Asian J. Pharm. Sci. **10**, 81 (2015).

37. B. Guchhait, R. Biswas and P. K. Ghorai, J. Phys. Chem. B **117**, 3345 (2013).

38. P. F. Barbara and W. Jarzeba, Adv. Photochem. **15**, (1990).

39. Š. Vajda, R. Jimenez, S. J. Rosenthal, V. Fidler, G. R. Fleming and E. W. Castner, J. Chem. Soc., Faraday Trans. **91**, 867 (1995).

40. N. Sarkar, A. Datta, S. Das and K. Bhattacharyya, J. Phys. Chem. **100**, 15483 (1996).

41. H. Shirota and K. Horie, J. Phys. Chem. B **103**, 1437 (1999).

42. K. Hara, N. Baden and O. Kajimoto, J. Phys.: Condens. Matter **16**, S1207 (2004).

43. N. E. Levinger, Curr. Opin. Colloid Interface Sci. **5**, 118 (2000).

44. H. Shirota, Y. Tamoto and H. Segawa, J. Phys. Chem. A **108**, 3244 (2004).

45. T. Pradhan, P. Ghoshal and R. Biswas, J. Chem. Sci. **120**, 275 (2008).

46. Y. Tamoto, H. Segawa and H. Shirota, Langmuir **21**, 3757 (2005).

47. T. Pradhan, H. A. R. Gazi, B. Guchhait and R. Biswas, J. Chem. Sci. **124**, 355 (2012).

48. R. Baumann, C. Ferrante, E. Kneuper, F.-W. Deeg and C. Bräuchle, J. Phys. Chem. A **107**, 2422 (2003).

49. M.-L. Horng, J. Gardecki and M. Maroncelli, J. Phys. Chem. A **101**, 1030 (1997).

50. S. Indra and R. Biswas, J. Chem. Phys. **142**, 204501 (2015).

51. B. D. Wagner, Molecules **14**, 210 (2009).

52. R. Karmakar and A. Samanta, J. Phys. Chem. A **106**, 4447 (2002).

53. M. Maroncelli and G. R. Fleming, J. Chem. Phys. **86**, 6221 (1987).

54. L. Reynolds, J. Gardecki, S. Frankland, M. Horng and M. Maroncelli, J. Phys. Chem. **100**, 10337 (1996).

55. D. Roy, S. K. Mondal, K. Sahu, S. Ghosh, P. Sen and K. Bhattacharyya, J. Phys. Chem. A **109**, 7359 (2005).

56. P. Hazra, D. Chakrabarty and N. Sarkar, Chem. Phys. Lett. **371**, 553 (2003).

57. F. Cichos, A. Willert, U. Rempel and C. Von Borczyskowski, J. Phys. Chem. A **101**, 8179 (1997).

58. F. Cichos, R. Brown, U. Rempel and C. Von Borczyskowski, J. Phys. Chem. A **103**, 2506 (1999).

59. T. Molotsky and D. Huppert, J. Phys. Chem. A **107**, 8449 (2003).

60. T. Molotsky and D. Huppert, J. Phys. Chem. A **107**, 2769 (2003).

61. A. Seret and M.-A. Bahri, Colloids Surf., A **339**, 153 (2009).

62. R. Zana and D. Guveli, J. Phys. Chem. **89**, 1687 (1985).

63. S. Gouin and X. X. Zhu, Langmuir **14**, 4025 (1998).

64. G. Li and L. B. McGown, J. Phys. Chem. **98**, 13711 (1994).

65. B. Bagchi and R. Biswas, Adv. Chem. Phys **109**, 207 (1999).

66. R. Biswas and B. Bagchi, J. Phys. Chem. A **103**, 2495 (1999).

67. H. K. Kashyap and R. Biswas, J. Phys. Chem. B **114**, 16811 (2010).

68. H. K. Kashyap and R. Biswas, J. Phys. Chem. B **112**, 12431 (2008).

69. S. Daschakraborty and R. Biswas, J. Chem. Phys. **137**, 114501 (2012).

70. B. Guchhait, S. Daschakraborty and R. Biswas, J. Chem. Phys. **136**, 174503 (2012).

71. B. Guchhait, H. A. R. Gazi, H. K. Kashyap and R. Biswas, J. Phys. Chem. B **114**, 5066 (2010).

72. C. Cametti, S. Marchetti, C. Gambi and G. Onori, J. Phys. Chem. B **115**, 7144 (2011).

73. R. Buchner, C. Baar, P. Fernandez, S. Schrödle and W. Kunz, J. Mol. Liq. **118**, 179 (2005).

74. C. Baar, R. Buchner and W. Kunz, J. Phys. Chem. B **105**, 2906 (2001).

75. C. Baar, R. Buchner and W. Kunz, J. Phys. Chem. B **105**, 2914 (2001).

76. T. Shikata and S.-i. Imai, Langmuir **14**, 6804 (1998).

77. R. Biswas, N. Rohman, T. Pradhan and R. Buchner, J. Phys. Chem. B **112**, 9379 (2008).

78. Y. Feldman, *Dielectric Relaxation in Biological Systems: Physical Principles, Methods, and Applications*. (Oxford University Press, USA, 2015).

79. S. K. Pal, J. Peon, B. Bagchi and A. H. Zewail, J. Phys. Chem. B **106**, 12376 (2002).

80. B. Bagchi, Chem. Rev. **105**, 3197 (2005).

81. N. Nandi, K. Bhattacharyya and B. Bagchi, Chem. Rev. **100**, 2013 (2000).

82. T. Pradhan and R. Biswas, J. Phys. Chem. A **111**, 11514 (2007).

83. H. A. R. Gazi, B. Guchhait, S. Daschakraborty and R. Biswas, Chem. Phys. Lett. **501**, 358 (2011).

84. B. Guchhait and R. Biswas, J. Chem. Phys. **138**, 114909 (2013).

85. H. A. R. Gazi, H. K. Kashyap and R. Biswas, J. Chem. Sci. **127**, 61 (2015).

86. A. Das and R. Biswas, J. Phys. Chem. B **119**, 10102 (2015).

87. R. Biswas, A. R. Das, T. Pradhan, D. Touraud, W. Kunz and S. Mahiuddin, J. Phys. Chem. B **112**, 6620 (2008).

88. N. Sarma, J. M. Borah, S. Mahiuddin, H. A. R. Gazi, B. Guchhait and R. Biswas, J. Phys. Chem. B **115**, 9040 (2011).

89.   M. Horng, J. Gardecki, A. Papazyan and M. Maroncelli, J. Phys. Chem. **99**, 17311 (1995).

90.   R. Buchner, Pure Appl. Chem. **80**, 1239 (2008).

91.   U. Kaatze and K. Giese, J. Phys. E **13**, 133 (1980).

92.   C. J. F. Böttcher and P. Bordewijk, *Theory of Electric Polarization*. (Elsevier: Amsterdam, The Netherlands, 1978).

93.   K. Mukherjee, A. Das, S. Choudhury, A. Barman and R. Biswas, J. Phys. Chem. B **119**, 8063 (2015).

94.   R. Buchner and J. Barthel, Annu. Rep. Prog. Chem. Sect. C: Phys. Chem. **91**, 71 (1994).

95.   R. Biswas, J. Lewis and M. Maroncelli, Chem. Phys. Lett. **310**, 485 (1999).

96.   J. Lewis, R. Biswas, A. Robinson and M. Maroncelli, J. Phys. Chem. B **105**, 3306 (2001).

97.   A. Das, S. Das and R. Biswas, Chem. Phys. Lett. **581**, 47 (2013).

98.   P. K. Mandal, M. Sarkar and A. Samanta, J. Phys. Chem. A **108**, 9048 (2004).

99.   Z. Hu and C. J. Margulis, Proc. Natl. Acad. Sci. U.S.A. **103**, 831 (2006).

100.   B. Guchhait, S. Das, S. Daschakraborty and R. Biswas, J. Chem. Phys. **140**, 104514 (2014).

101.   R. Jimenez, G. R. Fleming, P. Kumar and M. Maroncelli, Nature **369**, 471 (1994).

102.   N. Nandi, S. Roy and B. Bagchi, J. Chem. Phys. **102**, 1390 (1995).

103.   N. Nandi and B. Bagchi, J. Phys. Chem. B **101**, 10954 (1997).

104.   D. Mandal, A. Datta, S. K. Pal and K. Bhattacharyya, J. Phys. Chem. B **102**, 9070 (1998).

105.   R. Buchner, J. Barthel and J. Stauber, Chem. Phys. Lett. **306**, 57 (1999).

106.   K. Nörtemann, J. Hilland and U. Kaatze, J. Phys. Chem. A **101**, 6864 (1997).

107.   W. Qi, J. Chen, J. Yang, X. Lei, B. Song and H. Fang, J. Phys. Chem. B **117**, 7967 (2013).

108.   M. Neumann, J. Chem. Phys. **85**, 1567 (1986).

109.   T. Hatakeyama, H. Hatakeyama and K. Nakamura, Thermochimi. Acta **253**, 137 (1995).

110.   S. Indra, B. Guchhait and R. Biswas, J. Chem. Phys. **144**, 124506 (2016).

111.   T. Pal and R. Biswas, J. Phys. Chem. B **119**, 15683 (2015).

Chapter 10

Concluding Remarks and Future Problems

10.1 Concluding Remarks

To summarize, we have investigated in this Thesis the interaction and dynamics of ionic and non-ionic amide deep eutectics, polymer based systems and biologically relevant complex systems using dielectric relaxation spectroscopy, and steady state and time-resolved fluorescence spectroscopy. Ion-amide interactions in the studied deep eutectics have been found to generate a slow relaxation component with timescale in the range of nanosecond. In fact, presence of polymeric compounds in multi-component deep eutectics also leads to such a slow component in non-ionic deep eutectic systems. Absence of one hydroxyl group in one of the members of a given amphiphilic bile salt pair leads to different aggregation behavior and solution structure. The estimated static dielectric constants (ε_0) of acetamide and urea containing ionic DESs are smaller than those in molten neat acetamide and urea. For non-ionic DESs, in comparison, the estimated ε_0 values are comparable to the neat values. Moreover, the DR dynamics of the ionic DESs depends strongly on the identity of the electrolytes added in the medium. Additionally, we have revealed the interaction, dynamics and heterogeneity aspects of aqueous macromolecular systems and polymer gel electrolytes employing time-resolved fluorescence spectroscopic techniques. Since each chapter contains conclusions separately, no separate chapter has been included for over-all conclusion. A number of interesting and relevant problems are briefly discussed below for future studies.

10.2 Future Problems

10.2.1 Effects of Urea on Dielectric Relaxation Dynamics of ($acetamide + electrolyte$) DESs

Dielectric relaxation spectroscopic study in ($acetamide + electrolyte$) DESs, presented in chapter 3, shows that the ($acetamide + electrolyte$) DESs possess strong ion-acetamide interaction, inducing a slow relaxation in addition to the relaxation present in molten acetamide (at ~ 354 K).[1] Although the effects of urea in pure water and aqueous biomacromolecular systems is still under intense investigation,[2-5] it will be interesting to study the effects of urea on the dynamics of these ionic DESs, particularly the competitive ion-solvation aspect by both urea and acetamide. Moreover, recently performed (unpublished work) time-resolved fluorescence measurements along with simulation studies indicate urea-induced homogenization of dynamics of these DESs.[6] Additionally, the DR measurements of ($acetamide + urea$) DESs, presented in chapter 4, will help to understand the effects of urea more precisely.

10.2.2 Temperature Dependent DR Measurements of Ionic and Non-ionic DESs in a Broad Frequency Regime, $0.01 \leq \nu / GHz \leq 100$

Temperature dependent DR measurements for both ionic and non-ionic DESs in the frequency regime, $0.2 \leq \nu / GHz \leq 50$, (presented in chapter 3, chapter 5 and chapter 7), indicate that we miss a substantial part of the total DR dynamics.[1, 7-8] So DR measurements with a broader frequency window will help to reveal the total DR dynamics of these DESs comprehensively. It has been observed that with increases in temperature the estimated static dielectric constant (ε_0) the ionic DESs increases. It is noteworthy that neither a plateau in $\varepsilon'(\nu)$ nor a peak in $\varepsilon''(\nu)$ is observed in the DR spectra of the measured complex DR response and it may be due to the limited frequency coverage of our instrument. It is known that error-free estimation of ε_0 is a non-trivial exercise for these conducting solutions. However, DR measurements with broader frequency coverage, allowing the proper conductivity correction, would be useful to understand the full dynamics of these systems in the microwave region.

10.2.3 Structure and Dynamics of Non-ionic ($acetamide + urea + PEG$) DES

In chapter 7, we have revealed the DR dynamics of a new type of non-ionic DES consisting of acetamide, urea and polyethylene glycol (PEG) in the frequency regime $0.2 \leq \nu / GHz \leq 50$. This non-ionic DES exhibits exquisite solvent properties at close to room temperature. DR measurements show that the dielectric constant of this DES is quite high and comparable to that of ($acetamide + urea$) DESs. Interestingly, like ionic DESs, this non-ionic DES also possesses nanosecond relaxation time component which is absent in the DR dynamics of ($acetamide + urea$) DESs. However, DRS technique cannot provide any information about the liquid structure of this solvent. So sophisticated experimental techniques like small angle neutron scattering (SANS) and small angle X-ray scattering (SAXS) will be helpful to understand the structural properties of this multi-component system. A simulation study focusing on the orientational relaxation and H-bond fluctuation dynamics of the acetamide (or urea) molecules will be very helpful to explore the origin of the DR time scales reported in the present work. Higher frequency DR measurements would be needed to explore the librational dynamics of these extensively H-bonded systems, and compliment the ultrafast fluorescence Stokes shift measurements.

10.2.4 Effect of Polymer Structure and Chain Length on the Dynamics of Polymer Gel Electrolyte Systems

In chapter 8, we have discussed the viscosity coupling of rotation and solvation of C153 in a polymer gel electrolyte system.[9] We have found that the polymer has remarkable effect on the solvation dynamics of the photo-excited probe molecule. It will be very interesting to see the effect of polymer chain length on the dynamics of these gel electrolyte systems keeping the other two components unchanged. In addition, one can also play with the chemical structure of the polymer to explore the effect of polymer structure in the physicochemical properties of these systems. Moreover, there exists a huge scope for further investigation of these systems by performing atomistic simulations for complimentary information.

10.2.5 Interaction and Dynamics in Organic Electrolyte Systems

In chapter 8, we have investigated the dynamics of ($PC + LiClO_4$) using time-resolved fluorescence (TRF) measurement technique.[9] It reveals that the addition of electrolyte in PC changes the dynamics of the medium significantly. Previous studies indicate that Li^+ interacts strongly with organic solvents like ethylene carbonate (EC), propylene carbonate (PC) and diethyl carbonate (DEC) and forms adducts with the solvent molecules.[10-13] A comprehensive study of these organic electrolyte systems, involving the pure organic solvents as well as their mixtures, will enrich our understanding about the interaction and dynamics of these interesting systems. Additionally, one can also study the structure, dynamics and lifetime of the Li^+ adducts with required instrumental resolution.

10.2.6 Effect of Electrolytes on Structure and Dynamics of Aqueous Bile Salt Solutions

In Chapter 9, we have studied the impact of the aggregation behavior of sodium cholate and sodium deoxycholate on aqueous solution structure and dynamics.[14] It would be worth investigating the effects of electrolytes in the structure and dynamics of these aqueous bile salt solutions. It has already been reported that the counter ions play an important role in the aggregation of bile salts.[15] Hence, electrolytes containing the same counter ions as bile salts will be informative in this context. Moreover, some specific anions have ability to induce disorder in the hydrophobic aggregations as revealed by vibrational sum frequency spectroscopy (VSFS).[16-17] Thus, the effects of electrolytes can be an interesting problem to investigate.

10.2.7 Effects of Saccharides on Aggregation of Bile Salts in Aqueous solutions

In chapter 9, we have performed all the experiments above the primary critical micellization concentration (CMC[1]) of cholate and deoxycholate. Recent fluorescent studies show that the CMC[1] value decreases in presence of lactose (a disaccharide) in aqueous solution while with increasing temperature the CMC[1] increases.[18] The modulation of CMC[1] value by using saccharide molecules or by changing the temperature of the medium can be an interesting topic

to examine the driving force that leads to the formation of such aggregates in aqueous medium. Moreover, the interaction between the bile salt molecules forming an aggregate is still not clear. Further investigation of these biologically relevant macromolecular systems would therefore be necessary to understand the solution characteristics.

10.2.8 Interaction and Dynamics in Organogels Formed by AOT and Bile Salts

In chapter 9, we have studied the dynamics of aqueous solutions of sodium deoxycholate (SDC). AOT forms organogels in presence of SDC in organic solvents, like cyclohexane and n-alkanes.[19] Thus formed organogel is color less and stable upto 80°C. It has been found that among all the bile salts SDC is capable of forming such organogels. Understanding the structure and dynamics of these organogels can be an interesting topic to pursue. In addition, one can further study the effects of temperature and AOT concentration on the interaction and dynamics of these organogels. Moreover, the interaction and dynamics of cholic acids in organic solvents[20] should be understood clearly.

These are some representative interesting future problems that can be studied using dielectric relaxation and time-resolved fluorescence spectroscopic techniques suitably aided by computer simulations. These are complex systems which have relevance both to biology and industry. Reminding that life is an outcome of actions performed in unison by innumerable microsystems built of complex molecules, Chemists can indeed contribute positively to the over-all understanding of life by studying relevant complex systems revealing the structure and dynamics at the molecular length-scale. The high level of sophistication of various spectroscopic techniques and the present day efficiency of computation systems can be intelligently employed to conquer the barrier of the molecular world and gain precise knowledge of actions and driving force that allows the complex systems to perform seemingly simple actions. We look forward to that exciting future.

References

1. K. Mukherjee, A. Das, S. Choudhury, A. Barman and R. Biswas, J. Phys. Chem. B **119**, 8063 (2015).

2. J. D. Batchelor, A. Olteanu, A. Tripathy and G. J. Pielak, J. Am. Chem. Soc. **126**, 1958 (2004).

3. B. J. Bennion and V. Daggett, Proc. Natl. Acad. Sci. U.S.A. **100**, 5142 (2003).

4. S. Funkner, M. Havenith and G. Schwaab, J. Phys. Chem. B **116**, 13374 (2012).

5. G. Walrafen, J. Chem. Phys. **44**, 3726 (1966).

6. A. Das, S. Das and R. Biswas, (under preperation).

7. K. Mukherjee, A. Barman and R. Biswas (under preperation).

8. K. Mukherjee, A. Barman and R. Biswas (under preperation).

9. K. Mukherjee, A. Barman and R. Biswas (under preperation).

10. B. Klassen, R. Aroca, M. Nazri and G. Nazri, J. Phys. Chem. B **102**, 4795 (1998).

11. D. Battisti, G. Nazri, B. Klassen and R. Aroca, J. Phys. Chem. **97**, 5826 (1993).

12. H. L. Yeager and H. Reid, J. Phys. Chem. **80**, 850 (1976).

13. H. L. Yeager, J. D. Fedyk and R. J. Parker, J. Phys. Chem. **77**, 2407 (1973).

14. K. Mukherjee, A. Barman and R. Biswas, J. Mol. Liq. **222**, 495 (2016).

15. L. v. B. Pártay, M. Sega and P. Jedlovszky, Langmuir **24**, 10729 (2008).

16. M. C. Gurau, S.-M. Lim, E. T. Castellana, F. Albertorio, S. Kataoka and P. S. Cremer, J. Am. Chem. Soc. **126**, 10522 (2004).

17. Y. Zhang and P. S. Cremer, Annu. Rev. Phys. Chem. **61**, 63 (2010).

18. S. Chauhan, V. Sharma, K. Singh, M. Chauhan and K. Singh, J. Mol. Liq. **222**, 67 (2016).

19. S.-H. Tung, Y.-E. Huang and S. R. Raghavan, Soft Matter **4**, 1086 (2008).

20. A. N. Dıaz, F. G. Sánchez and A. G. Pareja, Colloids Surf., A **142**, 27 (1998).

Appendix A.a
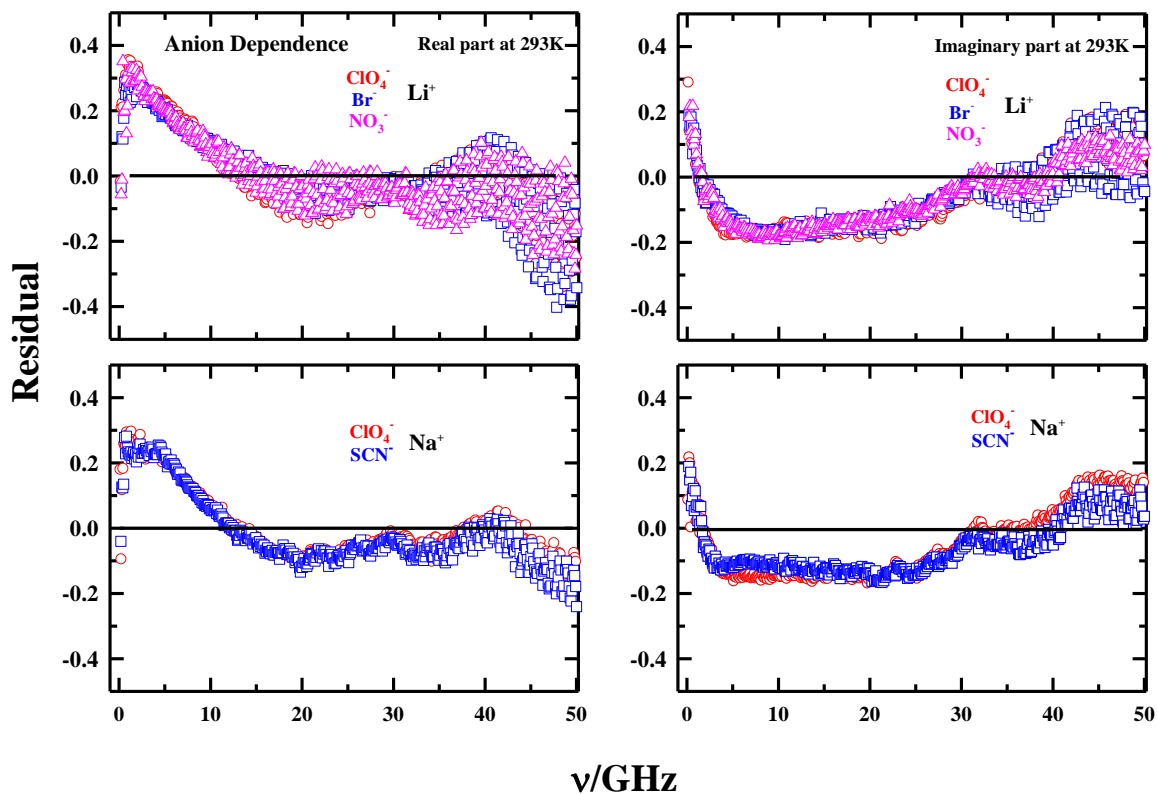
Fig. A.a.1: Residuals from 4-Debye simultaneous fits of the real and imaginary parts of the measured DR spectra for ($acetamide + electrolyt\,e$) deep eutectics at ~293 K. Two sets of electrolytes possessing different anions are considered here. Representations are color-coded.
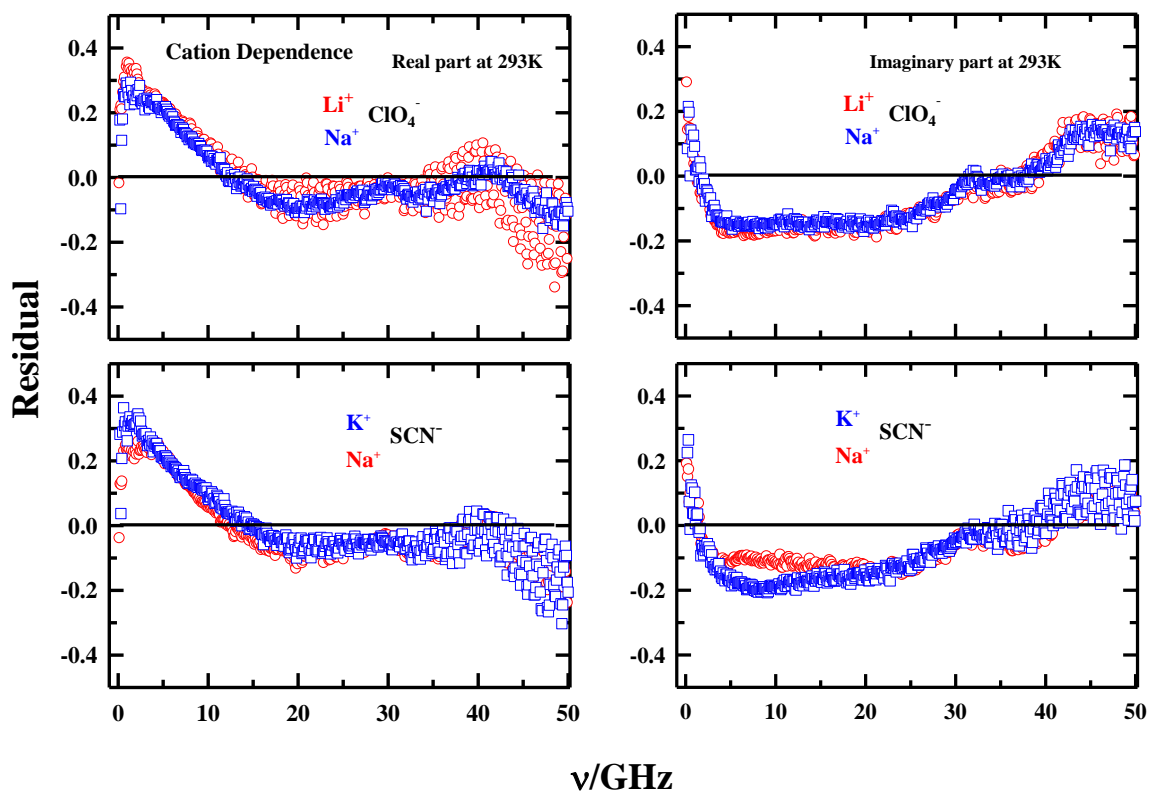
Fig. A.a.2: Residuals from 4-Debye simultaneous fits of the real and imaginary parts of the measured DR spectra for (*acetamide* + *electrolyte*) deep eutectics at ~293 K. Two sets of electrolytes possessing different cations are considered here. Representations are color-coded.
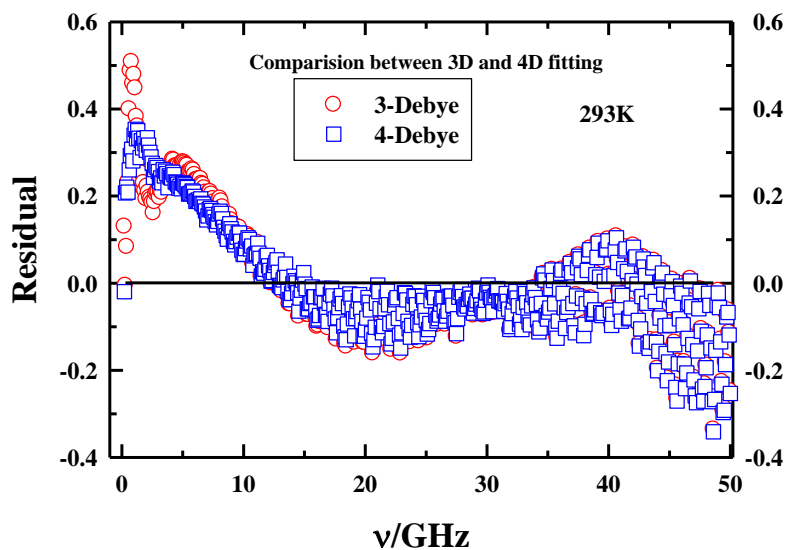
Fig. A.a.3: Comparison between residuals from 3-Debye and 4-Debye fits to the measured DR spectra for a representative system, (*acetamide + LiClO₄*), at ~293 K. Residuals shown here correspond to fits to real part of the DR spectrum. Representations are color-coded.

Table A.a.4: Viscosity coefficients (η) and conductivities of six (acetamide + electrolyte) deep eutectics studied.

System	η_{318K} (cp)[a]	η_{293K} (cp)[b]	κ(S/m) at 293K (from fits to DR spectra)	κ (S/m) at 293K (from measurements)
Acetamide + LiBr	360	1950	0.121	0.141
Acetamide + LiNO₃	82	263	0.095	0.103
Acetamide+LiClO₄	66	220	0.141	0.171
Acetamide +NaClO₄	57	195	0.082	0.145
Acetamide +NaSCN	235	-	0.041	0.055
Acetamide + KSCN	38	-	0.23	0.249

a) Viscosity values are from refs.21, 24 and 25 of the main text.

b) Viscosity values at ~293 K are obtained from extrapolation of the temperature dependent data available in refs. 21, 24 and 25.

Table A.a.5: Ion volumes and radii from ref. 66.

Anion	Volume (nm^3)	Radius(nm)	Cation	Volume (nm^3)	Radius(nm)
Br$^-$	0.056	0.34	Li$^+$	0.00199	0.11
NO$_3^-$	0.064	0.36	Na$^+$	0.00394	0.14
SCN$^-$	0.071	0.37	K$^+$	0.00986	0.19
ClO$_4^-$	0.082	0.39	-	-	
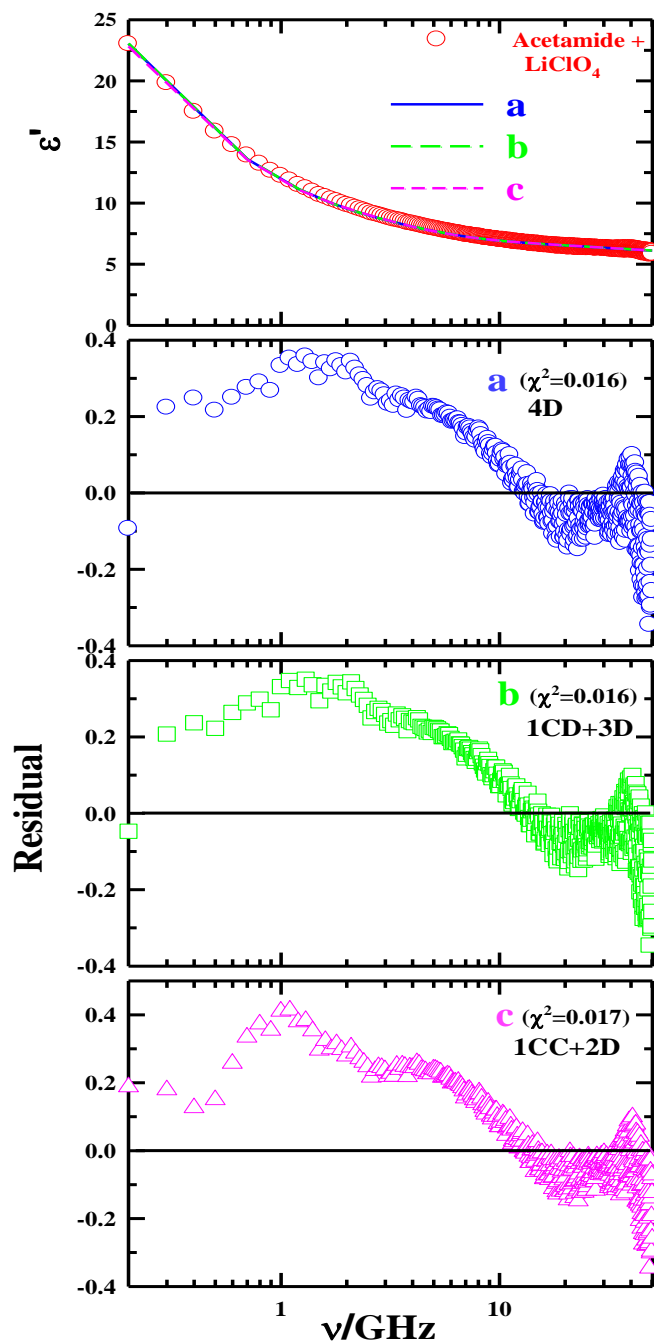
Fig A.a.6: Comparison among fits of real (ε') part of the measured DR spectra for (*Acetamide + LiClO_4*) DES at ~293 K to various relaxation models. While 'a' denotes fit to 4 Debye relaxation, 'b' and 'c' represent fits to a sum of Cole-Davidson (CD) and Debye (D), and a sum of Cole-Cole (CC) and Debye processes. Fits are shown by lines going through the data, and color-coded. Goodness-of-fit parameter (χ^2) for these fits are indicated in panels showing residuals. Similar comparison has also been found for the corresponding imaginary (ε'') part.
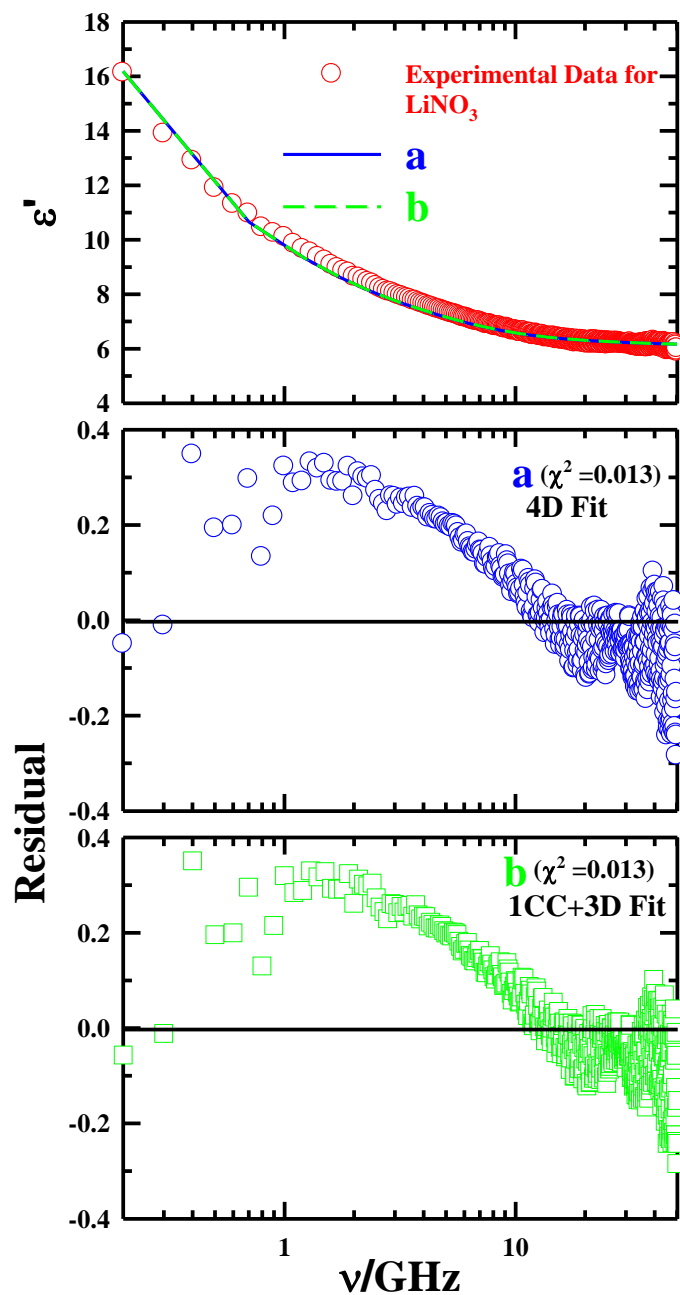
Fig A.a.7: Comparison among fits of real (ε') part of the measured DR spectra for (*Acetamide + LiNO₃*) DES at ~293 K to various relaxation models. While 'a' denotes fit to 4 Debye relaxation, 'b' represents fits to a sum of Cole-Cole (CC) and Debye (D) processes. Other representations remain the same as in Fig. A.a.6.

Table A.a.8: Fitting parameters for the fitting of experimental data in *Acetamide* + *LiClO*$_4$/ *LiNO*$_3$ DESs with different models at ~293K .

						Acetamide + *LiClO*$_4$ ($0.2 \leq \nu(GHz) \leq 50$)													
Model	ε_0	$\Delta\varepsilon_1$	τ_1	α	β	$\Delta\varepsilon_2$	τ_2	α	β	$\Delta\varepsilon_3$	τ_3	α	β	$\Delta\varepsilon_4$	τ_4	α	β	ε_∞	χ^2
4D[a]	29.4	16.2 (69%)	630	0	1	4.4 (19%)	160	0	1	2.3 (9%)	38	0	1	0.8 (3%)	4	0	1	5.8	0.016
1CD[b]+ 3D	29.3	14.5 (62%)	577	0	1.16	5.9 (25%)	162	0	1	2.3 (10%)	36	0	1	0.8 (3%)	4	0	1	5.8	0.016
1CC[c]+ 2D	31.0	22.4 (89%)	540	0.14	1	2.1 (8%)	45	0	1	0.7 (3%)	4	0	1	-	-	-	-	5.7	0.017

						Acetamide + *LiNO*$_3$ ($0.2 \leq \nu(GHz) \leq 50$)													
Model	ε_0	$\Delta\varepsilon_1$	τ_1	α	β	$\Delta\varepsilon_2$	τ_2	α	β	$\Delta\varepsilon_3$	τ_3	α	β	$\Delta\varepsilon_4$	τ_4	α	β	ε_∞	χ^2
4D	21.9	11.4 (72%)	790	0	1	2.9 (18%)	126	0	1	1.4 (9%)	29	0	1	0.1 (1%)	4	0	1	6.1	0.013
1CC+ 3D	21.9	11.3 (71%)	790	0	1	3.1 (20%)	127	0.02	1	1.3 (8%)	29	0	1	0.1 (1%)	4	0	1	6.1	0.013

a) D denotes Debye relaxation.

b) CD denotes Cole-Davidson relaxation.

c) CC denotes Cole-Cole relaxation.

Table A.a.9: Comparison between the fitting parameters for aqueous solutions of sodium chloride (NaCl) and potassium chloride (KCl) at ~293 K and ~298 K respectively obtained from our measurements and from the existing literature.

System	Model	ε_0	$\Delta\varepsilon_1$	τ_1	α	β	ε_∞	χ^2	Frequency range
Water+0.05M NaCl (Expt)	1CC	79.5	74.6	9.8	0.02	1	4.9	0.02	$0.2 \leq \nu/GHz \leq 50$
Water+0.05M NaCl (Lit)[a]	1CC	80.4	-	9.28	-	1	-	-	$0.02 \leq \nu/GHz \leq 40$
Water+0.61 M NaCl (Expt)	1CC	70.0	66.5	9.4	0.07	1	3.5	0.15	$0.2 \leq \nu/GHz \leq 50$
Water+0.61 M NaCl (Lit)[a]	1CC	72.0	-	8.7	-	1	-	-	$0.02 \leq \nu/GHz \leq 40$
Water+ 0.05M KCl (Expt)	1D	79.9	74.7	9.4	1	1	5.2	0.004	$0.2 \leq \nu/GHz \leq 50$
Water+ 0.05M KCl (Lit)[b]	1CC	77.7	71.4	8.24	0.002	1	6.3	0.02	$0.2 \leq \nu/GHz \leq 89$
Water+ 0.1M KCl (Expt)	1CC	79.0	73.9	9.3	0.004	1	5.1	0.015	$0.2 \leq \nu/GHz \leq 50$
Water+ 0.1M KCl (Lit)[b]	1CC	77.4	71.4	8.17	0.011	1	5.8	0.04	$0.2 \leq \nu/GHz \leq 89$
Water+ 0.6M KCl (Expt)	1CC	71.4	66.9	8.80	0.02	1	4.5	0.35	$0.2 \leq \nu/GHz \leq 50$
Water+ 0.6M KCl (Lit)[b]	1CC	72.9	68.6	7.71	0.034	1	4.3	0.14	$0.2 \leq \nu/GHz \leq 89$

[a]Ref. 85
[b]Ref. 86
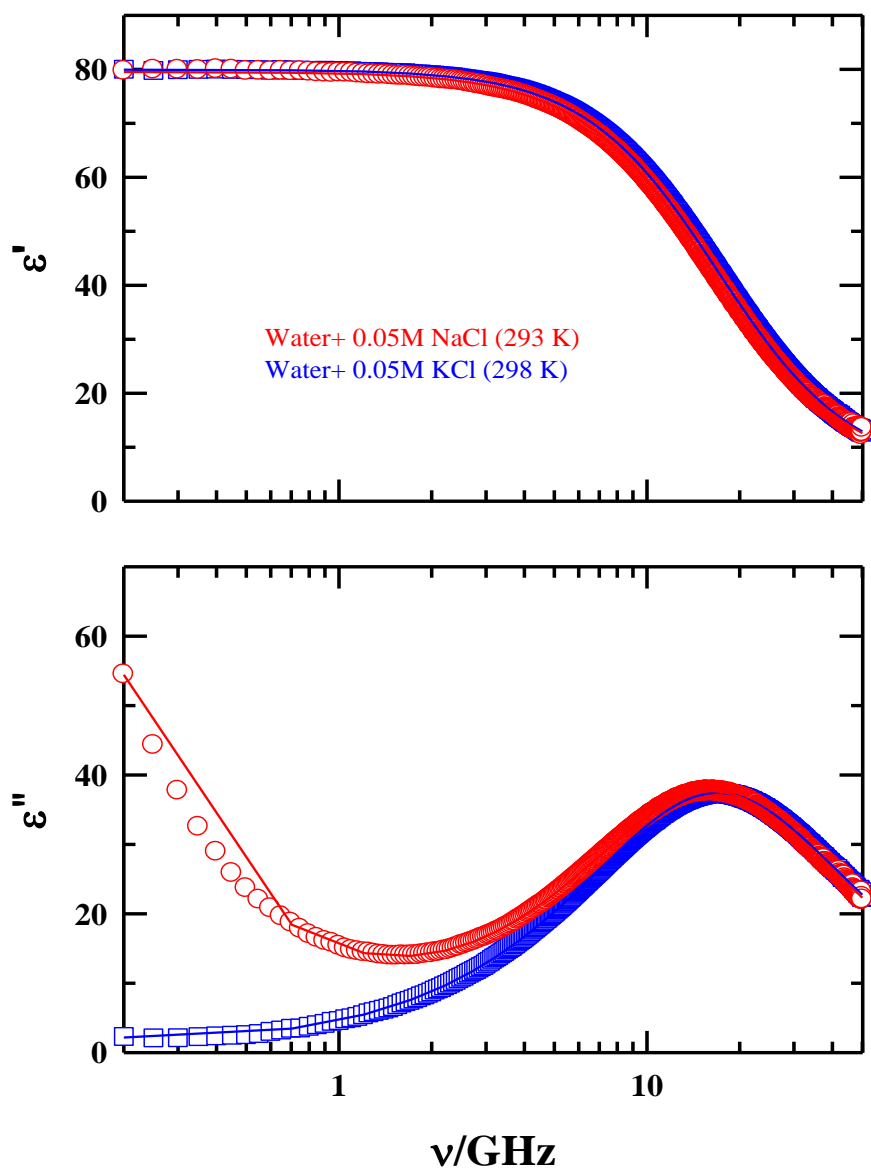
Fig. A.a.10: Real (ε') and imaginary (ε'') components of the measured complex dielectric spectra for aqueous solutions of NaCl (red circles) and KCl (blue squares), and fits (solid lines) through them. Fitted parameters are summarized in Table A.a.9 and compared with the corresponding literature data. Residuals are shown in Fig. A.a.11.
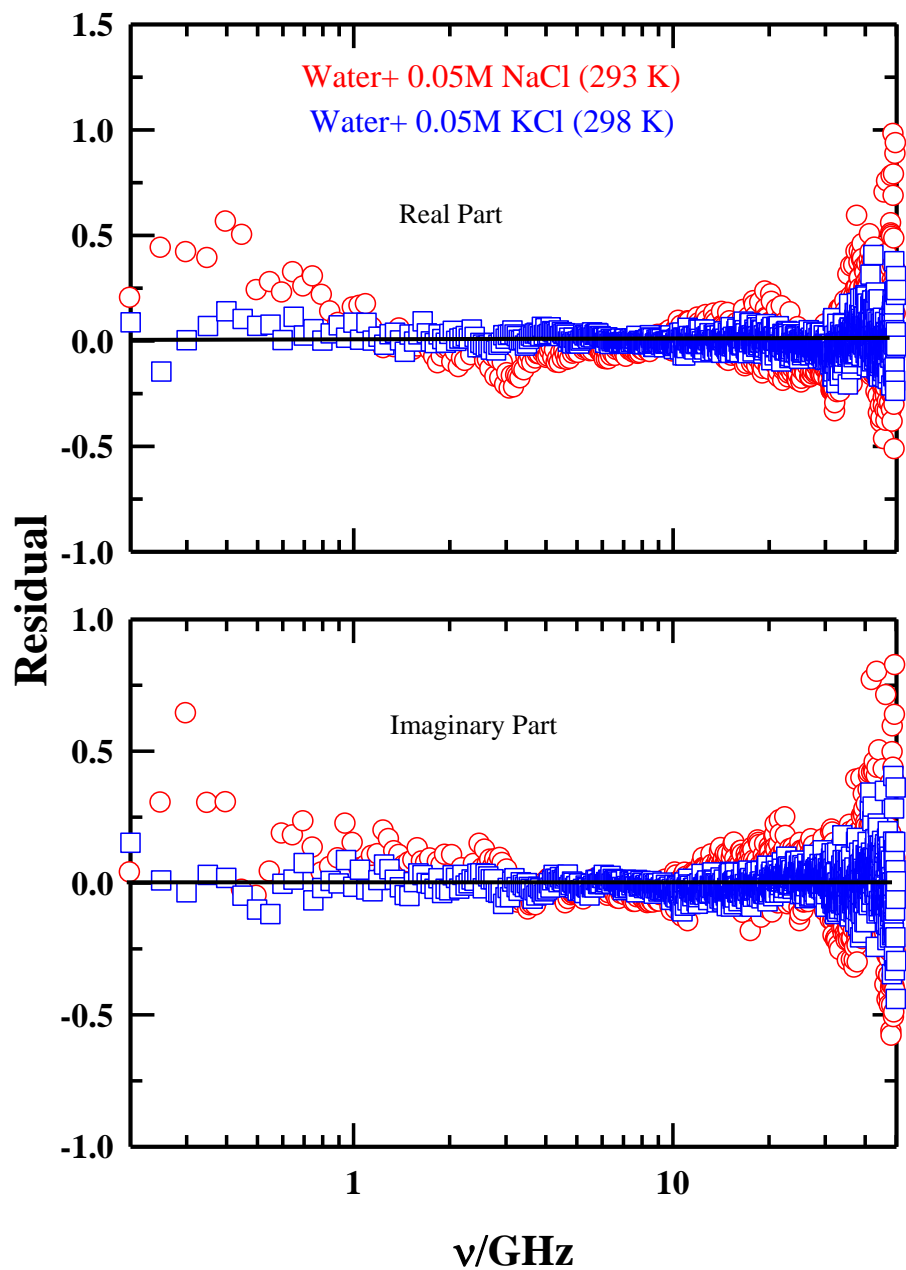
Fig. A.a.11: Residuals of fits to real (ε') and imaginary (ε'') components of the measured complex dielectric spectra for aqueous solutions of NaCl (red circles) and KCl (blue squares). Fits, and fit models have been described in the previous figure (Fig. A.a.10). Others representations remain the same as in Fig. A.a.10.

Appendix A.b

Table A.b.1: Temperature dependent DR parameters obtained from 3-Debye fits to the complex DR spectrum of molten urea in the frequency regime $0.2 \leq v/GHz \leq 50$.

Frequency range	Temp. (K)	ε_0	$\Delta\varepsilon_1$	τ_1 (ps)	$\Delta\varepsilon_2$	τ_2 (ps)	$\Delta\varepsilon_3$	τ_3 (ps)	ε_∞	χ^2	τ_{av}^{DR}	κ (S/m)
$0.2 \leq v(GHz) \leq 50$	406	69.0	6.7 (11%)	87	51.0 (83%)	29	4.0 (6%)	4.0	7.3	0.096	34	0.28
	408	69.7	5.1 (8%)	88	53.4 (86%)	28	3.8 (6%)	4.0	7.4	0.115	31	0.29
	411	70.4	4.2 (7%)	86	55.0 (87%)	27	3.9 (6%)	4.0	7.3	0.108	29	0.31
	416	70.0	3.7 (6%)	82	55.2 (88%)	25	4.0 (6%)	4.0	7.1	0.108	27	0.35
	421	69.6	3.4 (5%)	78	55.1 (88%)	23	4.1 (7%)	4.0	7.0	0.113	24	0.40
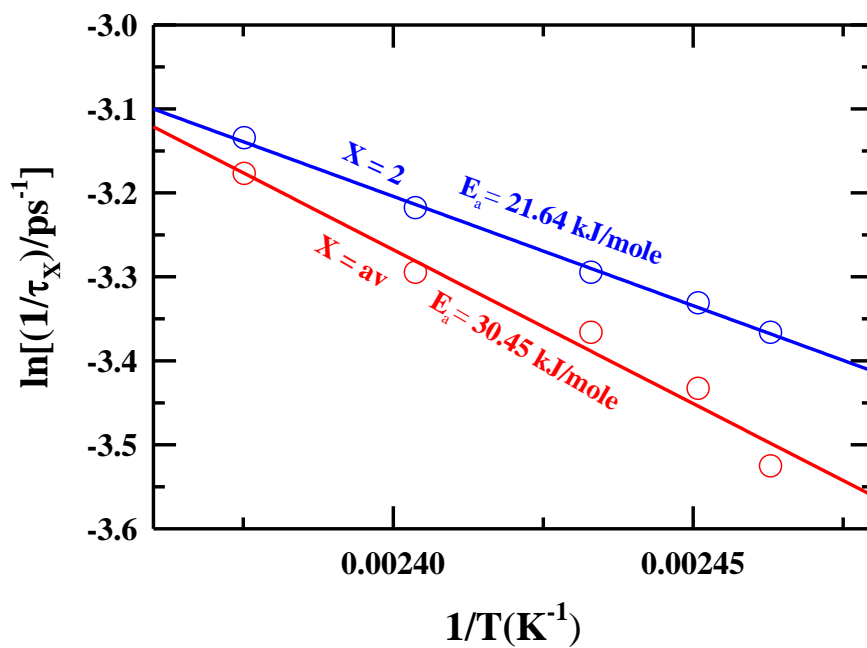
Fig. A.b.2: Arrhenius plot for the τ_2 and $\langle \tau_{av}^{DR} \rangle$ ($= \sum_{i=1}^{2} a_i \tau_i \Big/ \sum_{i=1}^{2} a_i$ where the amplitudes (a_i) and the time constants (τ_i) are taken from **Table A.b.1**) of molten urea. Solid lines depict the fit through the data points. Representations are color-coded.
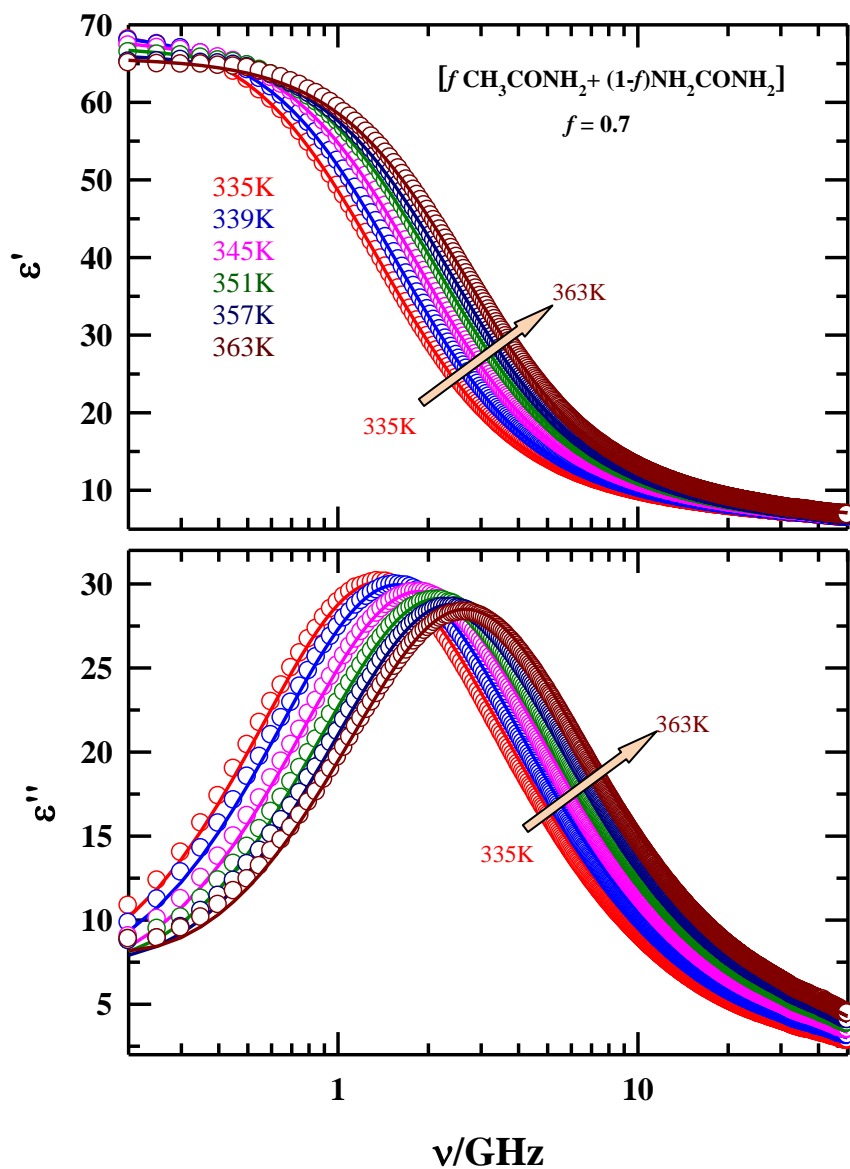
Fig. A.b.3: Temperature dependence of the real (ε') and imaginary (ε'') parts of the measured DR spectra for the DES at $f = 0.7$ within the frequency regime $0.2 \leq \nu / \mathrm{GHz} \leq 50$. Solid lines through the experimental data sets represent the 3-Debye fits. The arrows indicate the direction of temperature increase. Representations are color-coded.
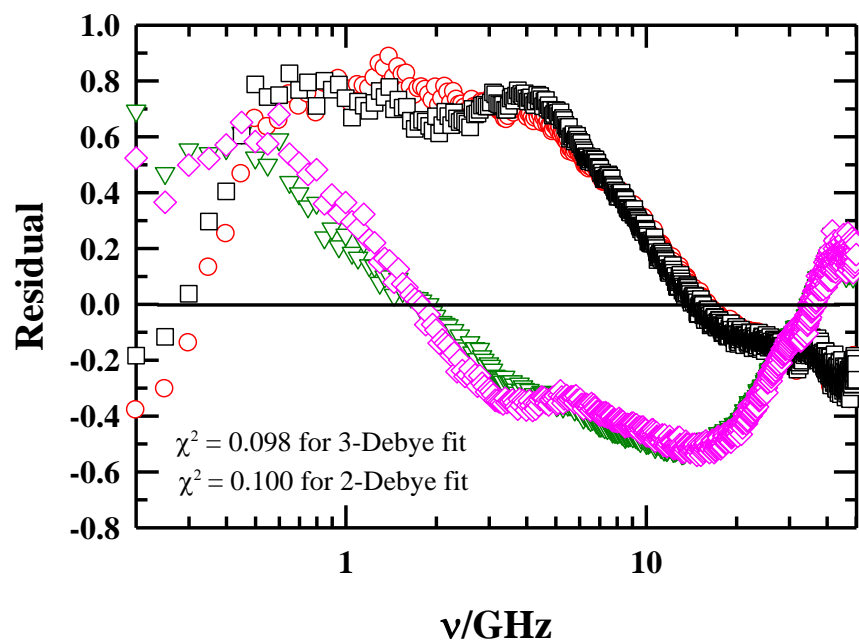
Fig. A.b.4: Comparison between 3-Debye and 2-Debye fit of the DR data for DES with f =0.7 at 363K. In the graph red circles and black boxes represent the residuals of the fitting of ε' by 3-Debye and 2-Debye model, respectively. In the same graph the dark green triangles and pink diamonds depicts the residual for the fitting of ε'' by 3-Debye and 2-Debye model, respectively.
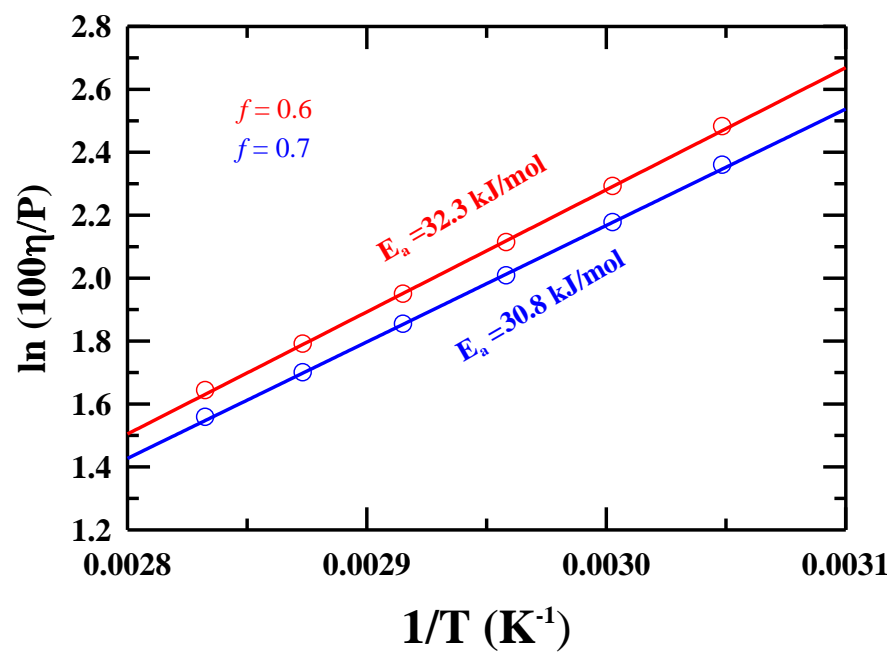
Fig. A.b.5: Arrhenius plots for viscosity coefficients for (*acetamide* + *urea*) DESs at two different compositions (data from Ref. 26). Representations are color-coded.
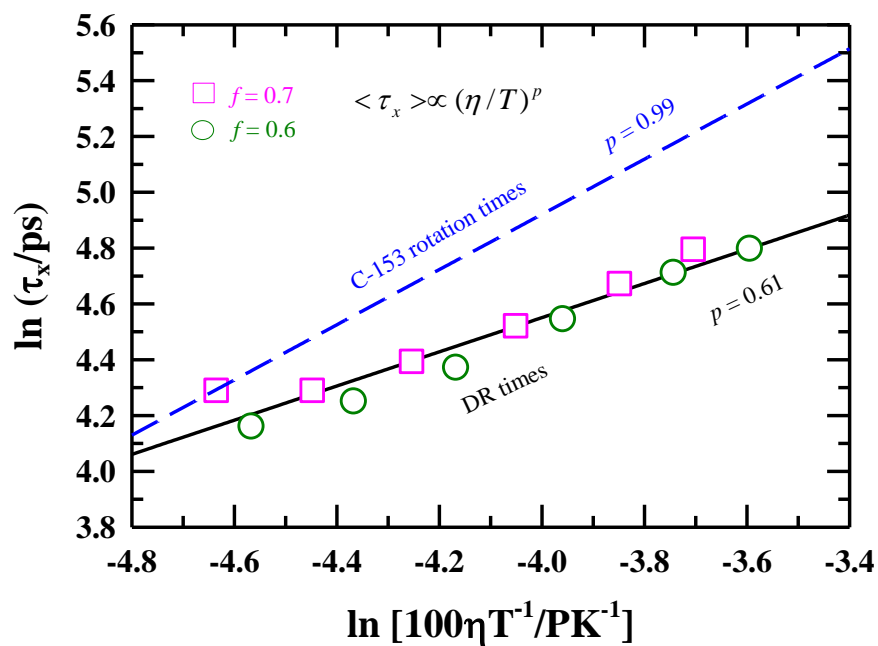
Fig. A.b.6: $\left(\dfrac{\eta}{T}\right)$ dependence of slowest DR times (τ_1) for the two different compositions. Solid

line represent the fit through the all ($f = 0.6$ and 0.7) τ_1 data. The long dash line represents the fit through the data points of fluorescence anisotropy measurements[26] using C153 as dipolar probe molecule.
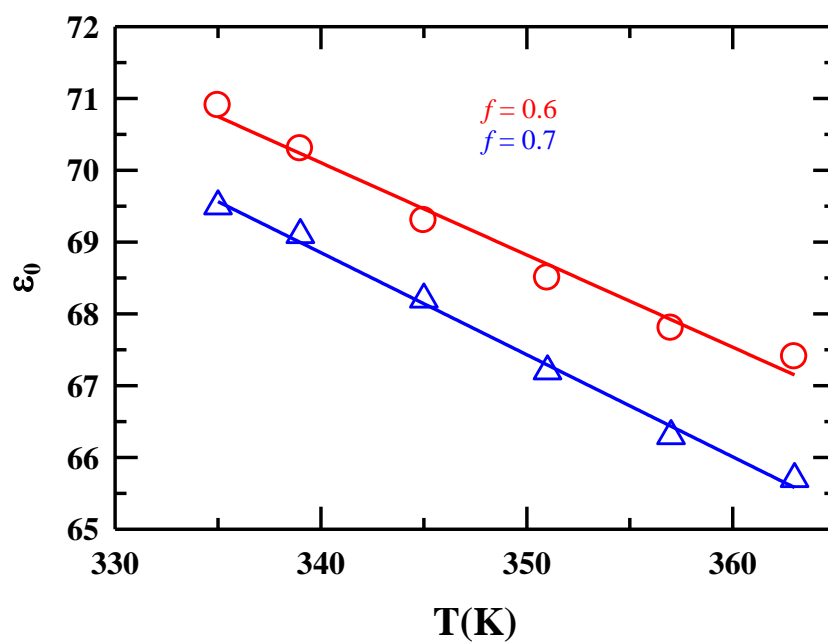
Fig. A.b.7: Temperature dependence of the static dielectric constants (ε_0) estimated from our measurements for the DESs at two different compositions. Representations are color-coded.

A.b.8: Simulation Results*

A.b.8.1 Viscosity Determination

Simulated viscosity coefficient are 0.7 ± 0.2 cP for molten urea at 406 K and 10.0 ± 2.0 cP for (*acetamide + urea*) DESs at 335 K. Note the experimental viscosity of the (*acetamide + urea*) DESs at 333 K is 9.87±0.2 cP.[26]
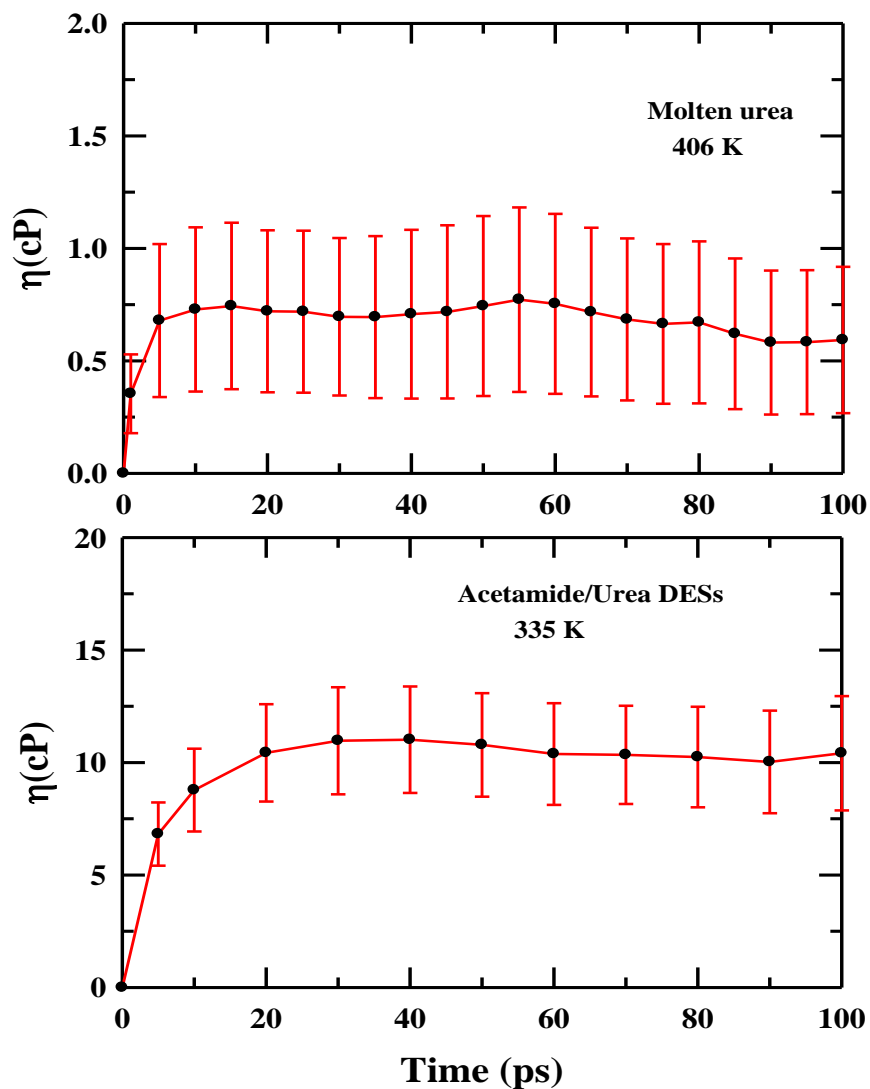
Fig. A.b.8.1: Time convergence of the viscosity as calculated from the integration of PACF. The upper panel shows the data for urea at 406 K and the lower panel shows the same for (*acetamide + urea*) DESs at 335 K. The calculated error bar is also shown with each data point.

A.b.8.2 H-bond Dynamics of Molten Urea and the DES
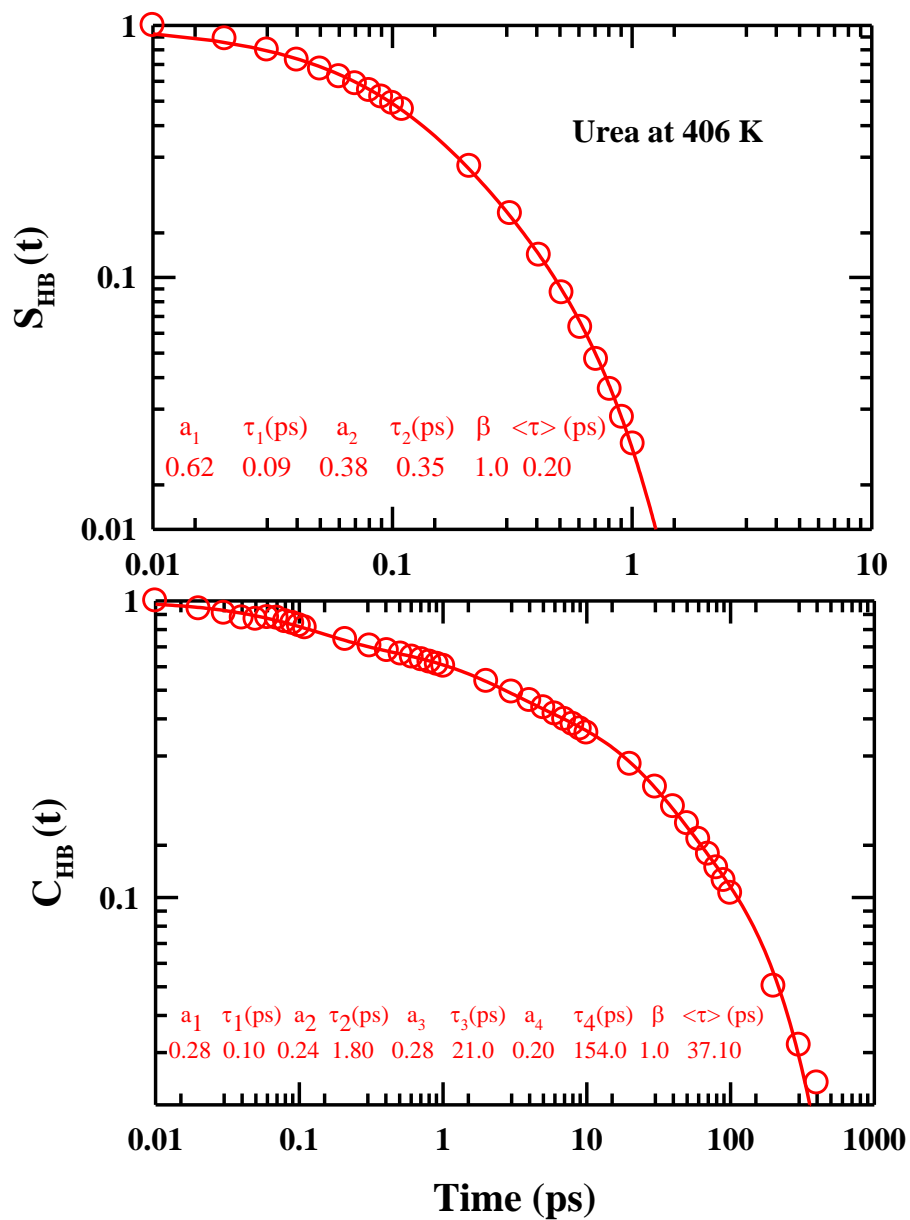
Fig. A.b.8.2: Simulated decay of the H-bond correlation functions $S_{HB}(t)$ and $C_{HB}(t)$, defined in the text, for urea at 406 K. Multi-exponential fitting parameters are shown inside the panels.
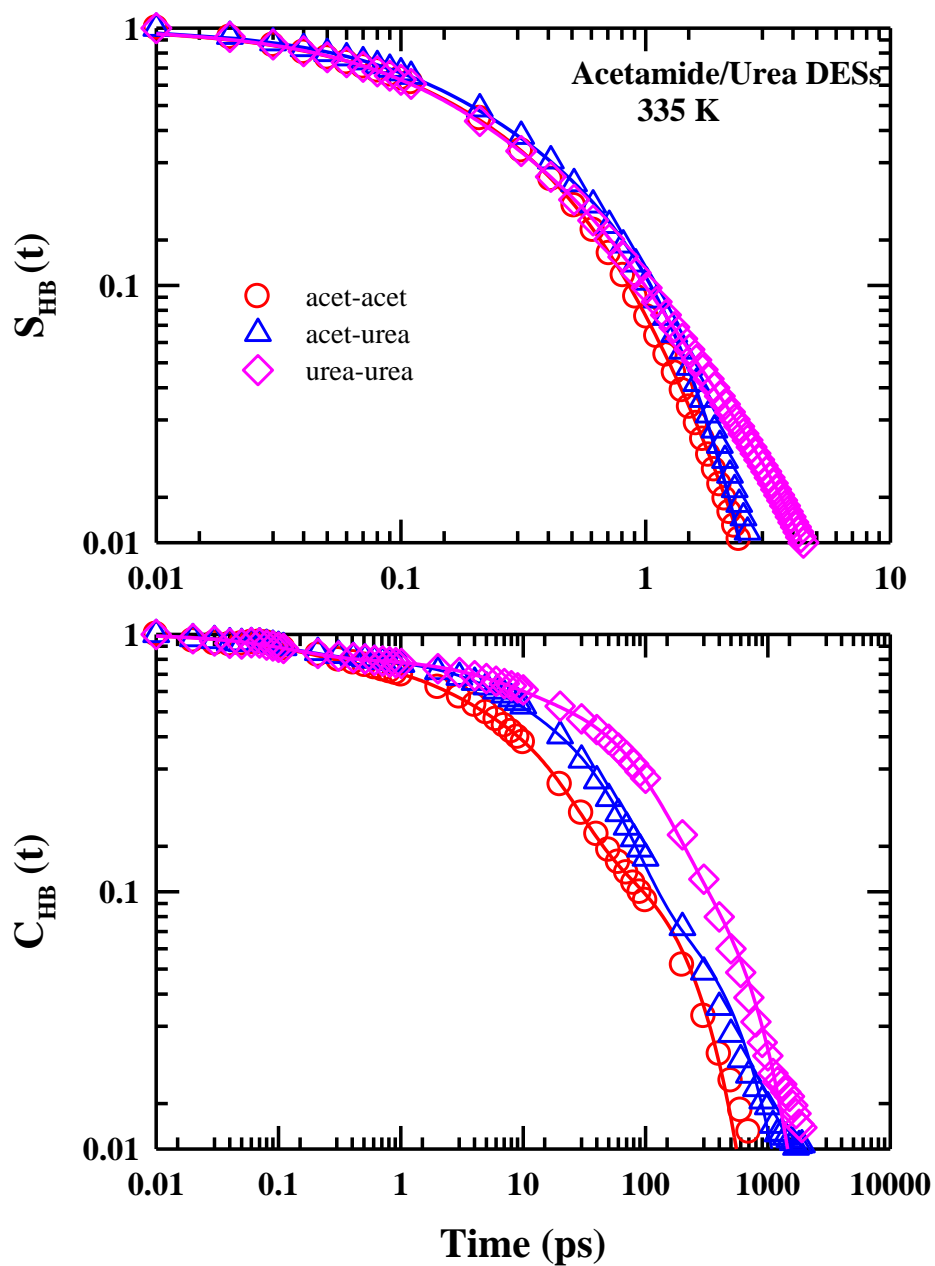
Fig. A.b.8.3: Simulated decay of various types of H-bond correlation functions $S_{HB}(t)$ and $C_{HB}(t)$, defined in the text, for (*acetamide* + *urea*) DESs at 335 K. Multi-exponential fitting parameters are provided in supporting information, **Table A.b.8.4**. Presentations are color-coded.

Table A.b.8.4: Multi-exponential fitting parameters extracted from fitting of the a) $S_{HB}(t)$ and b) $C_{HB}(t)$ for acetamide/urea DES mixture at 335 K.

a) $S_{HB}(t)$:

Type of H-bond	a_1	τ_1 (ps)	a_2	τ_2 (ps)	a_3	τ_3 (ps)	β	$\langle\tau\rangle$ (ps)
acet-acet	0.27	0.08	0.57	0.30	0.16	0.90	1.0	0.33
acet-urea	0.43	0.12	0.57	0.60	-	-	1.0	0.40
urea-urea	0.42	0.10	0.49	0.41	0.09	2.0	1.0	0.42

b) $C_{HB}(t)$:

Type of H-bond	a_1	τ_1 (ps)	a_2	τ_2 (ps)	a_3	τ_3 (ps)	a_4	τ_4 (ps)	β	$\langle\tau\rangle$ (ps)
acet-acet	0.19	0.13	0.20	1.80	0.45	15.0	0.16	200.0	1.0	39.1
acet-urea	0.19	0.12	0.23	5.60	0.48	41.3	0.10	454.5	1.0	66.6
urea-urea	0.20	0.12	0.19	6.10	0.44	80.0	0.17	500.0	1.0	121.4

*This work has been done in collaboration with Mr. Suman Das. For further details see his thesis "Heterogeneity and its effect on simple chemical events in molten multi-component systems".

Appendix A.c
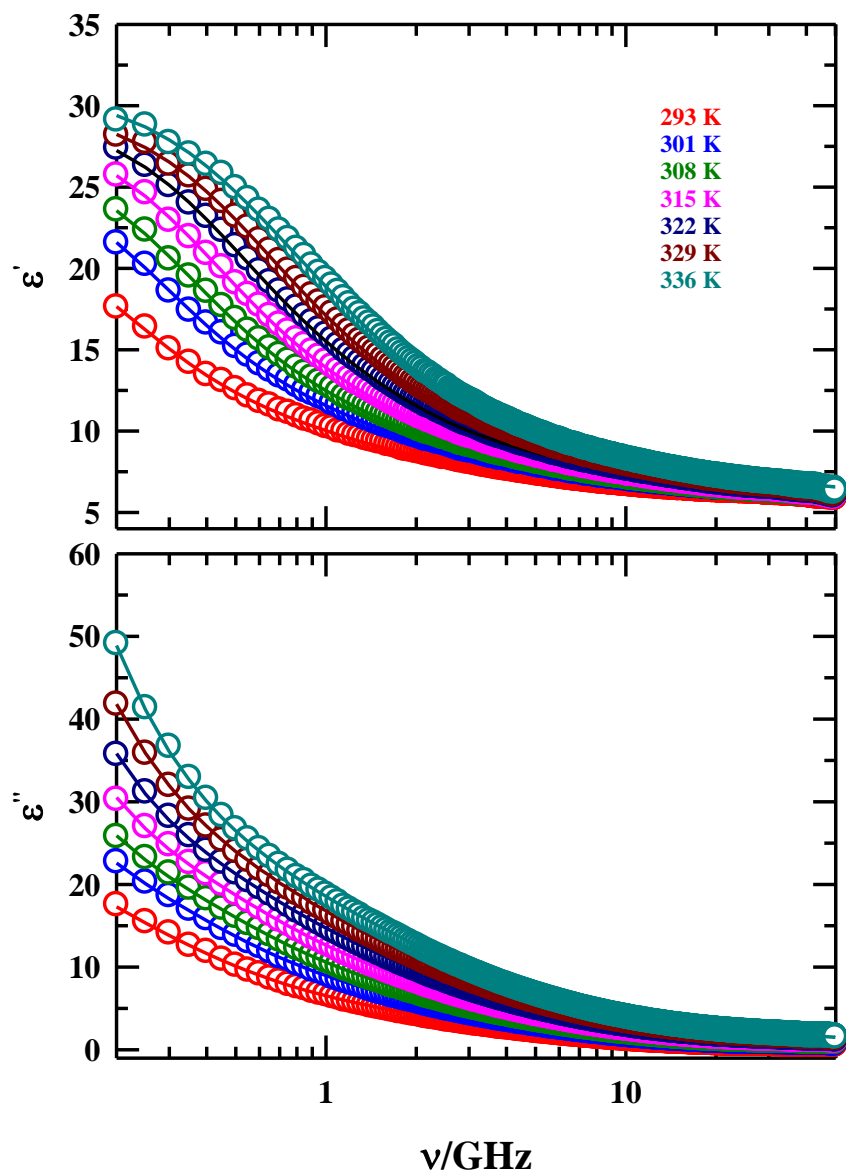
Fig. A.c.1: Temperature dependence of the real (ε') and imaginary (ε'') parts of the measured DR spectra for the (*acetamide + LiNO₃*) DES within the frequency regime $0.2 \leq \nu / \mathrm{GHz} \leq 50$. Solid lines through the experimental data sets represent the 4-Debye fits. Temperatures are color-coded.
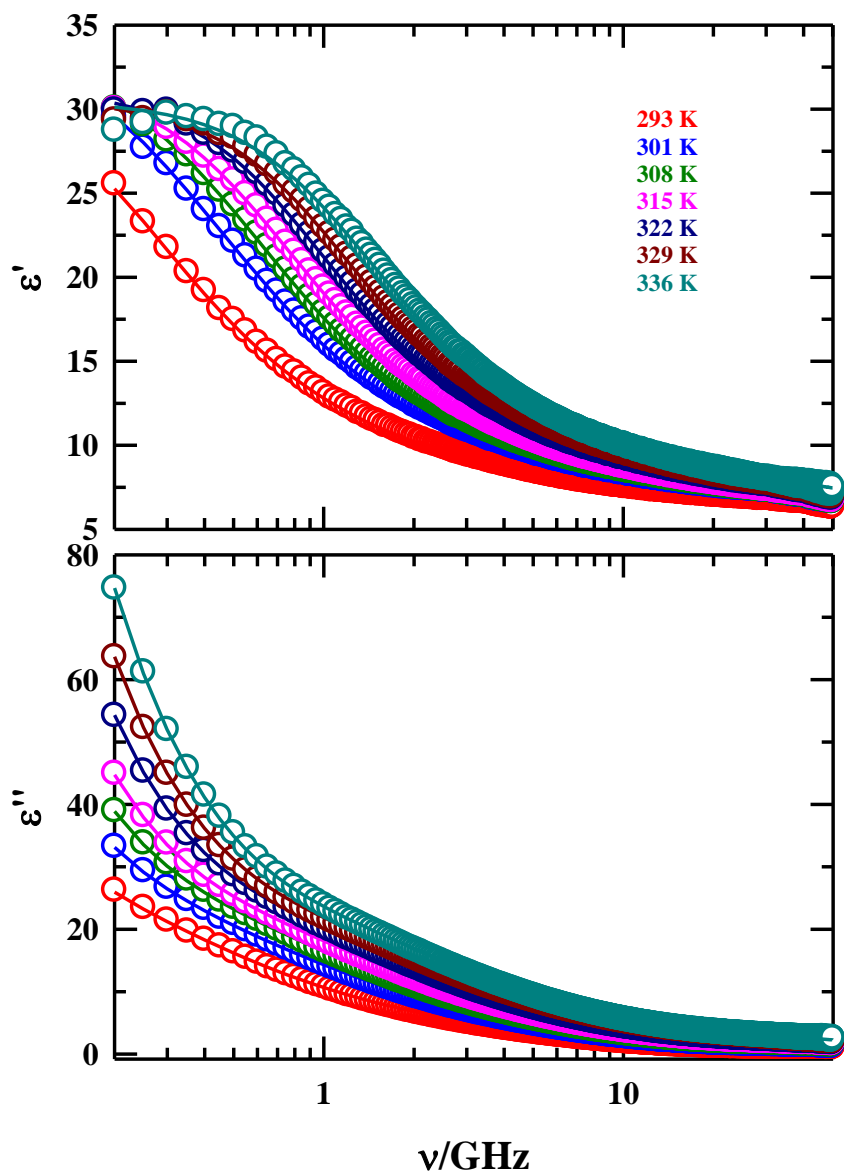
Fig. A.c.2: Temperature dependence of the real (ε') and imaginary (ε'') parts of the measured DR spectra for the (*acetamide + LiClO₄*) DES within the frequency regime $0.2 \leq \nu / \text{GHz} \leq 50$. Solid lines through the experimental data sets represent the 4-Debye fits. Temperatures are color-coded.
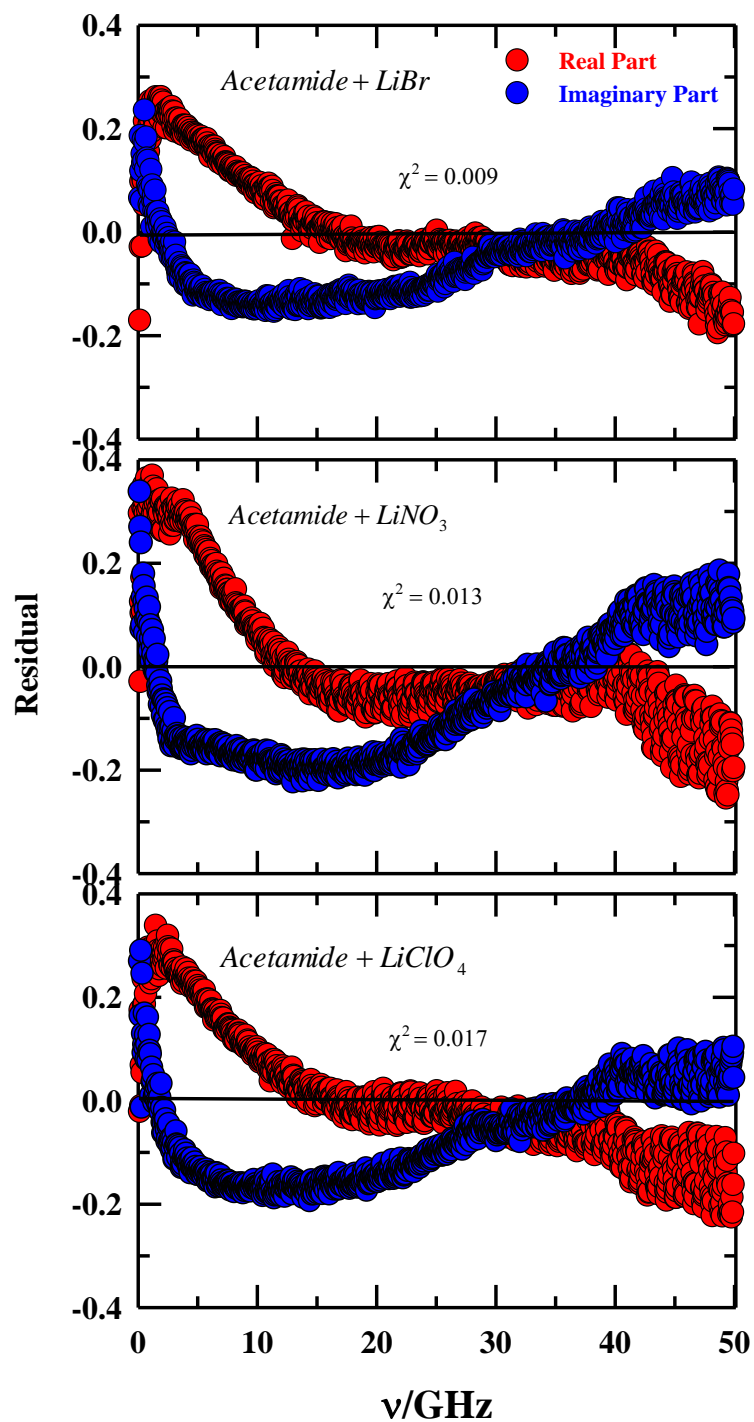
Fig. A.c.3: Residuals from 4-Debye simultaneous fits of the real and imaginary parts of the measured DR spectra for (*acetamide + electrolyte*) deep eutectics at ~293 K. Compositions of the DESs are given in the insets. Representations are color-coded.

Table A.c.4: Inaccessible part of the three DESs at 293 K.

System	$(\varepsilon_\infty - n^2)^a$ at 293 K
Acetamide + LiBr	3.320
Acetamide + LiNO$_3$	3.982
Acetamide + LiClO$_4$	4.220

a) Refractive index values has been collected from ref. 54 of chapter 5.

Appendix A.d
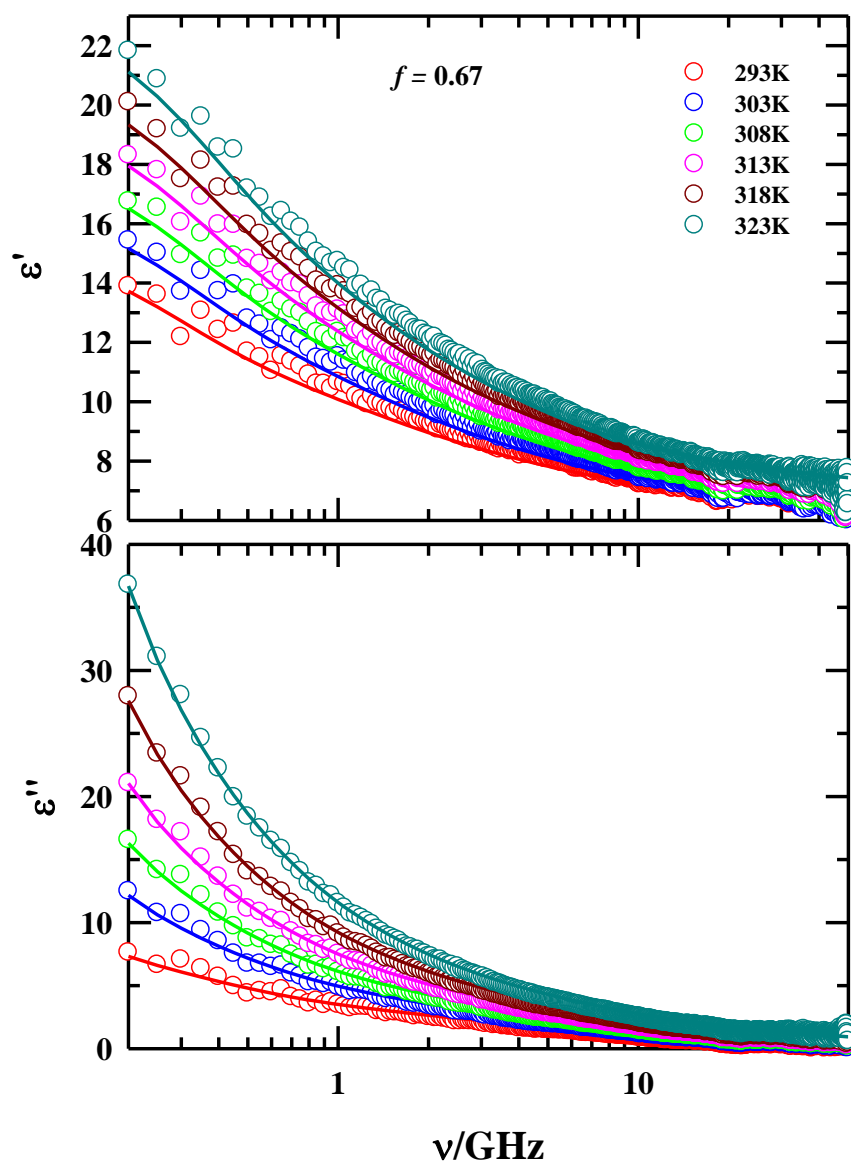
Fig. A.d.1: Temperature dependent DR spectra of (*urea + choline chloride*) DESs for *f* = 0.67 within the frequency window, $0.2 \leq \nu/GHz \leq 50$. Solid lines passing through the corresponding data points are the 4-Debye fits. Representations are color-coded.
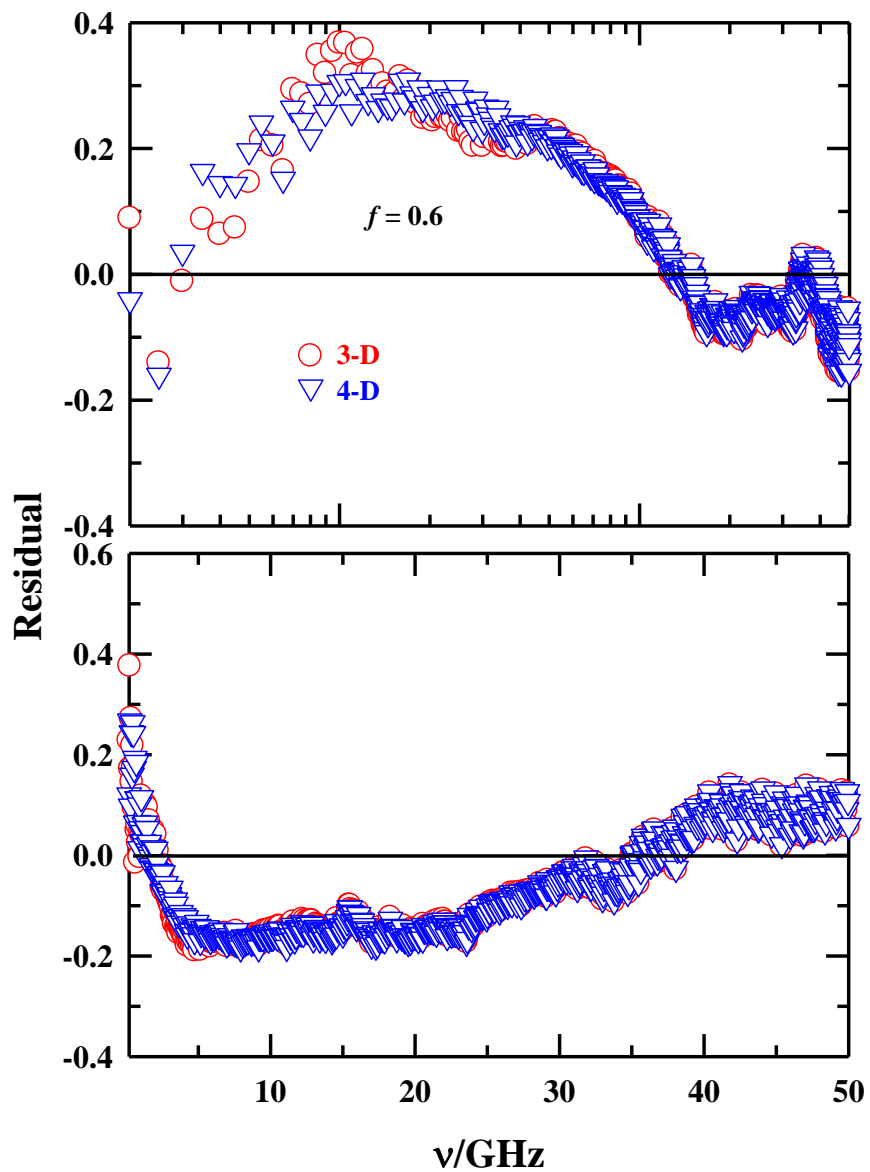
Fig. A.d.2: Comparison between 4-Debye and 3-Debye fits to the ε' (upper panel) and ε'' (lower panel) of the complex DR spectra of ($urea + choline\ chloride$) DES for $f = 0.6$ at 293K. Presentations are color-coded.
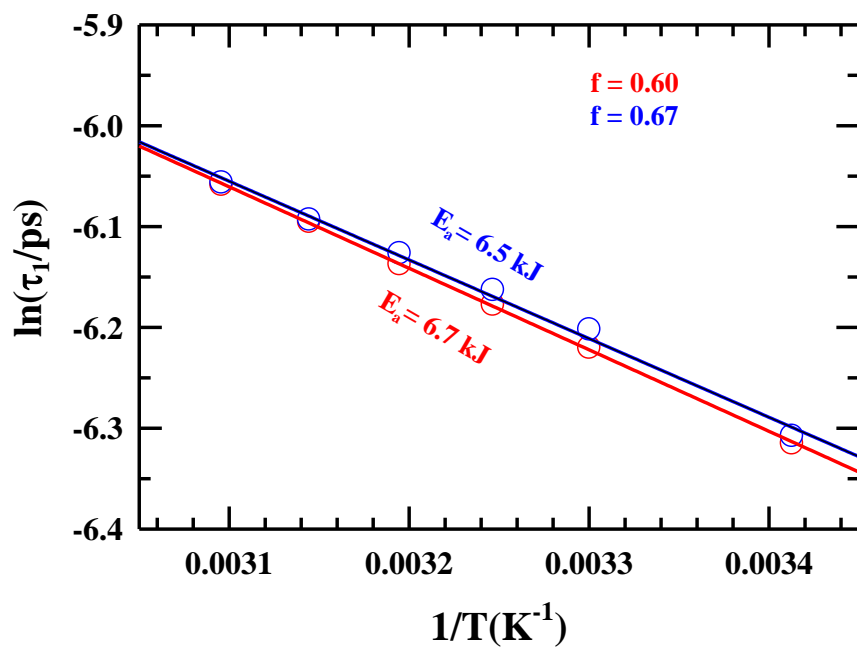
Fig. A.d.3: Arrhenius plot for the slowest DR time constant (τ_1) of ($urea + choline\ chloride$) DESs. Solid lines depict the fits through the data points. Representations are color-coded.

Appendix A.e
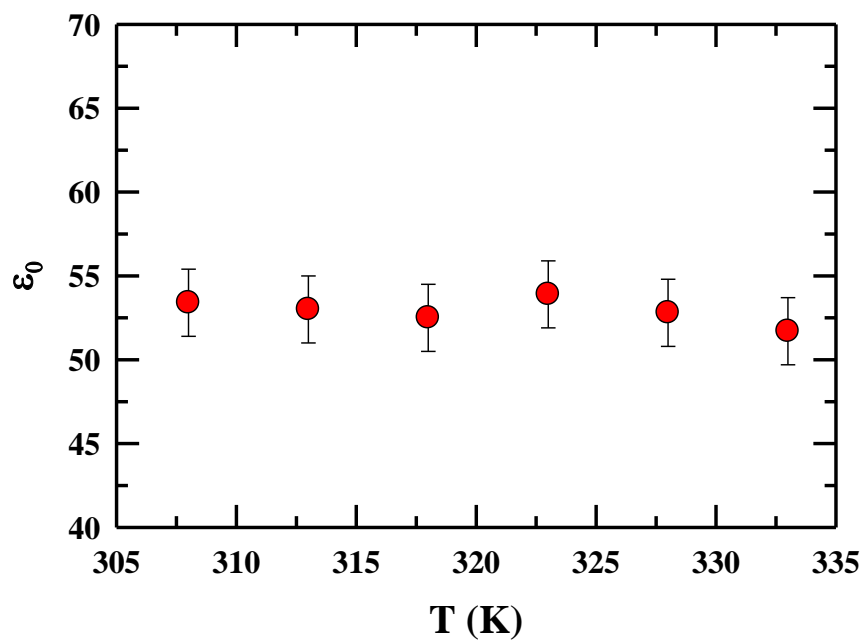
Fig. A.e.1: Temperature dependence of estimated static dielectric constant (ε_0) for the DES.
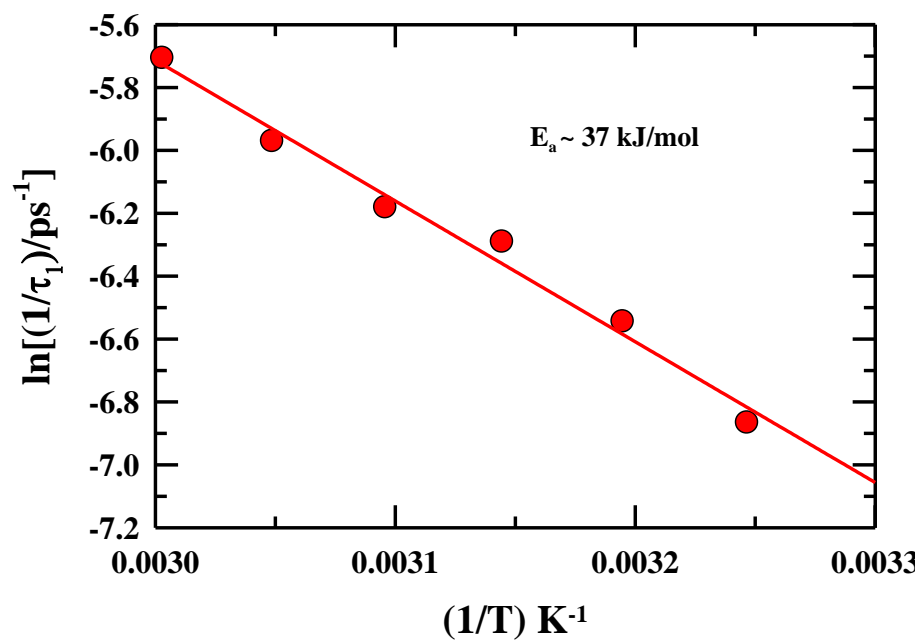
Fig. A.e.2: Arrhenius plot for the slowest DR time constant (τ_1) of the DES. Solid line depicts the fit through the data points.
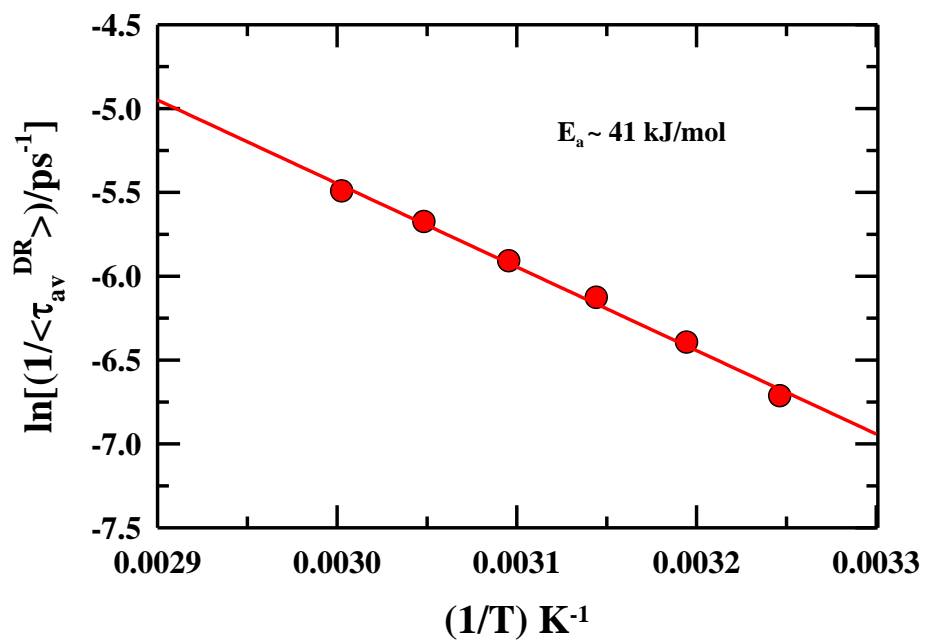
Fig. A.e.3: Arrhenius plot for the amplitude-averaged DR time constant ($\langle \tau_{av}^{DR} \rangle$) of the DES. Solid line depicts the fit through the data points.

Appendix A.f

Table A.f.1: Excitation wavelength dependent emission features for C153 in 40 wt% *PEG* containing polymer gel electrolyte at 298 K.

Excitation Wavelength (nm)	Spectral Width(FWHM) (10^3cm^{-1})	Average Frequency (10^3cm^{-1})
375	2.681	18.827
385	2.676	18.765
395	2.693	18.742
405	2.682	18.721
415	2.698	18.714
425	2.698	18.705
435	2.693	18.706
445	2.678	18.699
455	2.656	18.707
465	2.652	18.696
475	2.634	18.665
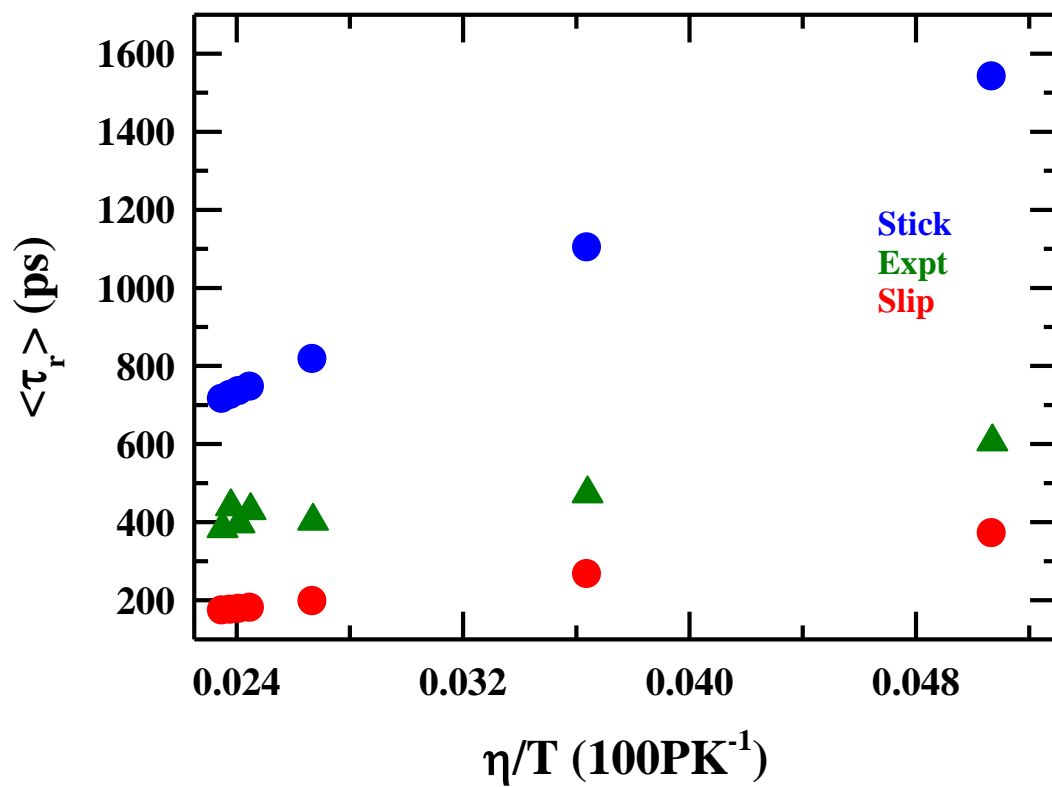
Fig. A.f.2: Representative plot of average rotation time ($\langle \tau_r \rangle$) versus temperature-reduced viscosity (η/T) for C153 in 40 wt% *PEG* containing polymer gel electrolyte. Here $T = 298$ K. Blue and red circles represent the stick and slip boundary limits, respectively. Green triangles represent the experimental data points.
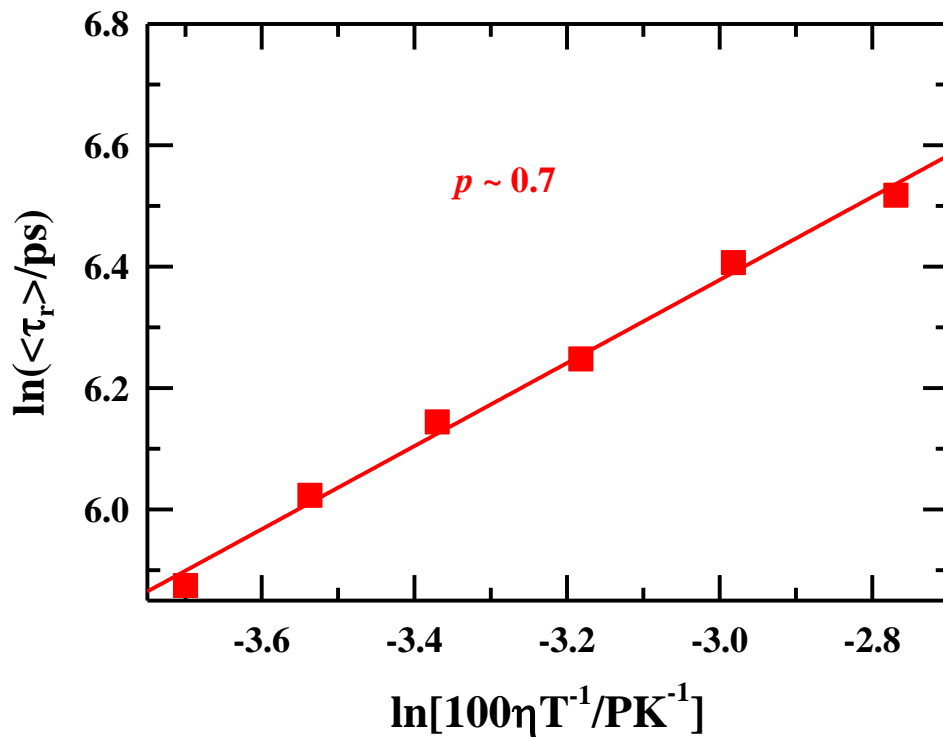
Fig. A.f.3: Representative spectra for average rotation time ($\langle \tau_r \rangle$) versus temperature-reduced viscosity (η/T) for C153 in 40 wt% *PEG* containing polymer gel electrolyte. Here we have tuned the viscosity of the medium by varying the temperature, keeping the polymer concentration fixed.
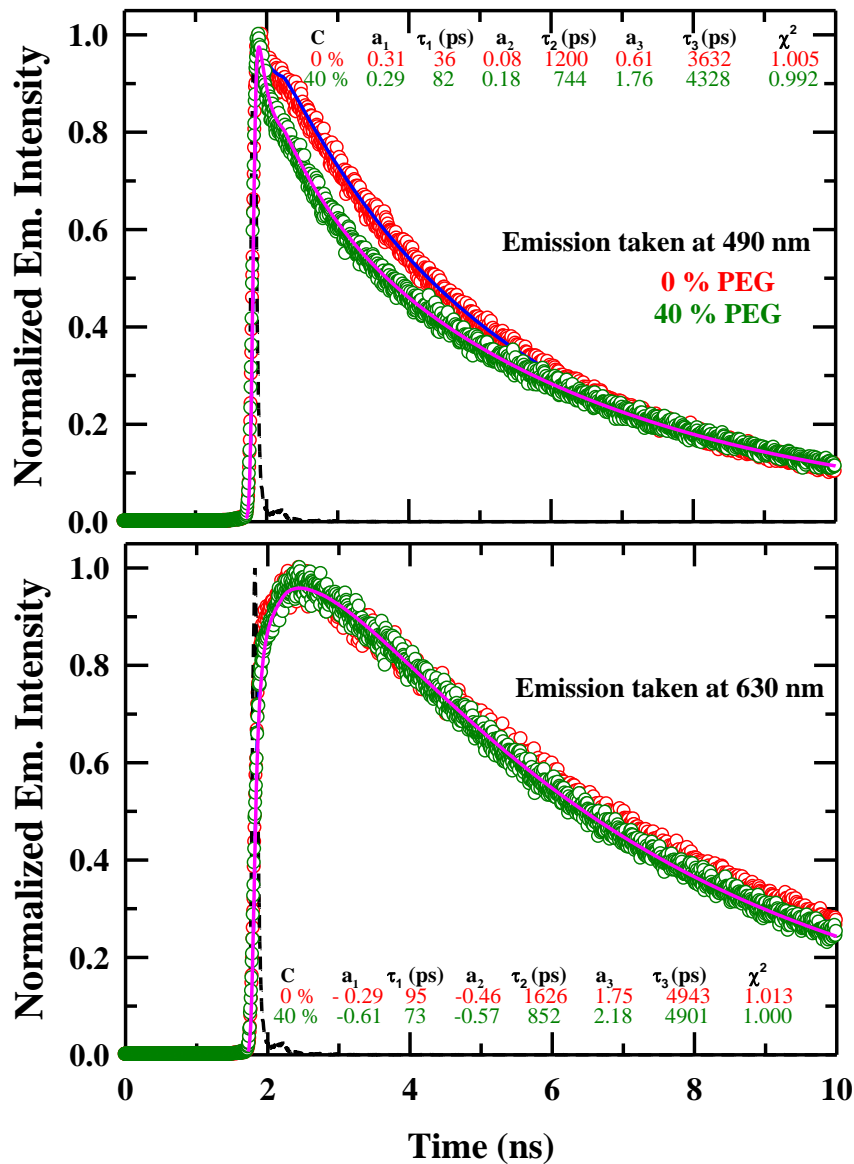
Fig. A.f.4: Representative intensity decay profiles collected at blue (490 nm), presented in upper panel, and red (630 nm), shown in lower panel, wavelengths for 0 wt% and 40 wt% *PEG* containing polymer gel electrolyte systems are shown as a function of time. The solid lines passing through the data sets depict the tri-exponential fits through them. Fit parameters are given in the inset. All representations are color-coded.
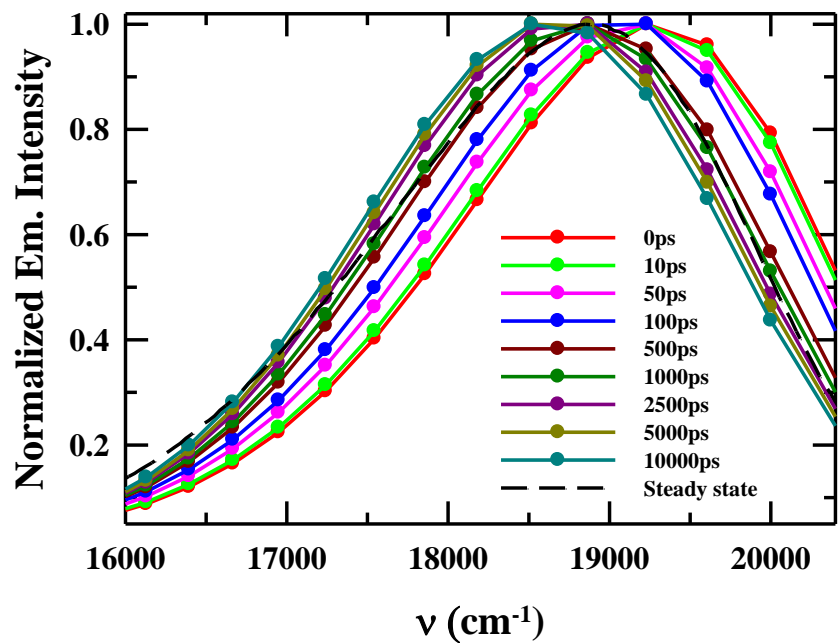
Fig. A.f.5: Synthesized time resolved emission spectra (TRES) of C153 at different time slices from the experimentally measured decays in the 40 wt% *PEG* containing polymer gel electrolyte system. TRES at different time intervals are color coded. The steady state emission spectrum of solute in this composite is also shown in this figure.
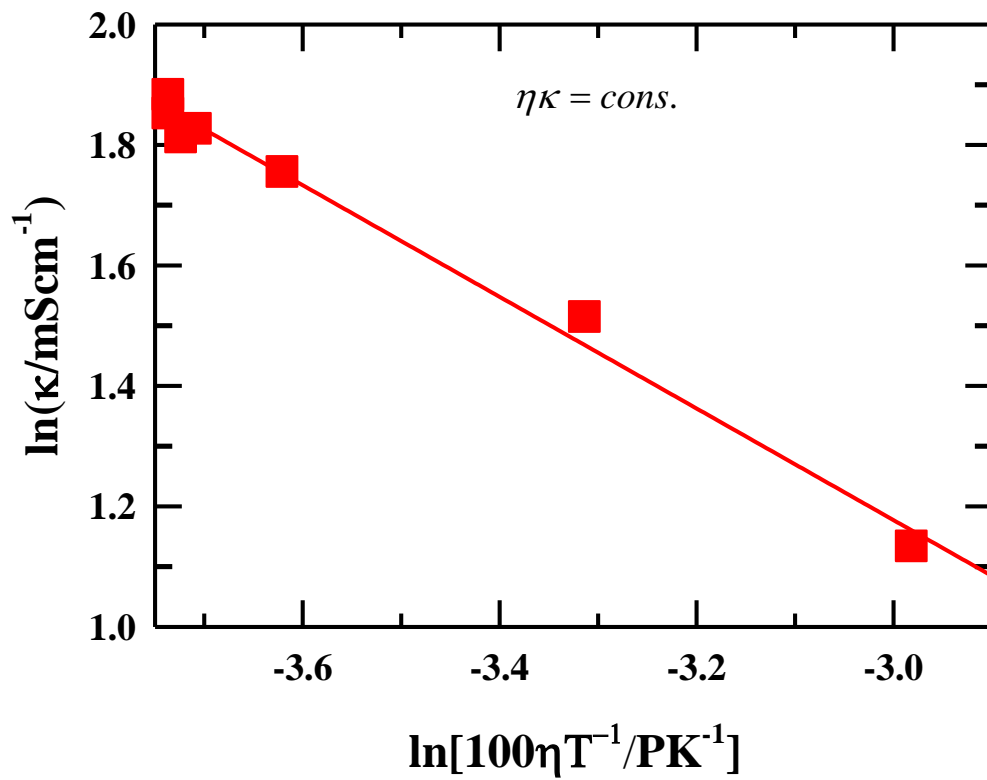
Fig. A.f.6: Represents the viscosity (η/T) dependence of the measured conductivity (κ) for different *PEG* concentrations at 298 K.
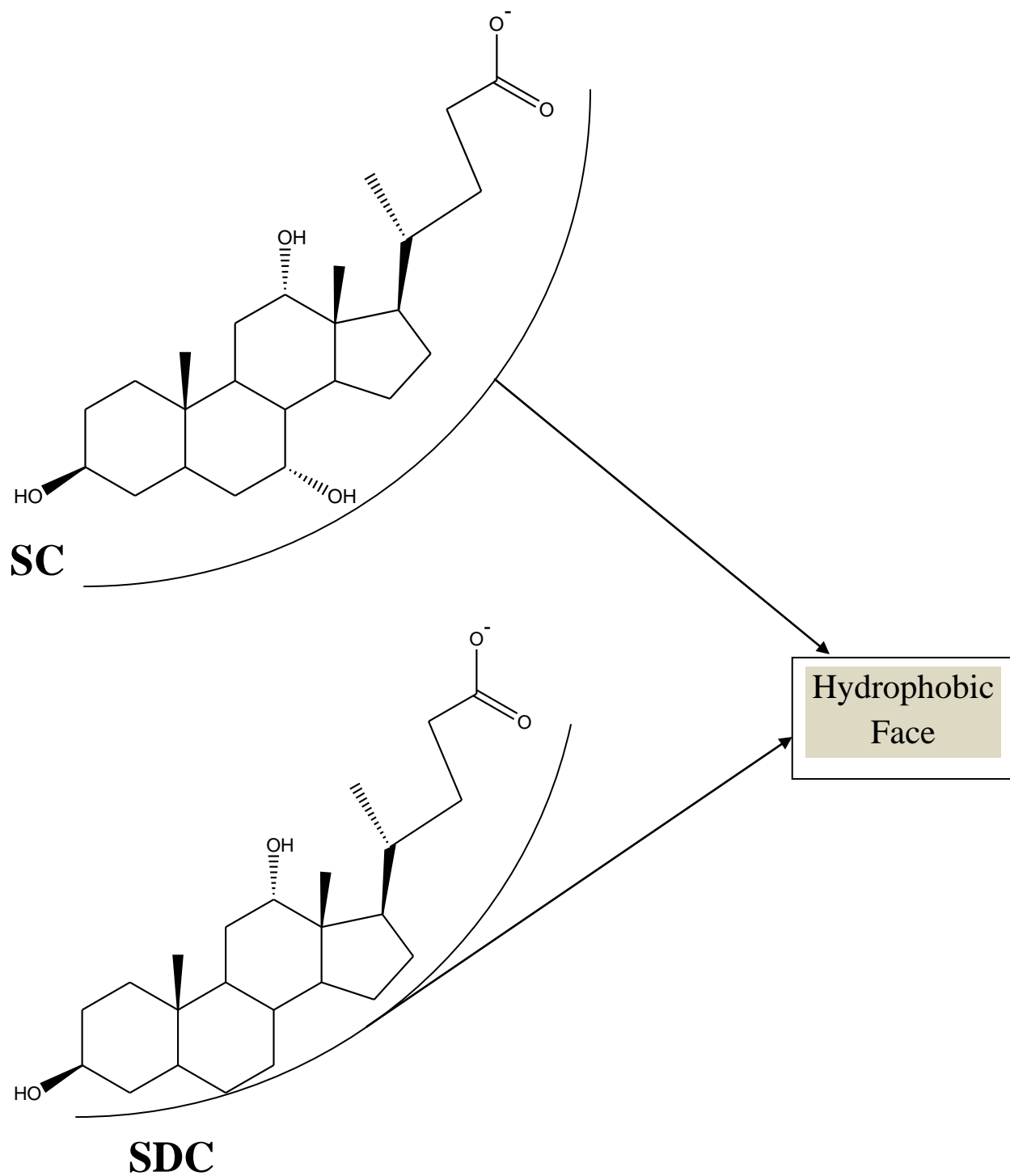
Fig. A.g.1: Chemical structures of SC and SDC showing hydrophobic faces.
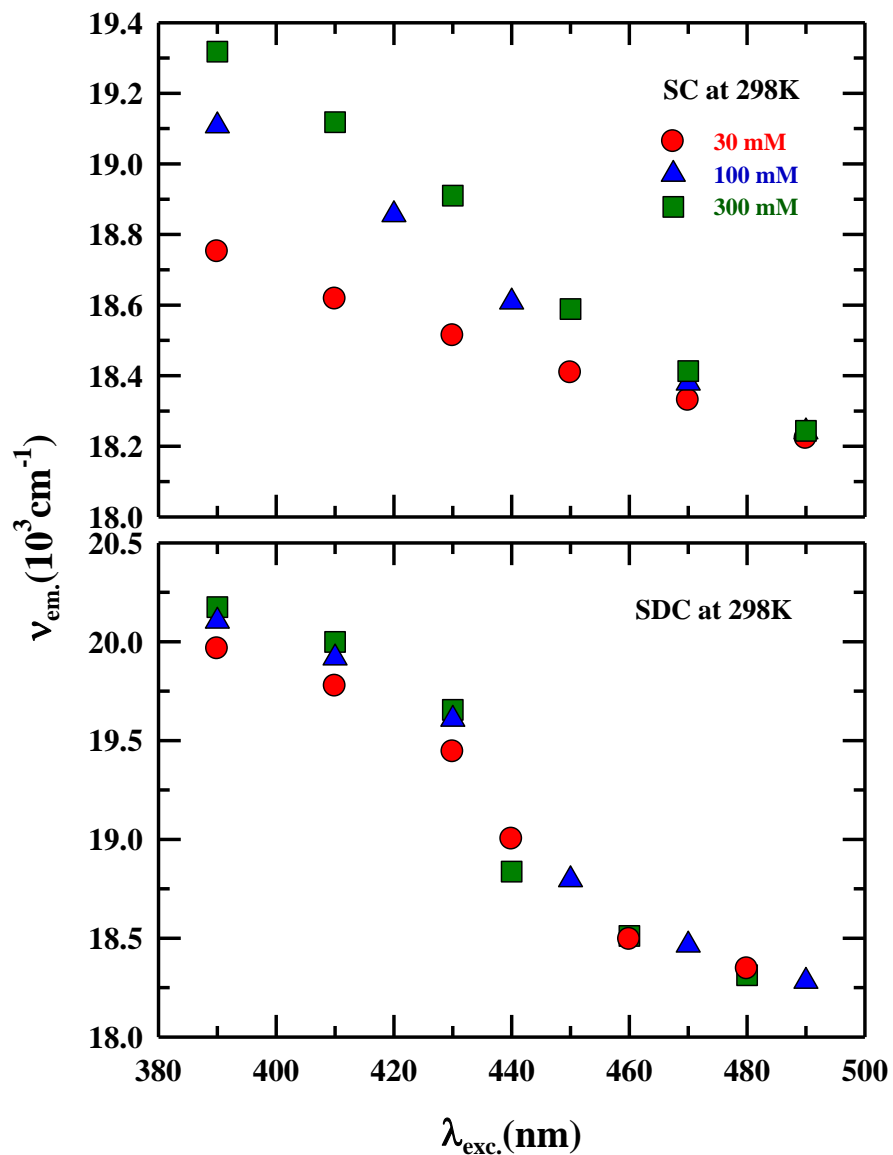
Fig. A.g.2: Excitation wavelength ($\lambda_{exc.}$) dependent emission peak frequency ($\nu_{em.}$) of C153 in SC (upper panel) and SDC (lower panel) solutions of three different bile salt concentrations for each bile salt at 298K. Circles indicate the 30 mM concentration where as the triangles and the squares represent the 100 mM and 300 mM concentrations, respectively.
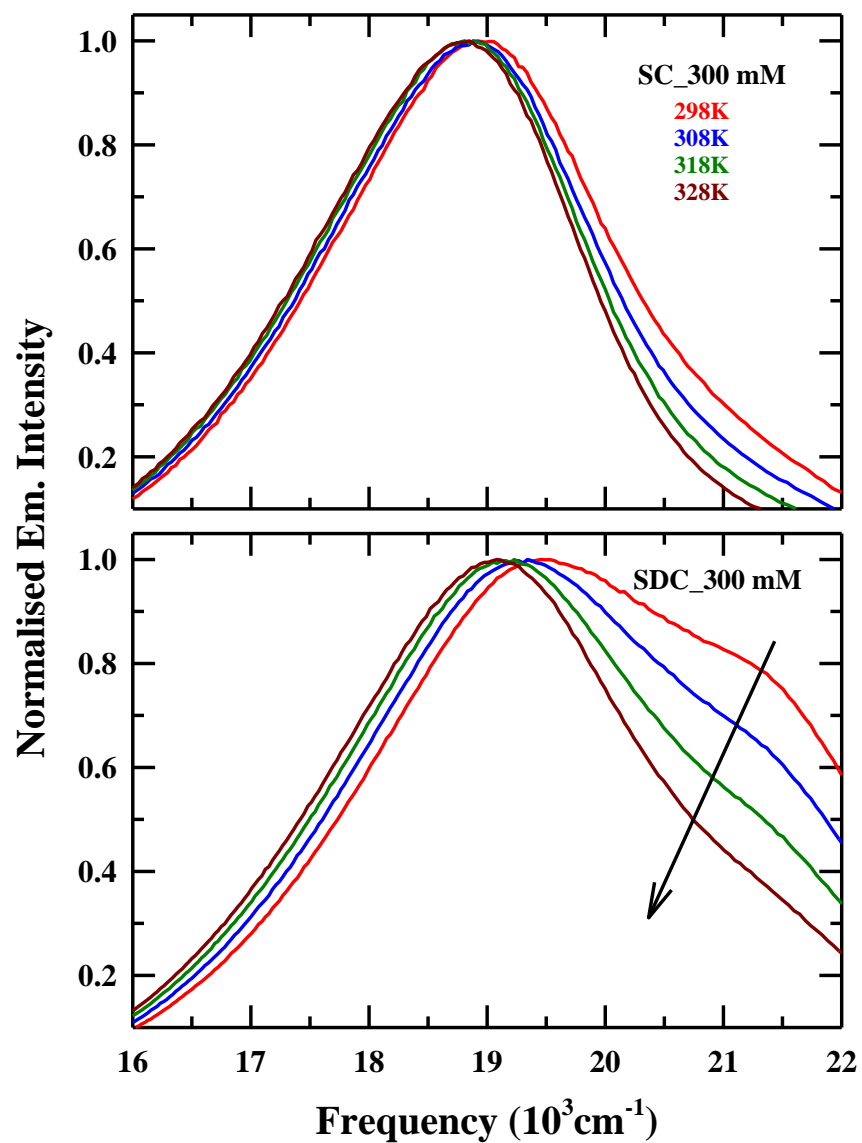
Fig. A.g.3: Representative spectra for temperature dependent emission spectra of C153 in 300 mM aqueous solutions of SC (upper panel) and SDC (lower panel). Different temperatures are color coded. The arrow indicates the direction of temperature increase.
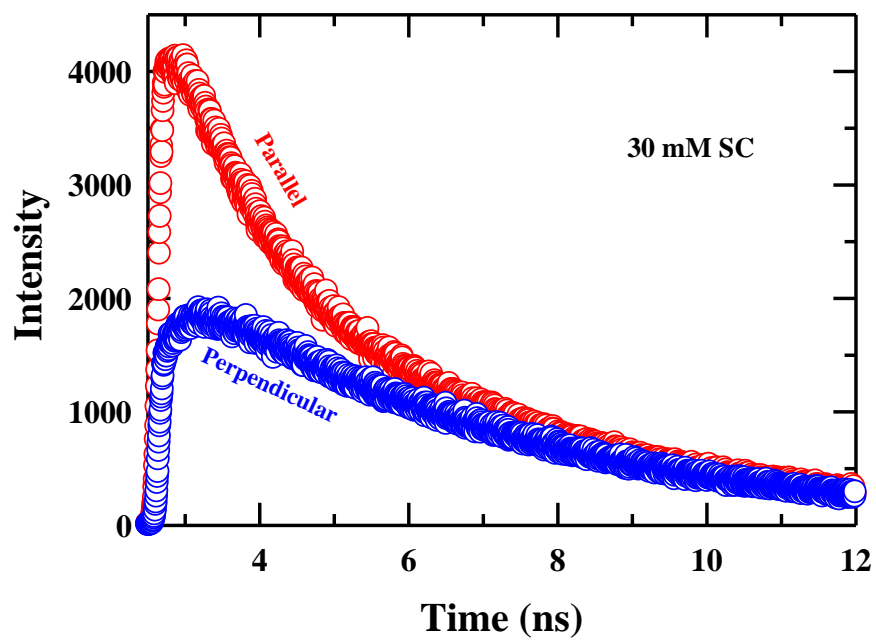
Fig. A.g.4: Representative fluorescence intensity decay profiles for 30 mM SC solution, collected with different polarizations. Representations are color-coded.
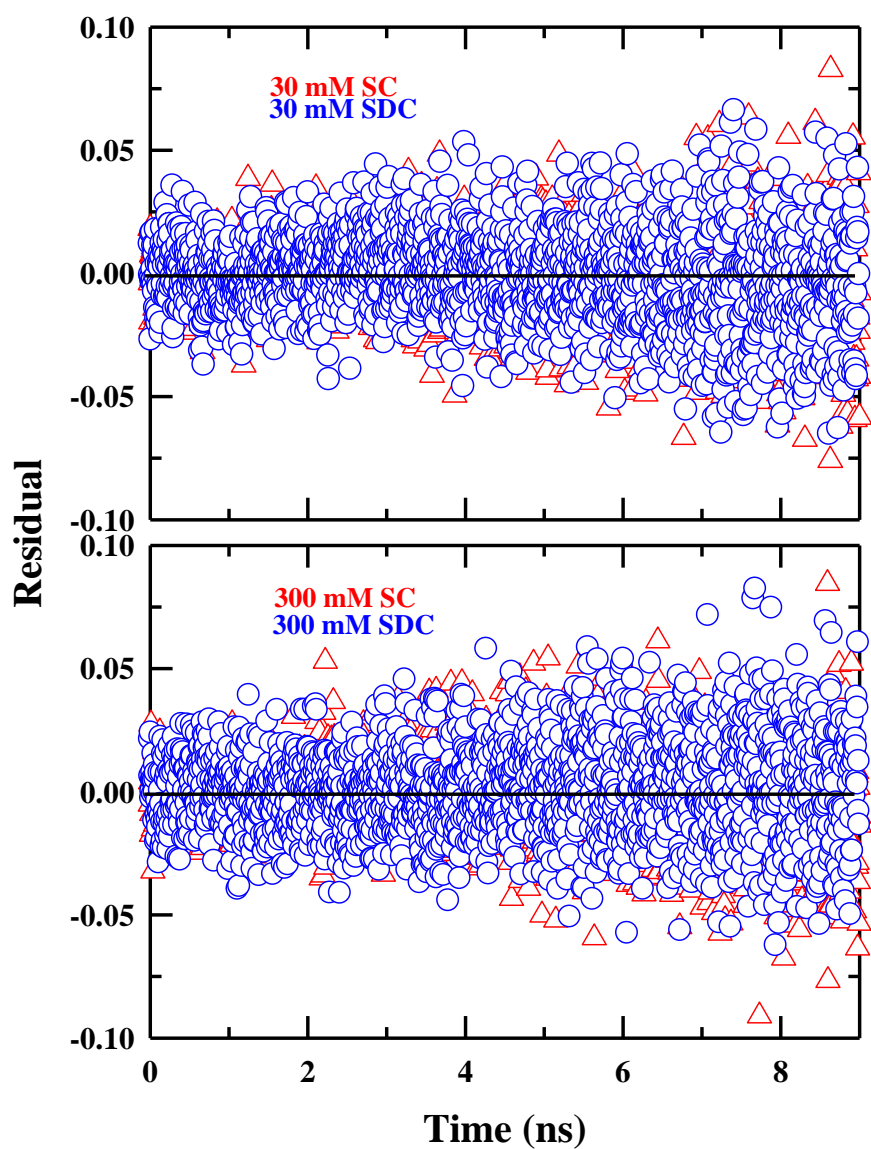
Fig. A.g.5: Residuals for the fitting of fluorescence anisotropy decay (r(t)) of C153 in 30 mM (upper panel) and 300 mM (lower panel) SC and SDC solutions. Red triangles and blue circles indicate SC and SDC, respectively.

Table A.g.6: Temperature dependence of viscosity coefficient (η) for the aqueous solutions of SC and SDC with three different concentrations.

Temperature (K)	η (cp)					
	30 mM		100 mM		300 mM	
	SC	SDC	SC	SDC	SC	SDC
293	1.054	1.075	1.230	1.318	1.993	3.521
303	0.844	0.862	0.980	1.045	1.552	2.526
313	0.702	0.716	0.807	0.855	1.070	1.880
323	0.601	0.614	0.684	0.719	0.889	1.452
333	0.527	0.570	0.595	0.619	0.758	1.154
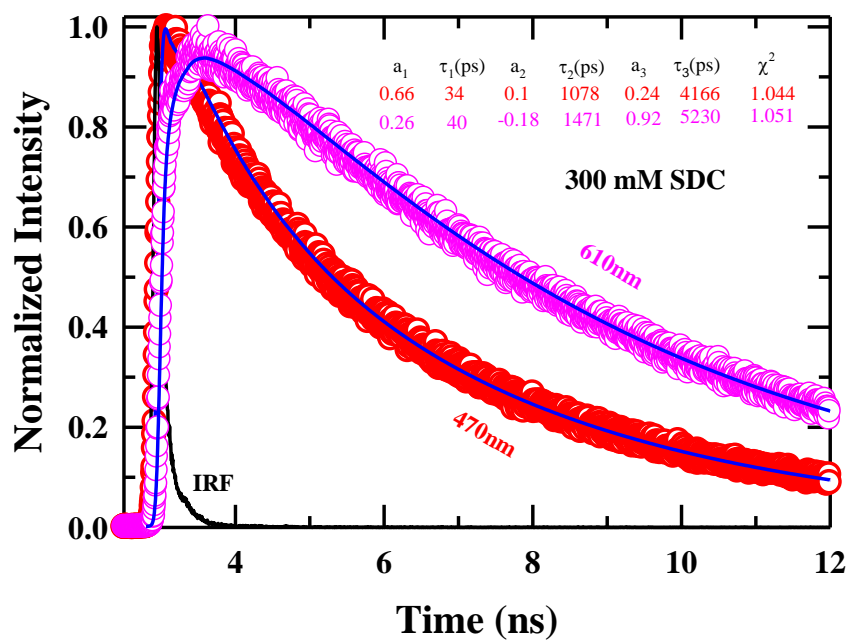
Fig. A.g.7: Representative intensity decay profiles collected at red (610 nm) and blue (470 nm) wavelengths for 300 mM SDC solution are shown as a function of time. The blue solid lines passing through the data sets depict the tri-exponential fits through them. Fit parameters are given in the inset. All representations are color-coded.
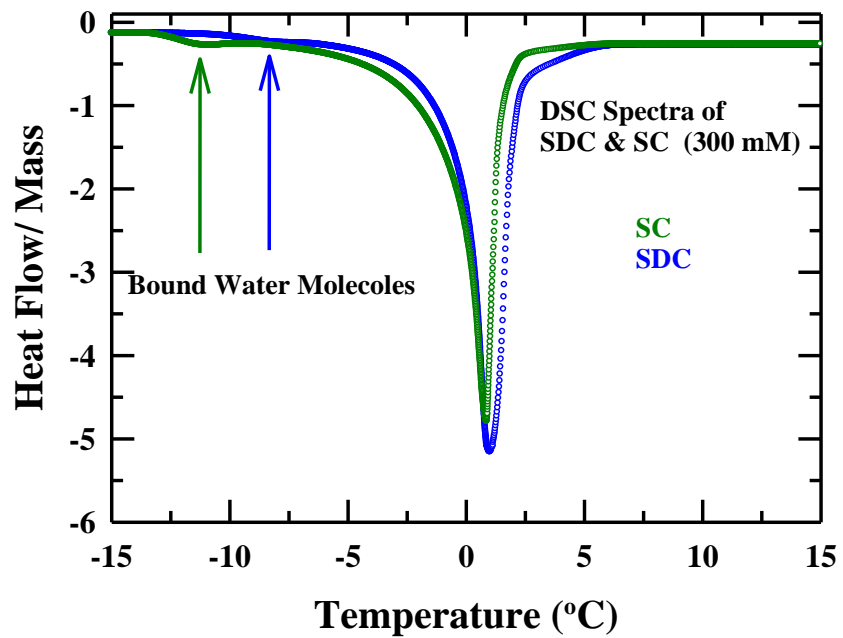
Fig.A.g.8: Representative DSC data of SC and SDC solutions with 300 mM concentration. Salt identities are color-coded and the arrows indicate the sub-melting peak positions for comparison.